

**FIELD SCALE HISTORY MATCHING AND ASSISTED HISTORY
MATCHING USING STREAMLINE SIMULATION**

A Dissertation

by

ARUN KHARGHORIA

Submitted to the Office of Graduate Studies of
Texas A&M University
in partial fulfillment of the requirements for the degree of

DOCTOR OF PHILOSOPHY

August 2003

Major Subject: Petroleum Engineering

**FIELD SCALE HISTORY MATCHING AND ASSISTED HISTORY
MATCHING USING STREAMLINE SIMULATION**

A Dissertation

by

ARUN KHARGHORIA

Submitted to Texas A&M University
in partial fulfillment of the requirements
for the degree of

DOCTOR OF PHILOSOPHY

Approved as to style and content by:

Akhil Datta-Gupta
(Chair of Committee)

Daulat D. Mamora
(Member)

W. John Lee
(Member)

Yalchin Efendiev
(Member)

Hans C. Juvkam-Wold
(Head of Department)

August 2003

Major Subject: Petroleum Engineering

ABSTRACT

Field Scale History Matching and Assisted History Matching Using Streamline Simulation.

(August 2003)

Arun Kharghoria, B.S., Indian School of Mines, Dhanbad, India;

M.S., University of Tulsa

Chair of Advisory Committee: Dr. Akhil Datta-Gupta

In this study, we apply the streamline-based production data integration method to condition a multimillion cell geologic model to historical production response for a giant Saudi Arabian reservoir. The field has been under peripheral water injection with 16 injectors and 70 producers. There is also a strong aquifer influx into the field. A total of 30 years of production history with detailed rate, infill well and re-perforation schedule were incorporated via multiple pressure updates during streamline simulation. Also, gravity and compressibility effects were included to account for water slumping and aquifer support. To our knowledge, this is the first and the largest such application of production data integration to geologic models accounting for realistic field conditions. We have developed novel techniques to analytically compute the sensitivities of the production response in the presence of gravity and changing field conditions. This makes our method computationally extremely efficient. The field application takes less than 6 hours to run on a PC.

The geologic model derived after conditioning to production response was validated using field surveillance data. In particular, the flood front movement, the aquifer encroachment and bypassed oil locations obtained from the geologic model was found to be consistent with field observations. Finally, an examination of the permeability changes during production data integration revealed that most of these changes were aligned along the facies distribution, particularly the 'good' facies distribution with no resulting loss in geologic realism.

We also propose a novel assisted history matching procedure for finite difference simulators using streamline derived sensitivity calculations. Unlike existing assisted history matching techniques where the user is required to manually adjust the parameters, this procedure combines

the rigor of finite difference models and efficiencies of streamline simulators to perform history matching. Finite difference simulator is used to solve for pressure, flux and saturations which, in turn, are used as input for the streamline simulator for estimating the parameter sensitivities analytically. The streamline derived sensitivities are then used to update the reservoir model. The updated model is then used in the finite difference simulator in an iterative mode until a significant satisfactory history match is obtained.

The assisted history matching procedure has been tested for both synthetic and field examples. The results show a significant speed-up in history matching using conventional finite difference simulators.

DEDICATION

To my beloved parents and brothers and sister, to my lovely wife and her family, and to my friends.

ACKNOWLEDGMENTS

I would like to express my deep gratitude to my graduate advisor Dr. Akhil Datta-Gupta for his invaluable advice, financial support, and especially for academic guidance.

I would like to thank Dr. John W. Lee, Dr. Daulat D. Mamora, and Dr. Yalchin Effendiev for serving as committee members and Dr. Tanya Pankiw for serving as the Graduate Council Representative. I acknowledge their helpful comments and suggestions in shaping this dissertation. I would like to thank Dr. Sang Heon Lee and Zhong He for their help and fruitful discussion during the research work. I would also like to thank Dr. Neil Barman and Seongsik Yoon of Veritas DGC and Manoj Choudhary of Chevron Technology for their help, support and valuable advices at the early days of my research and beyond.

I would like to acknowledge financial support from the *Joint Industry Project* members and also from the U. S. Department of Energy.

I want to thank my friends in the reservoir characterization group, Harshal Parikh, Ichiro Osako, Nam Il, Hao Cheng, Adel, Ahmed Daoud, Ahmed Alhuthali, Mishal, Eduardo, Dayo and Leonardo for making my graduate years enjoyable and memorable. The facilities and resources provided by the Petroleum Engineering Department, Texas A&M University, are gratefully acknowledged.

I would also like to express my sincere acknowledge to Weipeng Jiang who provided me with some critical guidance with ECLIPSE.

Finally, I would like to say my sincere 'thank you' to my wife Shabnam who bore with me all the difficulties while at Texas A&M and sacrifices made during my studies.

TABLE OF CONTENTS

	Page
ABSTRACT.....	iii
DEDICATION.....	v
ACKNOWLEDGMENTS.....	vi
TABLE OF CONTENTS.....	vii
LIST OF TABLES.....	x
LIST OF FIGURES.....	xi
CHAPTER I INTRODUCTION.....	1
1.1 Motivation for the Study.....	1
1.2 Introduction.....	2
1.3 Literature Review.....	3
1.4 Objectives of the Study.....	4
1.5 Dissertation Outline.....	5
CHAPTER II THEORETICAL BACKGROUND OF PRODUCTION DATA	
INTEGRATION AND STREAMLINE SIMULATION.....	6
2.1 Introduction.....	6
2.2 Production Data Integration - Theoretical Background.....	8
2.3 Sensitivity Computation.....	8
2.3.1 Sensitivity of Tracer Concentration Response.....	8
2.3.2 Sensitivity of Two-Phase Production Response.....	10
2.4 Travel Time Sensitivity.....	11
2.5 Construction of the Inverse Model.....	11
2.6 Optimization with LSQR.....	13
2.7 Forward Model.....	13
2.8 Illustrative Example of Production Data Integration.....	14
2.9 Streamline Simulation Fundamentals.....	23
2.9.1 Pressure Solving.....	26
2.9.2 Streamline Tracing and Time of Flight Computation.....	26
2.9.3 Saturation Advancing Along Streamlines.....	27
2.9.4 Pressure Updating.....	29
2.10 Incorporating Effect of Compressibility and Aquifer Influx.....	30
2.11 Implementing Horizontal Well.....	30
2.12 Chapter Summary.....	31

	Page
CHAPTER III PRODUCTION DATA INTEGRATION - A LARGE SCALE	
FIELD EXAMPLE.....	32
3.1 Introduction.....	32
3.2 Objective.....	33
3.3 Geology and Geologic Model.....	34
3.4 Approach for Data Integration.....	35
3.4.1 Two Step Approach.....	35
3.4.2 Setup of Coarse Scale Model.....	37
3.4.3 Results.....	43
3.4.4 Conditioning Coarse Scale Model to Water Cut Responses.....	51
3.4.5 Downscaling.....	75
3.4.6 Finescale Simulation with the Updated Model.....	75
3.4.7 Direct Integration into the Finescale Modle.....	75
3.5 Statistics after Inversion.....	87
3.6 Comparison with ECLIPSE.....	87
3.7 Chapter Summary.....	98
CHAPTER IV ASSISTED HISTORY MATCHING.....	100
4.1 Introduction.....	100
4.2 Methodology.....	100
4.2.1 Comparison of Velocity Fields.....	102
4.3 Assisted History Matching : A Synthetic Example with Infill Wells.....	106
4.4 Assisted History Matching : Field Applications.....	106
4.4.1 Goldsmith Field Example.....	106
4.4.2 Giant Middle Eastern Field Example.....	111
4.5 Sensitivity Studies for the History Match Process.....	123
4.5.1 Goldsmith Field Example.....	123
4.5.2 Giant Middle Eastern Field Example.....	131
4.6 Time Comparison.....	131
4.7 Advantages of Assisted History Matching.....	131
4.8 Chapter Summary.....	131
CHAPTER V CONCLUSIONS AND RECOMMENDATIONS.....	140
5.1 Conclusions.....	140
5.2 Recommendations.....	143

	Page
NOMENCLATURE.....	145
REFERENCES.....	147
APPENDIX A DYNAMIC MEMORY ALLOCATION	150
APPENDIX B HORIZONTAL WELL.....	162
APPENDIX C USER INTERFACES	165
VITA.....	173

LIST OF TABLES

TABLE	Page
3.1 Comparison of CPU Time for Parameter Estimation.....	91
4.1 CPU Time Comparison for Goldsmith Field Case for Different Scenarios..	139
4.2 CPU Time Comparison for Giant Middle Eastern Field Case (Upscaled Model) for Different Scenarios..	139

LIST OF FIGURES

FIGURE	Page
2.1 Well Locations for the Synthetic Example.....	15
2.2 Reference Permeability Model for Synthetic Example.	16
2.3 Tracer Response from Reference and Initial Model.	17
2.4 Tracer Response after Arrival Time Match.	18
2.5 Permeability Field after Arrival Time Match.	19
2.6 Tracer Response after Amplitude Match.	20
2.7 Comparison of Permeability Fields after Amplitude Match.....	21
2.8 Root Mean Squared Error of Tracer Concentration Misfit as a Function of Number of Iterations.....	22
2.9 A Stepwise Illustration of Streamline Simulation.....	25
3.1 Well Location Map of the Giant Middle Eastern Field. The Dotted Line Denotes the Simulation Area..	36
3.2 Cross Section Map of Porosity and Permeability Model Based on Full Geologic Model (128x16128)	36
3.3 Cross Section Map of Porosity and Permeability Model Based on Upscaled Model (128x160x13) from Geologic Model	38
3.4 Relative Permeability Curves	38
3.5 Facies Based J-Curves for Initial Water Saturation Estimation.....	39
3.6 Fieldwide Facies Model and N-S Cross Section of the Facies Model.	40
3.7 Initial Water Saturation Distribution of Geologic Model.....	40
3.8 N-S Cross Section of Initial Water Saturation of the Geologic Model	41
3.9 Examples of Actual Flow Rates vs. Averaged Flow Rates Used for Streamline Simulation	44
3.10 Pressure Distribution at Three Different Times for Layer 1, 4 and 8 without Gravity.	45
3.11 Time of Flight Distribution at Three Different Times for Layer 1, 4 and 8 without Gravity	46
3.12 Water Saturation Distribution at Three Different Times for Layer 1, 4 and 8 without Gravity	47
3.13 Areal Map of Streamline Distribution at Three Different Times without Gravity	48
3.14 Examples of Water Cut Responses without Gravity Effect.....	49
3.15 Pressure Distribution at Three Different Times for Layer 1, 4 and 8 with Gravity	52

FIGURE	Page
3.16 Time of Flight Distribution at Three Different Times for Layer 1, 4 and 8 with Gravity	53
3.17 Water Saturation Distribution at Three Different Times for Layer 1, 4 and 8 with Gravity	54
3.18 Areal Map of Streamline Distribution at Three Different Times with Gravity	55
3.19 Water Cut Responses with Gravity Effect.....	56
3.20 Travel Time Match at Four Different Iterations without Gravity	59
3.21 Water Cut Matches for Upscale Model without Gravity Effect	60
3.22 Changes in Pressure Distribution at Three Different Times without Gravity	62
3.23 Changes in Water Saturation Distribution at Three Different Times without Gravity ..	64
3.24 Permeability Change (md) from the Initial Model for Layer 1, 4 and 8 without Gravity	66
3.25 Travel Time Matches at Four Different Iterations with Gravity.....	66
3.26 Water Cut Matches for Upscale Model with Gravity Effect	67
3.27 Changes in Pressure Distribution at Three Different Times with Gravity.	70
3.28 Changes in Water Saturation at Three Different Times with Gravity.....	72
3.29 Permeability Change (md) from the Initial Model for Layer 1, 4 and 8 with Gravity...	74
3.30 Permeability Change (md) from the Initial Model in Fine Scale Model.....	76
3.31 Comparison of Permeability Change (md) from the Initial Model (Left) and Facies Distribution (Right) at Different Layers in Fine Scale Model.....	77
3.32 Initial (at 60 Days) and Final (at 10290 Days) Pressure Distributions for Layer 10, 50 and 70 for Fine Scale Simulation.	81
3.33 Areal View of Streamline Distributions for Updated Model for Fine Scale Simulation	82
3.34 Time of Flight Distributions at Initial and Final Time for Layer 10, 50 and 70 for Fine Scale Simulation	83
3.35 Saturation Distributions at Initial and Final Time for Layer 10,50 and 70 for Fine Scale Simulation.	84
3.36 Water Cut Matches for Updated Fine Scale Model	86
3.37 Travel Time Match at Four Different Iterations for Direct Integration	88
3.38 Examples of Water Cut Matches from Direct Fine Scale Integration.....	89
3.39 Change in Permeability (md) for Direct Fine Scale Integration for Layer 10, 50 and 70.....	91
3.40 Histogram of Two Models	92
3.41 Examples of Comparison of Water Cut Match with ECLIPSE	95

FIGURE	Page
3.42 Comparison of Water Saturation Distributions (10290 days) Estimated by ECLIPSE and Streamline Simulation with Initial Permeability	96
3.43 Comparison of Water Saturation Distributions (10290 days) Estimated by ECLIPSE and Streamline Simulation with Inverted Permeability	97
4.1 Flowchart for Assisted History Matching	101
4.2 Velocity Comparison for the Synthetic Example	103
4.3 Velocity Comparison for NRU Field Example	104
4.4 Well Pattern and Reference Permeability Field for the Synthetic Example.....	105
4.5 Water Cut Response from Initial and Final Model for Synthetic Example	107
4.6 Initial and Final Permeability Multipliers for the Synthetic Example	108
4.7 Initial and Final Permeability Distribution for the Synthetic Example.....	108
4.8 Initial and Final Travel Time Match for the Synthetic Example	109
4.9 Reduction in Travel Time RMS Error and Total RMS Error for Different Iterations for the Synthetic Example.....	109
4.10 Goldsmith Study Area.....	110
4.11 Reference Permeability and Porosity Distribution for Goldsmith Field Example.....	112
4.12 Initial and Final Water Cut Matches for Goldsmith Field Example	112
4.13 Initial and Final Permeability Multipliers for Goldsmith Field Example.....	113
4.14 Initial, Final and Change in Permeability for Goldsmith Field Example.....	114
4.15 Initial and Final Travel Time Match for Goldsmith Field Example	115
4.16 Reduction in Error for Goldsmith Field Example.....	115
4.17 Initial and Final Travel Time Matches for Giant Middle Eastern Field Example	116
4.18 Reduction in Travel Time RMS Error and Total RMS Error for the Giant Middle Eastern Field Example	117
4.19 Initial and Final Permeability Multipliers for the Giant Middle Eastern Field Example	118
4.20 Permeability Difference (md) for the Giant Middle Eastern Field Example.....	119
4.21 Final Water Saturation Profile for the Giant Middle Eastern Field Example.....	120
4.22 Examples of Water Cut Match for the Giant Middle Eastern Field Example	121
4.23 Comparison of Facies Trends with Change in Permeability (md) for Layer 58, 64 and 67 Respectively from Top to Bottom	122
4.24 Comparison of Misfit Reduction for Goldsmith Example.	124
4.25 Comparison of Initial and Final Travel Time Matches for the Goldsmith Field Example	125

4.26	Comparison of Initial Permeability Multipliers for the Goldsmith Field Example	126
	FIGURE	Page
4.27	Comparison of Final Permeability Multipliers for the Goldsmith Field Example	127
4.28	Comparison of Estimated Permeability with Reference Model for the Goldsmith Field Example	128
4.29	Comparison of Permeability Change for the Goldsmith Field Example	129
4.30	Comparison of Initial and Final Water Cut Matches for the Goldsmith Field Example	130
4.31	Comparison of Reduction in Errors for Giant Middle Eastern Field Example	133
4.32	Comparison of Initial and Final Travel Time Match for the Giant Middle Eastern Field Example	134
4.33	Comparison of Initial Permeability Multipliers for the Giant Middle Eastern Field Example	135
4.34	Comparison of Final Permeability Multipliers for the Giant Middle Eastern Field Example	135
4.35	Comparison of Permeability Difference for the Giant Middle Eastern Field Example	136
4.36	Comparison of Final Water Saturation Profiles for the Giant Middle Eastern Field Example	137
4.37	Comparison of Water Cut Response from Initial and Final Models for the Giant Middle Eastern Field Example	138

CHAPTER I

INTRODUCTION

This chapter presents the motivation and objectives of the research work carried out for this dissertation. Dynamic data integration technologies are being increasingly used as a tool in petroleum industry for history matching with high resolution geological model. Use of streamline simulator as a forward model in data integration process makes it at least an order of magnitude faster compared to the use of conventional finite difference simulator. However, till date, history matching using streamline simulation technique has been applied to synthetic and small scale field applications. Present study focuses on improvement of the existing techniques and their application to a large scale field example. A brief literature review has been presented followed by objective of the study. Finally, the organization of this dissertation is outlined.

1.1 Motivation for the Study

Incorporation of all available data for reservoir history matching is an important aspect for optimal reservoir management and reliable performance forecasting. Recent developments in reservoir characterization and in the management of uncertainty have led to the ability of the petroleum industry to routinely generate large multimillion-cell detailed geologic models. Reconciling such high-resolution models with dynamic reservoir behavior (transient pressure and tracer response, multiphase production history) is essential to develop a reliable reservoir model for performance forecasting. However, dynamic data integration still remains an outstanding challenge because of the high expenses in terms of time and also the subjectivity and non uniqueness associated with conventional history matching approach. Considering the above challenges during production data integration, the major motivations for this study could be stated as below:

1. Generalization of Streamline based history matching to account for realistic field conditions.
2. Application of dynamic data integration techniques for a large scale field example accounting for rate change, infill drilling, recompletions and also reservoir mechanisms such as gravity and aquifer influx.

This dissertation follows the style and format of the *SPE Journal*.

3. Enhancement of conventional history matching using finite difference simulator with streamline derived sensitivities. This will retain the full-physics from the finite difference model and also result in a significant reduction in history matching cycle time.

1.2 Introduction

It is a well established fact that incorporation of dynamic data into geostatistical models is necessary for reliable reservoir descriptions. Dynamic data, time variant measurements such as transient pressure response, tracer or production history can be particularly effective in identifying preferential flow paths or barriers to flow that can adversely impact sweep efficiency. Reservoir models derived from static data such as geological descriptions, well logs, seismic attributes, or core data need to be further revised by integrating dynamic data to account for these flow characteristics of reservoirs. The past few years have seen significant developments in the area of dynamic data integration in the framework of inverse modeling, particularly for estimating reservoir parameters such as permeability or porosity.

Use of fast streamline-based simulation techniques offers significant potential in terms of computational efficiency. Streamline models can be advantageous in two ways for inverse modeling. First, the streamline simulator can serve as an efficient forward model for the inverse problem. Streamline methods have been gaining popularity with the increase of demand for fast fine scale simulation. Its high computational speed (in general, 1 to 3 orders of magnitude faster than conventional finite difference type flow simulators) makes it well suited for describing flow characteristics for high resolution reservoir models. Second, and more importantly, sensitivities to reservoir parameters can be formulated along streamlines. This reduces the governing sensitivity equations to series of one-dimensional integrals. This is particularly advantageous because parameter sensitivities and transport equation can be solved along the same one-dimensional path. Sensitivities are obtained from the single streamline simulation, resulting in significant savings in computation time and making dynamic data integration into high resolution reservoir description possible.

In this study, the above mentioned advantages of streamline simulator has been further explored in combination with finite difference simulator. The velocity field required for streamline simulator has been obtained from the finite difference simulator and both water saturation and water cut responses are estimated from the finite difference simulator. The results

are supplied to the streamline simulator and then sensitivity computation along the streamlines is carried out. The streamline-derived sensitivities are then used in the data integration process. This results in a robust technique for assisted history matching that retains the full physics of from the finite difference simulator and utilizes the analytic sensitivities from the streamline model.

1.3 Literature Review

The fundamentals of potential flow theory can be traced back to the nineteenth century. Muskat¹ proposed modeling of fluid flow and transport using streamlines and streamtubes back in 1937. Since then, several authors have extended the underlying concepts of streamline into petroleum reservoir modeling. Notable works among these are from Fay and Prats², Higgins and Leighton³, Pitts and Crawford⁴, and Martin and Wagner⁵. Many of these applications used a 2-D streamtube based approach to model multiphase fluid displacement. The direct extension of the 2-D streamtube based approach to 3-D flow is non-trivial because of the complexities associated with the tracking of tube geometries in 3-D space.

The streamline method utilizes the concepts of particle tracking to define the pathlines in three-dimensional space. Unlike streamtube approach, streamline approach does not require tube geometries to be explicitly evaluated. This makes it suitable for modeling flow and transport in three dimensional space.

The key underlying concept behind the computation of streamlines in three dimensions is the ‘time-of-flight’ coordinate which was proposed by Datta-Gupta and King⁶. The ‘time-of-flight’ approach decouples the flow from transport and thus greatly facilitates analytical and numerical solutions along the streamlines. The advantage of this approach is the simplicity, computational efficiency and ready generalization.

Streamline simulation has become a viable alternative to conventional finite difference type reservoir simulator due to its high speed performance.^{7,8} It has been gaining popularity in petroleum industry in recent years and has been successfully used as a forward model in dynamic data integration process. Datta-Gupta *et al.*,⁹ Vasco and Datta-Gupta,¹⁰ Xue and Datta-Gupta¹¹ have employed streamline simulation to overcome computational burden in using conventional finite difference type simulator. First truly three dimensional streamline simulator applied to field level simulation was presented by Peddibholta¹² *et al.* Another advantage associated with streamline method is that it is possible to analytically derive a relationship

between perturbations in reservoir properties, such as permeability, porosity, or residual saturation, and changes in observables such as water-cut and tracer response. Vasco *et al.*¹³ have presented streamline-based production data integration approach in which sensitivity of water-cut with respect to reservoir parameters are computed semi-analytically along streamlines and demonstrated the inversion with more than 30,000 parameters. Yoon *et al.*¹⁴ applied this method for estimation of residual oil phase saturation by integrating interwell partitioning tracer tests. Further improvement on the streamline-based method was made by adapting hierarchical parameterization and scale-by-scale inversion in Yoon *et al.*¹⁵

Most recently, streamline technique has been applied to production data integration under changing field conditions¹⁶ and for identification of reservoir compartmentalization and flow barriers using primary production¹⁷.

1.4 Objectives of the Study

Our goal is to develop a systematic procedure for reconciling high-resolution geologic models to production data such as water-cut and pressure data, which ultimately improves reliability in the reservoir performance forecasting. Specifically, we want to establish a methodology that is computationally efficient and also can account for well scheduling such as infill drilling and rate changes during the course of field production history. We also want to incorporate all dominant reservoir mechanisms such as gravity and aquifer influx.

We demonstrate the practical feasibility of the streamline based production data integration technique by application to a giant middle-eastern filed with 30 years of production history As a part of the study, it was necessary to formulate and modify the existing streamline simulator to the capacity to handle large scale full field model. Also, an assisted history matching technique for finite difference simulator was proposed and tested for both synthetic and field examples.

Followings are the basic objectives :

- Enhance the capability of the present streamline simulator to handle large scale full field model with varying degree of heterogeneity.
- Extend the data integration process to include the effect of gravity, rock compressibility and aquifer influx in streamline simulation for field application.
- Implement horizontal well in well model.
- Test the developed concepts with synthetic and real field examples.

- Use the streamline simulator for assisted history matching for finite difference simulation models.

1.5 Dissertation Outline

Chapter II explains the fundamentals of streamline simulation and dynamic data integration based on streamline technology.

Chapter III presents the conditioning of a large scale geological model with production data using streamline based inversion technique. The application contains integration of 30 years of production history for history match purposes.

Chapter IV deals with the development and application of a novel streamline based assisted history matching procedure for finite difference simulators.

Chapter V summarizes the dissertation with conclusions and recommendations.

CHAPTER II

THEORETICAL BACKGROUND OF PRODUCTION DATA INTEGRATION AND STREAMLINE SIMULATION

This chapter discusses the theoretical background of production data integration and the use of streamline simulation technique as the forward model. Production data integration is essentially an inverse modeling problem consisting of three major components. First, forward model which is a mathematical or numerical model of the physics of the system of interest. Second, objective function that provides the measure of deviation of the model performance from the actual system response. Finally, optimization process which is a numerical technique to minimize the objective function to improve the estimation of model parameters.

2.1 Introduction

It is well known that geological models derived from static data only, such as geological, well log, core and seismic data, often fail to reproduce the production history. Reconciling geologic models to the dynamic response of the reservoir is critical to building reliable reservoir models. In recent years there have been significant developments in the area of dynamic data integration through the use of inverse modeling. Streamline models have shown great promise in this regard. The key advantages of streamline-based production data integration are its computational efficiency as a “forward” model and analytic computations of sensitivities of the production response with respect to reservoir parameters using a single flow simulation. Sensitivities describe the change in production response due to a small perturbation in reservoir properties such as porosity and permeability and are a vital part of the dynamic data integration process.

In recent years, researchers at Texas A&M have developed a streamline-based production data integration technique that is similar to seismic waveform inversion and utilizes a two-step procedure

1. A travel time match that involves matching of the ‘first arrival’ or breakthrough times,
2. An amplitude match involving matching of the actual production response.

The two-step approach has been shown to substantially speed-up the computation and also prevents the solutions from being trapped by secondary peaks in the production response. However, a majority of the production data misfit reduction occurs during the travel time inversion and most of the large-scale features of heterogeneity are resolved at this stage.

There are several advantages associated with a travel time inversion of production data. First, it is robust and computationally efficient. Unlike conventional ‘amplitude’ matching which can be highly non-linear, it has been shown that the travel time inversion has quasilinear properties. As a result, the minimization proceeds rapidly even if the initial model is not close to the solution. Second, the travel time sensitivities are typically more uniform between wells compared to ‘amplitude’ sensitivities that tend to be localized near the wells. This prevents over-correction in the near-well regions. Finally, during practical field applications, the production data are often characterized by multiple peaks (for example, tracer response). Under such conditions, the travel time inversion can prevent the solution from converging to secondary peaks in the production response.

Recently, the concept of assisted history matching has been introduced to facilitate conventional history matching. This approach is a manual history matching aided by the use of streamlines simulation and consists of the following major steps:

1. Assess the difference between model and field performance.
2. Use streamlines to assign grid blocks to wells. This identifies the grid blocks that need to be changed during history matching.
3. Manually change pre-specified properties (for example permeability multipliers).
4. Iterate.

This method utilizes unique information contained in the streamlines and helps history matching providing several advantages:

1. It considerably simplifies history matching by targeting changes to match specific well response,
2. it can be applied to finite-difference models.

However, it still requires subjective judgment during history matching and can introduce ‘artifacts’ by limiting changes along streamlines. Also it is hard to assess model through resolution and uncertainty analysis.

2.2 Production Data Integration – Theoretical Background

Briefly, the approach for production data integration using streamline model consist of the following steps:

- **Analytic Computation of Sensitivity** : We derive expressions for sensitivity of streamline time of flight to reservoir properties such as porosity and permeability. The time of flight sensitivities can then be easily translated to tracer concentration and water-cut sensitivities using chain rule of differentiation. The sensitivity computation simply involves evaluation of one-dimensional integrals along streamlines and requires a single simulation run.
- **Two-Step Inversion** : This involves iterative linearization of the time of flight expression about a known initial model based on static data to match the arrival time first, followed by amplitude matching. Integration of production data involves a two-step procedure:
 1. matching of the ‘first arrival’ or travel times.
 2. matching of the ‘amplitudes’ of the production response.

A brief discussion on computation of sensitivities followed by construction of inversion model and the LSQR optimization method is presented below.

2.3 Sensitivity Computation

By sensitivity, we mean the partial derivative of the production response with respect to model parameters such as permeability, porosity and saturation. Although several methods are available for computing sensitivities, for example, numerical perturbation method, direct method, or adjoint state method, these are limited by their computational costs and complex implementations. (For details on these methods, see reference 18.) Streamline-based analytic sensitivity computation approach is extremely efficient and requires only a single simulation run.

2.3.1 Sensitivity of Tracer Concentration Response

As described earlier, streamline method decouples flow and transport by a coordinate transformation from the physical space to one following flow directions viz. the tracer time of flight along streamlines. The time of flight can be defined as

$$\tau = \int_{\psi} s(\mathbf{x}) dr \quad (2-1)$$

where the integral is along the streamline trajectory, ψ and $s(\mathbf{x})$ is the 'slowness' defined as¹⁴

$$s(\mathbf{x}) = \frac{1}{|v(\mathbf{x})|} (S_w + K_o S_o) = \frac{\phi(\mathbf{x})}{\lambda_f k(\mathbf{x}) |\nabla P|} (S_w + K_o S_o) \quad (2-2)$$

where K_o is the partitioning coefficient of tracer defined as the ratio of tracer concentration in oil phase to that in water phase. For an injected concentration history, $C_o(t)$ the corresponding tracer concentration response at the producer along a single streamline can be written as

$$C(t) = C_0(t - \int_{\psi} s(\mathbf{x}) dr) \quad (2-3)$$

Consider a small perturbation in reservoir properties about an initial reservoir model, let us say based on static data. The resulting changes in slowness and tracer concentrations can be written as

$$\begin{aligned} s(\mathbf{x}) &= s^0(\mathbf{x}) + \delta s(\mathbf{x}) \\ C(\mathbf{x}, t) &= C^0(\mathbf{x}, t) + \delta C(\mathbf{x}, t) \end{aligned} \quad (2-4)$$

If it is assumed that streamlines do not shift as a result of small perturbations in medium properties, then the change in concentration response at the producing well can be derived based on a Taylor series expansion¹⁹

$$\delta C(\mathbf{x}, t) = -C_0'(t - \tau) \int_{\psi} \delta s(\mathbf{x}) dr \quad (2-5)$$

Because $s(\mathbf{x})$ is a composite function involving reservoir properties, its variation will be given by

$$\delta s(\mathbf{x}) = \frac{\partial s(\mathbf{x})}{\partial k} \delta k(\mathbf{x}) + \frac{\partial s(\mathbf{x})}{\partial \phi} \delta \phi(\mathbf{x}) + \frac{\partial s(\mathbf{x})}{\partial S_w} \delta S_w \quad (2-6)$$

where the partial derivatives are

$$\begin{aligned}
\frac{\partial s(\mathbf{x})}{\partial k} &= \frac{-\phi(\mathbf{x})}{\lambda_t k^2(\mathbf{x})|\nabla P|} (S_w + K_o S_o) = -\frac{s(\mathbf{x})}{k} (S_w + K_o S_o) \\
\frac{\partial s(\mathbf{x})}{\partial \phi} &= \frac{1}{\lambda_t k(\mathbf{x})|\nabla P|} (S_w + K_o S_o) = \frac{s(\mathbf{x})}{\phi} (S_w + K_o S_o) \\
\frac{\partial s(\mathbf{x})}{\partial S_w} &= \frac{\phi(\mathbf{x})}{\lambda_t k(\mathbf{x})|\nabla P|} (1 - K_o) = s(\mathbf{x})(1 - K_o)
\end{aligned} \tag{2-7}$$

Note that in the above expressions, we have ignored pressure changes resulting from small variations in permeability. Also, for unit partitioning coefficient, the tracer response will be insensitive to saturation changes as one might expect. Tracer travel time and concentration sensitivities with respect to permeability, porosity, and water saturation can be obtained by integrating Eq. 2-5 over all streamlines contributing to a producer.

2.3.2 Sensitivity of Two-Phase Production Response

Similarly, we can easily translate a perturbation in slowness to a corresponding perturbation in fractional flow. The perturbation in the fractional flow can be written as

$$\delta f_w = \frac{\partial f_w}{\partial \tau} \delta \tau \tag{2-8}$$

where $\delta \tau$ is related to reservoir properties through the integral equation

$$\delta \tau(x) = \int_{\psi} \delta s(x) dr \tag{2-9}$$

In this case, the slowness is defined as¹³

$$s(\mathbf{x}) = \frac{1}{|v(\mathbf{x})|} \tag{2-10}$$

The slowness variations with respect to the changes of reservoir parameters are

$$\begin{aligned}
\frac{\partial s(\mathbf{x})}{\partial k} &= \frac{-\phi(\mathbf{x})}{\lambda_t k^2(\mathbf{x})|\nabla P|} = -\frac{s(\mathbf{x})}{k(\mathbf{x})} \\
\frac{\partial s(\mathbf{x})}{\partial \phi} &= \frac{1}{\lambda_t k(\mathbf{x})|\nabla P|} = \frac{s(\mathbf{x})}{\phi(\mathbf{x})}
\end{aligned} \tag{2-11}$$

The water-cut sensitivities with respect to reservoir properties can now be obtained by integrating Eq. 2-11 over all streamlines reaching the producing well.

Note that the above expressions for sensitivity of tracer concentration and water cut response only involve quantities that are readily available once we generate the velocity field and define the streamline trajectories in a streamline simulator. Thus, in a single forward run of a streamline simulator we may derive all the sensitivity coefficients required to solve the inverse problem.

2.4 Travel Time Sensitivity

For the case of travel time inversion, we need sensitivity of travel time with respect to reservoir parameters. In tracer data integration, we can simply integrate Eq. 2-7 over all streamlines contributing to a producer at particular time to get the sensitivity of travel time. However, simple integration of Eq. 2-11 over the streamlines is not sufficient in the water-cut data integration case. That is because the speed of saturation front is different from that of neutral tracer particle. To get the correct travel time of the saturation front and corresponding sensitivity, we need to divide the time of flight by the fractional flow slope at breakthrough, $(\partial f_w / \partial S_w)_{bt}$.

2.5 Construction of the Inversion Model

Our approach to production data integration using streamlines consists of two distinct steps:

1. an ‘arrival time’ or fluid breakthrough matching.
2. an ‘amplitude’ or water-cut/pressure response matching.

During inverse modeling or production data integration, we want to minimize the differences between observed production responses and our model predictions. Mathematically, this can be expressed as

$$\min_{\mathbf{m}} \|\mathbf{d} - \mathbf{g}[\mathbf{m}]\|^2 \quad (2-12)$$

where \mathbf{d} is the data vector with N observations, \mathbf{g} is the forward model, \mathbf{m} is the vector of M parameters. Because of the nonlinearity between data and model parameters, we resort to an iterative minimization procedure. For example, at the k -th iteration step we obtain the following using a first order Taylor series expansion of $\mathbf{g}[\mathbf{m}]$ around \mathbf{m}^k ,

$$\mathbf{g}[\mathbf{m}] = \mathbf{g}[\mathbf{m}^k] + \mathbf{G} \delta \mathbf{m} \quad (2-13)$$

where $\delta \mathbf{m}$ is the parameter perturbation at k -th step and \mathbf{G} is the sensitivity matrix with sensitivity coefficient entries as discussed above coefficient entries discussed above and defined by

$$\mathbf{G} = \left. \frac{\partial \mathbf{g}[\mathbf{m}]}{\partial \mathbf{m}} \right|_{\mathbf{m}^k} \quad (2-14)$$

The residual (data misfit) vector $\boldsymbol{\varepsilon}$ at the k -th iteration step will be given by

$$\boldsymbol{\varepsilon} = \mathbf{d} - \mathbf{g}[\mathbf{m}^k] \quad (2-15)$$

We can for $\delta \mathbf{m}$ at each step by minimizing the linear least squares

$$\|\boldsymbol{\varepsilon} - \mathbf{G} \delta \mathbf{m}\|^2 = \sum_{i=1}^N \left(\varepsilon_i - \sum_{j=1}^M G_{ij} \delta m_j \right)^2 \quad (2-16)$$

and update our parameter vector with

$$\mathbf{m} = \mathbf{m}^k + \delta \mathbf{m} \quad (2-17)$$

In field situations, very often we have a large number of unknown parameters and limited measurements. Thus, the inverse problem tends to be ill-posed.^{20,21} Solutions of such ill-posed problems suffer from non-uniqueness and instability. To circumvent the problem, we augment the linear system of Eq. 2-15 by incorporating additional penalty terms. This is called regularization.²² Two common approaches are to include a model norm constraint and a model roughness constraint. The norm constraint (2nd term in Eq. 2-18 below) ensures that our final model is not significantly different from our initial model. This makes physical sense because typically our initial model already incorporates sufficient geologic and other prior information. The roughness constraint (3rd term in Eq. 2-18 below) accounts for the fact that production data is an integrated response and is best suited to resolve large-scale trends rather than small-scale fluctuations.

The penalized objective function is now given by

$$\|\boldsymbol{\varepsilon} - \mathbf{G}\boldsymbol{\delta\mathbf{m}}\|^2 + \gamma_1^2\|\boldsymbol{\delta\mathbf{m}}\|^2 + \gamma_2^2\|\mathbf{L}\boldsymbol{\delta\mathbf{m}}\|^2 \quad (2-18)$$

The minimization of Eq. 2-18 is equivalent to solving the following augmented linear system in a least square sense,

$$\min_{\boldsymbol{\delta\mathbf{m}}} \left\| \begin{bmatrix} \mathbf{G} \\ \gamma_1 \mathbf{I} \\ \gamma_2 \mathbf{L} \end{bmatrix} \boldsymbol{\delta\mathbf{m}} - \begin{bmatrix} \boldsymbol{\varepsilon} \\ \mathbf{0} \\ \mathbf{0} \end{bmatrix} \right\|^2 \quad (2-19)$$

where γ 's are the weighting factors, \mathbf{I} is an identity matrix and \mathbf{L} is a spatial difference operator, for example the second spatial derivative of parameters measuring the model roughness. An efficient iterative linear system solver, LSQR^{23,24} is used for solving this augmented linear system of equations.

2.6 Optimization with LSQR

For large and sparse matrix systems, conjugate gradient type solvers have been popular for discrete inverse problems in the earth science literature.²³⁻²⁵ The mathematically equivalent algorithm LSQR is based on the Lanczos bidiagonalization process and is particularly well-suited for highly ill-conditioned matrices.²¹ The method seeks for the minimum over a Krylov subspace spanned by a sequence of orthonormal basis vectors that are generated from the Lanczos bidiagonalization.

The computational efficiency of the LSQR lies on the Lanczos process. In general, our linear system contains a large sparse and ill-conditioned matrix \mathbf{A} . Thus, the first few large singular values of \mathbf{A} play important roles in the solution of the linear system. The Lanczos process generates a sequence of bidiagonal matrices \mathbf{B}_k with the property that the large singular values of \mathbf{B}_k tend to be progressively better approximations to those of \mathbf{A} . Thus, with fewer iterations than the rank(\mathbf{A}), we obtain reasonable approximations to the large singular values, making the LSQR attractive for sparse matrix systems.

2.7 Forward Model

Given a parameter set, forward model predicts the system responses. Unlike inverse modeling, forward modeling can be stable one-to-one mapping due to the well-determined nature. In this

dissertation, an efficient three-dimensional streamline simulator is used for forward modeling. Fundamentals of streamline simulation are discussed in great detail later in this chapter.

2.8 Illustrative Example of Production Data Integration

In this section, we will illustrate the procedure for dynamic data integration for reservoir parameter estimation using synthetic examples that involve integration of tracer response as well as two-phase production history.

Our synthetic model is a single layer, heterogeneous permeability field with a mesh size of 21x21. The well locations before and after infill are shown in **Fig. 2.1**. The reference permeability field is shown in **Fig. 2.2**. The overall structure consists of a high permeability trend extending in a northeastern direction. The tracer responses from the eight producing wells in the 9-spot pattern are shown in **Fig. 2.3**. The tracer response exhibits multiple peaks indicating the complex nature of the heterogeneity pattern. Also, superimposed on Fig. 2.3 are the tracer responses corresponding to the initial model, a homogeneous permeability field conditioned at the wells.

As discussed in the previous section, dynamic data integration involves two step process – namely travel time match and amplitude match. In matching the arrival time or breakthrough time, we ‘line-up’ the observed and computed production responses at all the wells by minimizing the misfit between the observed and calculated peak concentration time. This is illustrated in **Fig. 2.4**. We observe that the peak arrival times for all the wells are now in agreement, although the magnitudes of the concentration response differ substantially. This arrival time match constitutes by far the most critical aspect of the inversion. In fact most of the dominant features of the permeability field becomes apparent at this stage. Also, we accomplish the largest reduction in overall misfit. Another important benefit of the travelttime matching is that it prevents the solution from being trapped by secondary peaks in multi-peaked production responses that are commonly associated with field data. This is related to the quasi-linear characteristic of the travelttime inversion approach. The permeability field derived after travel time match is shown in **Fig. 2.5**. It is evident that most of the dominant features become apparent after matching the peak arrival times. The arrival time matching is followed by amplitude matching. In this stage, we minimize the misfit between the magnitudes of the observed and computed production response at all times. **Fig. 2.6** shows the tracer response compared to the responses obtained from the reference permeability field. As we can see, the

peak tracer concentrations and locations are resolved at this stage. The amplitude matching further improves the permeability field by incorporating small-scale variations as shown in **Fig. 2.7**. **Fig. 2.7** also shows the comparison of the final (i.e. after amplitude match) permeability field with the reference permeability field. **Fig. 2.8** shows the overall misfit reduction as a function of number of iterations. The first 10 iterations consist of arrival time matching. The importance of arrival time matching is evident from the fact that about 70% of the misfit reduction is accomplished at this stage.

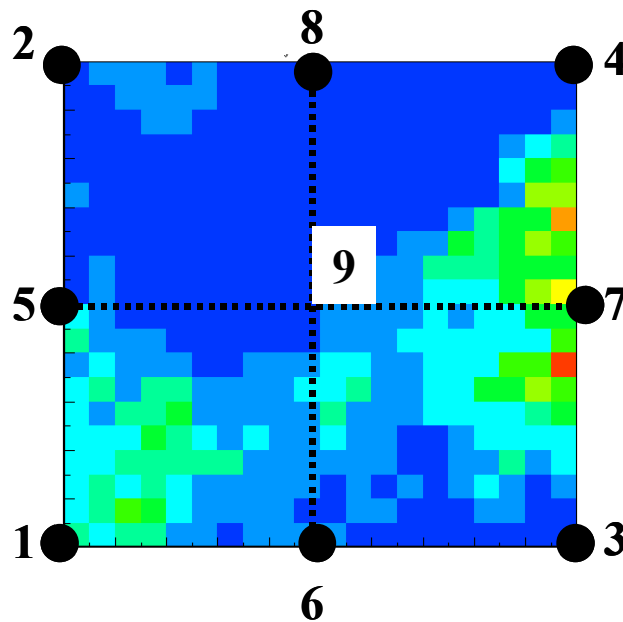


Figure 2.1 – Well Locations for the Synthetic Example. Well 5,6,7, and 8 are Infill Wells. Well 9 is Injection Well.

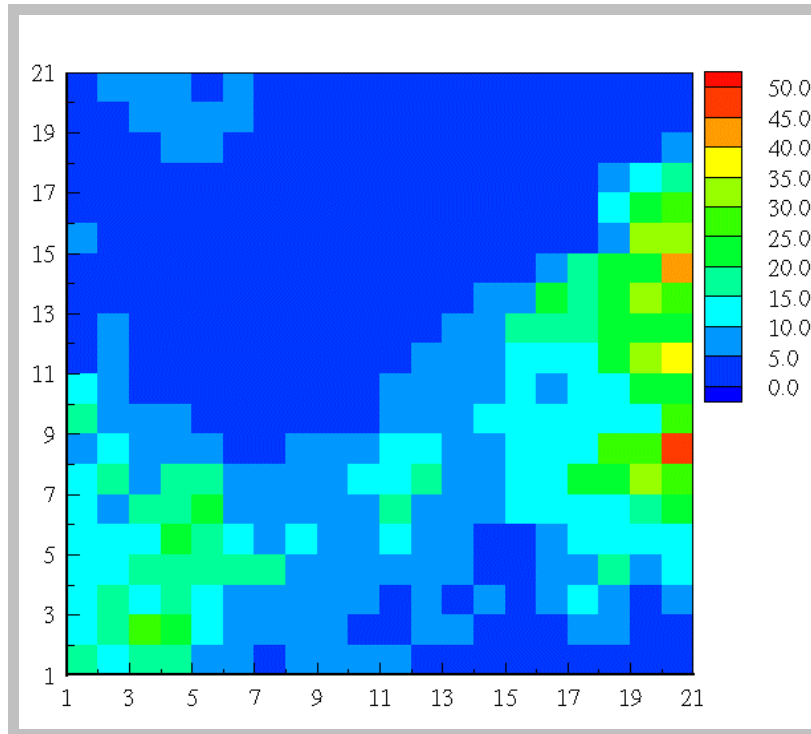


Figure 2.2 – Reference Permeability Model for Synthetic Example.

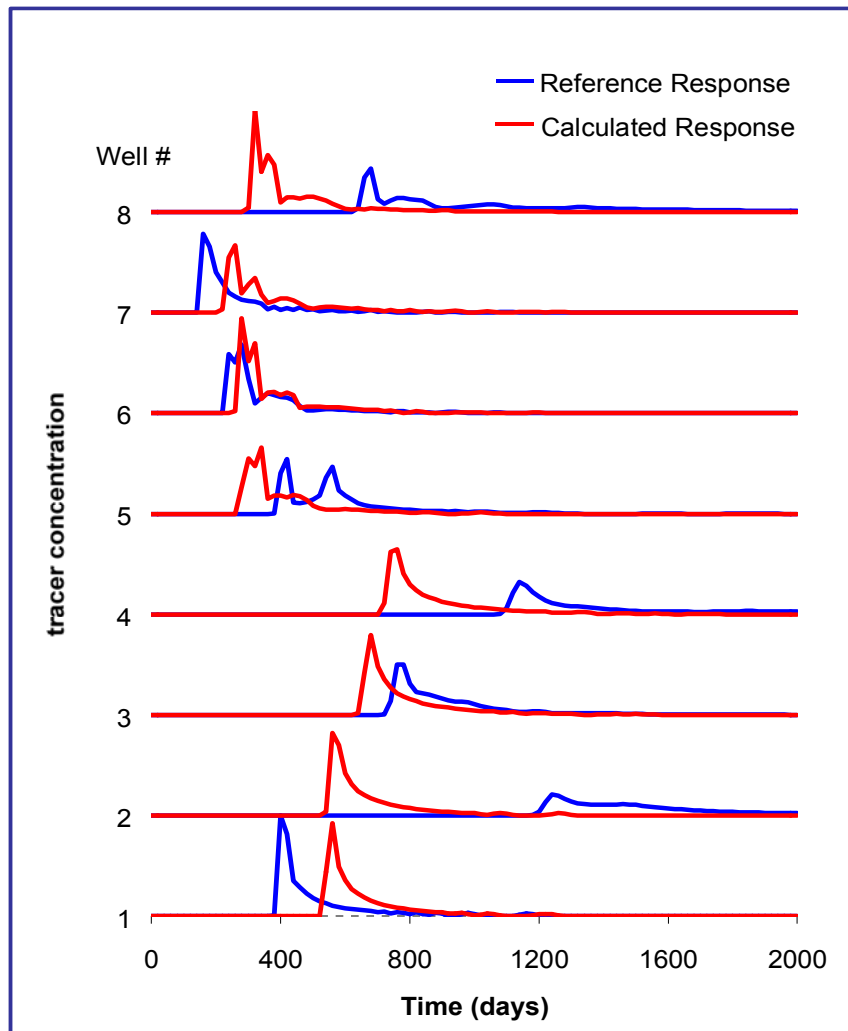


Figure 2.3 – Tracer Response from Reference and Initial Model.

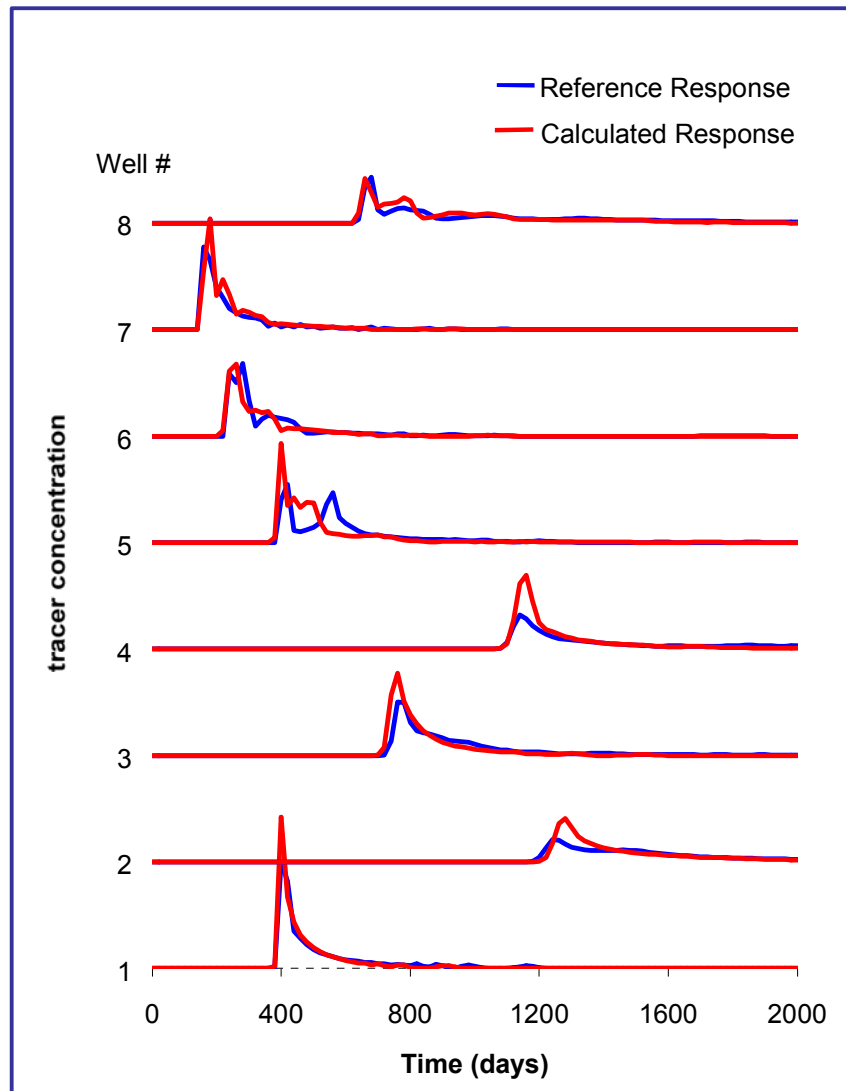


Figure 2.4 – Tracer Response after Arrival Time Match.

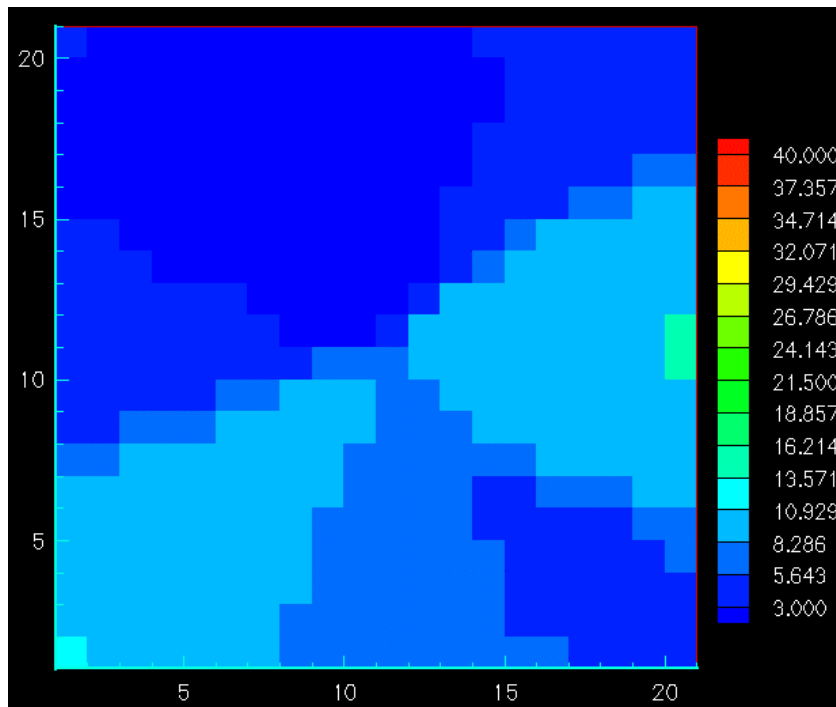


Figure 2.5 – Permeability Field after Arrival Time Match.

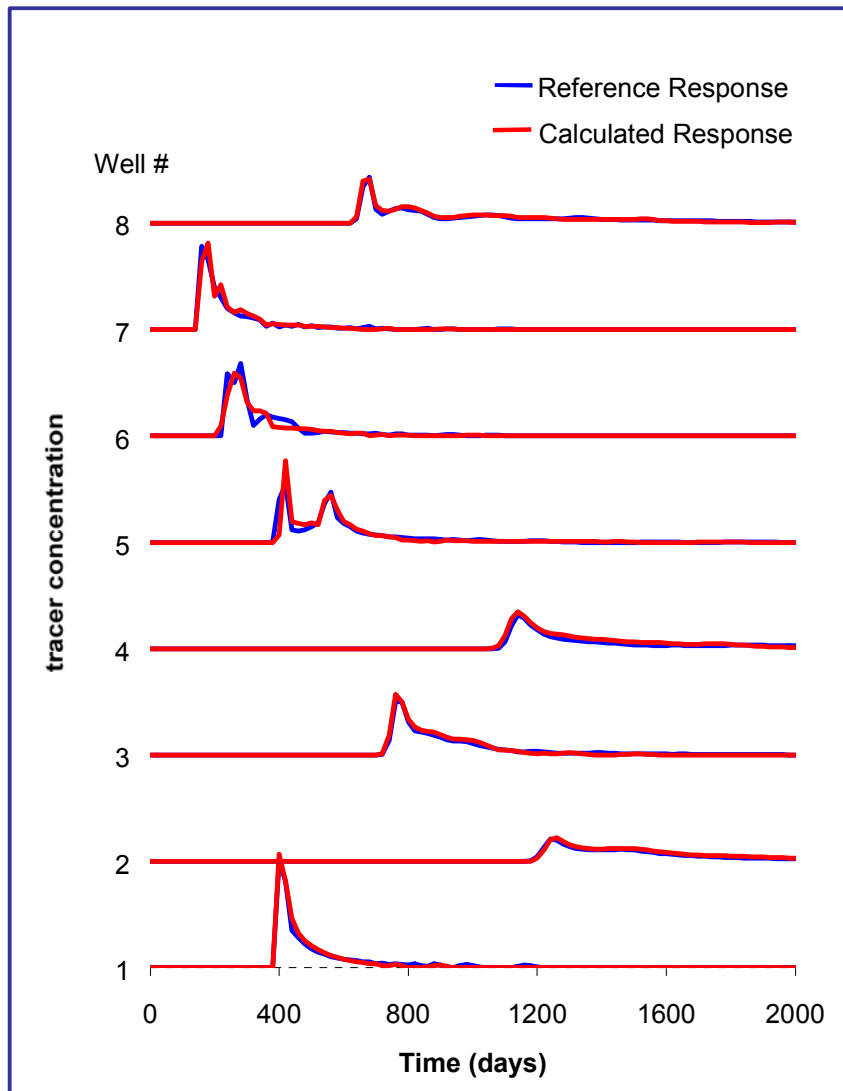
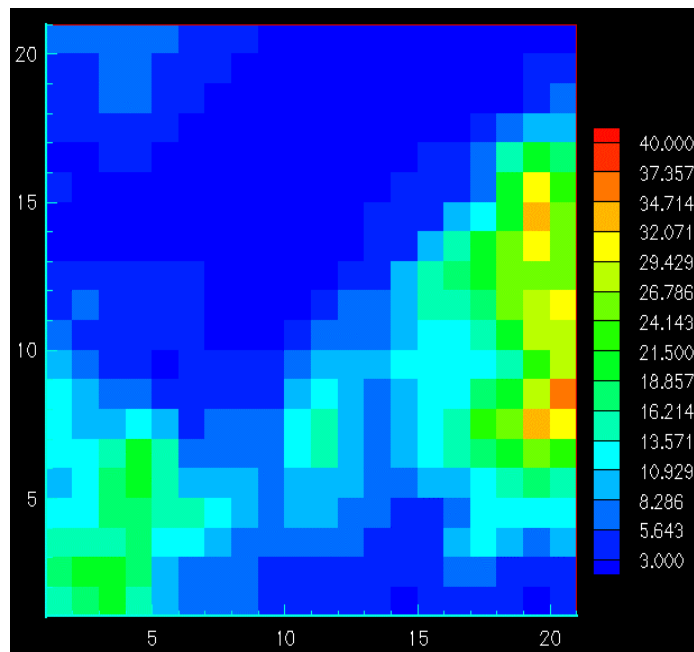
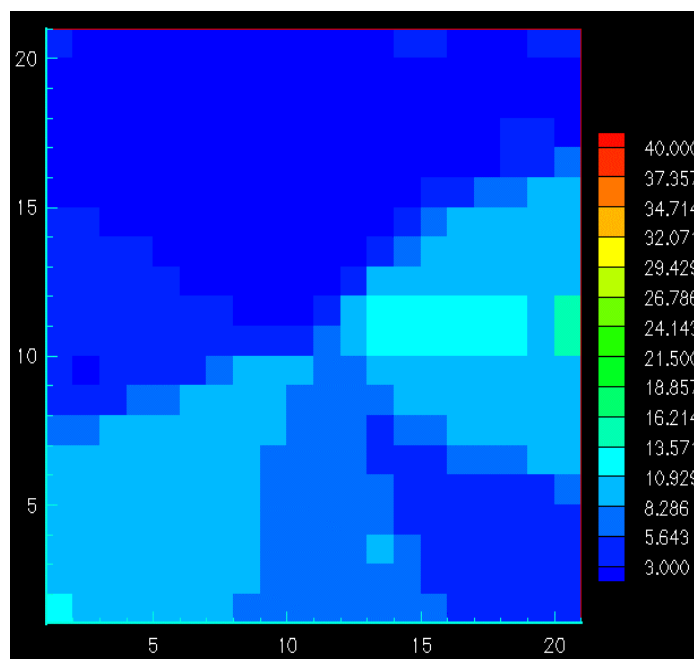


Figure 2.6 – Tracer Response after Amplitude Match.



(a) Reference



(b) Estimated

Figure 2.7 – Comparison of Permeability Fields after Amplitude Match. (a) Reference, (b) Estimated.

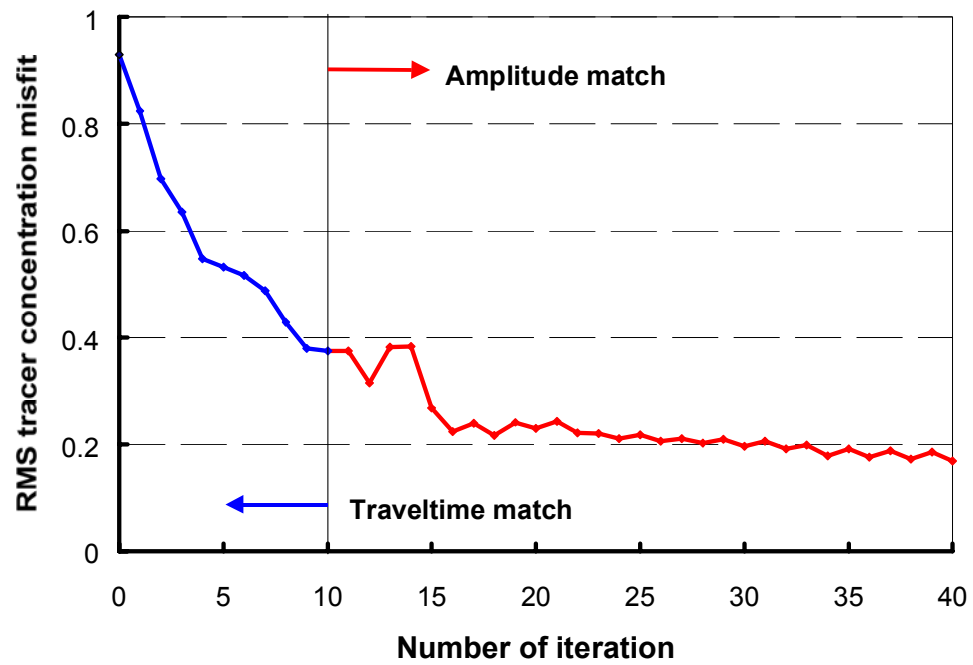


Figure 2.8 - Root Mean Squared Error of Tracer Concentration Misfit as a Function of Number of Iterations.

2.9 Streamline Simulation Fundamentals

Due to the recent advances in geostatistics, fine scale reservoir description has become a current trend. However, fine scale conventional flow simulation is still limited because of high computational costs. Streamline simulation can be the viable alternative in this regard. Its high speed performance is well suited for integrated reservoir descriptions, specifically, production data (dynamic data) integration, ranking of multiple geostatistical reservoir models,²⁶ or mitigation of upscaling problems like pseudo function usage or grid orientation problems.¹⁰ Streamline simulator can be characterized by its high simulation speed (can be orders of magnitude faster than conventional finite difference type simulators) and numerical dispersion free results. Conceptually, streamline simulation is IMPES type simulation: Solving for pressure first and then saturation and occasional updating of pressure field. Its difference from a conventional numerical type simulation lies on the way fluid transport is modeled. Streamline method decouples the transport from the physical underlying grid on which pressure field is obtained. Saturation is moved along streamlines characterized by time of flight coordinate. Due to the decoupling and infrequent pressure updating, streamline method can have large time stepping for saturation computation without suffering from numerical instability or dispersion and consequently have a superior simulation speed. A recent study demonstrates how time steps could be selected for saturation calculations.²⁷

The governing equation for fluid flow in porous media is based on the fundamental laws of physics. Conventional reservoir simulators solve the governing differential equation that is based on the following three equations:

1. Continuity Equation (Conservation of Mass),
2. Darcy Equation: empirical solution of Equation of Motion (Conservation of Momentum), and
3. Equation of State.

Streamline simulators share the same basis. The basic steps for streamline simulation can be summarized as below:

- **Step 1: Solving for Pressure**

Given petrophysical properties and boundary conditions, pressure field is computed on physical grid like the way the finite difference simulator does.

- **Step 2: Streamline Tracing and Time of Flight Computation**

Based on the pressure field, velocity field is generated and streamline is traced. Then particle traveltime along streamline is computed.

- **Step 3: Saturation Advancing Along Streamlines**

Using coordinate transformation, 3D spatial coordinate is transformed into 1D traveltime coordinate along streamline. Then fluid saturation is advanced along the streamlines by solving the 1D saturation equation analytically or numerically. Finally the saturation along streamlines are mapped onto the underlying grid.

- **Step 4: Pressure Updating**

Occasional pressure updating is necessary to take into account total mobility changes due to saturation changes over times or well condition changes such as rate changes and infill drilling. For this updated pressure field, the streamlines are retraced and saturation remapped onto the new streamlines.

These steps are illustrated in **Fig. 2.9** below. Notice the grouping of streamlines along the high permeability streak and the flow channeling as indicated by the time of flight and saturation contours. In particular, the time of flight formulation offers a natural and quantitative way of flow visualization that can provide a mechanism for dynamic reservoir characterization. Now, let us discuss each step in more detail.

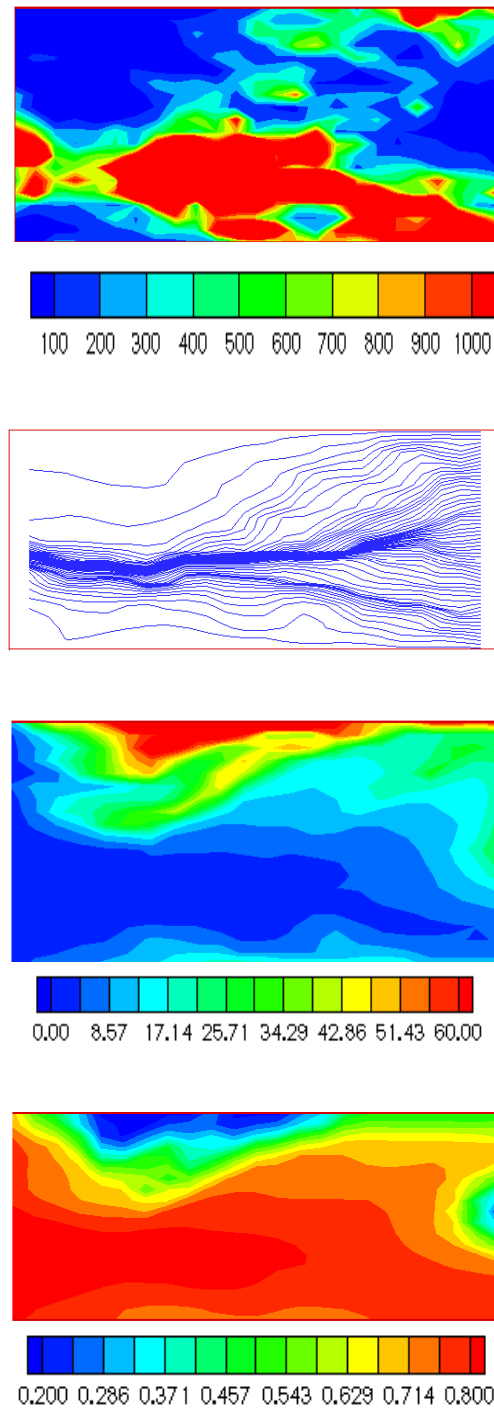


Figure 2.9 – A Stepwise Illustration of Streamline Simulation. An Injector Well is Placed on the Left Side and a Producer on the Opposite Side.

2.9.1 Pressure Solving

For incompressible flow, the continuity equation is given by

$$\nabla \cdot u_t = 0 \quad (2-20)$$

where u_t is the total phase velocity. Applying the Darcy's equation and including gravitational effects and away from source or sink, we can rewrite the Eq. 2-20 in terms of pressure distribution as

$$\nabla \cdot \mathbf{k} (\lambda_{rt} \nabla P + \lambda_{rtg} \nabla D) = 0 \quad (2-21)$$

where \mathbf{k} is the permeability tensor, $\lambda_{rt} = \lambda_{rw} + \lambda_{ro}$ is the total relative mobility for the water-oil system, and $\lambda_{rtg} = (\lambda_{rw} \rho_w + \lambda_{ro} \rho_o) g$. Pressure field over the entire grids can be obtained by solving the above equation with finite difference scheme. Upon obtaining this pressure field, velocity field can be derived by applying Darcy's law on every grid basis.

2.9.2 Streamline Tracing and Time of Flight Computation

By definition, streamlines are tangential to velocity field at a moment and can be represented by

$$\frac{dx_1}{u} = \frac{dx_2}{u} = \frac{dx_3}{u} = \frac{d\tau}{\phi} \quad (2-22)$$

where u is i^{th} component of the Darcy velocity, ϕ is porosity, and τ is the time of flight, or actual transit time of particle. Assuming linear velocity variation within a grid block,⁶ a particle transit time within a grid block, $\Delta\tau$ can be computed by direct integration of the above equation and multiplying porosity.

$$\Delta T_{i2} = \int_{inlet}^{outlet} \frac{dx_1}{u_t} = \frac{1}{a_i} \ln \left[\frac{u_{i2}}{u_{i1}} \right] \quad (2-23)$$

$$\Delta \tau_{i2} = \phi \Delta T_{i2}$$

where a_i is i^{th} component linear velocity gradient across the grid block, u_{i1} is the inlet i^{th} component velocity, and u_{i2} is outlet i^{th} component velocity. Since the particle must exit through

one of the faces, the actual transit time of the particle is given by the minimum time. Then the outlet (or exit) location of the streamline within the grid block can be given by

$$x_i = \frac{1}{a_i} [u_{i1} \exp(a_i \Delta T) - u_{i0}] \quad (2-24)$$

where u_{i0} is the i^{th} component velocity at grid origin (or center of the grid block), and ΔT is the minimum time in the grid block. Thus streamline locus can be obtained by backtracking the particle movement from the point of interest to an injector. The time of flight τ can be obtained by integrating individual transit time $\Delta \tau$ along a streamline ψ .

2.9.3 Saturation Advancing Along Streamlines

For 3D flow, the streamfunctions are related to velocity by

$$u = \nabla \psi \times \nabla \chi \quad (2-25)$$

where ψ and χ are stream functions of three-dimensional flow. Now we are to consider saturation movement along the streamlines. This can be achieved by the coordinate transformation from actual grid coordinates (x, y, z) to streamline coordinates (τ, ψ, χ) .

From the elementary calculus, transformation of gradient operator to (τ, ψ, χ) coordinate can be given by

$$\nabla = \nabla \tau \frac{\partial}{\partial \tau} + \nabla \psi \frac{\partial}{\partial \psi} + \nabla \chi \frac{\partial}{\partial \chi} \quad (2-26)$$

where ∇ is evaluated in (x, y, z) coordinate system. Time of flight is defined as

$$\tau(x, y, z) = \int_0^{(x, y, z)} \frac{\phi}{\|u\|} dr \quad (2-27)$$

Eq. 2-29 can be written as follows

$$u \cdot \nabla \tau = \phi \quad (2-28)$$

Combining Eq. 2-26 and 2-28 and the orthogonality condition between gradient of stream function and velocity, we can simplify the coordinate transformation as

$$\begin{aligned}
u \cdot \nabla &= u \cdot \nabla \tau \frac{\partial}{\partial \tau} + u \cdot \nabla \psi \frac{\partial}{\partial \psi} + u \cdot \nabla \chi \frac{\partial}{\partial \chi} \\
&= \phi \frac{\partial}{\partial \tau}
\end{aligned} \tag{2-29}$$

From the material balance, the flow of water phase away from source and sink can be expressed by

$$\phi \frac{\partial S_w}{\partial t} + u \cdot \nabla f_w = 0 \tag{2-30}$$

After the coordinate transformation, the above three-dimensional differential equation is reduced to series of one-dimensional ones along the streamlines in the time of flight coordinate.

$$\frac{\partial S_w}{\partial t} + \frac{\partial f_w}{\partial \tau} = 0 \tag{2-31}$$

This can be solved for saturation explicitly in time by either using single point upstream or TVD (Total Variation Diminishing) numerical scheme. The corresponding single point upstream solution is

$$(S_w)_i^{n+1} = (S_w)_i^n - \frac{\Delta t}{\Delta \tau} \left((f_w)_i^n - (f_w)_{i-1}^n \right) \tag{2-32}$$

where n is time index and i denotes streamline node. If uniform initial saturation assumption is applicable, Buckley-Leverett type analytical solution can be used to estimate water flood performance. The corresponding analytical solution is

$$\frac{\tau}{t} = \frac{\partial f_w}{\partial S_w} \tag{2-33}$$

The self-similarity of the solution along streamlines allows us to compute the solution only once and map it directly to the time of interest.

Another important aspect of the coordinate transformation is that the coordinate transformation preserves pore volume.

$$\frac{\partial(\tau, \psi, \chi)}{\partial(x, y, z)} = u \cdot \nabla \tau = \phi, \text{ i.e.} \tag{2-34}$$

$$d\tau \, d\psi \, d\chi = \phi \, dx \, dy \, dz.$$

In order to include the gravity effect, the flow of water phase away from source can be expressed by,

$$\phi \frac{\partial S_w}{\partial t} + u_t \cdot \nabla f_w - \nabla \cdot \left(k \frac{\lambda_{rw} \lambda_{ro}}{\lambda_{rt}} \Delta \rho g \nabla D \right) = 0 \quad (2-35)$$

Using operator splitting, Eq. 2-35 can be split into two parts: a convective step and a gravity step. First, after the coordinate transformation from the physical space to the time of flight coordinates, the convective term of Eq 2-35 is reduced to series of one-dimensional ones along the streamlines in the time of flight coordinate.

$$\frac{\partial S_w}{\partial t} + \frac{\partial f_w}{\partial \tau} = 0 \quad (2-36)$$

Then fluid saturation is advanced along the streamlines by solving the 1D saturation equation analytically or numerically. After that, a gravity step is taken along gravity lines and saturation are updated using

$$\phi \frac{\partial S_w}{\partial t} - \frac{\partial}{\partial z} \left(k_z \frac{\lambda_{rw} \lambda_{ro}}{\lambda_{rt}} \Delta \rho g \right) = 0 \quad (2-37)$$

2.9.4 Pressure Updating

We can often encounter such cases that the stationary streamline assumption is violated. In the cases of changing well conditions or more drastically, infill drilling cases, regeneration of streamline trajectories by updating pressure field is necessary to account for new well conditions. Even if constant well conditions are assumed, occasional pressure updates might be necessary to take into account of the total mobility changes due to the saturation variation over the flooding period.

After first pressure updating, the Buckley-Leverett analytical solution cannot be used to the one-dimensional hyperbolic equation of Eq. 2-31. That is because the uniform initial condition is no longer valid due to the saturation movement in earlier step. It should be noted that, however, Thiele²⁸ showed the usage of analytical solutions could be tolerable, as long as constant well conditions are met.

2.10 Incorporating Effect of Compressibility and Aquifer Influx

The existing streamline simulator was modified to handle the total compressibility in terms of fluid and rock compressibilities, and associated change in porosity as a result of variation in magnitude of pressure. In the presence of compressibility, the generation of streamlines will still be a rigorous exercise which will involve the determination of number and trajectory of streamlines based on velocity field obtained after obtaining the pressure solution.²⁹

Additionally, the simulator is enhanced to incorporate the effect of influx from surrounding or bottom aquifer. The effect of aquifer plays a significant role in the history matching process for large water drive reservoirs. However, incorporating its effect in terms of additional grid blocks representing the aquifer is expensive in terms of computing time and efficiency. To replicate the effect of influx from the aquifer, the concept of pore volume multipliers has been implemented. This requires to modify the origin and termination criteria for streamlines so that streamlines can start and end in aquifer. This implementation also enables the field applications to be modeled in a more efficient and faster way.

2.11 Implementing Horizontal Well

An algorithm to handle the production from horizontal wells has been implemented. A horizontal well is treated as a rectangular pipe with interconnected blocks in either in x or y direction depending on the direction of the well. Also, special care has been taken to ensure that interconnected faces of the horizontal well are not active for launching streamlines. Productivity index for the horizontal well is calculated using the equivalent well block radius proposed by Peaceman,³⁰ (as given below). More detail of horizontal well is presented in Appendix B.

In x - direction:

$$r_o = 0.28 \frac{\left(\left[\frac{K_y}{K_z} \right]^{0.5} \Delta z^2 + \left[\frac{K_z}{K_y} \right]^{0.5} \Delta y^2 \right)^{0.5}}{\left[\frac{K_y}{K_z} \right]^{0.25} + \left[\frac{K_z}{K_y} \right]^{0.25}} \quad (2-38)$$

In y - direction:

$$r_o = 0.28 \frac{\left(\left[\frac{K_x}{K_z} \right]^{0.5} \Delta z^2 + \left[\frac{K_z}{K_x} \right]^{0.5} \Delta x^2 \right)^{0.5}}{\left[\frac{K_x}{K_z} \right]^{0.25} + \left[\frac{K_z}{K_x} \right]^{0.25}} \quad (2-39)$$

2.12 Chapter Summary

In this Chapter, we have reviewed the fundamentals of production data integration with emphasis on the details of the theoretical background of the forward model. The discussion showed that production data integration technique is essentially an ill-posed inverse problem involving minimization of a penalized objective function which uses streamline simulator as a fast forward model. We have also discussed additional enhancements of the existing streamline simulator for practical field application.

CHAPTER III

PRODUCTION DATA INTEGRATION : A LARGE SCALE FIELD

EXAMPLE

3.1 Introduction

Recent developments in reservoir characterization and in the management of uncertainty have lead to the ability of the petroleum industry to routinely generate large multimillion-cell detailed geologic models. Reconciling such high-resolution models to dynamic reservoir behavior (transient pressure and tracer response, multiphase production history) is essential to develop a reliable reservoir model for performance forecasting. However, dynamic data integration still remains an outstanding challenge because of the high man- power costs, subjectivity and non uniqueness associated with conventional history matching approach. Streamline methods have shown significant potential in this regard. Streamline methods can be advantageous in two specific ways. First, streamline models can be significantly faster than conventional finite-difference simulators. Second, the sensitivities of the production response with respect to reservoir parameters can be computed very efficiently using a single simulation. Such sensitivities quantify changes in the production response because of small perturbation in reservoir properties such as porosity, permeability and relative permeability parameters. These sensitivities form a critical component of any dynamic data integration process

The principle objective of this work has been to demonstrate the feasibility of streamline-based dynamic data integration techniques under realistic field conditions relevant to middle eastern oil fields. Specifically, we want to develop a geologic model for a giant middle eastern field that is conditioned with respect to water-cut responses at the wells. The conditioning process is to account for all major well events such as rate changes, infill drilling, zone isolation and pattern conversions etc. in addition to dominant physical mechanisms such as gravity and aquifer influx. The work involved substantial enhancement of the existing streamline-based production data integration techniques.

We successfully applied the streamline-based production data integration method to the giant middle eastern field. The geologic model studied to integrate production data included 48 wells showing water-cut response out of a total of 70 producers. The production history included a period of 30 years. During streamline simulation, we used 34 pressure updates to consider the detailed rate schedule to account for infill drilling, reperforations and significant

rate changes. Gravity effects have also been included in the modeling and had a significant impact on the results, especially water-cut matches. Also streamline flow simulation incorporated fluid compressibility and aquifer influx to obtain pressure history consistent with the field observations. For aquifer influx, we used pore volume multiplier in aquifer regions to obtain reasonable overall field pressure and fluid flow rates.

A two-step approach that utilizes an upscaled model for production data integration and then propagates changes to the fine scale model through downscaling was developed. The two-step approach appears to be robust, computationally efficient (about 6 hrs in a PC) and results in significant improvement in the production history match. Almost all (about 90%) of the wells showed improvement in the breakthrough time matches. About 70% of the wells exhibited good to moderate matches in the overall production history. A comparison of the saturation distribution derived from streamline simulation with the field surveillance data appear to indicate that the model reproduces the gross fluid movement in the reservoir quite well. The waterfront movement and aquifer encroachment are consistent with field observations. The model indicates water coning and bypassed oil as observed in the field. Also, the unswept areas in the model are consistent with field observations. Finally, an examination of the permeability changes resulting from production data integration appears to indicate that most of the dominant trends are along the 'good' facies. These changes are considered geologically plausible and are consistent with prior observations. The integrated geological model derived after incorporating the water-cut history should significantly reduce the cycle time for full-physics history matching. This is confirmed by preliminary comparison of the streamline simulation results with those from a commercial numerical simulator (ECLIPSE).

It is important to point out that the streamline-based production data integration is not a substitute for conventional finite-difference based simulation and history matching. In fact, it is complementary and should facilitate the history matching process by identifying potential inconsistencies between field production response and the geologic model.

3.2 Objective

Traditional geostatistical models are well-suited to integrate static data such as well log, core and seismic data. However, integration of dynamic data such as pressure and multiphase production response (for example, water-cut data) typically requires the solution of an inverse problem. Such inverse problems are computationally intensive and require many solutions of the flow and transport problem. In particular, for field scale application with high-resolution

geologic models consisting of multimillion cells, dynamic data integration using conventional numerical simulators can become computationally infeasible.

Our goal is to develop a systematic procedure for reconciling high-resolution geologic models to production data such as water-cut and pressure data using streamline models. Such conditioning to dynamic data is expected to improve the reliability in the reservoir performance forecasting and also significantly reduce the cycle time associated with history matching using full-physics finite-difference simulators. Specifically, we want to establish a methodology that is computationally efficient and also can account for realistic field conditions such as gravity effects, compressibility and aquifer influx and changing well events, for examples, infill drilling, zone isolation and rate changes during the course of field production history.

It is important to point out that the streamline-based production data integration is not a substitute for conventional finite-difference based simulation and history matching. In fact, it is complementary and should facilitate the history matching process by identifying potential inconsistencies between field production response and the geologic model.

3.3 Geology and Geologic Model

A limited literature survey was performed to gather as much as possible information and to understand previous studies on the giant middle eastern field. The giant middle eastern field is a large anticline measuring 25 km in length and 15 km in width. It contains extra light crude at an average subsea depth of 8000 ft. The oil accumulation is bounded by oil-water contact in the north and reservoir pinch-out in the south. It was first produced in September of 1970, with a peripheral water flood initiated in January of 1973. Injection wells were drilled close to the trailing edge of the OWC and completed open hole.

The giant middle eastern field is a large heterogeneous carbonate reservoir. The geologic model included a series of lithofacies, porosity, and permeability models. In addition, the following engineering data for the field were delivered:

- monthly well injection data and production data.
- reservoir pressure data, fluid properties.
- J curves and relative permeability curves.
- well completion data and flow meter measurements.

The geologic model provided were constructed using a 250m areal grid size in the horizontal direction. In general, the it consists of two major units:

1. a lower non-reservoir unit of organic rich laminated lime mud stone and low porosity skeletal wackstone and,
2. an upper reservoir unit of grain rich carbonates including skeletal packstone, grainstone and boundstone.

Permeability and porosity models were obtained by facies dependent sequential Gaussian simulation with collocated cokriging using well data and seismic data. The reservoir has 70 producers and 16 injectors. Most injection wells are located peripherally with respect to production wells (**Fig. 3.1**).

3.4 Approach for Data Integration

We attempted two different methods to integrate water cut data into fine scale geologic model for the reservoir. The first method is a two-step approach that utilizes an upscaled model for production data integration and then propagates the changes in permeability to the fine scale model via downscaling. It is computationally efficient because the production data inversion is performed using the upscaled model and thus, requires relatively few unknown parameters. This method takes about 6 hours in a PC. The second method is a single-step approach that performs direct integration of production data into the fine scale model. This is more time consuming and takes about 20 hours in a PC. Although both the methods result in the same general trend in permeability changes, the two-step approach appears to be more stable and is our preferred method in this case.

3.4.1 Two Step Approach

This approach consists of the following major steps:

Step I:

- Upscaling to set up coarse scale model,
- Inversion to generate coarse scale model conditioned to water cut response at wells,

Step II:

- Downscaling to update the fine scale model based on permeability changes in the upscaled model,
- Fine scale simulation with the updated model.

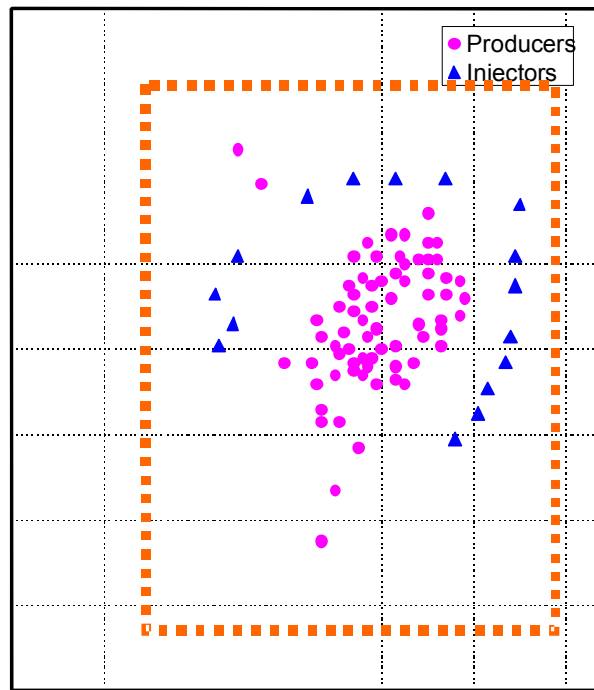
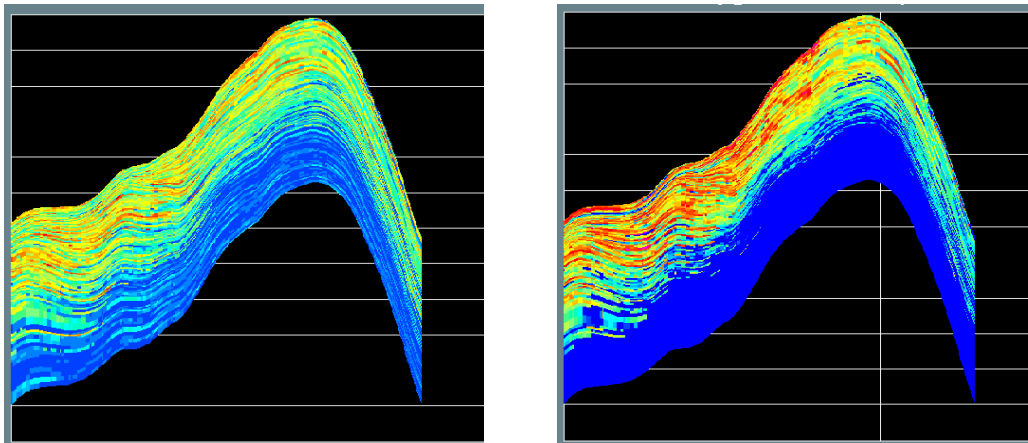


Figure 3.1- Well Location Map of the Giant Middle Eastern Field. The Dotted Line Denotes the Simulation Area.



(a) Porosity

(b) Permeability

Figure 3.2 - Cross Section Map of Porosity and Permeability Model Based on Full Geologic Model (128x160x128). (a) Porosity, (b) Permeability.

3.4.2 Setup of Coarse Scale Model

In coarse scale model, we take into account the following elements:

1. Vertical Upscaling

For the preliminary simulation studies to investigate the flow characteristics in the reservoir (Fig. 3.1), we performed only vertical upscaling of geologic model (128x160x128: 49 zones) into 13 layer model. Upscaled model comprises 13 zones. The areal dimensions of the upscaled model for reservoir simulation were kept the same as the geologic model dimensions (250 meters by 250 meters) to avoid relocation of wells. The vertically upscaled model combines several geologic layers into one simulation layer. Because the lower part of the reservoir consists of tight and non reservoir formation, a relatively large part of the formation was grouped into an upscaled block. **Figs. 3.2** and **3.3** show the detailed geologic model and the corresponding upscaled model.

While porosity is calculated using bulk-volume-weighted arithmetic averaging to preserve the pore volume of the original fine scale model, upscaled permeabilities are determined by the combination of arithmetic and harmonic averaging. To consider the effect of flow direction, arithmetic averaging is used for x-directional upscaled permeability, K_x and harmonic averaging for z-directional upscaled permeability, K_z .

2. Removal of Aquifer Blocks

In upscaled simulation model, we also eliminate the grid blocks in the aquifer region, which helps reducing the number of grid blocks and the computational cost significantly. Note that removal of some of the aquifer blocks resulted in a large reduction in the number of grid blocks from 2.6 million down to 1.0 million without upscaling in vertical direction. Therefore, though above two steps, the resulting simulation model becomes 72x100x13 (93600 cells). In **Fig. 3.1**, the dotted line indicates the simulation model region.

3. Boundary Condition for Aquifer Flux

To consider aquifer flux in the simulation, we tried two approaches: pressure-specified imaginary injection wells and PV multipliers. First, we put imaginary injection wells along the boundary to emulate the aquifer influx in the reservoir. This approach entails specifying pressure constraints at the imaginary injection wells. In practice it is very difficult to obtain proper pressure values at the boundary. On the other hand, to account for the unknown aquifer size, we can use pore volume multiplier in aquifer regions to obtain reasonable overall field

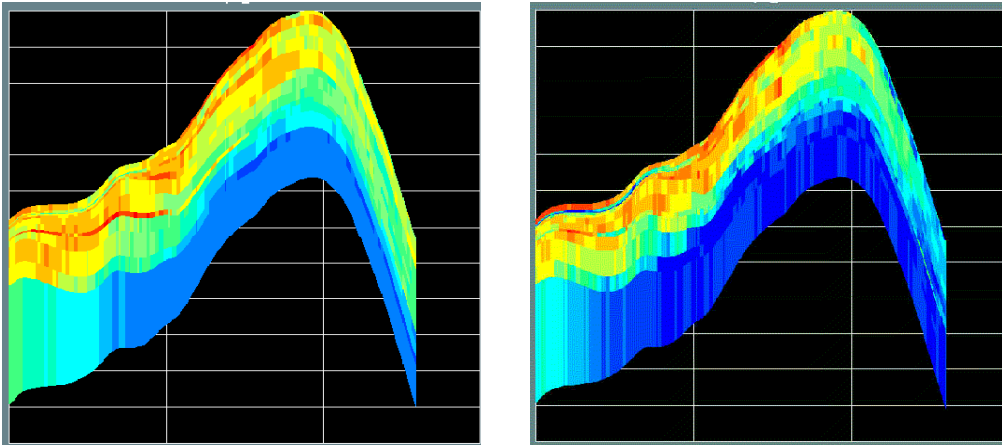


Figure 3.3 - Cross Section Map of Porosity and Permeability Model Based on Upscaled Model (128x160x13) from Geologic Model. On the Left is Porosity, On the Right is Permeability (md).

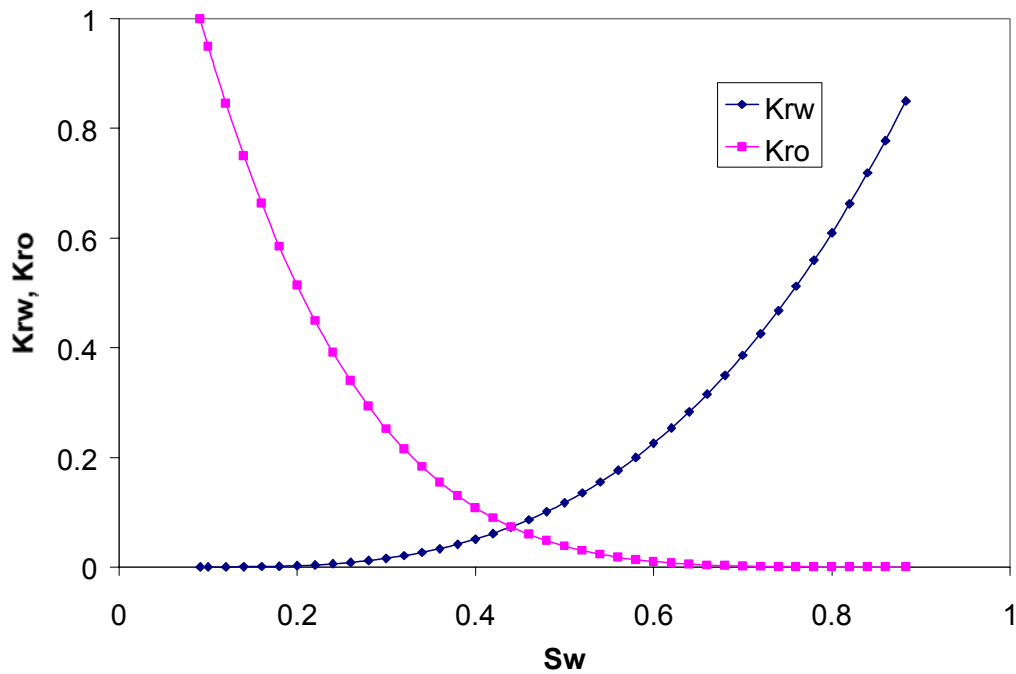


Figure 3.4 - Relative Permeability Curves. $S_{wi} = 0.091$, $S_{or} = 0.12$, $K_{rwendpt} = 0.85$, $n_o = 4.5$, $n_w = 3$.

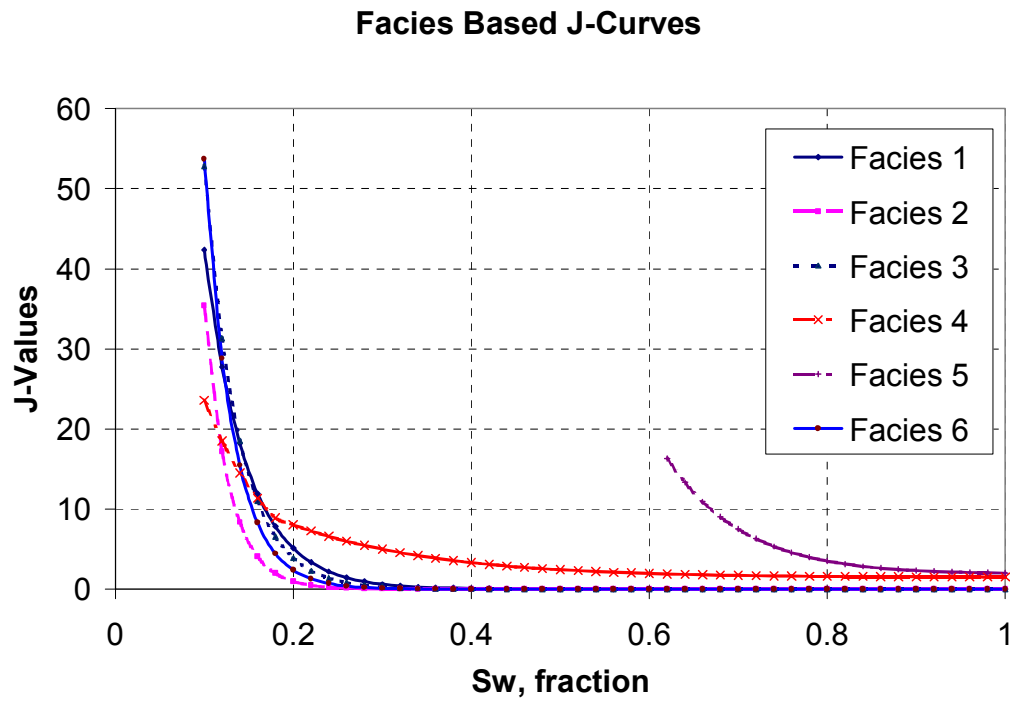


Figure 3.5 - Facies Based J-Curves for Initial Water Saturation Estimation.

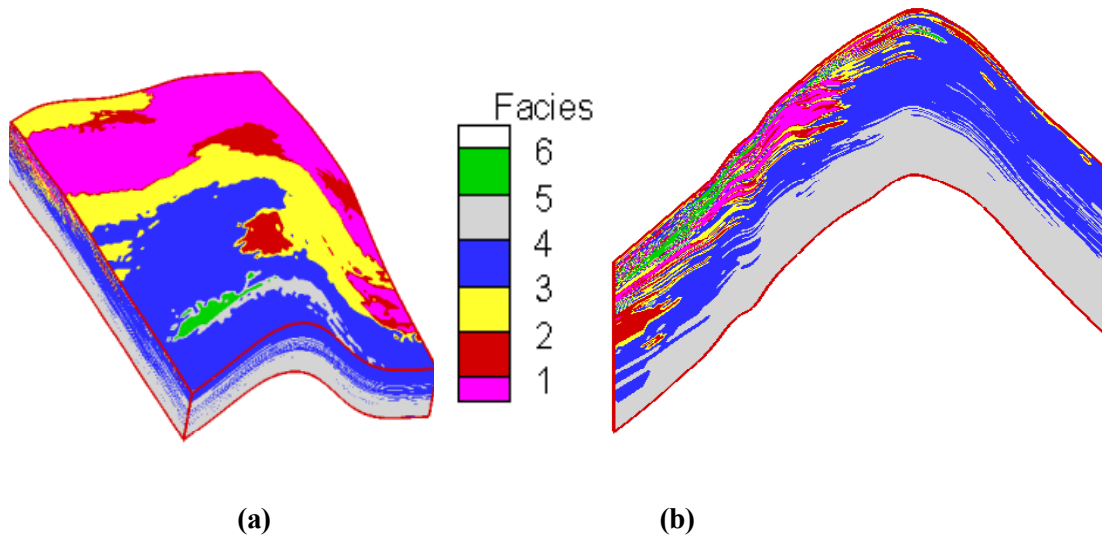


Figure 3.6 - Fieldwide Facies Model and N-S Cross Section of the Facies Model. (a) 3-D View, (b) N-S Cross Section.

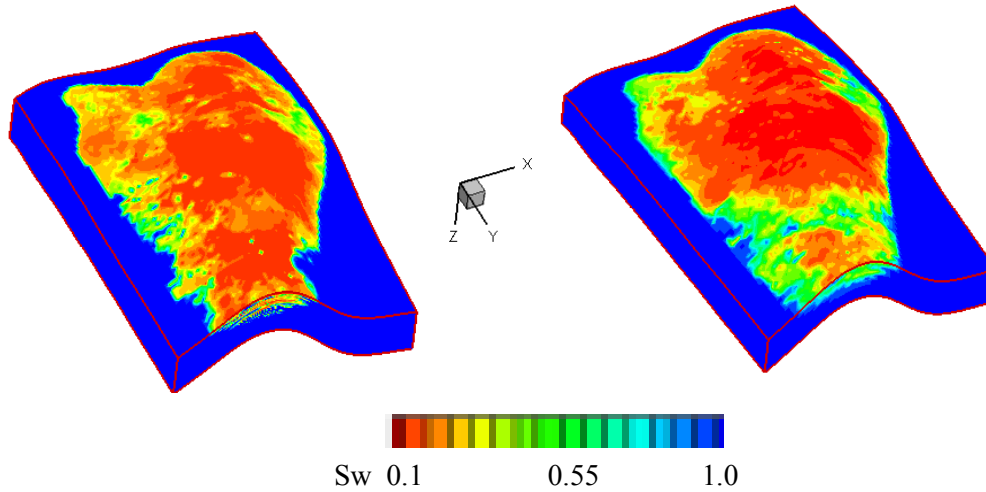


Figure 3.7 - Initial Water Saturation Distribution of Geologic Model. On the Left is Fine Scale Model, On the Right is Upscaled Model.

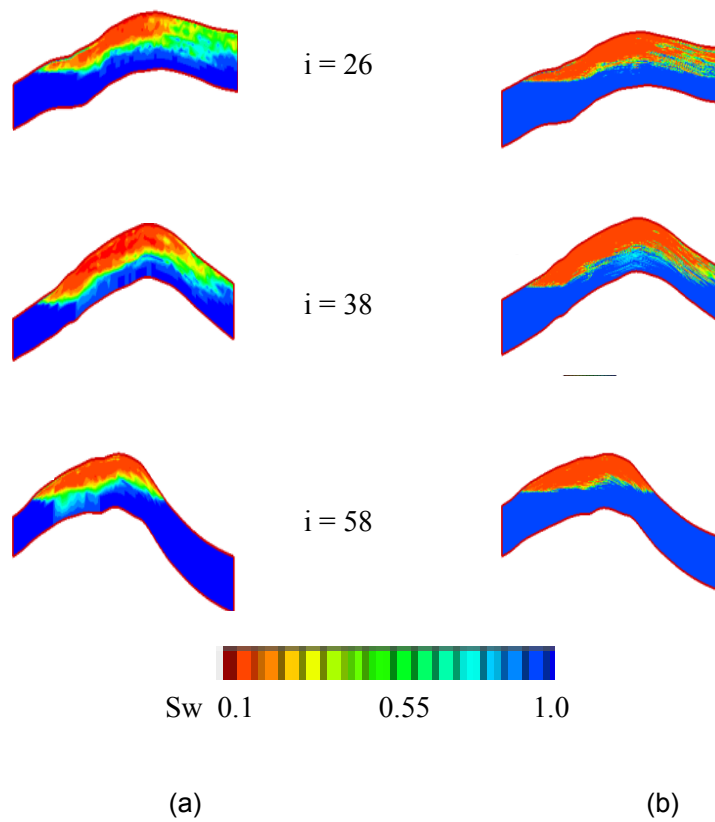


Figure 3.8. - N-S Cross Section of Initial Water Saturation of the Geologic Model. (a) Upscale Model, (b) Fine Scale.

pressure and fluid flow rates. In this study, we used 20 PV multiplier at the edge grid blocks along three sides: North, East, and West.

4. Initial Water Saturation

To preserve the OOIP, water saturation for the upscaled model is calculated using a pore-volume weighted arithmetic averaging of the initial water saturation (Eq. 3.1) in the fine scale geologic model as follows:

$$S_w = \frac{\sum_{i=1}^{nb} S_{wi} PV_i}{\sum_{i=1}^{nb} PV_i}, \quad PV_i = \phi_i V_i \quad (3-1)$$

To initialize water saturation of the fine scale geologic model, we used given relative permeability curves (**Fig. 3.4**), J curves (**Fig. 3.5**) and facies information (**Fig. 3.6**). The procedure for computing the S_{wi} in Eq. 3.1 consists of the following two steps:

- The J-function value was computed from the subsea depth, porosity, and permeability at each cell by the following equation. It was assumed that the capillary pressure at the WOC (8230 subsea depth in the model) was zero.

$$J(S_w) = \frac{0.2166H(\rho_w - \rho_o)}{144\sigma \cos\theta} \sqrt{\frac{k}{\phi}} \quad (3-2)$$

where $\sigma \cos\theta = 18.5$ dynes/cm, $\rho_w = 61.582$ lb/ft³, and $\rho_o = 45.979$ lb/ft³.

- Based on the J vs. S_w curves at each facies, this J-value was then used to determine the initial water saturation at that cell location.

Note that scale geologic model with 6 facies-specific J curves yields 7.93 MMSTBOOIP. **Figs. 3.7** and **3.8** show the initial oil saturation of fine scale model and upscaled model and as expected, they look very similar.

5. Gravity Effect and Compressibility of Fluid

Commonly, streamline model is used for incompressible multiphase flow in porous model. But when the effect of compressibility of fluid is too significant to ignore, we should take into account it during pressure solving. In this study, we have 16.1×10^{-6} psi⁻¹ oil compressibility and 3.3×10^{-6} psi⁻¹ water compressibility at reservoir condition. Also, in gravity dominated

waterflood displacement, it is important to account for multiphase gravity effects in the simulation. The gravity force caused by the density difference of oil and water ($\rho_w = 61.582 \text{ lb/ft}^3$, and $\rho_o = 45.979 \text{ lb/ft}^3$) may affect final saturation distribution and water-cut responses. Thus, in this study, we extend a streamline-based history matching technique to include gravity and compressibility of fluid.

6. Pressure-Update Schedule

Another important factor that affects the computational cost is the number of pressure updates that will be used in simulation process. Therefore, we need to time-average the well rate schedules in order to reduce the number of pressure updates in the simulation without compromising the accuracy of the simulation. Actual well production rates were averaged with the consideration of major events in well flow rate, schedule and completion data. To account for the changing production rates and different starting times of the injection and production wells, 34 pressure updates were defined during 1/1/73 to 4/1/2001. **Fig. 3.9** shows the actual well rates and the averaged production rates for these 34 time periods. Also we performed a sensitivity study on the number of pressure updates. In terms of water cut matches and saturation distribution, a model with 45 pressure updates does not show significant changes.

3.4.3 Results

With coarse scale model, we performed two case studies to investigate the impact of gravity on flow characteristics in the reservoir. In Case 1, we did not consider gravity segregation phenomena during simulation. This case is computationally efficient because of not calculating saturation change due to gravity force. Case 2 involves the gravity effect to account for gravity segregation via operator splitting, which increases computation time requirements.

Case 1: Without Gravity Effect

Fig. 3.10 shows the pressure distribution at three different times. As expected, in the central region of the reservoir where most production wells are located, a significant pressure reduction

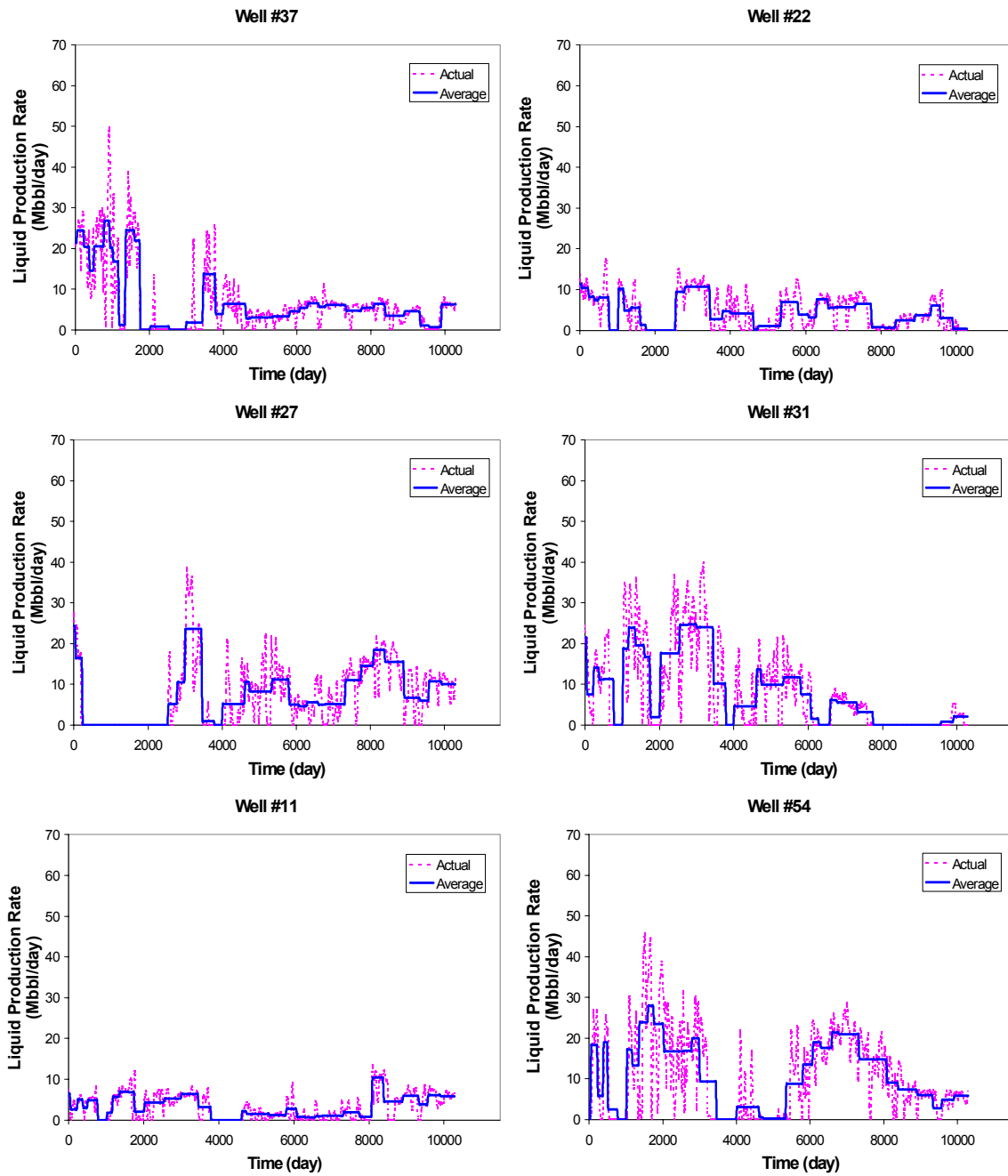
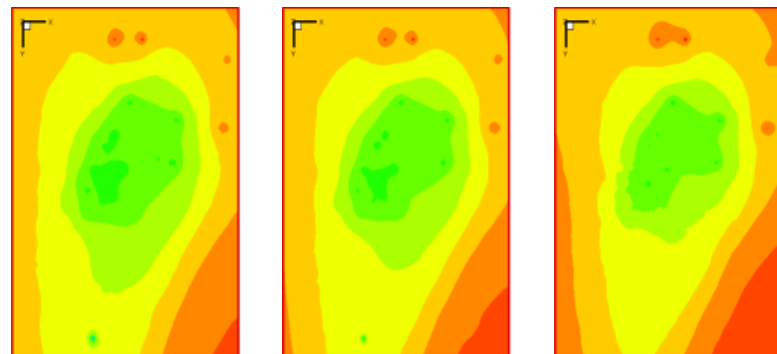
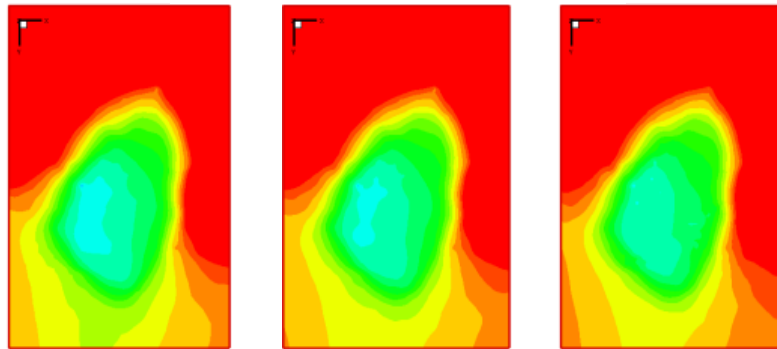


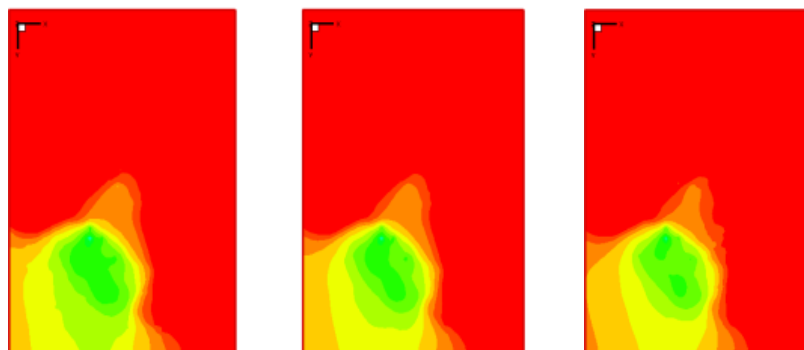
Figure 3.9 - Examples of Actual Flow Rates vs. Averaged Flow Rates Used for Streamline Simulation.



(a) at 60 Days



(b) at 5350 Days



(c) at 10290 Days

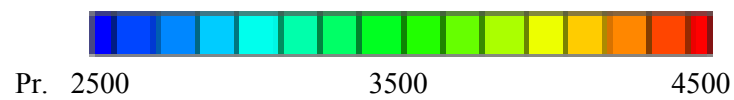


Figure 3.10 - Pressure Distribution at Three Different Times for Layer 1, 4 and 8 without Gravity.

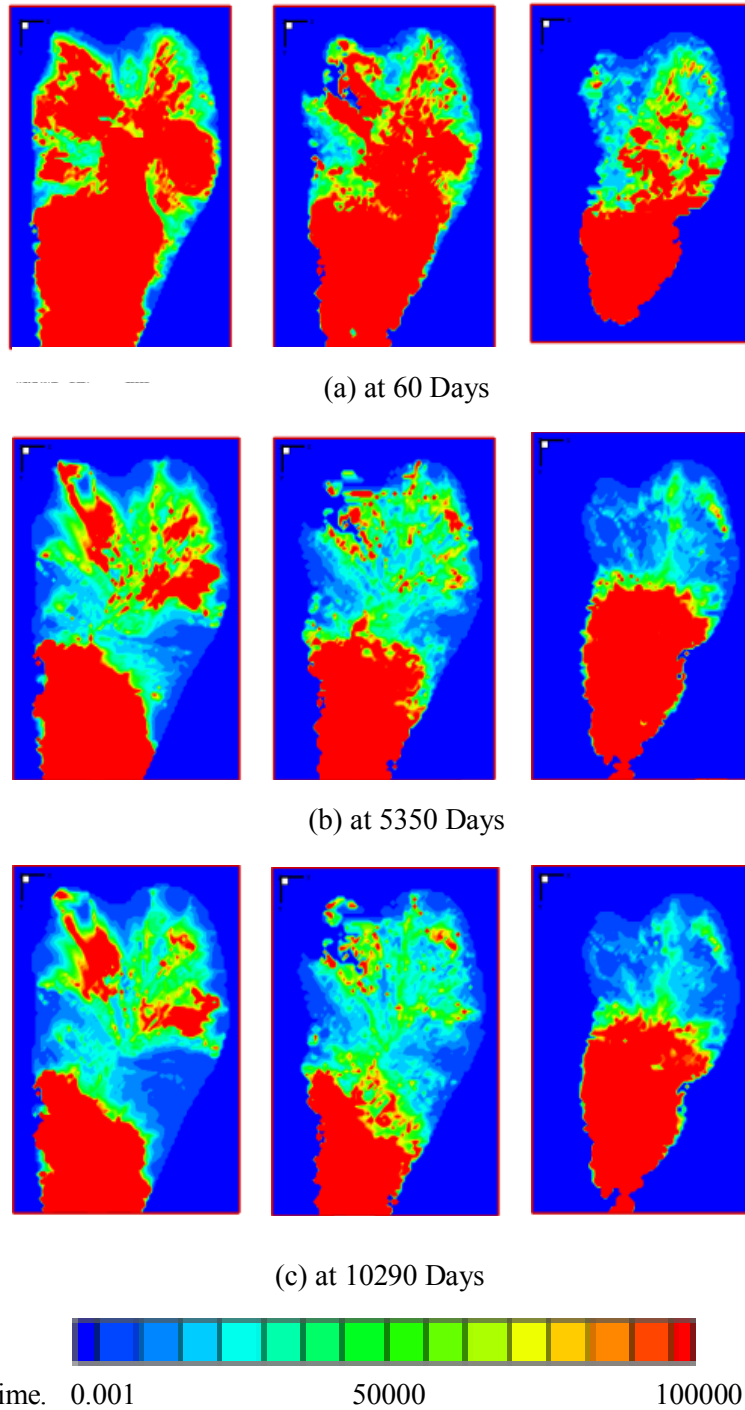


Figure 3.11 - Time of Flight Distribution at Three Different Times for Layer 1, 4 and 8 without Gravity.

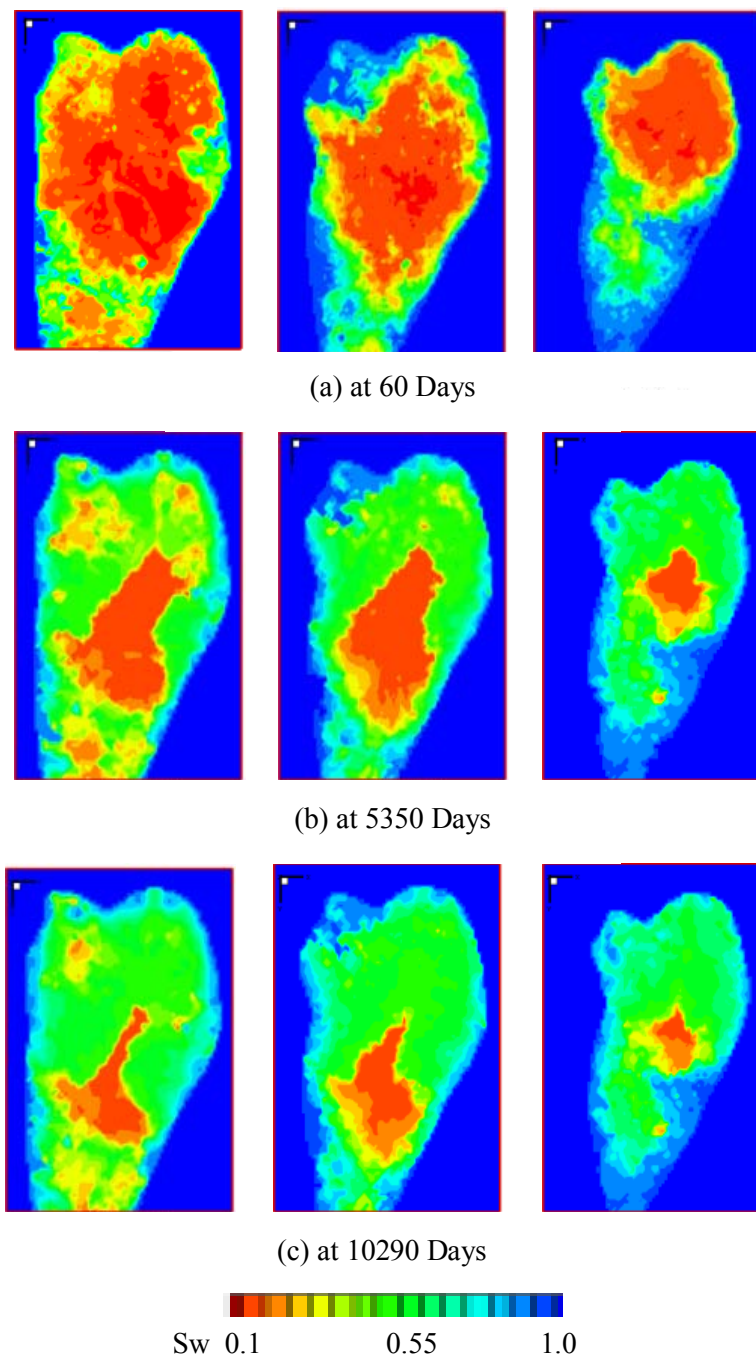


Figure 3.12 - Water Saturation Distribution at Three Different Times for Layer 1, 4 and 8 without Gravity.

Streamlines after 60 Days



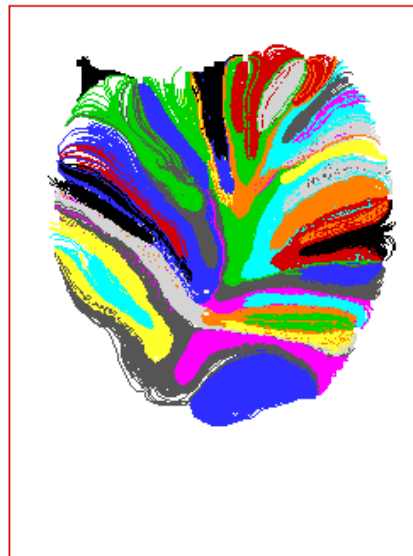
(a)

Streamlines after 5350 Days



(b)

Streamlines after 10290 Days



(c)

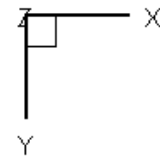


Figure 3.13 - Areal Map of Streamline Distribution at Three Different Times without Gravity. (a) Initial at 60 Days, (b) Middle at 5350 Days, (c) End at 10290 Days.

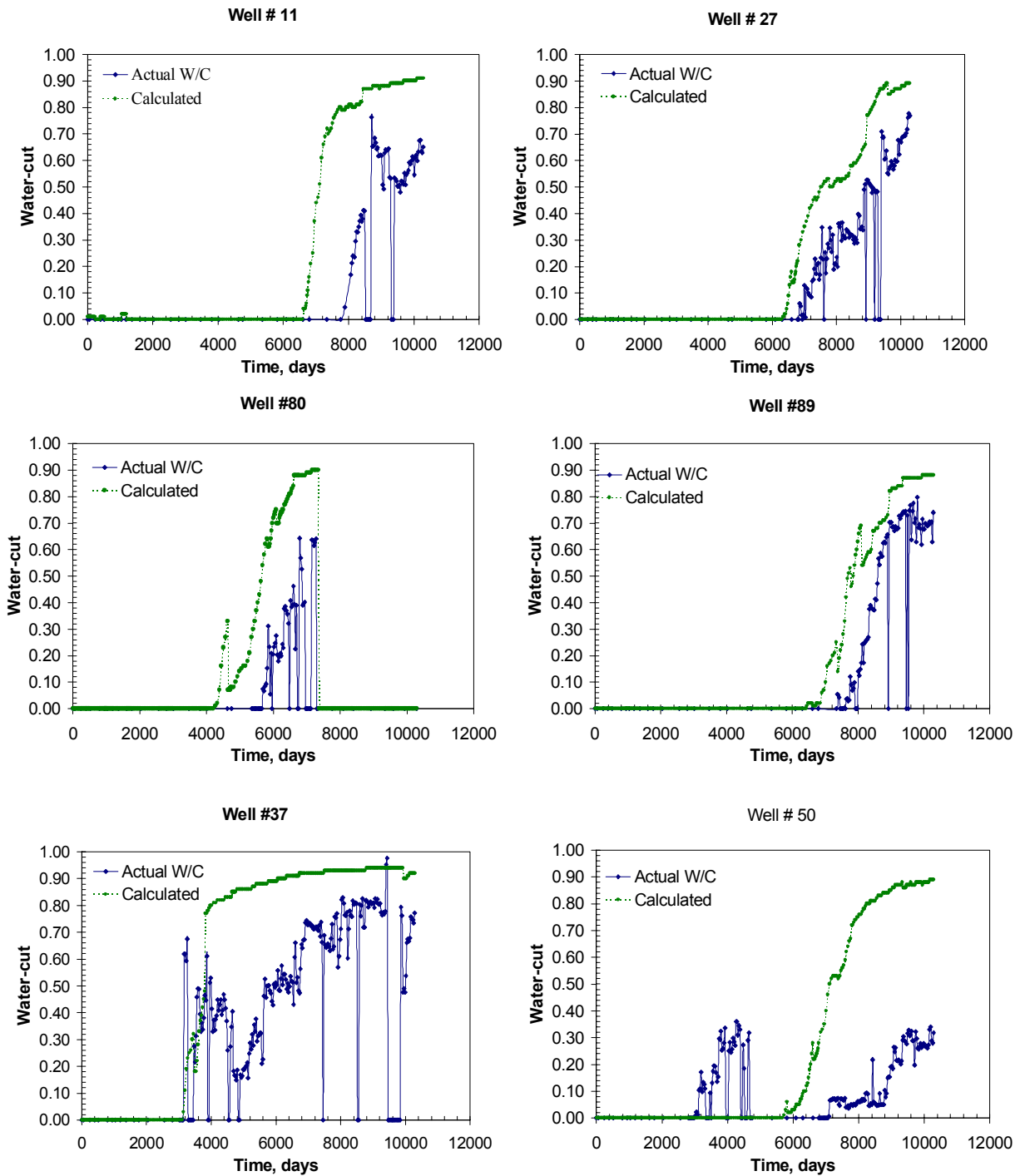


Figure 3.14 - Examples of Water Cut Responses without Gravity Effect.

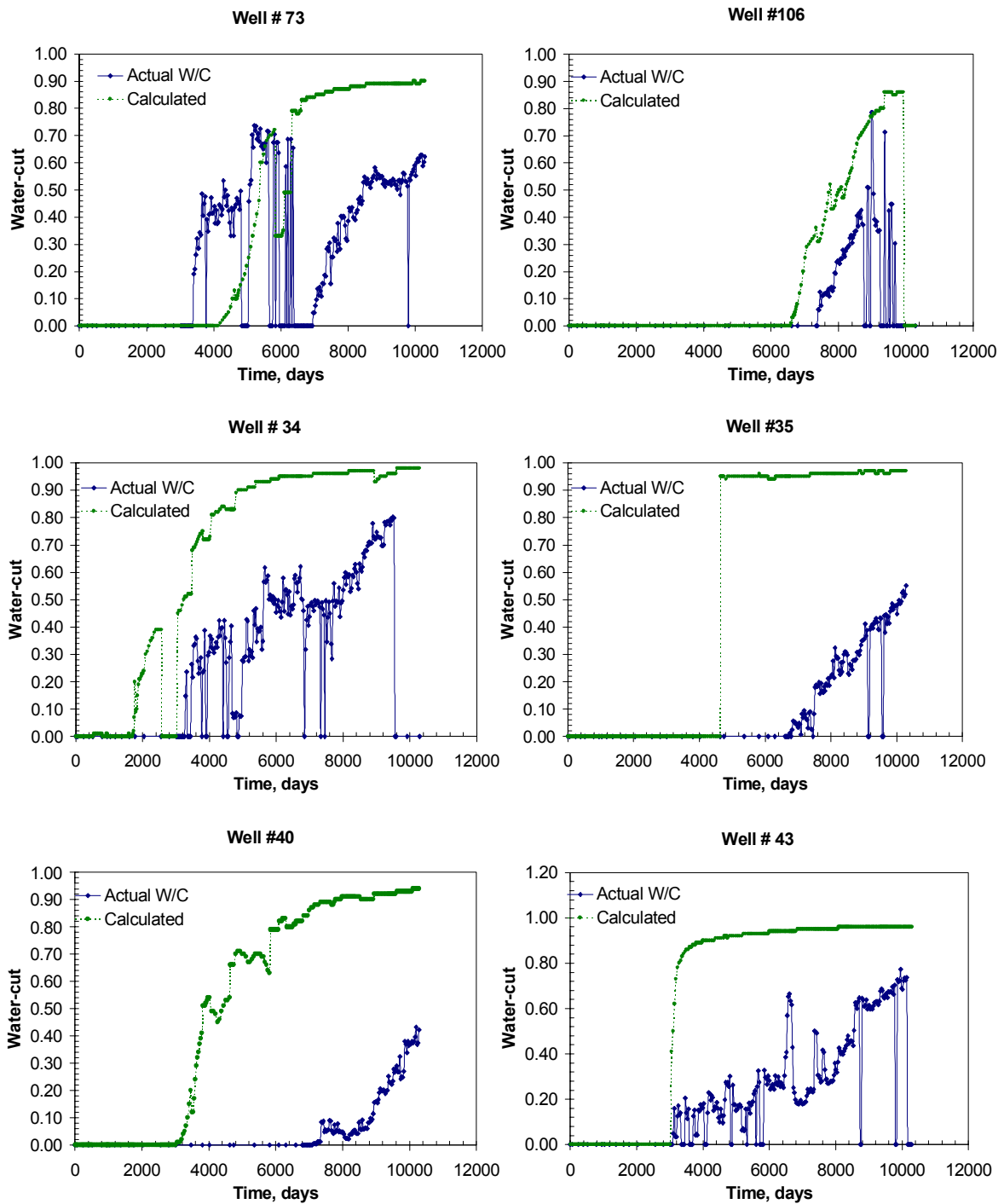


Figure 3.14 Continued.

is observed. **Fig. 3.11** indicates the streamline Time of Flight (TOF) distribution which also reflect the gross fluid movement in the reservoir. In the southern part of reservoir, we have high TOF values compared to northern part because of low permeability values. As the well configuration changes, TOF distribution also varies. As the water flooding proceeds, the unswept area in the reservoir becomes smaller. The water saturation distribution at three different times are shown **Fig. 3.12**. As the water flooding proceeds, most area except of the southern part of the reservoir was swept. In the final stage of production, the flood front is apparently formed in the middle of the reservoir. The streamline distribution during three stages of production (**Fig. 3.13**) provides a convenient way to observe injector/producer contributions and make subsequent adjustments to the allocation factors. Also, in Fig. 3.13 (a), the compressibility effects are clearly apparent in the streamlines at 60 days for the single producer that has no aquifer or injection support. As mentioned above, once pressure is updated due to infill wells, well conversions, mobility change and production rates changes of the wells, a new set of streamlines is computed. Then the simulator maps the locations of the saturation fronts in old streamlines onto new streamlines. **Fig. 3.14** shows the water-cut responses at 12 producers.

Case 2: With Gravity Effect

This case includes the impact of gravity in reservoir simulation and is thus more realistic representation of the reservoir flow. For this reservoir, we find that gravity over-ride is significant and the gravity impacts the water movement and saturation distribution. We use operator-splitting technique to perform streamline simulation with gravity, as described in Chapter II.

The broad trends in pressure distribution (**Fig. 3.15**), Time of Flight distribution (**Fig. 3.16**) and the water saturation distribution at three different times (**Fig. 3.17**) and the streamline distributions (**Fig. 3.18**) are similar to the results of Case 1. However, the gravity causes water-oil segregation and results in localized changes in saturation distribution which in turn affects the water-cut at the wells. In fact, inclusion of gravity effect in streamline simulation improves the water-cut matches, as can be seen in **Fig. 3.19** compared to **Fig. 3.14**.

3.4.4 Conditioning Coarse Scale Model to Water Cut Responses

We performed a streamline-based inversion to generate a coarse scale model conditioned to water cut responses. In the model, compressibility effects and aquifer support are included. The production data integration was carried out using water-cut data at 48 wells, which show

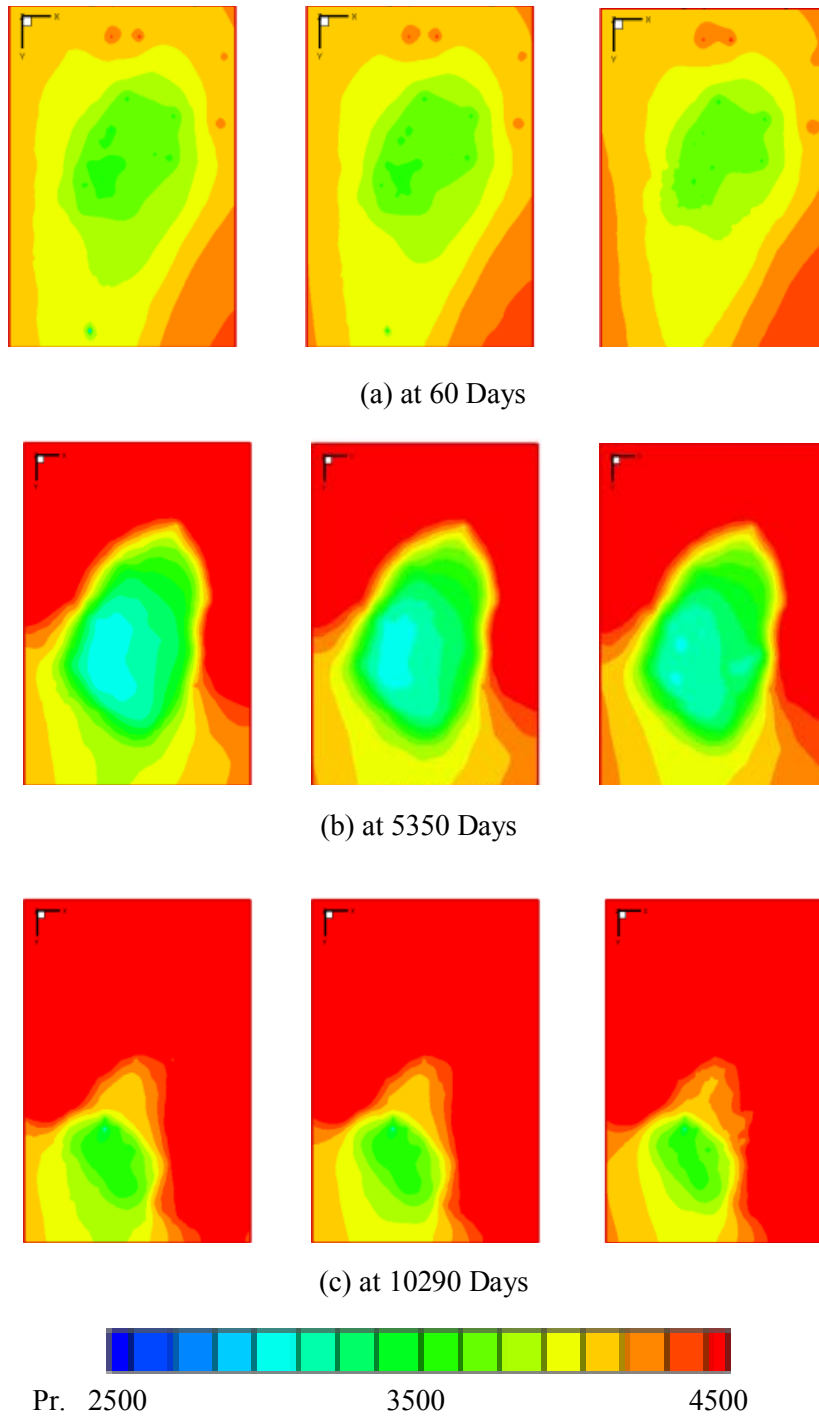


Figure 3.15 - Pressure Distribution at Three Different Times for Layer 1, 4 and 8 with Gravity.

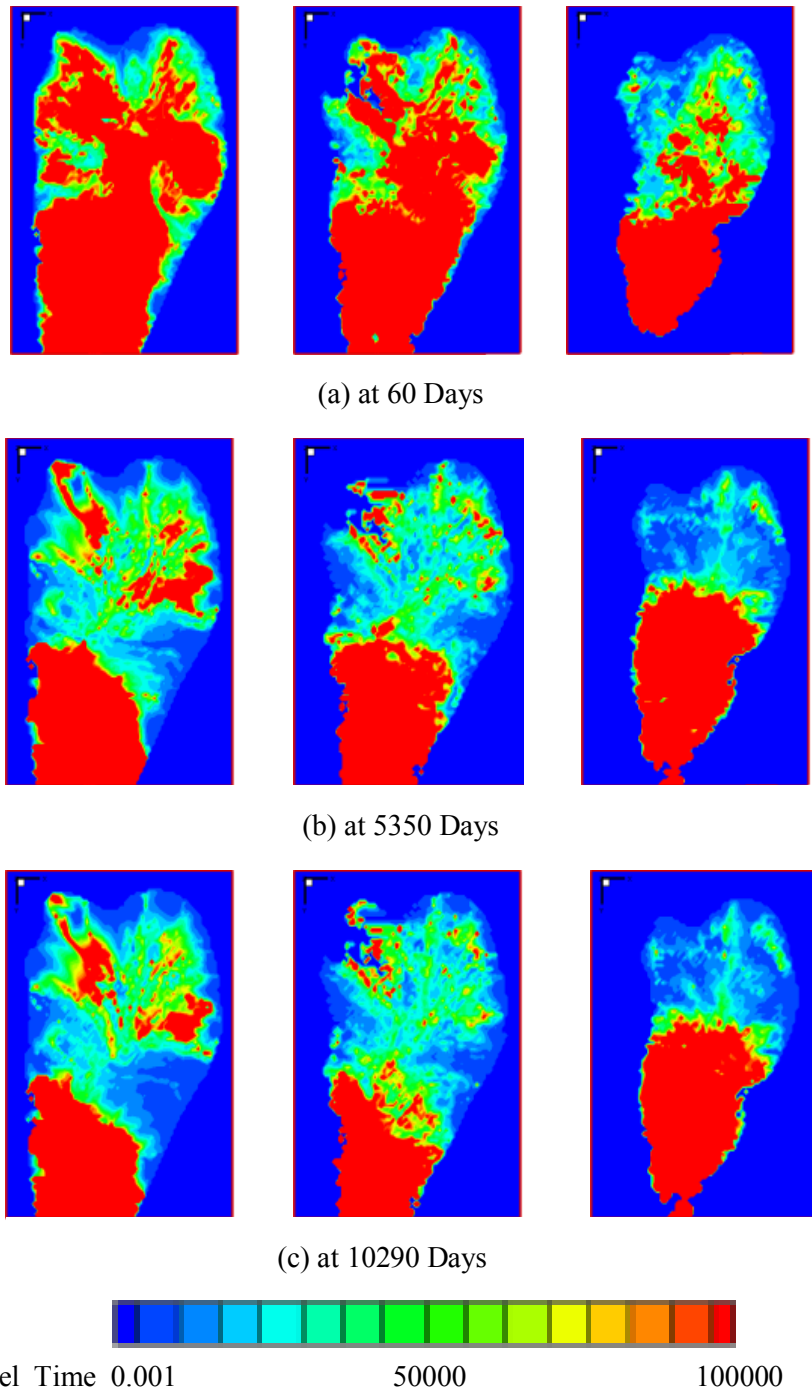


Figure 3.16 - Time of Flight Distribution at Three Different Times for Layer 1, 4 and 8 with Gravity.

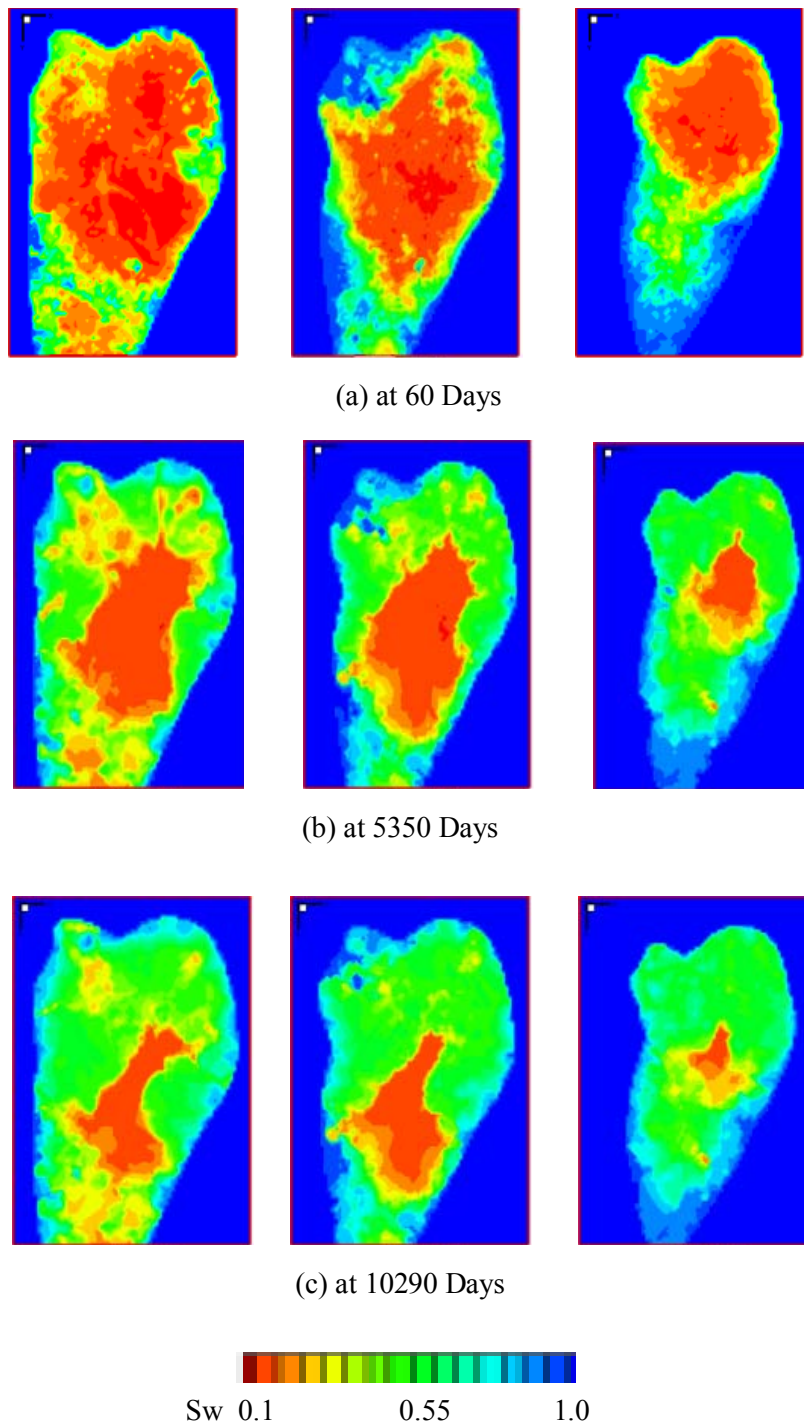


Figure 3.17 - Water Saturation Distribution at Three Different Times for Layer 1, 4 and 8 with Gravity.

Streamlines after 60 Days



(a)

Streamlines after 5350 Days



(b)

Streamlines after 10290 Days



(c)

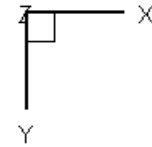


Figure 3.18 - Areal Map of Streamline Distribution at Three Different Times with Gravity. (a) Initial at 60 Days, (b) Middle at 5350 Days, (c) End at 10290 Days.

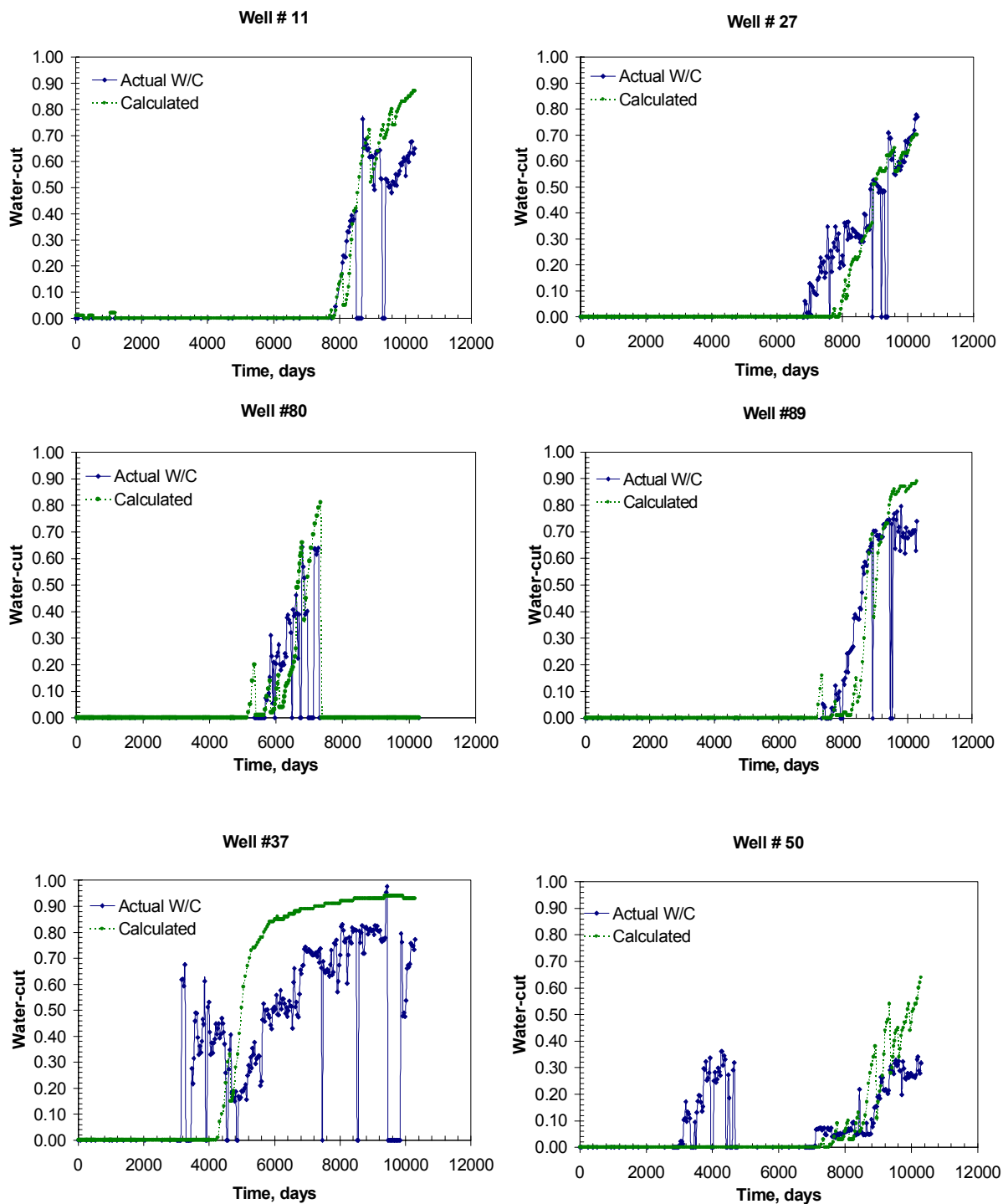


Figure 3.19 - Water Cut Responses with Gravity Effect.

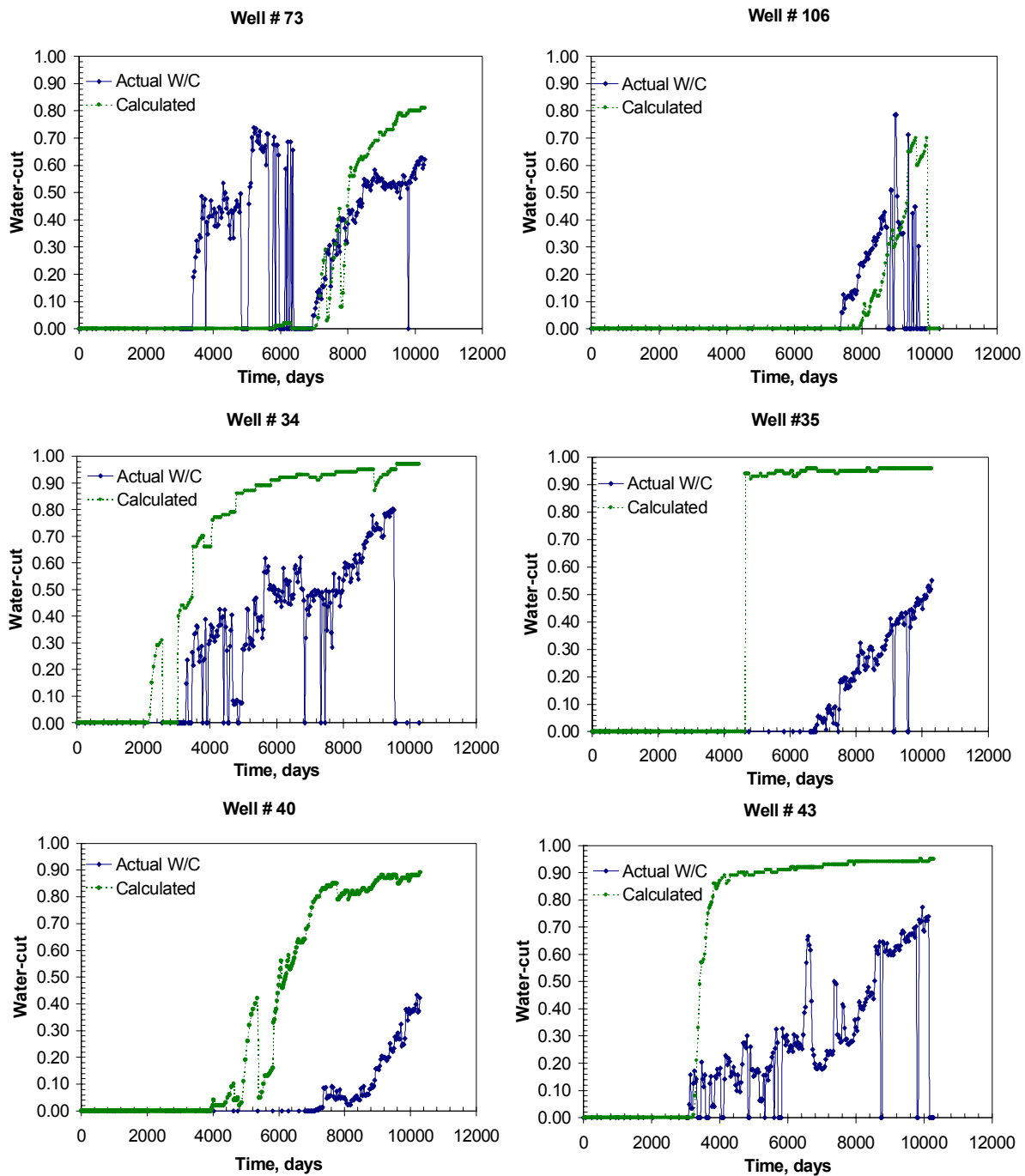


Figure 3.19 Continued

significant water cut responses. During inversion, the range of permeability was chosen to be the same as that in the static model. As in the preliminary simulation study, we examine the impact of gravity using two case studies.

Case 1: Without Gravity Effect

As mentioned in Chapter II, our approach to integration of production data into reservoir models is analogous to seismic waveform inversion. Thus, we first 'line-up' the observed and computed production response at all the wells by minimizing the misfit between the observed and calculated 'first arrival' or breakthrough times. **Fig. 3.20** illustrates the observed and calculated breakthrough times for all 48 producers at four different iterations. As the number of iteration increases, the scatteredness of the points significantly decreases which indicates the reduction of travel time misfit. We can see that at 6th iteration, the breakthrough times for all the wells are now in good agreement. Another important benefit of the travel time matching is that it prevents the solution from being trapped by secondary peaks in multi-peaked production responses that are commonly associated with field data. It is worth-mentioning here an important practical aspect of the travel time matching. Since the observation data usually contains measurement error, we do not have to make an effort to achieve the perfect match of breakthrough times. The water cut matches at individual wells are shown in **Fig. 3.21**. About 70% of the wells exhibited good to moderate matches in the overall production history. **Fig. 3.22** indicates the pressure distribution changes at two different time steps with initial model and model after inversion. In **Fig. 3.23** water saturation distribution changes at two different time steps are shown. To demonstrate the permeability change after inversion, a "difference model" was constructed by subtracting the inversion generated model from the initial geologic permeability model (**Fig. 3.24**). The computation time for the travel time match was just 4.5 hrs on the Pentium IV.

Case 2: With Gravity Effect

It is very important to consider the impact of gravity on the displacement of oil by water drive if the gravitational forces are not negligible in production mechanism. **Fig. 3.25** indicates breakthrough times match at four different iterations. At 6th iteration, the breakthrough times for 48 producers are now in good agreement. As concluded in simulation study with upscaled model, the consideration of gravitational drainage effect in the simulation substantially

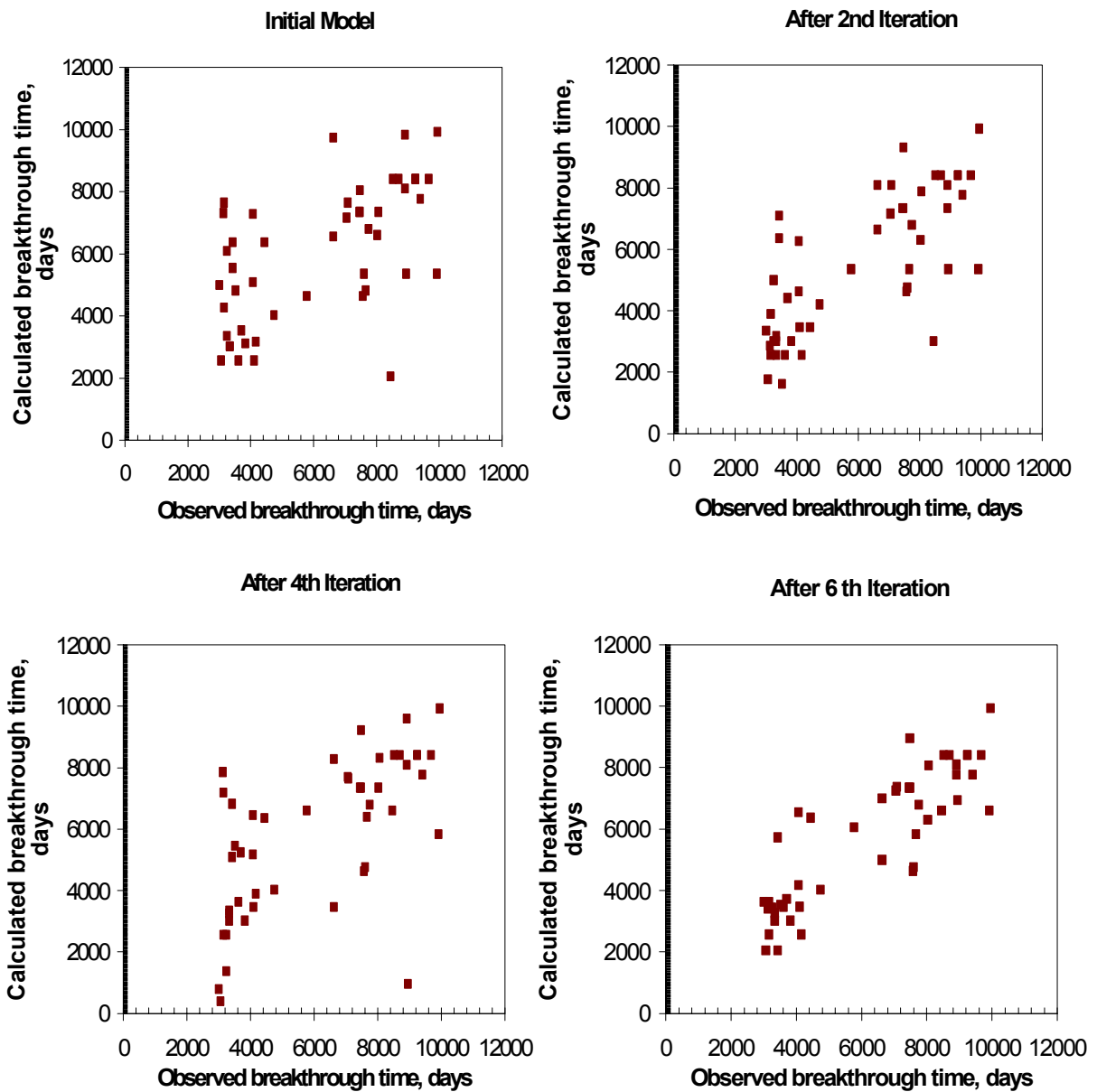


Figure 3.20 - Travel Time Match at Four Different Iterations without Gravity.

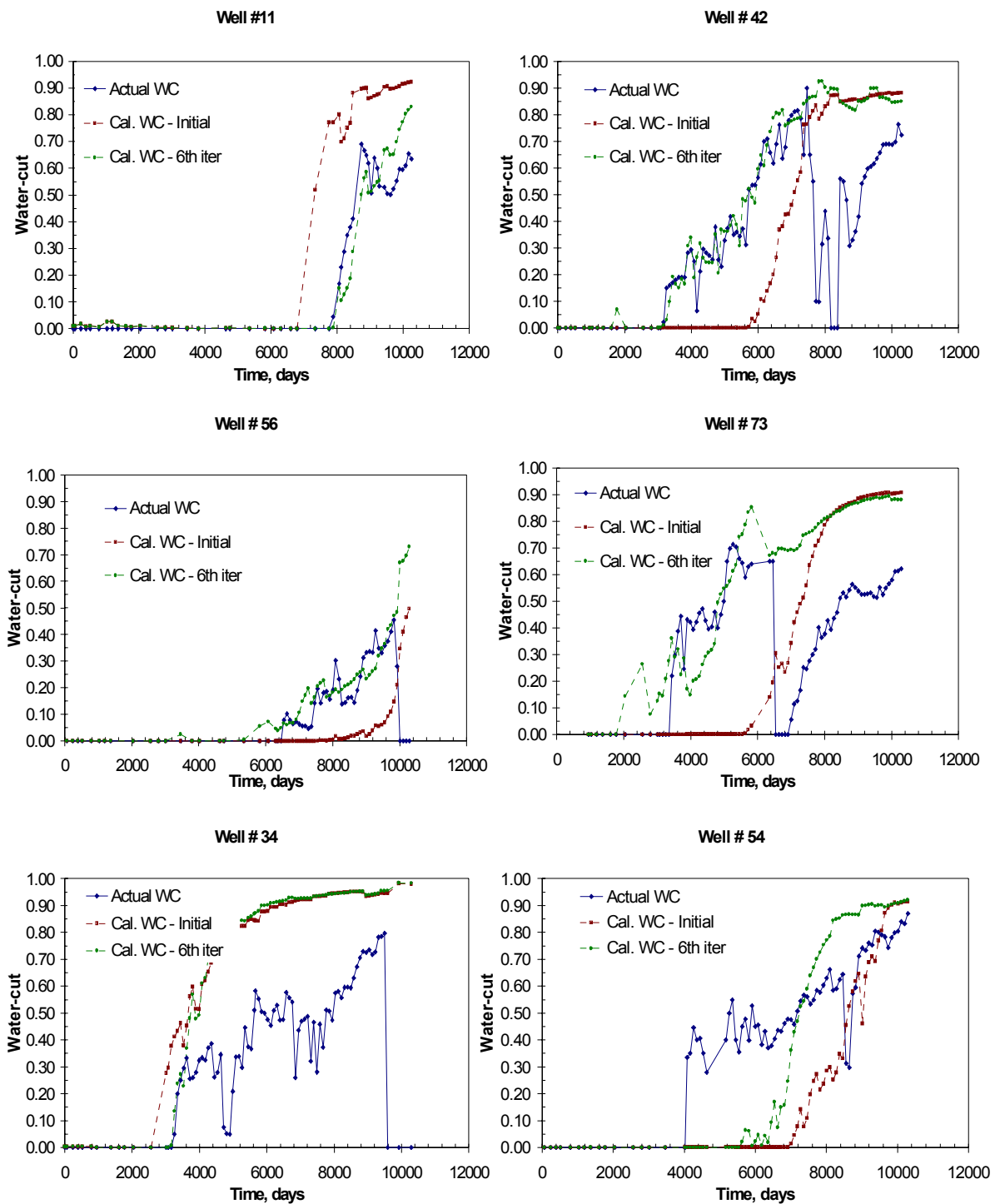


Figure 3.21 - Water Cut Matches for Upscale Model without Gravity Effect.

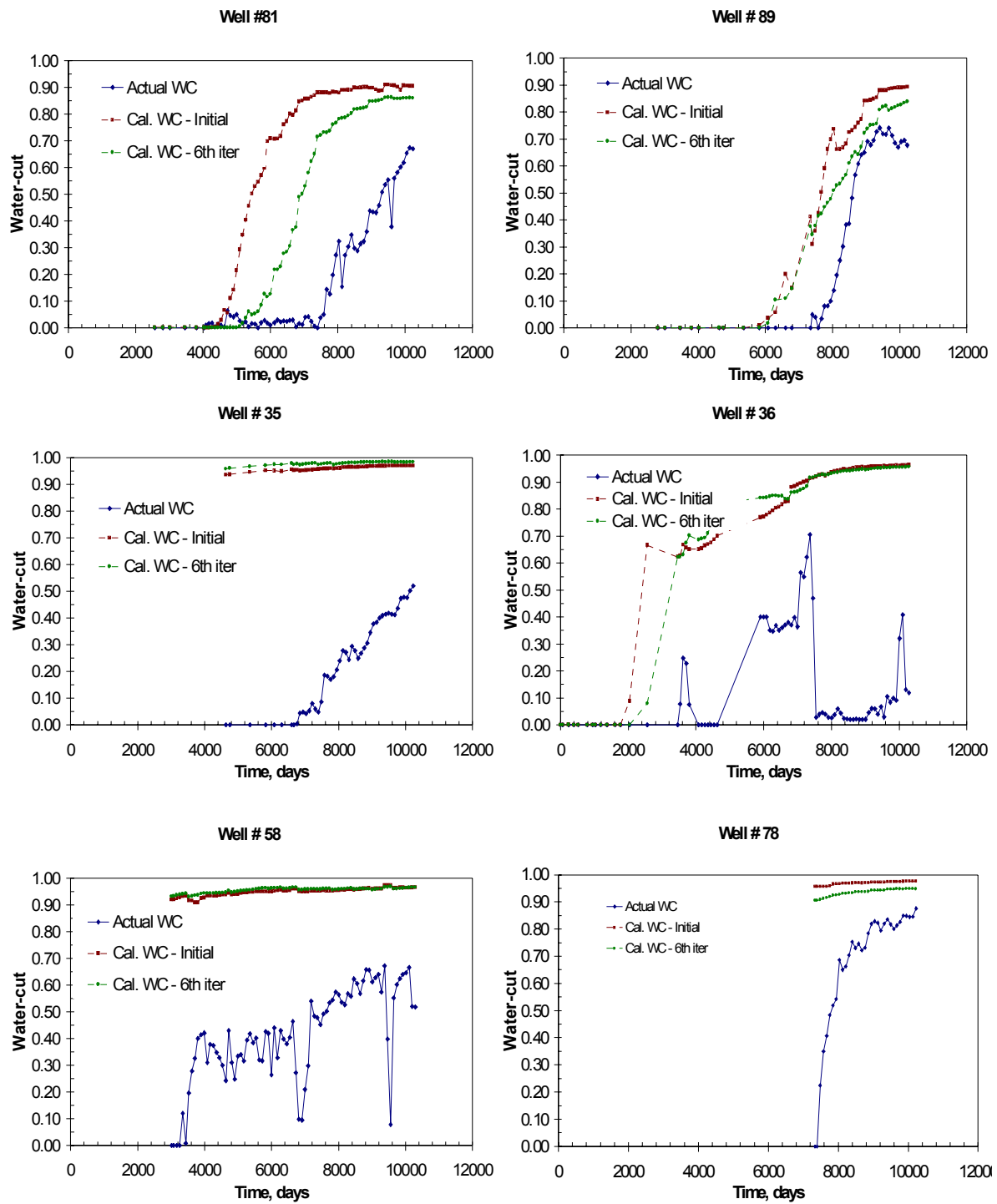
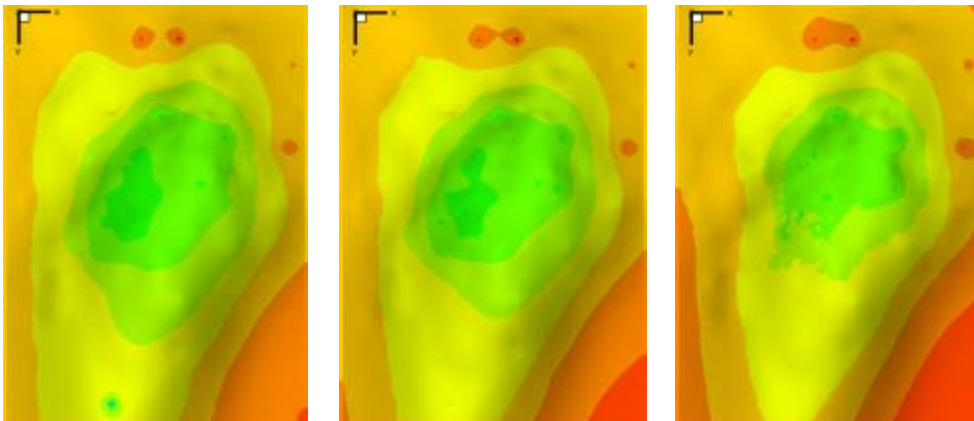
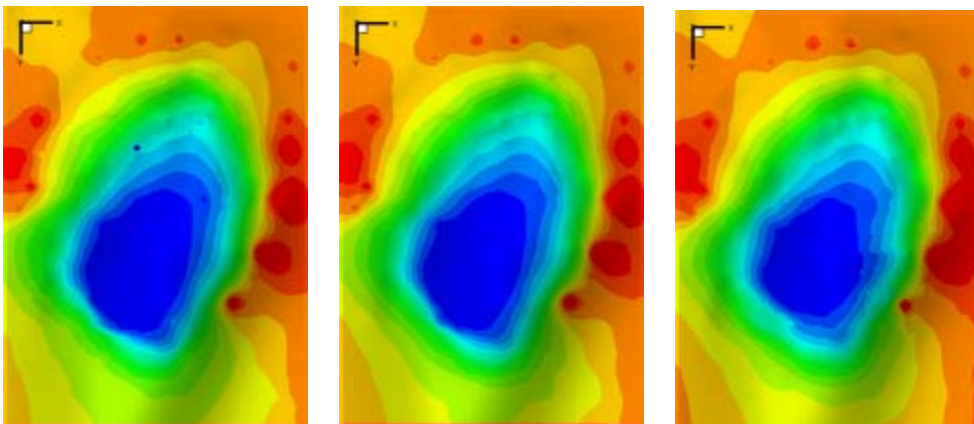


Figure 3.21 Continued.



(a) at 60 Days



(b) at 10290 Days

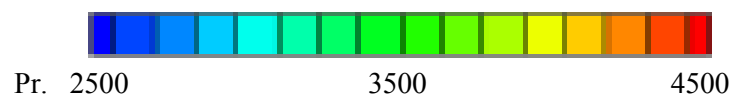
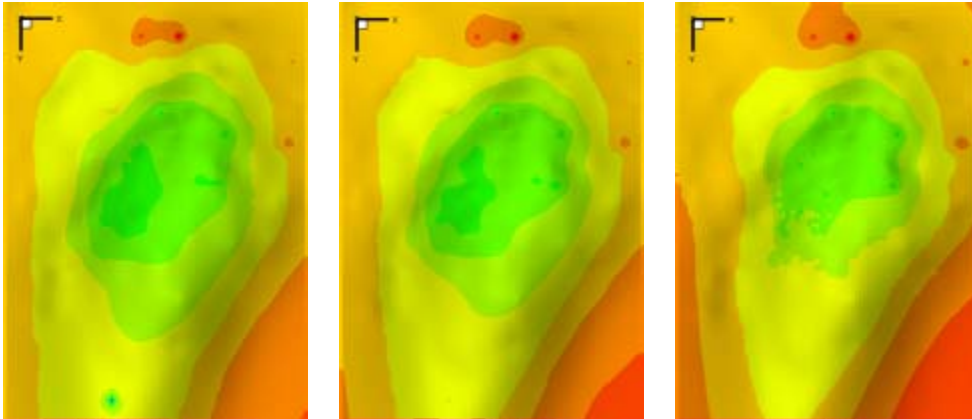
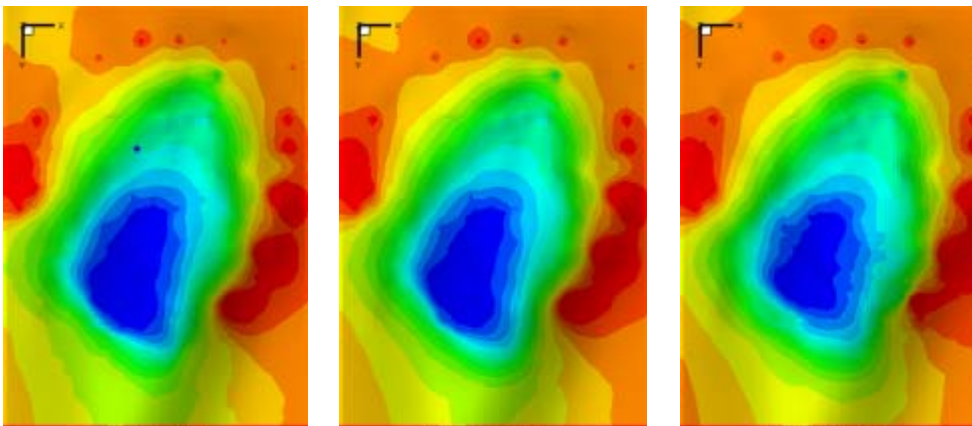


Figure 3.22 - Changes in Pressure Distribution at Three Different Times without Gravity. (a) at 60 Days from Initial Model, (b) at 10290 Days from Initial Model, (c) at 60 Days from Final Model, (d) at 10290 Days from Final Model.



(c) at 60 Days for Layer 1, 4 and 8.



(d) at 10290 Days for Layer 1, 4 and 8.

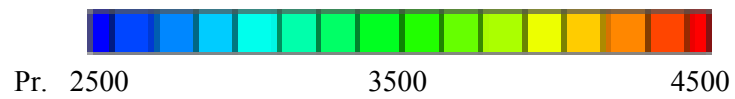
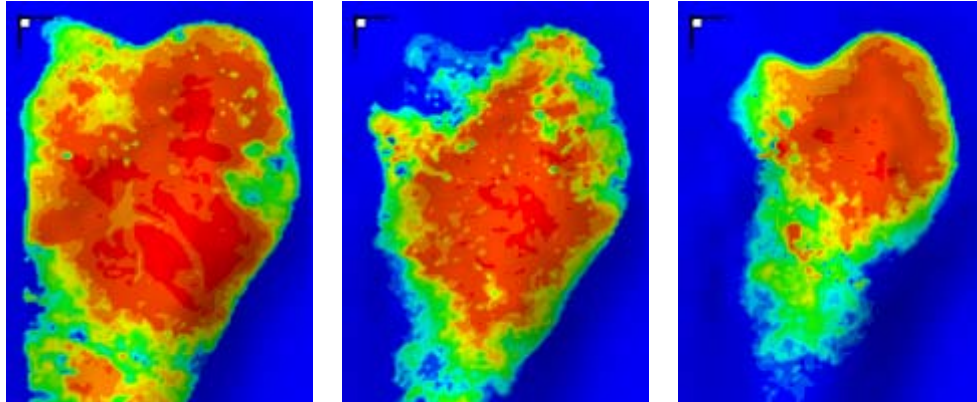
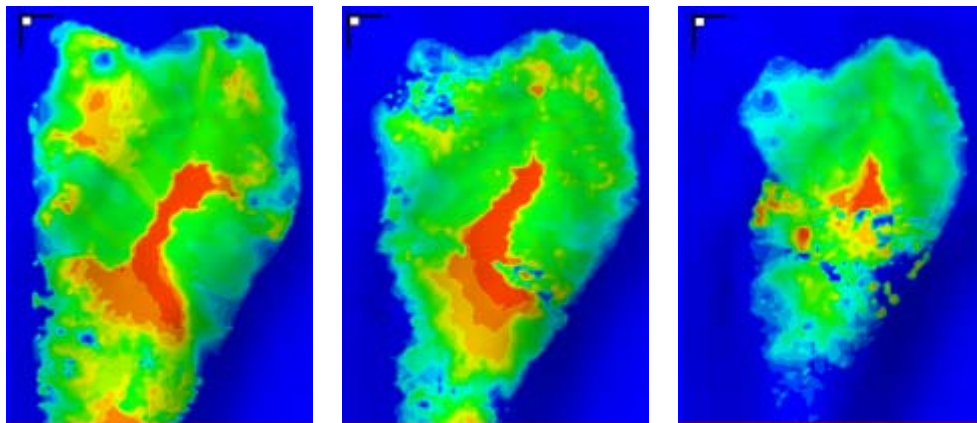


Figure 3.22 Continued.



(a) at 60 Days for Layer 1, 4 and 8.



(b) at 10290 Days for Layer 1, 4 and 8.

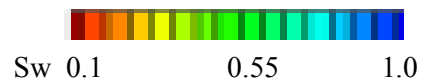
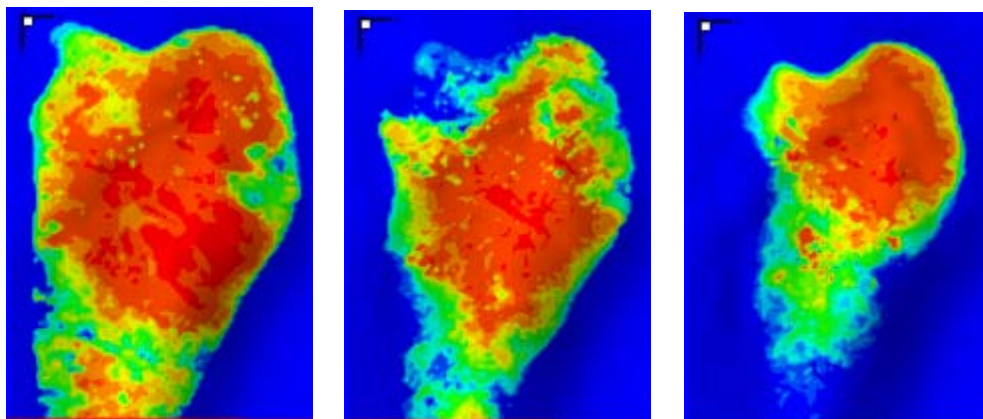
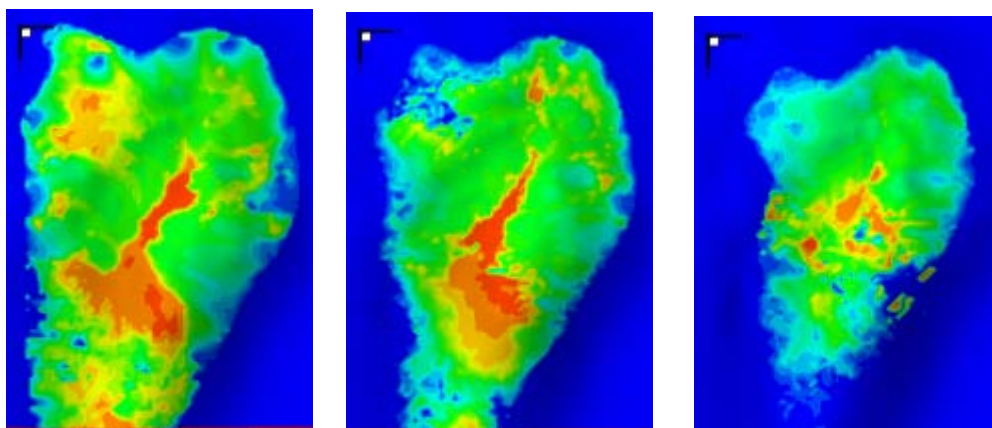


Figure 3.23 - Changes in Water Saturation Distribution at Three Different Times without Gravity. (a) at 60 Days from Initial Model, (b) at 10290 Days from Initial Model, (c) at 60 Days from Final Model, (d) at 10290 Days from Final Model.



(c) at 60 Days for Layer 1, 4 and 8.



(d) at 10290 Days for Layer 1, 4 and 8.

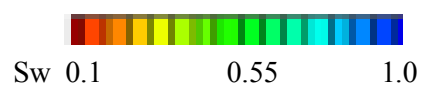


Figure 3.23 Continued.

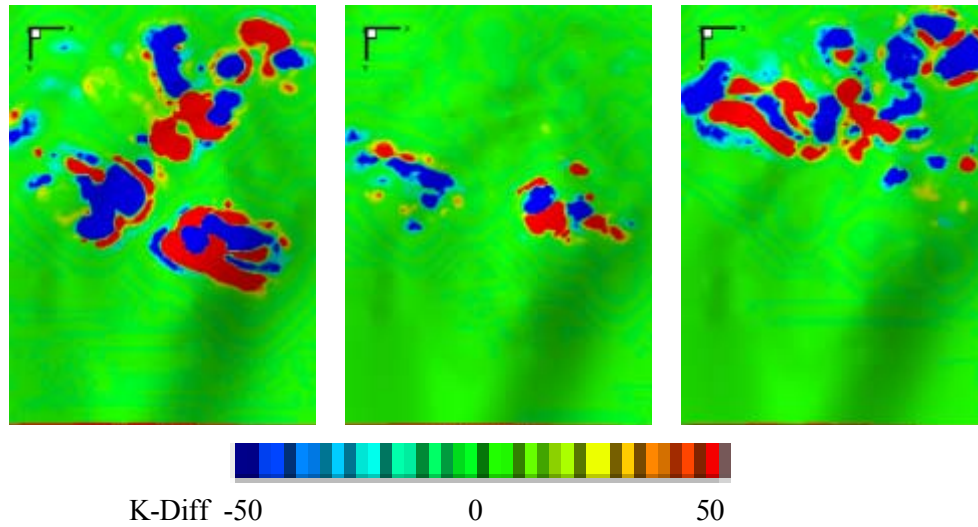


Figure 3.24 - Permeability Change (md) from the Initial Model for Layer 1, 4 and 8 without Gravity.

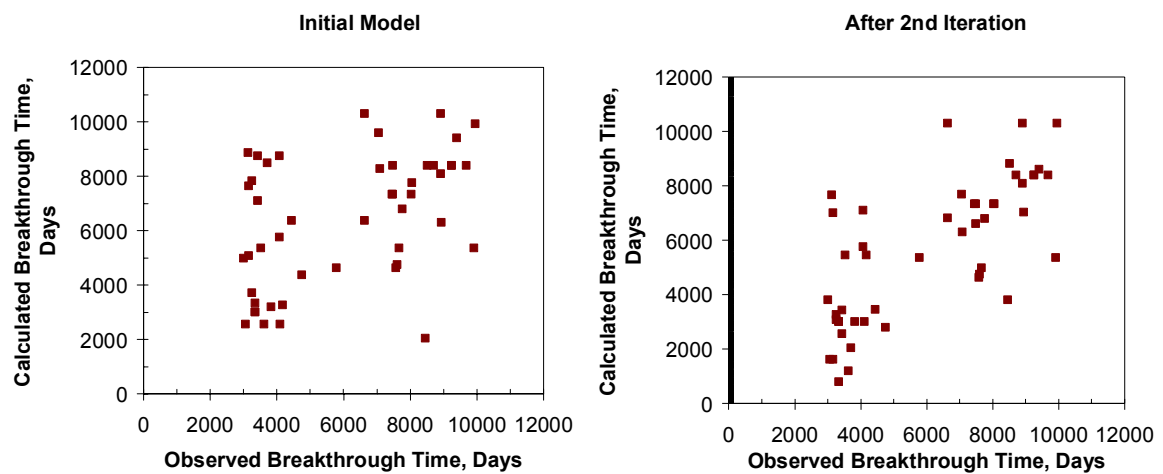


Figure 3.25 – Travel Time Matches at Four Different Iterations with Gravity.

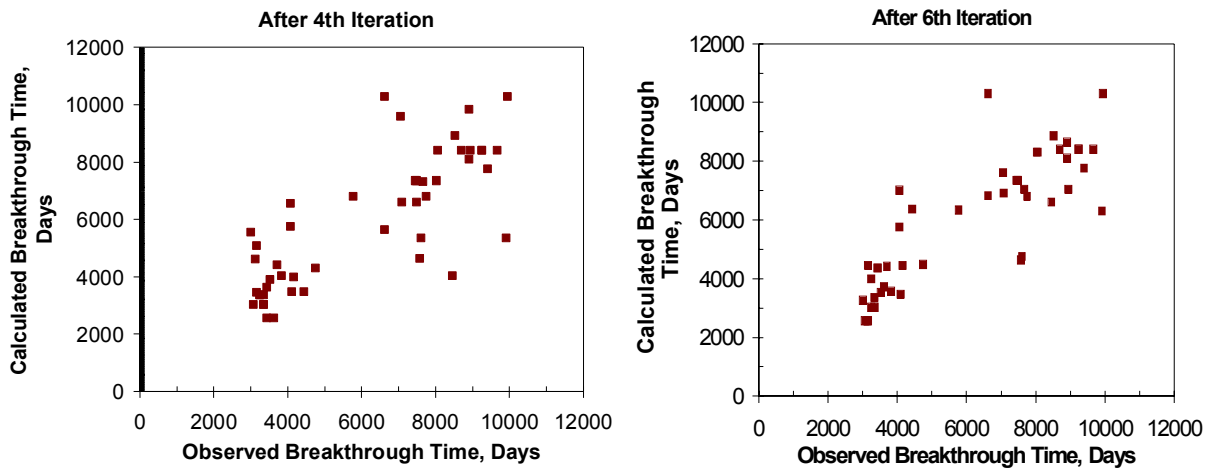


Figure 3.25 Continued.

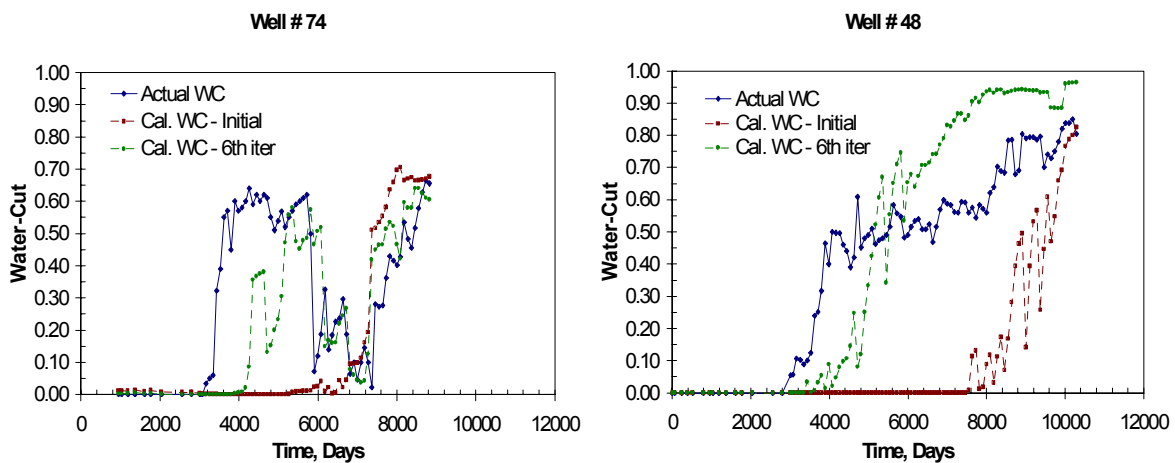


Figure 3.26 - Water Cut Matches for Upscale Model with Gravity Effect.

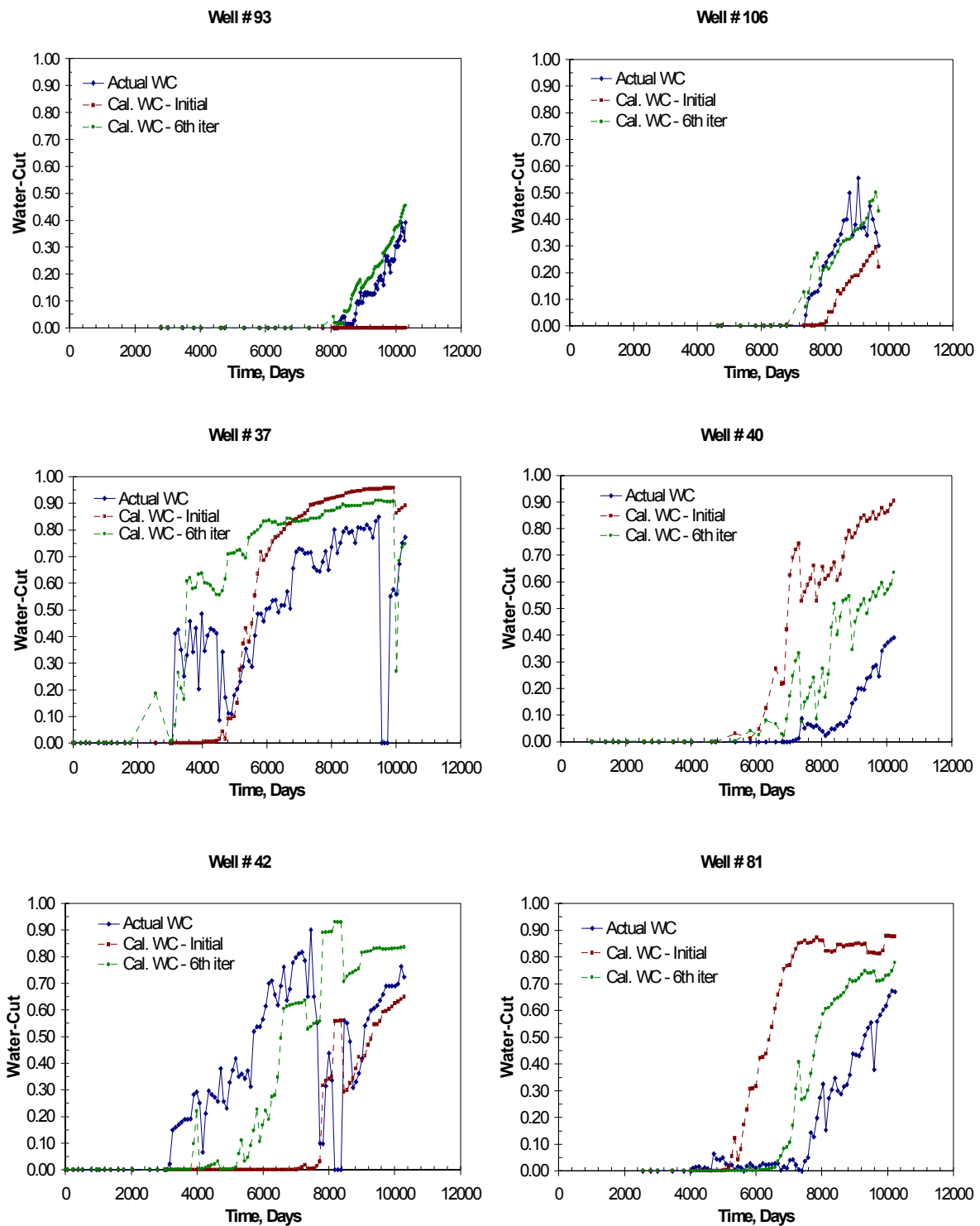


Figure 3.26 Continued.

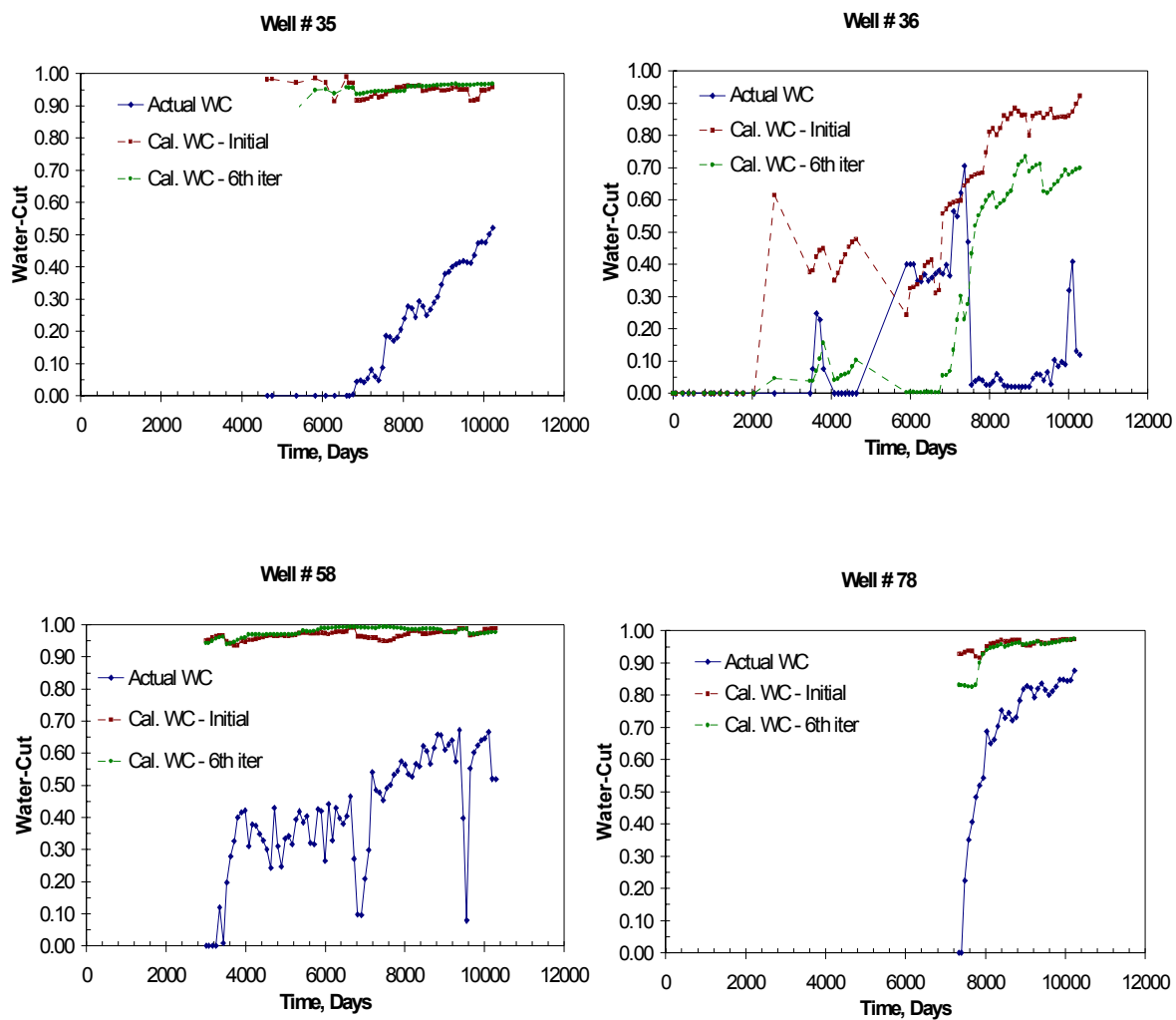
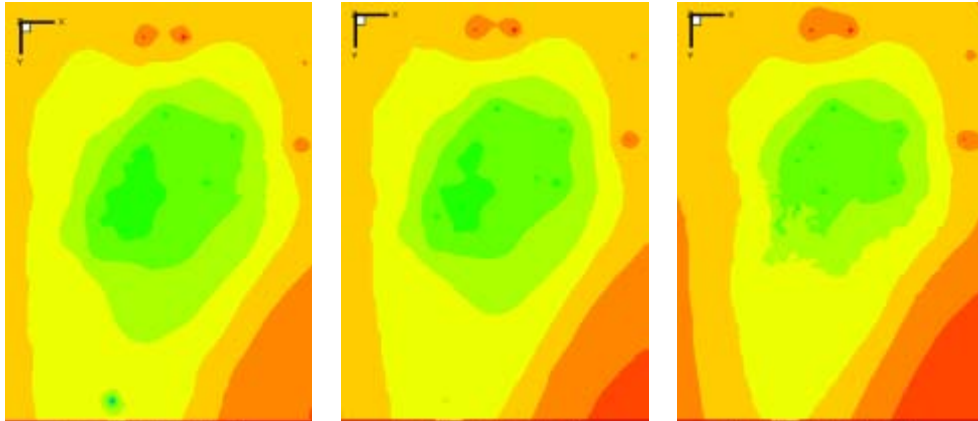
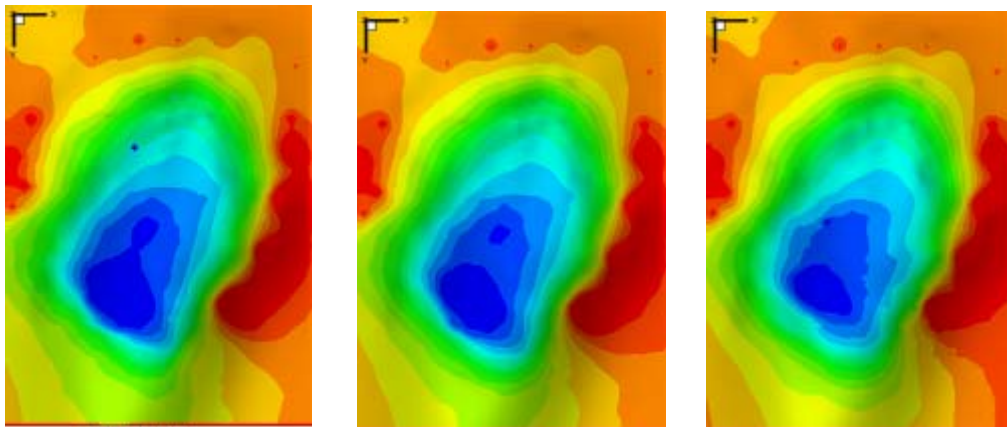


Figure 3.26 Continued.



(a) at 60 Days for Layer 1, 4 and 8.



(b) at 10290 Days for Layer 1, 4 and 8.

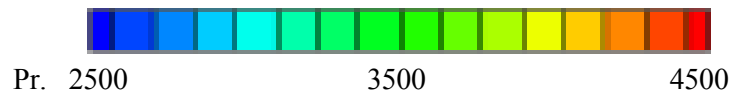
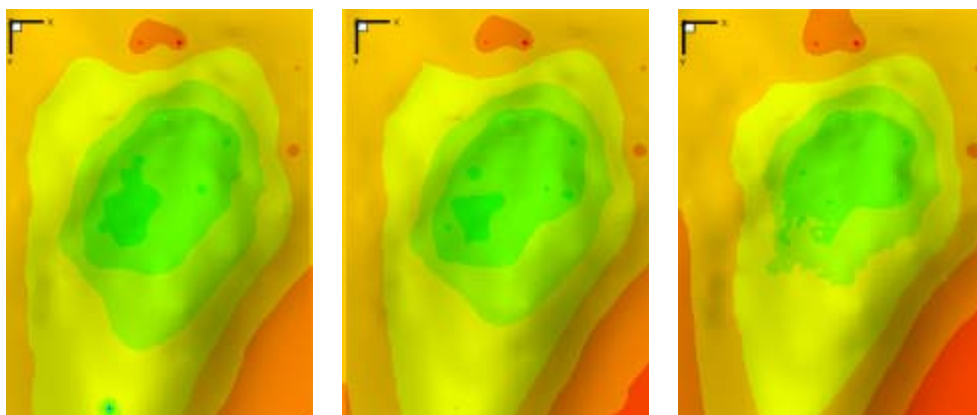
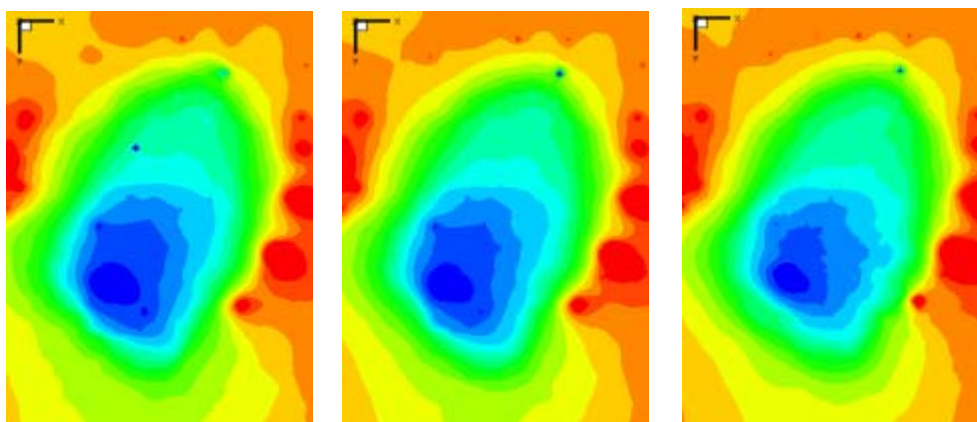


Figure 3.27 - Changes in Pressure Distribution at Three Different Times with Gravity. (a) at 60 Days from Initial Model, (b) at 10290 Days from Initial Model, (c) at 60 Days from Final Model, (d) at 10290 Days from Final Model.



(c) at 60 Days for Layer 1, 4 and 8.



(d) at 10290 Days for Layer 1, 4 and 8.

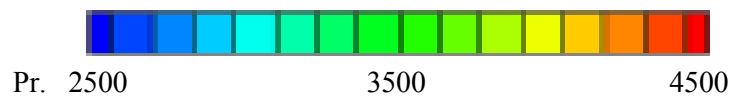
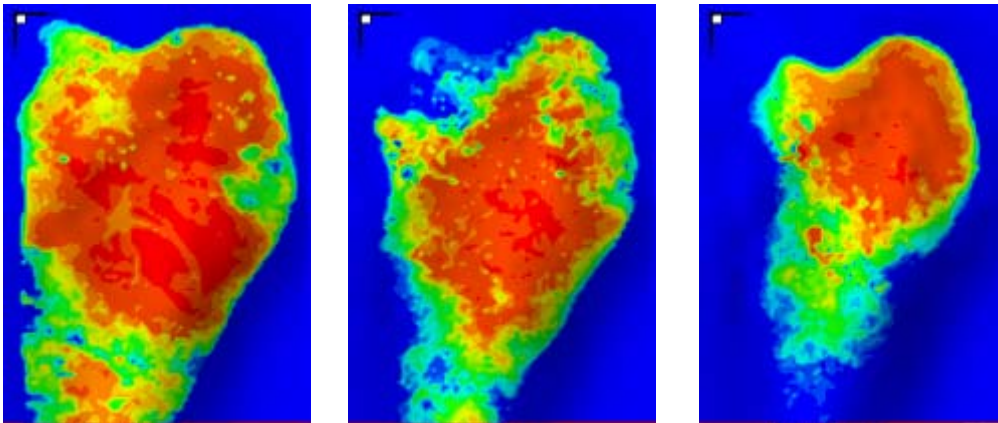
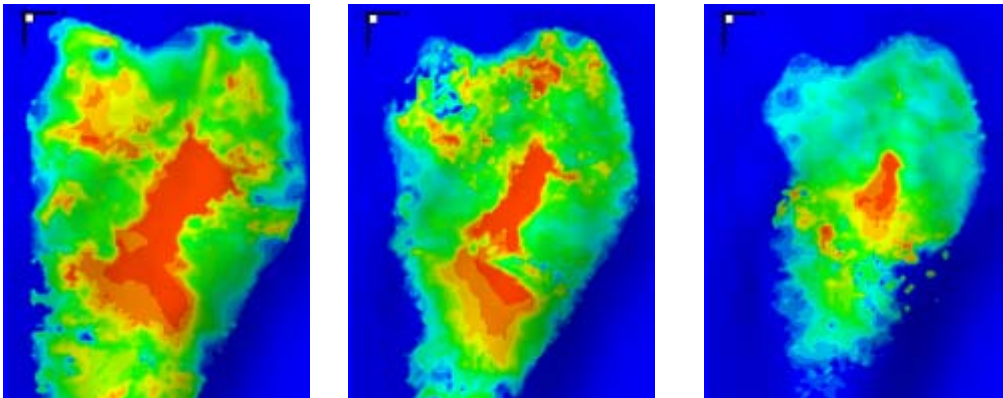


Figure 3.27 Continued.



(a) at 60 Days for Layer 1, 4 and 8.



(b) at 10290 Days for Layer 1, 4 and 8.

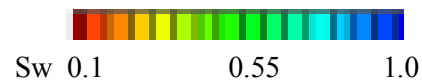
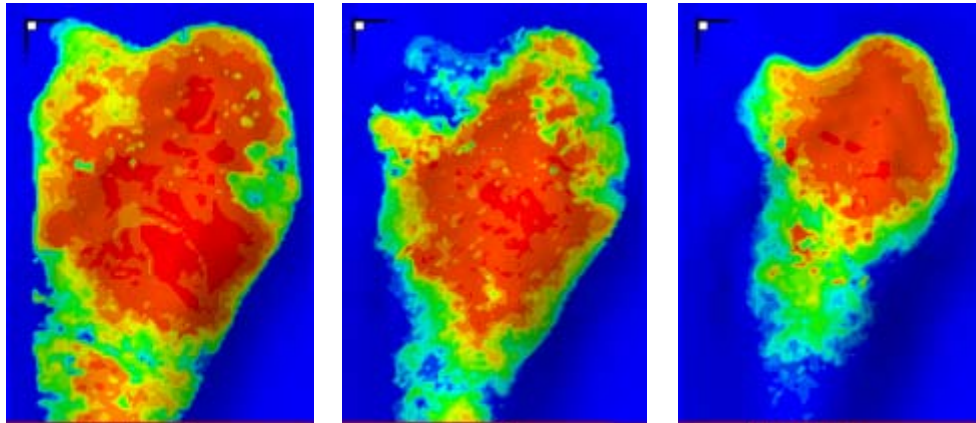
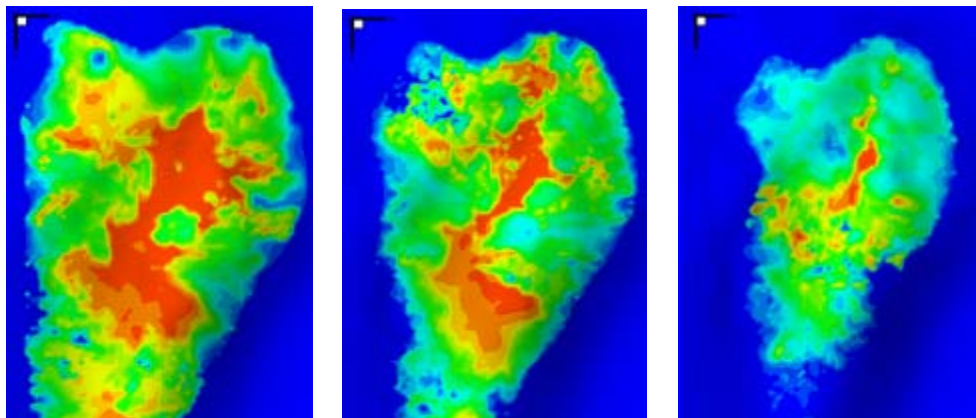


Figure 3.28 - Changes in Water Saturation at Three Different Times with Gravity. (a) at 60 Days from Initial Model, (b) at 10290 Days from Initial Model, (c) at 60 Days from Final Model, (d) at 10290 Days from Final Model.



(c) at 60 Days for Layer 1, 4 and 8.



(d) at 10290 Days for Layer 1, 4 and 8.

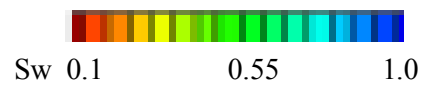


Figure 3.28 Continued.

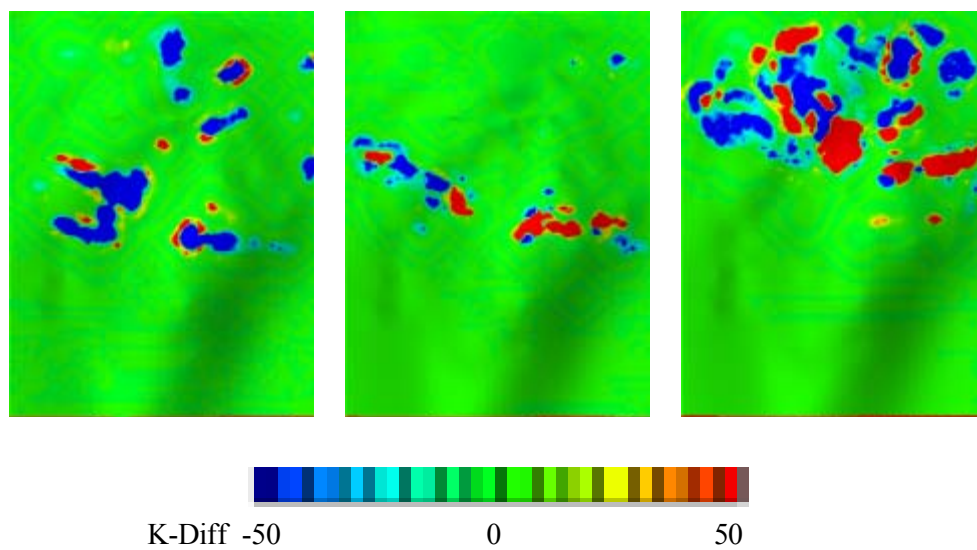


Figure 3.29 - Permeability Change (md) from the Initial Model for Layer 1, 4 and 8 with Gravity. (from Left to Right).

improves the water-cut matches (**Fig. 3.26**). In **Fig. 3.27**, **Fig. 3.28** and **Fig. 3.29**, pressure, water saturation, and changes in permeability distribution are shown. For this example with gravity option, the computation time requirement was less than 6 hrs in a PC.

3.4.5 Downscaling

Permeability changes in the upscaled model that occurred during the inversion process were transferred to the fine-scale model via a downscaling. A simple procedure based on permeability multipliers computed from the ratio of the grid-block permeabilities of the conditioned and unconditioned upscaled models was used to adjust the permeabilities in the fine-scale model. Finally, the permeability changes were compared with the facies map to examine any underlying trends. **Fig. 3.30** indicates permeability changes in fine scale model. **Fig. 3.31** compares the permeability change from the initial model with facies distribution at different layers in fine scale model, mainly located in between the upper and the middle region of the reservoir. As shown in **Fig. 3.31**, the trends of permeability changes are seen to follow the same trends as the facies distribution. An examination of the permeability changes appears to indicate that most of the dominant trends are along the ‘good’ facies. This is consistent with prior observations and has been found to be geologically realistic.

3.4.6 Finescale Simulation with the Updated Model

The permeabilities in the x- and y-directions were assumed to be same. Since previous reservoir simulation study ³¹ concluded that the ratio $K_z/K_x=0.2$, produced a reasonable pressure distribution and matched water breakthrough, we used the same ratio in fine scale streamline simulation model. In the fine scale simulation model, we used 20,000 PV multipliers along three edges. The pressure distribution are shown in **Fig. 3.32**. At different time steps, the distribution of streamline (**Fig. 3.33**), Time of Flight (**Fig. 3.34**) and Saturation (**Fig. 3.35**) are demonstrated. In **Fig. 3.36**, water cut matches compared to the observed responses are shown.

3.4.7 Direct Integration into the Finescale Model

In oil field situations, very often we have a large number of unknown parameters and limited measurement with error. Thus, inverse problem tends to be ill-posed which solution does not satisfy three conditions: Existence, Uniqueness, Stability. Especially since inversion of multiphase production data in highly non-linear in nature, it is easy for the solution to be

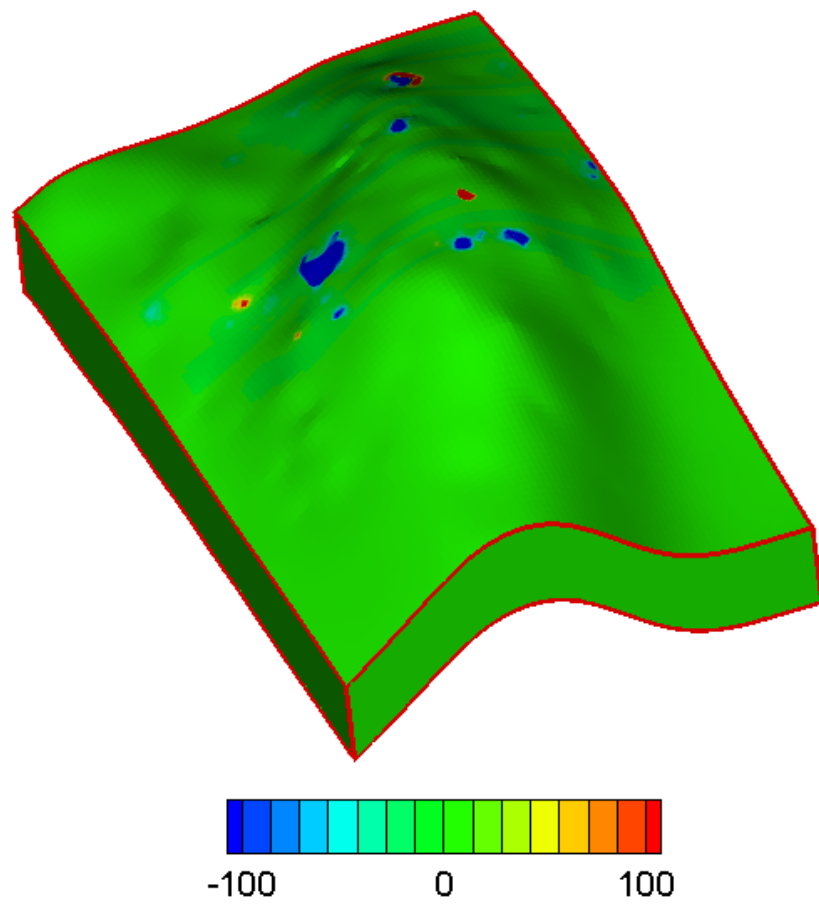


Figure 3.30 - Permeability Change (md) from the Initial Model in Fine Scale Model.

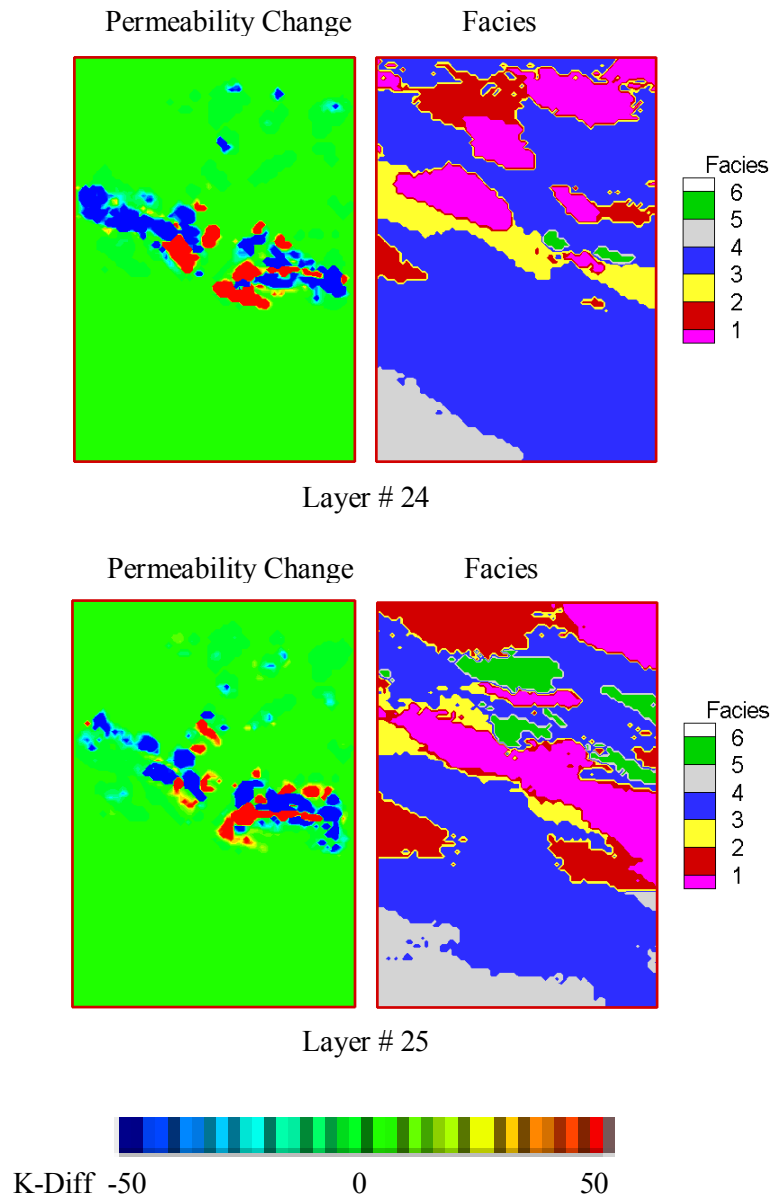


Figure 3.31- Comparison of Permeability Change (md) from the Initial Model (Left) and Facies Distribution (Right) at Different Layers in Fine Scale Model.

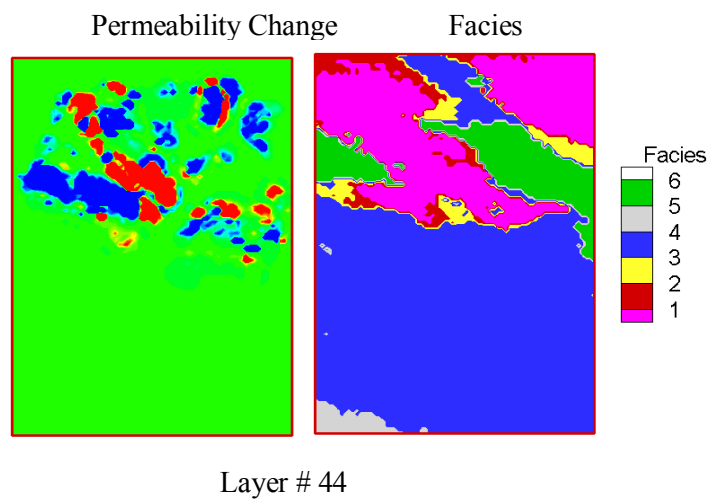
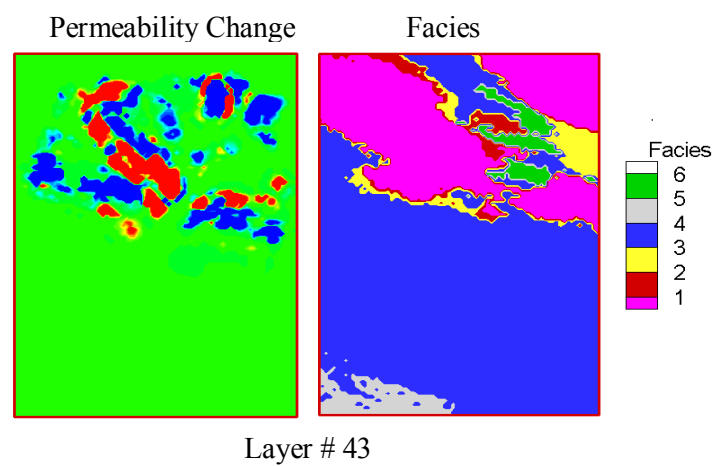
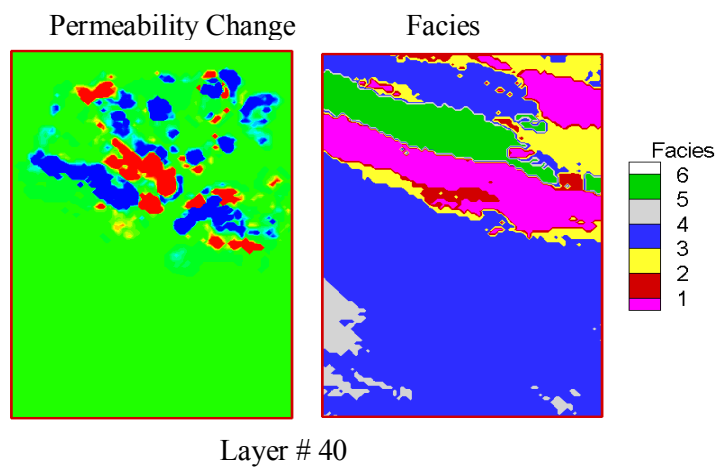


Figure 3.31 Continued.

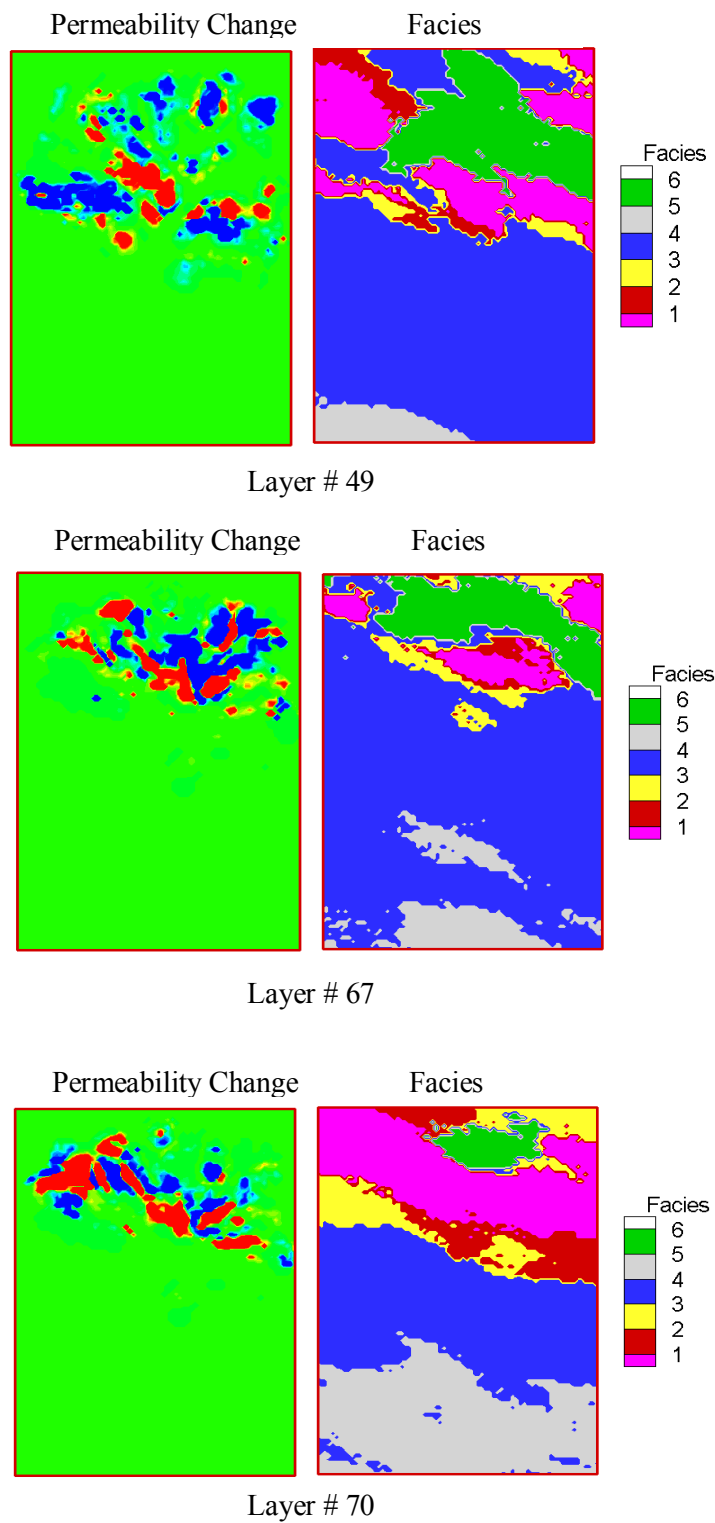
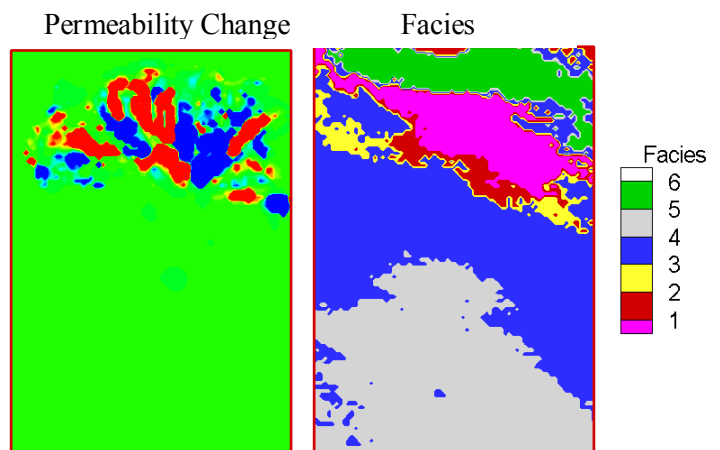
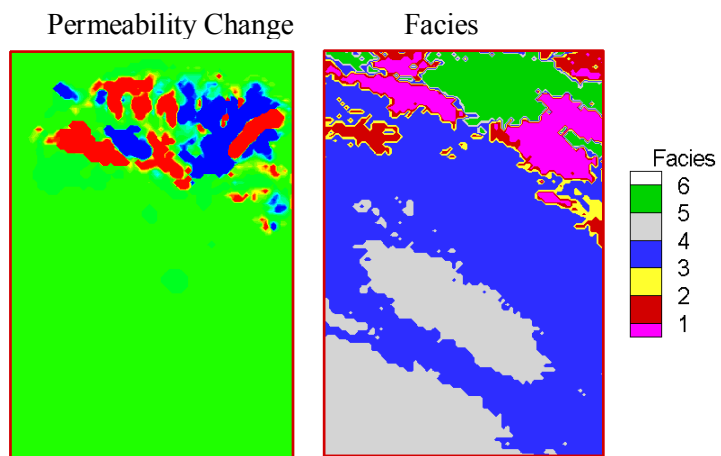


Figure 3.31 Continued.



Layer # 74



Layer # 76

Figure 3.31 Continued.

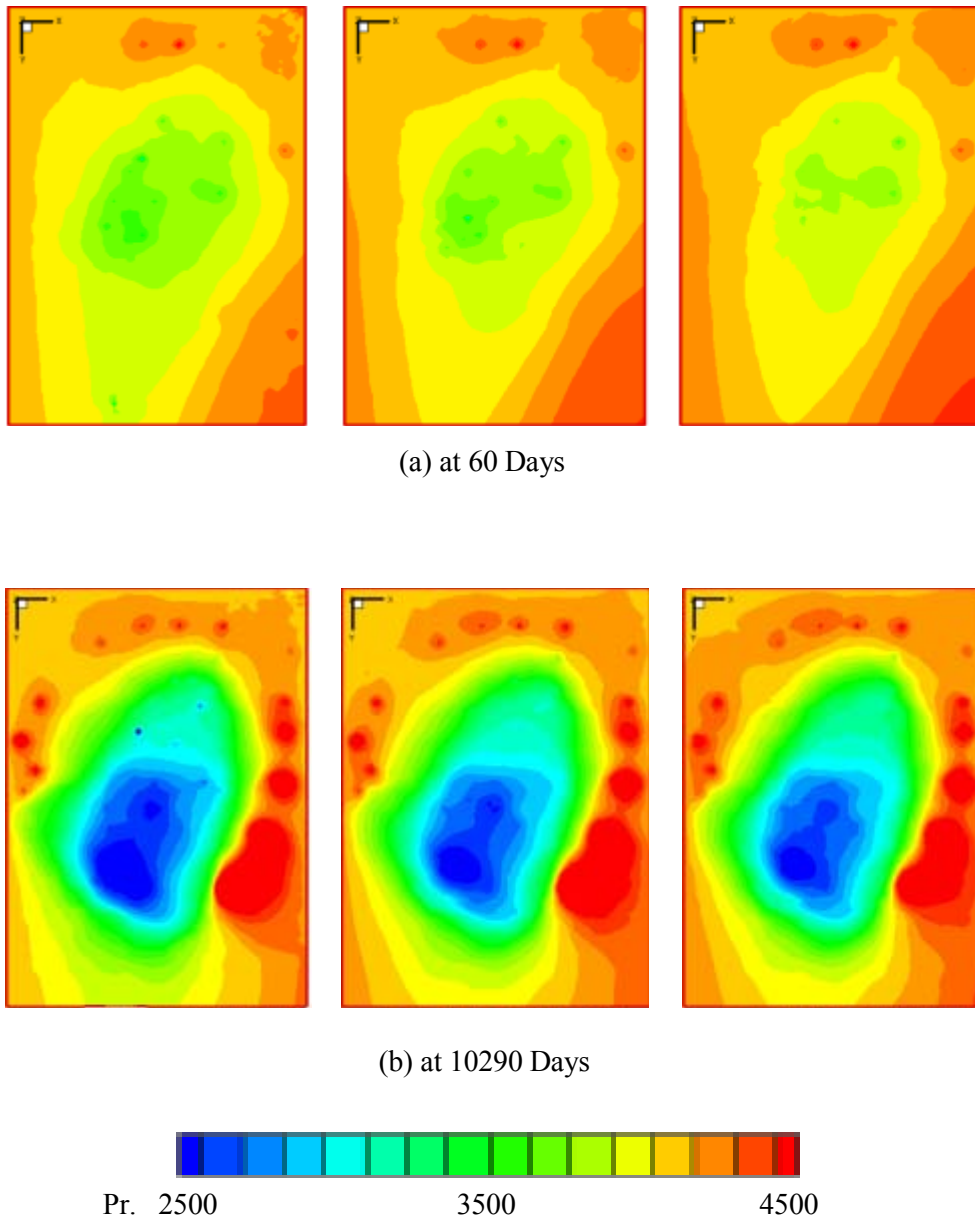


Figure 3.32 - Initial (at 60 Days) and Final (at 10290 Days) Pressure Distributions for Layer 10, 50 and 70 for Fine Scale Simulation.

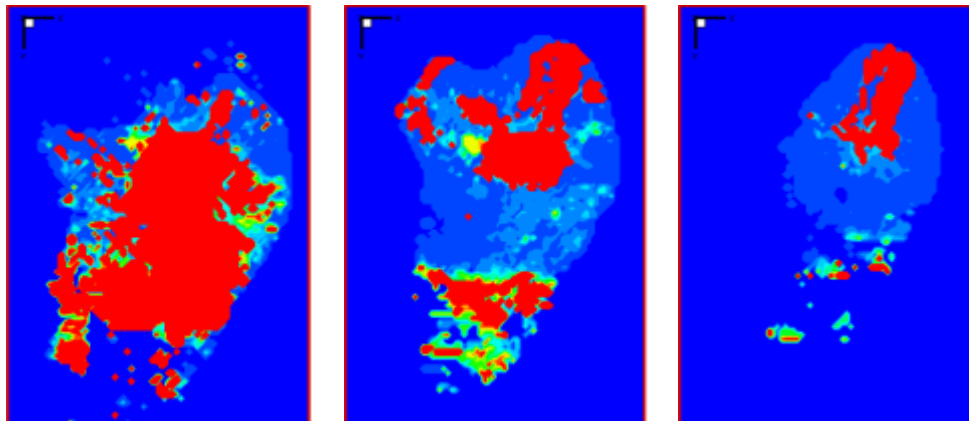
Streamlines after 60 Days



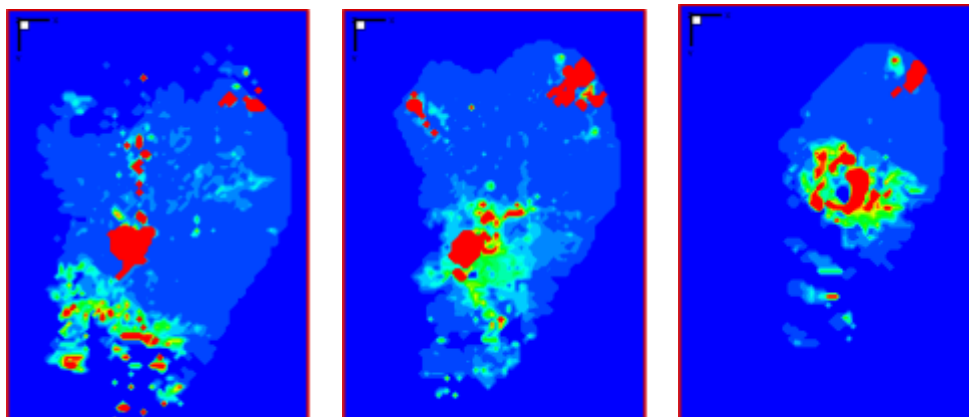
Streamlines after 10290 Days



Figure 3.33 - Areal View of Streamline Distributions for Updated Model for Fine Scale Simulation.



(a) at 60 Days



(b) at 10290 Days

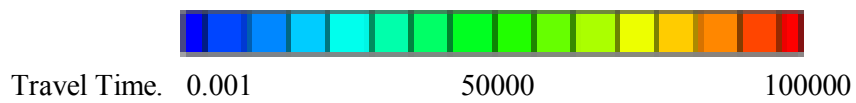


Figure 3.34 - Time of Flight Distributions at Initial and Final Time for Layer 10, 50 and 70 for Fine Scale Simulation.

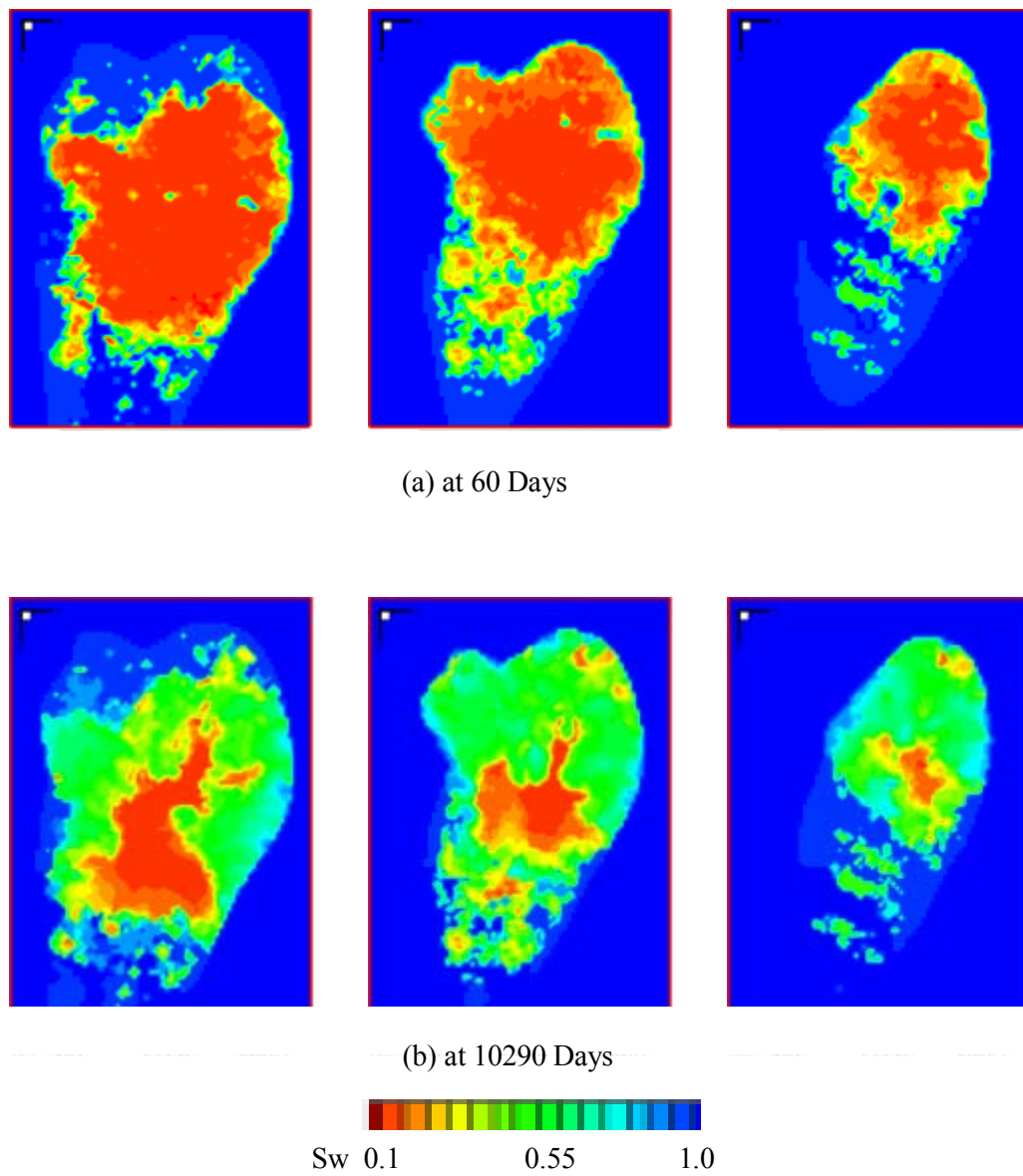


Figure 3.35 - Saturation Distributions at Initial and Final Time for Layer 10,50 and 70 for Fine Scale Simulation.

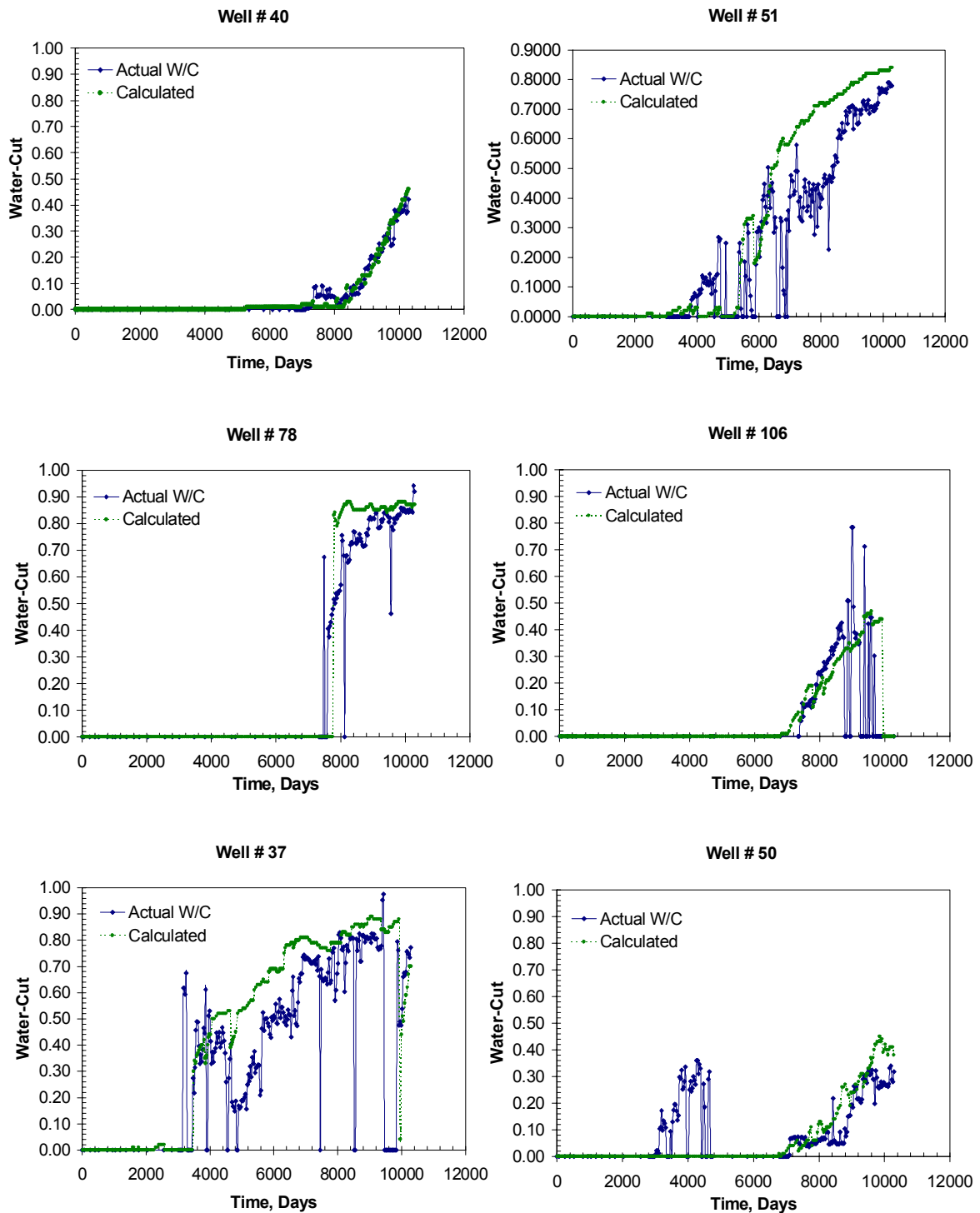


Figure 3.36 - Water Cut Matches for Updated Fine Scale Model.

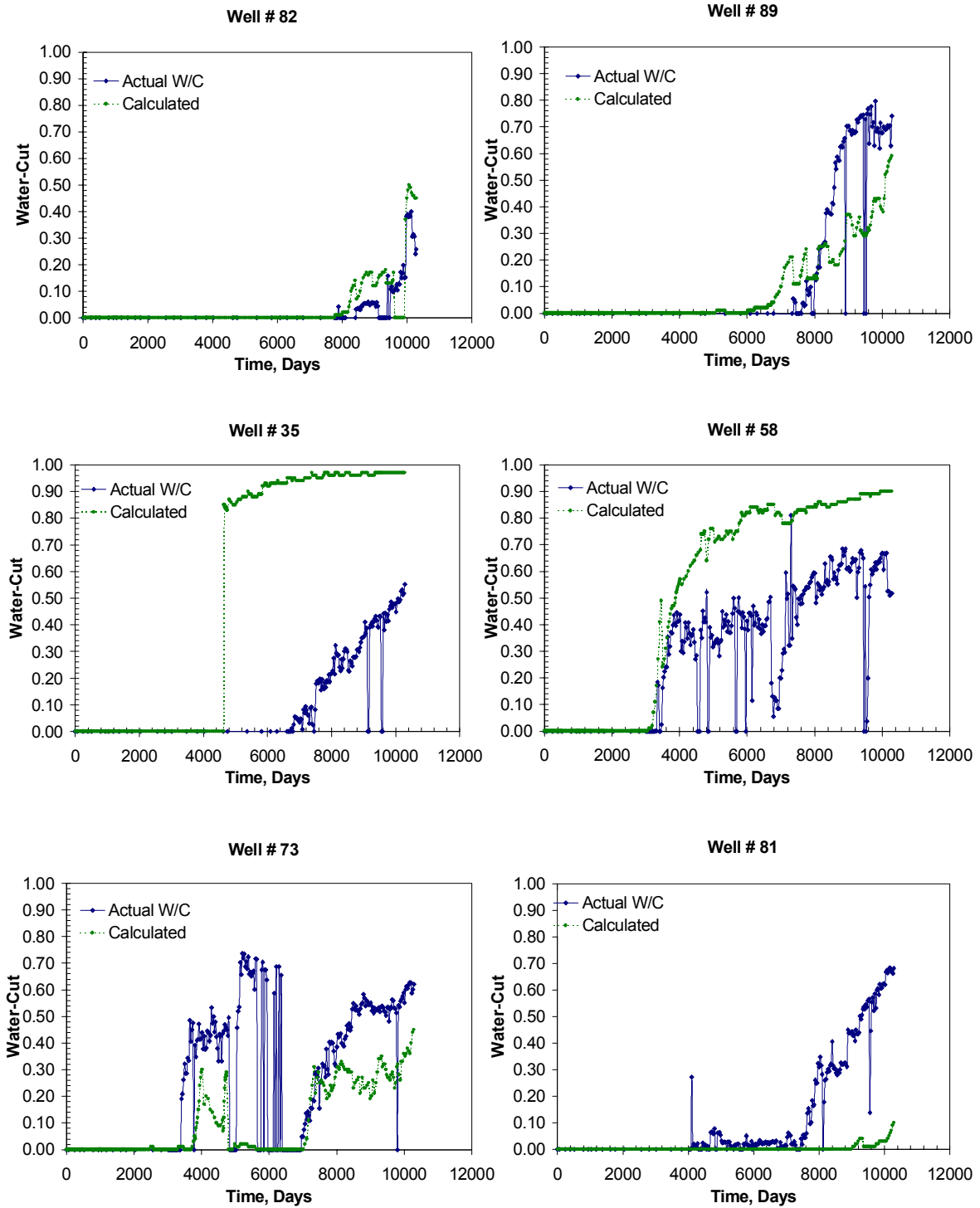


Figure 3.36 Continued.

entrapped into numerous local minima in the objective function. Thus proper parameterization based on data resolution greatly facilitates the inversion performance to circumvent the problem associated with the ill-posed nature of the inverse problem and the difficulties with the existence of local minima.

In this section, we performed a direct fine scale inversion with initial fine scale geologic model. In that case, to speed up inversion, we did not take into account for gravity effect during streamline simulation. **Fig. 3.37** indicates the progressive travel time misfits reduction at different iterations. The water cut matches at individual wells are shown in **Fig. 3.38**. **Fig. 3.39** shows the changes of permeability form the initial model.

The computation time for this example with 0.95 million grid cells and 34 pressure updates was about 20 hours in a PC, even if we ignore the gravity effect in the forward model. **Table 3.1** summarizes overall CPU time consumption of the two approaches.

3.5 Statistics after Inversion

We examined the impact of inversion on the permeability distribution by comparing the statistics of the initial and the inverted permeability fields. As indicated in **Fig. 3.40**, the histograms of both the models are almost identical in terms of the median and the upper and the lower quantiles of permeability. In other words, the shape of the distribution has essentially remained unchanged. The mean permeability, however, is slightly higher. This is primarily because integration of production data has resulted in flow channels and preferential flow paths with high permeabilities. Note that our dynamic data integration approach is designed to preserve the prior geologic model. Thus, some of the high permeabilities (of the order of 30000 md) in the original geologic model are also present in the final model.

3.6 Comparison with Eclipse

Streamline models offer an efficient means for flow simulation and dynamic data integration to high-resolution geologic models. However, such models are not a substitute for full physics of reservoir. To maintain the reasonable balance between computational efficiency and the modeling of physical processes, in this study we used a streamline model including gravity, compressibility of fluids, and aquifer flux with PV multipliers. As a final step we compared our

streamline simulation results with a commercial numerical simulator (ECLIPSE). **Figure 3.41** shows water cut responses from the inverted permeability field using the streamline model and

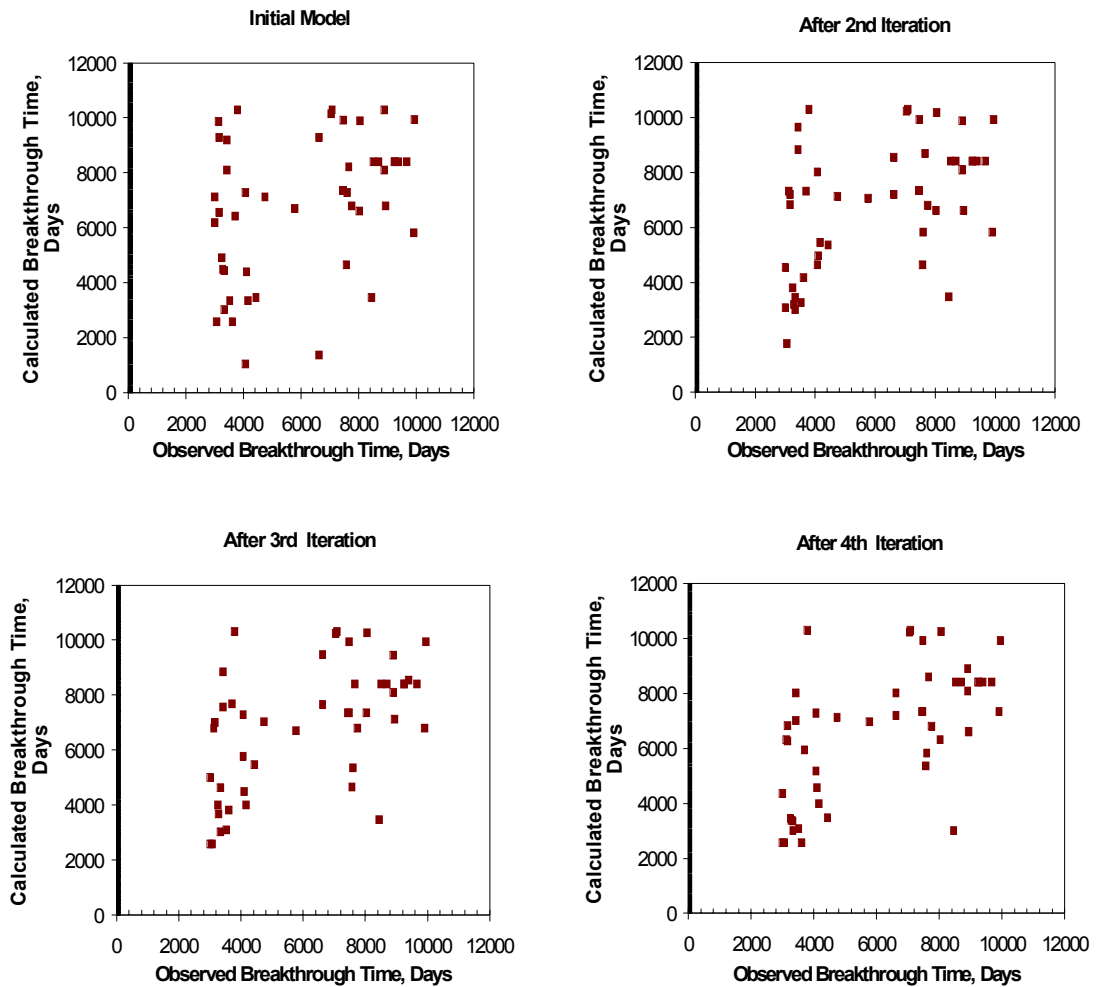


Figure 3.37 - Travel Time Match at Four Different Iterations for Direct Integration.

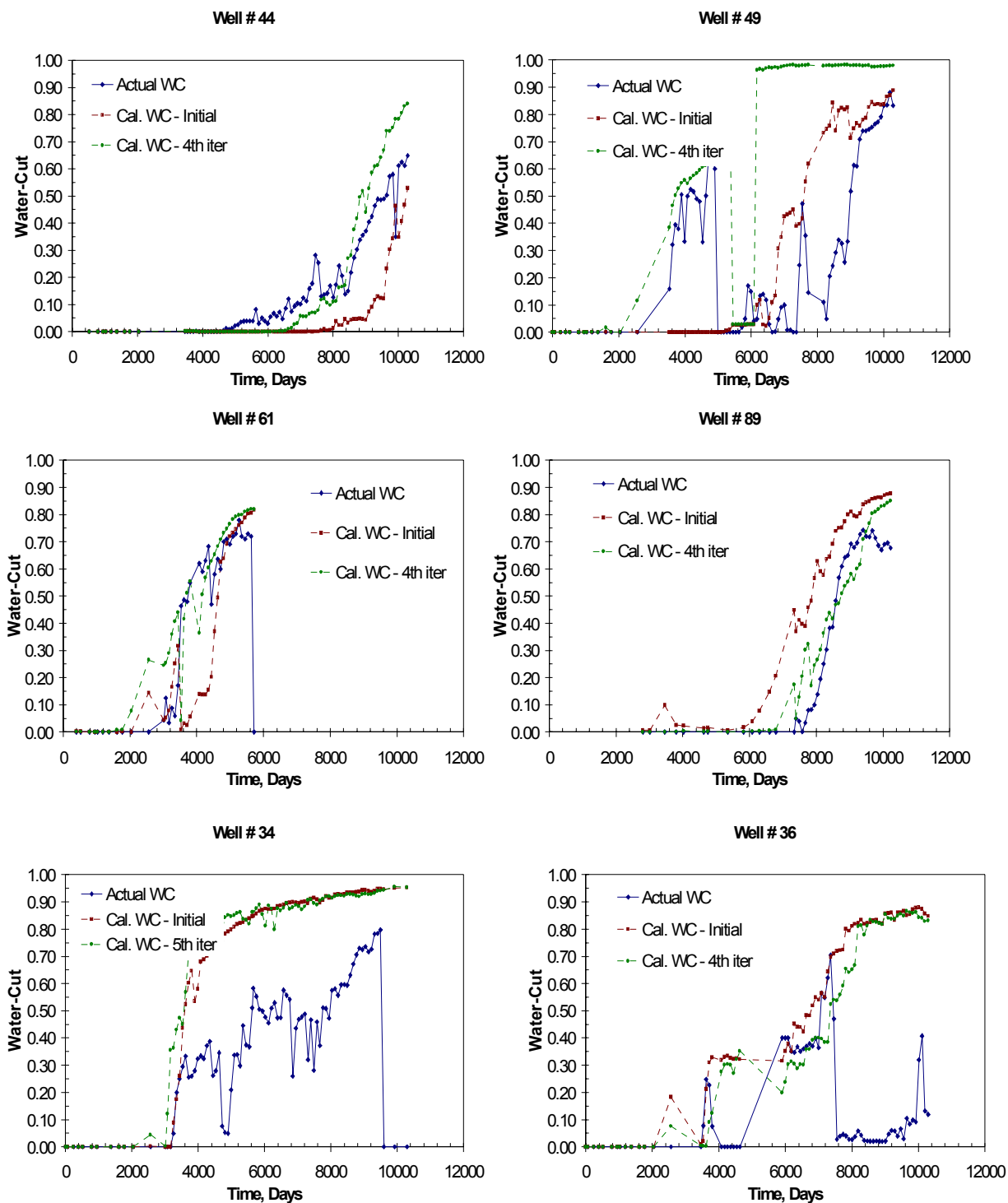


Figure 3.38 - Examples of Water Cut Matches from Direct Fine Scale Integration.

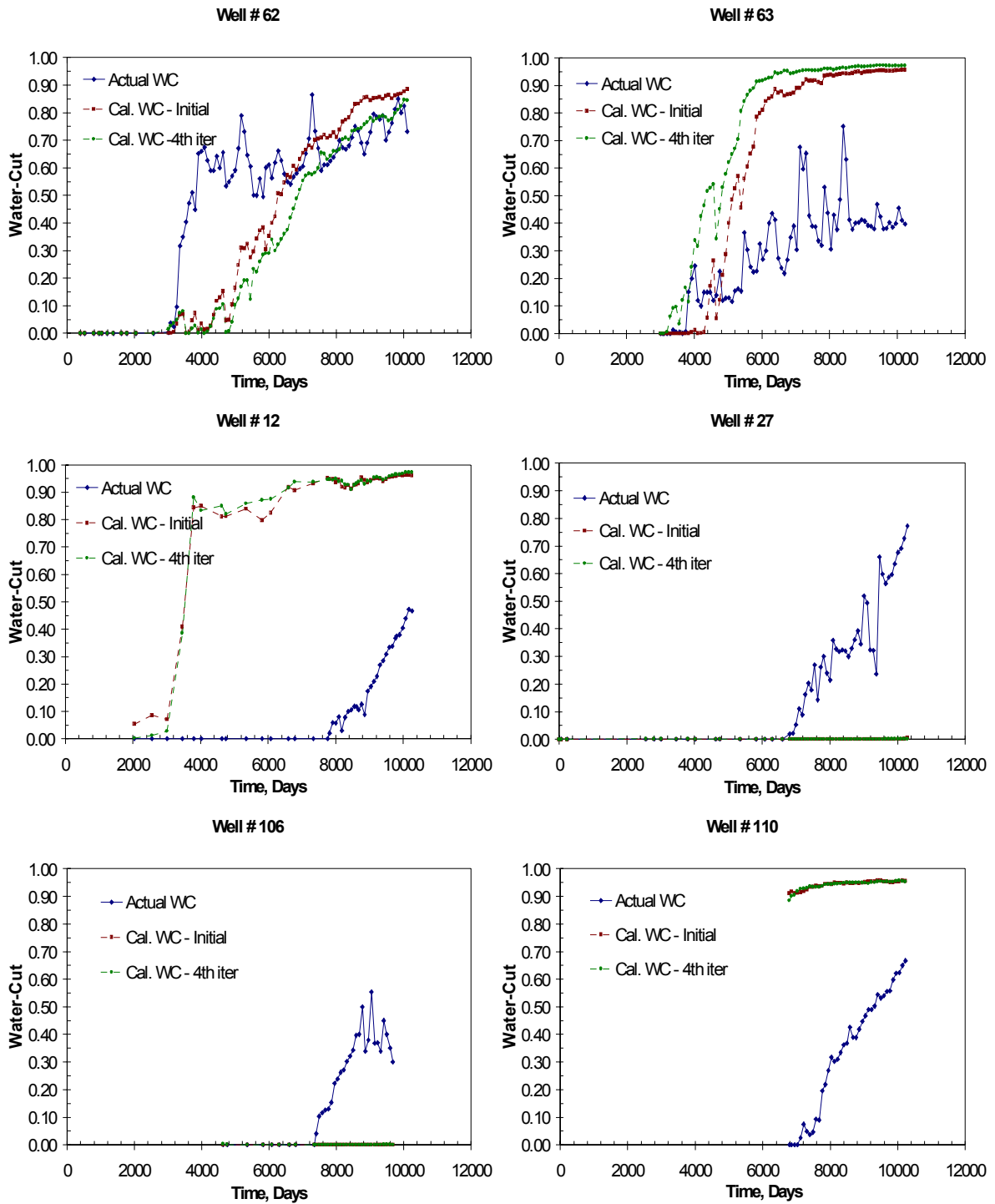


Figure 3.38 Continued.

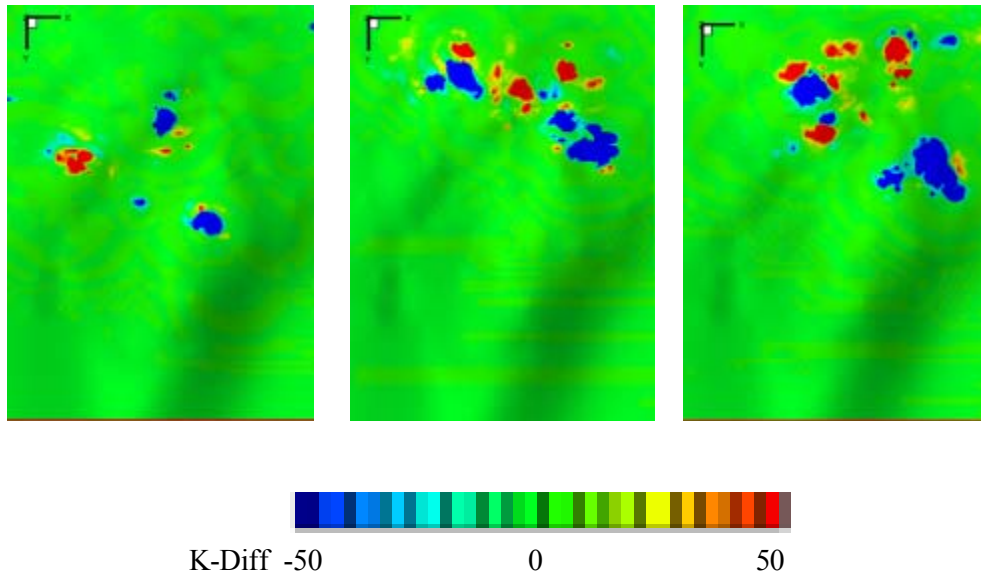
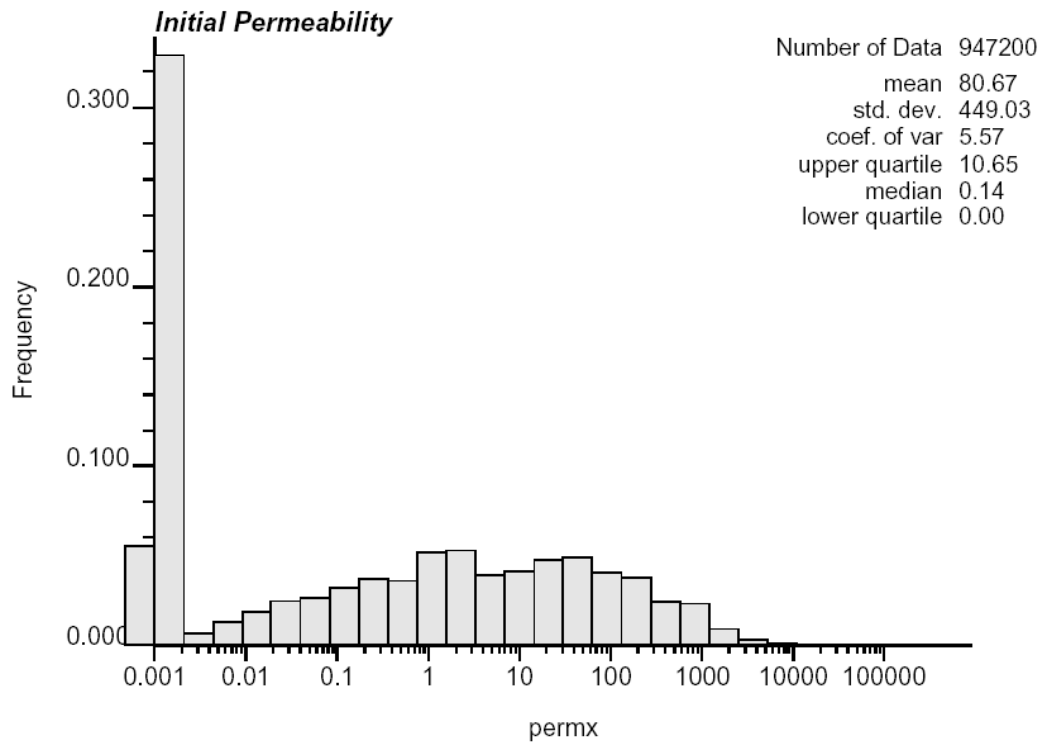


Figure 3.39 - Change in Permeability (md) for Direct Fine Scale Integration for Layer 10, 50 and 70.

Table 3.1 – Comparison of CPU Time for Parameter Estimation.

Model	Case	CPU Time (Hrs)
Upscale	With Gravity	6.00
	Without Gravity	4.50
Fine Scale	Without Gravity	20.00



(a)

Figure 3.40 - Histogram of Two Models. (a) Initial Permeability Field and (b) Inverted Permeability Field. All Units of Permeability in md.

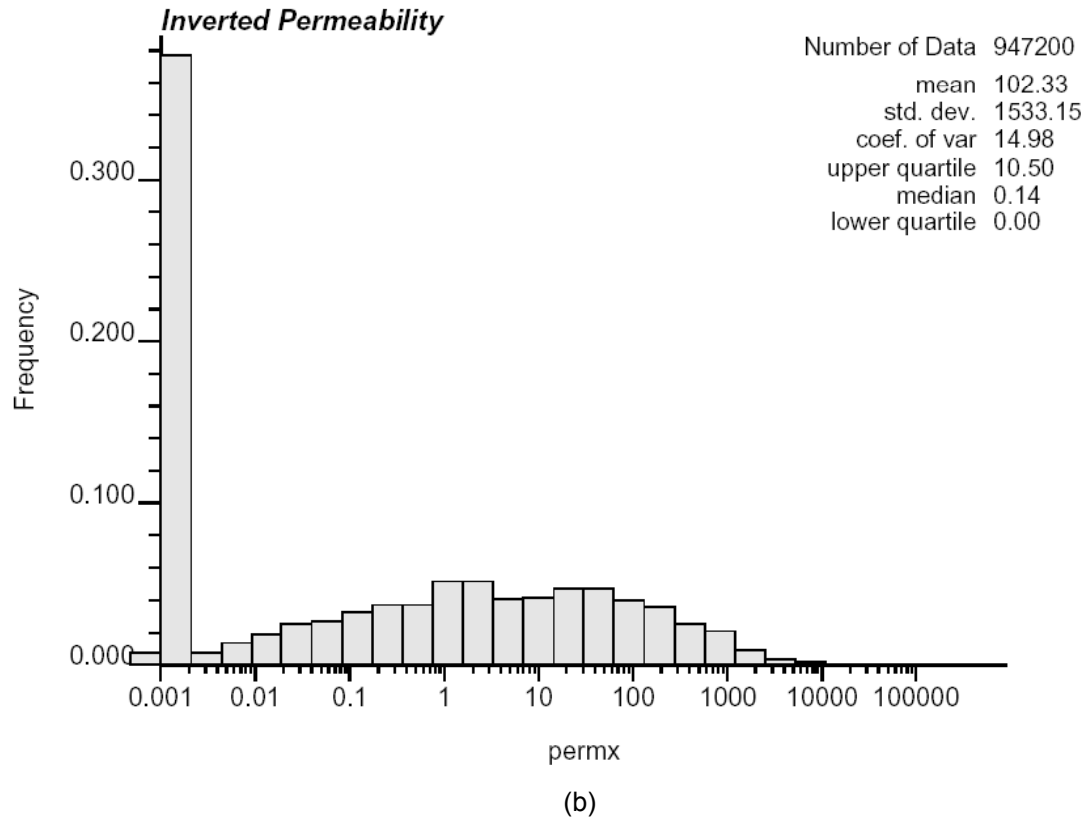


Figure 3.40 Continued.

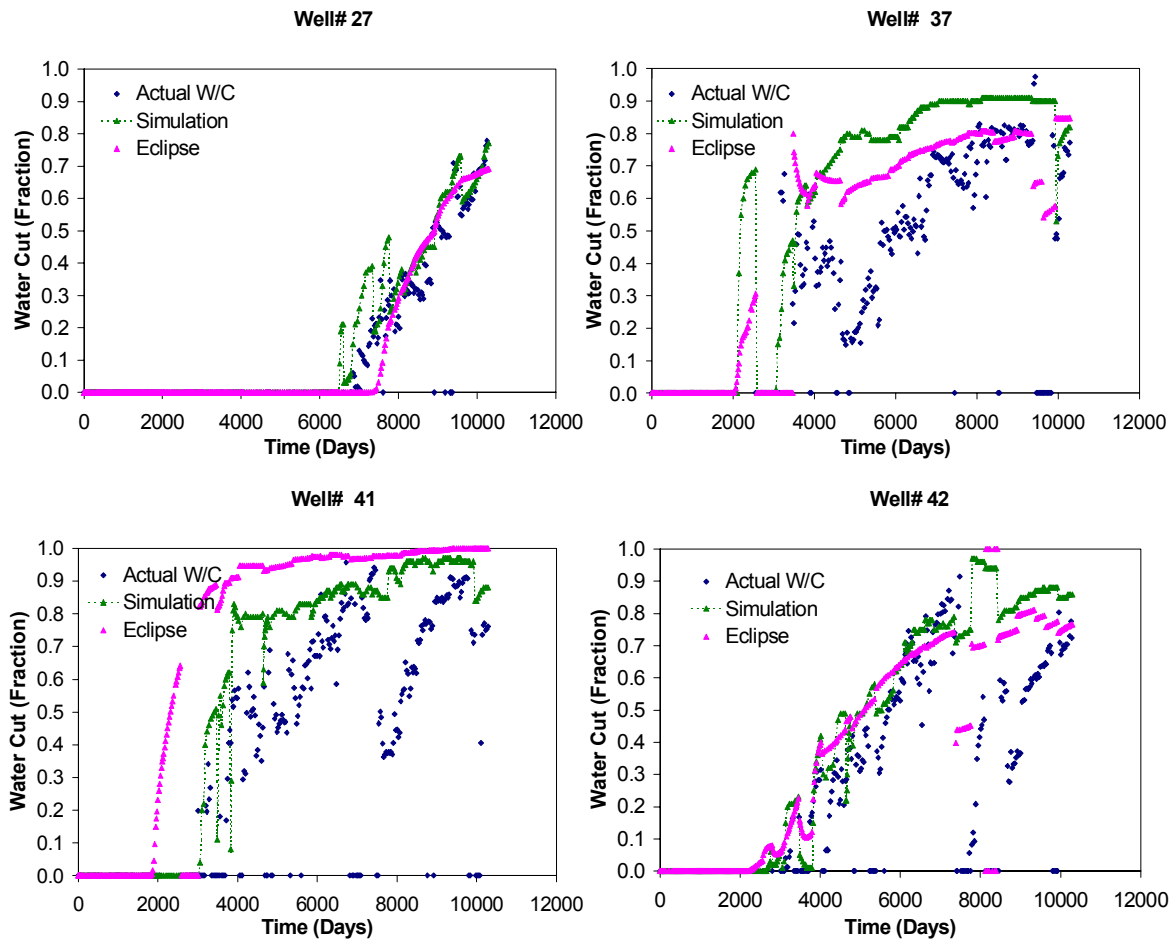


Figure 3.41 - Examples of Comparison of Water Cut Match with ECLIPSE.

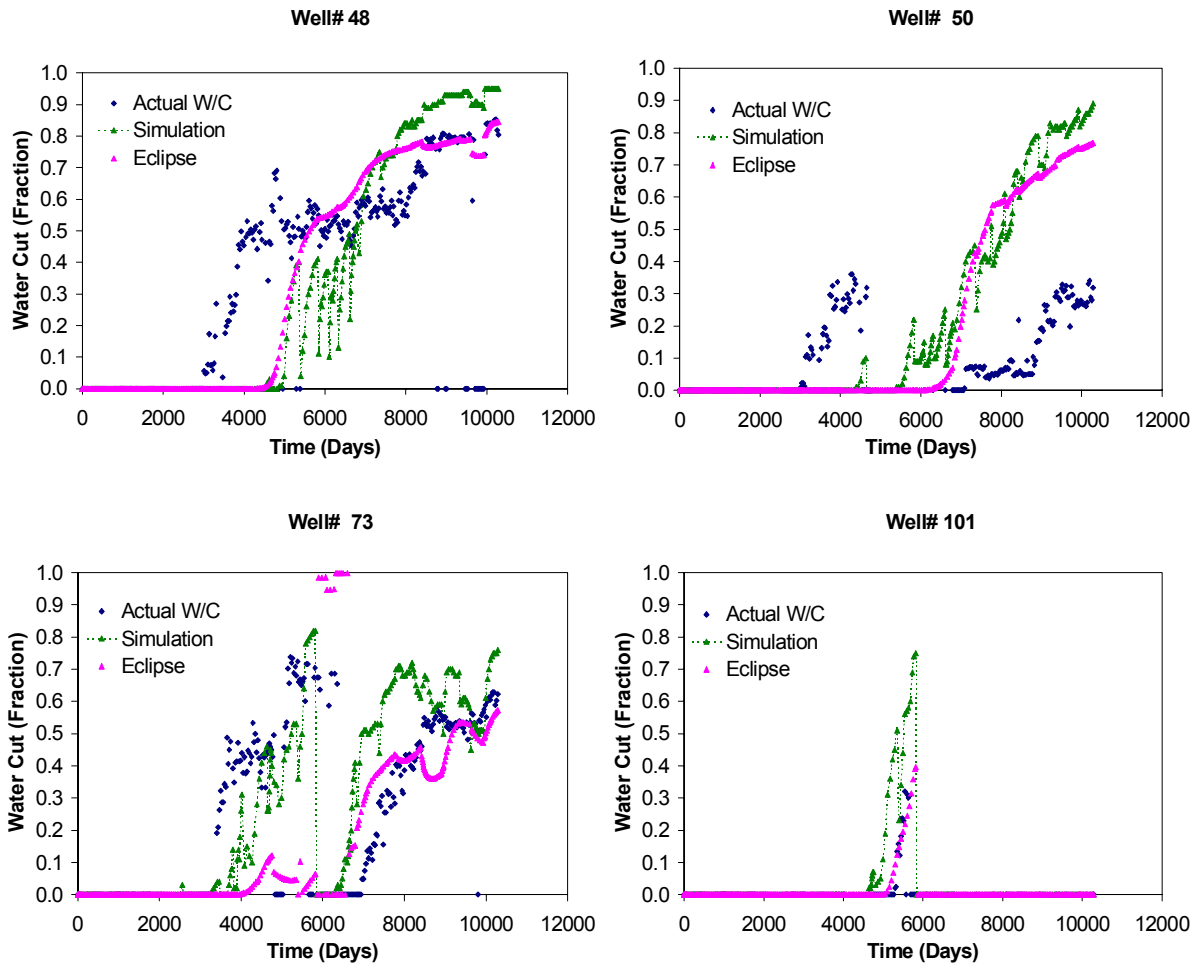


Figure 3.41 Continued.

Layer 2

Layer 6

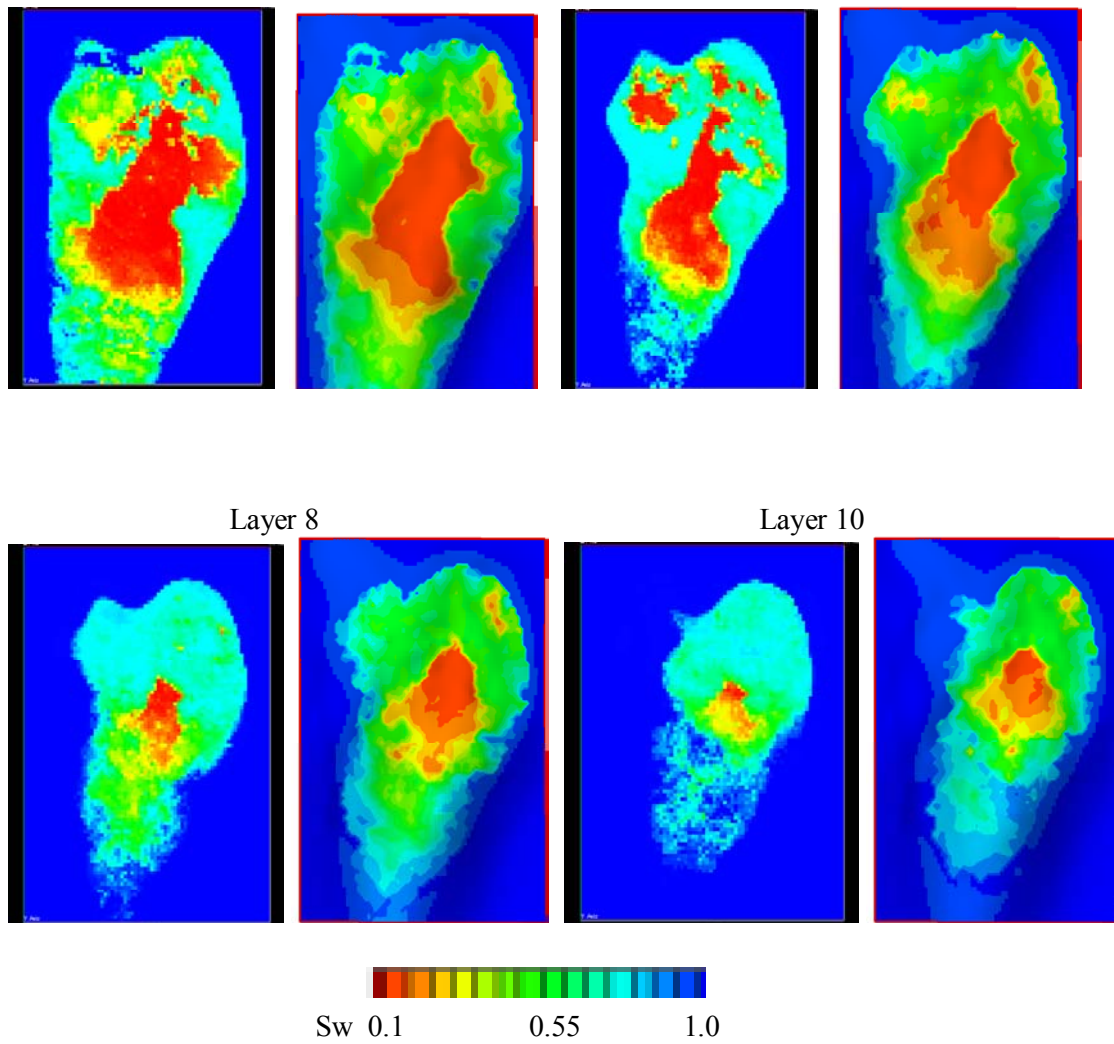


Figure 3.42 - Comparison of Water Saturation Distributions (10290 days) Estimated by ECLIPSE and Streamline Simulation with Initial Permeability.

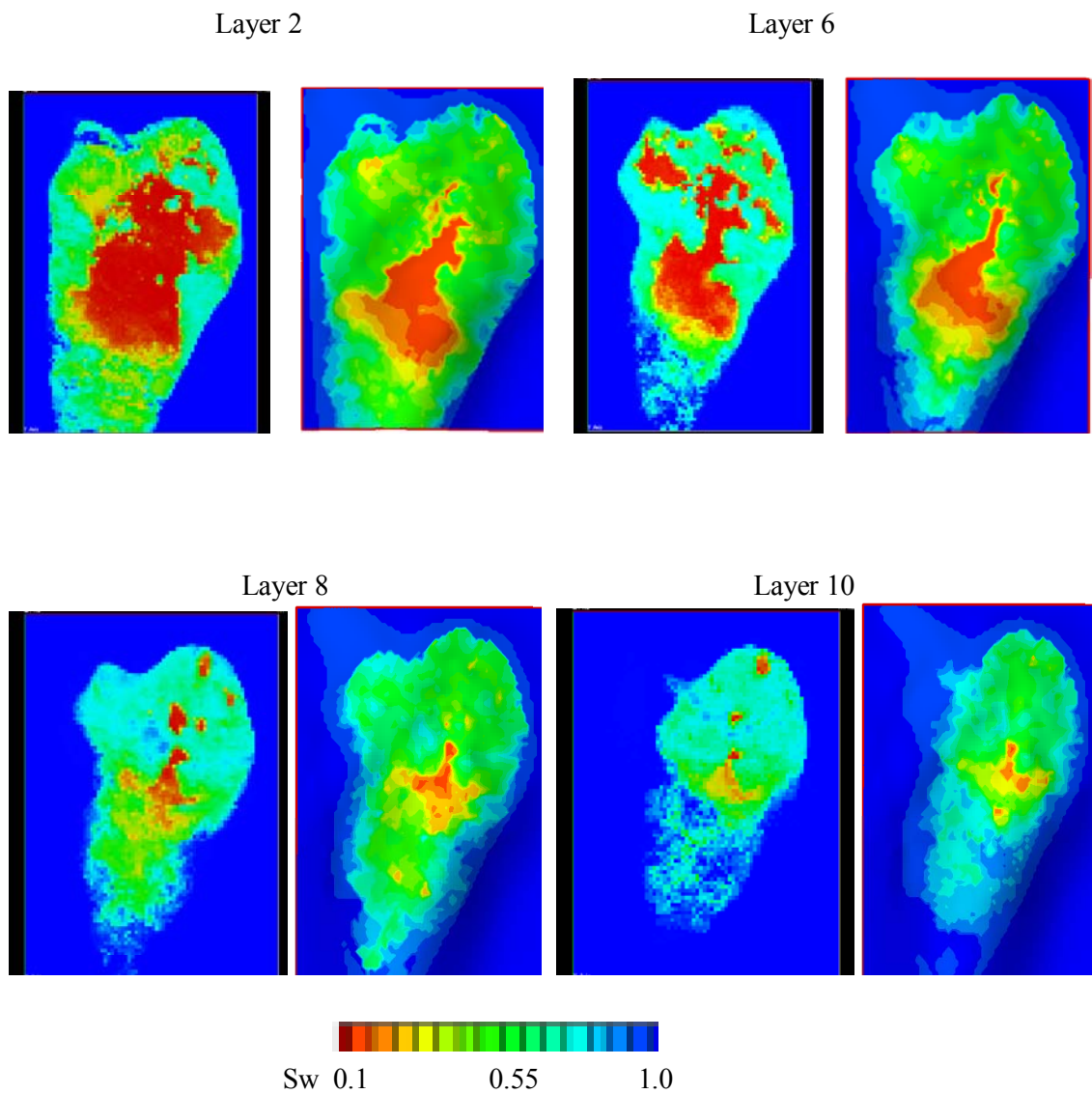


Figure 3.43 - Comparison of Water Saturation Distributions (10290 days) Estimated by ECLIPSE and Streamline Simulation with Inverted Permeability.

the ECLIPSE. For comparison purposes, we have also superimposed the field data on this plot. Overall, we see a reasonable agreement between the streamline results, ECLIPSE results and the field data. Note that for some of the wells there are differences between the streamline and ECLIPSE results. In particular, the ECLIPSE time-step is limited by the CFL criterion and thus some of the results tend to show instability in water-cut for some of the wells. Also, unlike the streamline simulator, the ECLIPSE results will also be impacted by numerical dispersion and this causes the water breakthrough to occur earlier in some cases compared to the streamline simulator. **Figs. 3.42** and **3.43** compare the water-saturation distribution for various layers in the initial and final permeability distribution from the streamline simulator and the ECLIPSE. Again, there seems to be a general agreement in the overall trend in the saturation distribution from both the models.

3.7 Chapter Summary

We have proposed a two-step approach to production data integration into high-resolution geologic models. The approach has been successfully applied to giant middle eastern reservoir. Our approach is very general and can account for gravity and changing field conditions such as rate changes, infill drilling and reperfurations via pressure updating. Also we have accounted for rock and fluid compressibilities as well as aquifer expansion during streamline simulation. To our knowledge, this is the first time streamline-based production data integration has been carried out under such general conditions. In this field application, almost 70% of the wells showed significant improvement in the water-cut matches. An examination of the saturation distribution in the reservoir from the simulation indicated that our results are consistent with the field surveillance data and appear to represent the gross fluid movement in the reservoir. Finally, a comparison of the streamline model with a commercial numerical simulator (ECLIPSE) showed that the water-cut matches are preserved during the full-physics numerical simulation.

Some specific findings from this study can be summarized as follows:

1. The proposed approach has accounted for the detailed rate schedule to account for infill drilling, reperfurations and significant rate changes using 34 pressure updates.
2. Gravity effects have been included in the modeling and appear to have a significant impact on the results.

3. Compressibility and aquifer influx were incorporated in order to obtain pressure history consistent with the field observations.
4. The two-step approach (upscaling-downscaling) appears to be robust, computationally efficient (about 6 hrs in a PC) and result in significant improvement in the production history match.
5. Almost all (about 90%) of the wells showed improvement in the breakthrough time matches.
6. About 70% of the wells exhibited good to moderate matches in the overall production history.
7. An examination of the permeability changes appears to indicate that most of the dominant trends are along the 'good' facies. This is geologically consistent and appears to confirm prior observations.
8. The permeability model derived from the production data integration should significantly reduce the cycle time for detailed full-physics history matching.
9. The wells that did not show improvements in matching appear to be the ones with incomplete or inconsistent data.
10. Further improvements in matching can also be obtained by adjusting the relative permeability curves (not attempted here).

CHAPTER IV

ASSISTED HISTORY MATCHING

4.1 Introduction

This chapter discusses the development and implementation of a new assisted history matching technique which combines the efficient sensitivity computing procedure using streamline simulator with the generality of a finite difference simulator. Some of the previous assisted history matching procedures using conventional simulator as forward model makes use of manual adjustment of parameters to obtain history match. However, the present procedure makes use of an automated routine to combine the sensitivity calculations along a streamline with the pressure and saturation derived from a finite difference simulator. This approach makes the history matching procedure more robust, general and at the same time computationally efficient.

4.2 Methodology

This proposed method for assisted history matching makes use of the efficiencies of both streamline based sensitivity computation and the ability to include detailed physics in finite difference simulation techniques. The basic philosophy of the production data integration remains the same, as discussed in Chapter II.

Streamline based flow simulation technique follows an IMPES (**IM**PLICIT **P**RESSURE **E**XPlicit **S**ATURATION) scheme. After obtaining the pressure solution, velocity for fluid phases in all coordinate directions are computed. Then the total phase velocity is used to trace the trajectory of a streamline. In the present method, instead of solving for pressure in the streamline simulator itself, we use a commercially available finite difference simulator to obtain the pressure and flux distribution at the start of each time step (which corresponds to every pressure update in the streamline simulator). This pressure field from the finite difference simulator is then used as input into the streamline simulator. In particular, fluid fluxes obtained from the finite difference simulator is converted to total phase velocity and is used to trace the trajectory of a streamline. Time of flight calculations along the streamline trajectory are carried out in the same manner based on the algorithm proposed by Datta-Gupta and King⁸.

A working flowchart of the process is presented in the **Fig. 4.1**

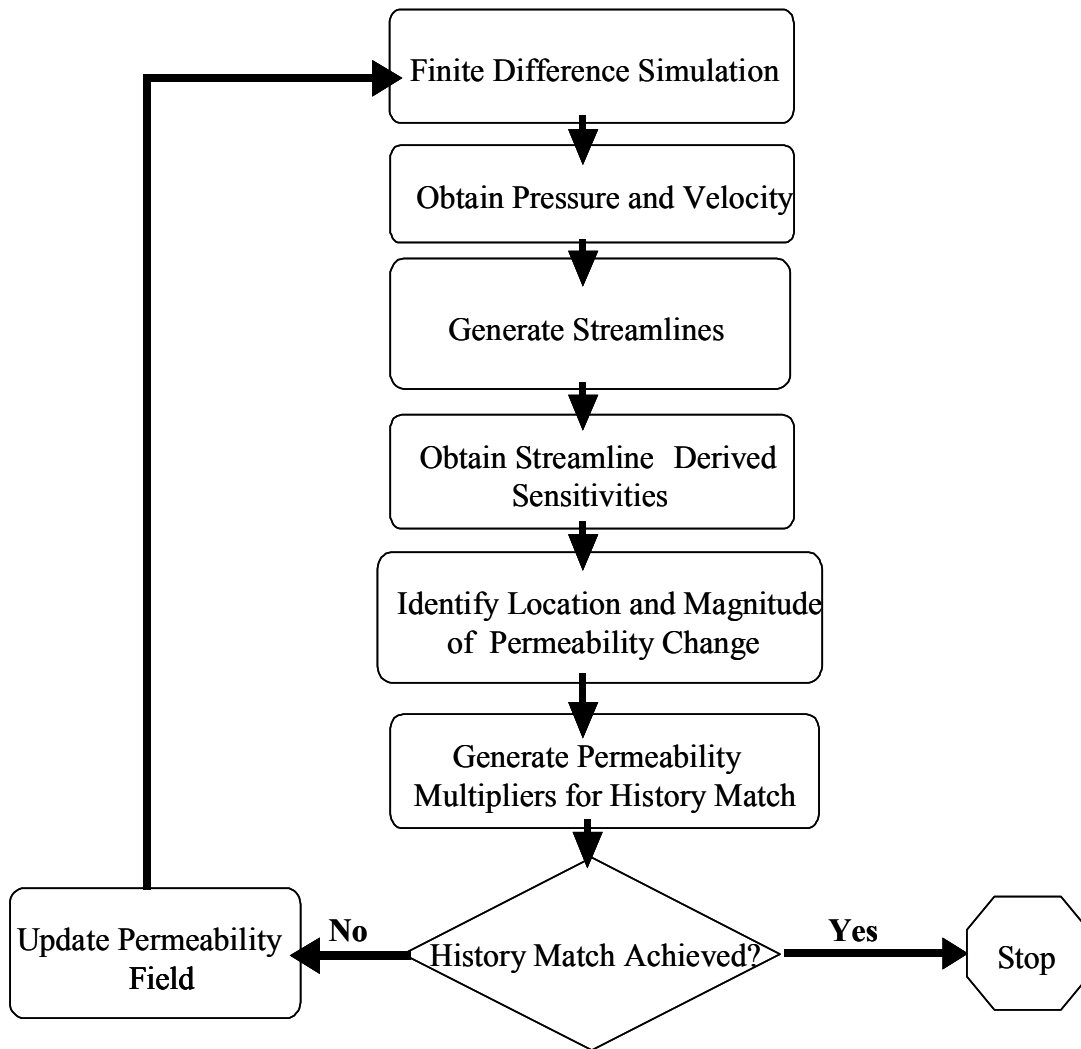


Figure 4.1 - Flowchart for Assisted History Matching.

There are two ways that the information from the finite difference simulator could be used for computation of the sensitivities.

1. The water saturation from the finite difference simulator (obtained at the same time step as pressure and flux) can be mapped onto the streamlines. We calculate the saturation propagation along the streamline to obtain production response at the wells. This procedure uses the finite difference saturation field, but computes the saturation propagation and water cut sensitivities along the streamline with streamline formulations.
2. We can use both water saturation and production response (water cut information) from the finite difference simulator. We can then use these information for water cut sensitivity calculations.

In the above procedure, it should be noted that to obtain the pressure, saturation and flux information from finite difference simulator at the start of each time period (corresponding to each streamline pressure update) for entire simulation time requires only one finite difference simulation in each iteration. The information written out from the finite difference simulation could be done in a very systematic manner so that it can be easily read from the streamline simulator.

Once the sensitivities are computed, the production data integration is carried out via inverse modeling as discussed in Chapter II. The iterative inversion algorithm generates permeability multipliers which are used to modify the initial geologic model.

4.2.1 Comparison of Velocity Fields

As a first step to use the information from finite difference simulator into the streamline technique, comparison of the velocity fields was derived from finite difference and the streamline simulator carried out.

1. A 21 x 21 synthetic example for a 5 spot pattern was used to generate the velocity fields in x-direction from both streamline and finite difference simulators. **Fig. 4.2** shows the velocity fields for both simulation techniques. It could be observed that both velocity fields are very similar in magnitude.
2. Velocity fields in x-direction were generated for the North Robertson Unit field example. NRU has 27 producers and 15 injectors and the details for the field can be

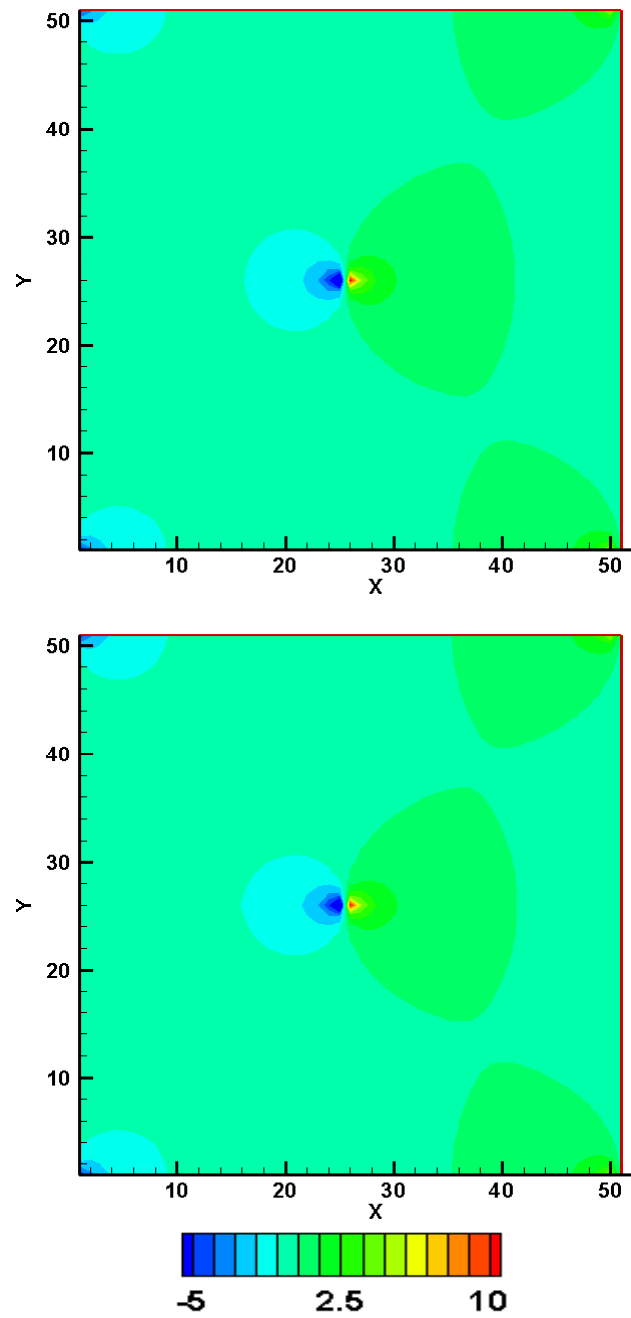


Figure 4.2 - Velocity Comparison for the Synthetic Example. On the Top is from Streamline Simulator, On the Bottom is from Eclipse.

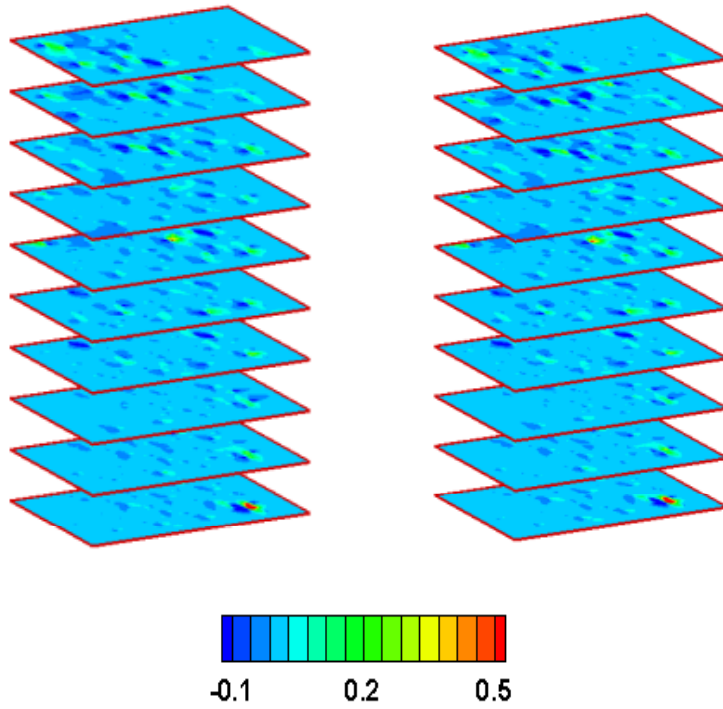
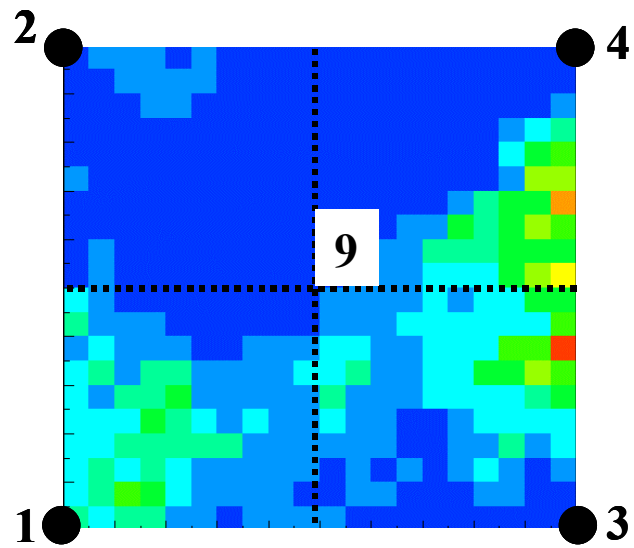
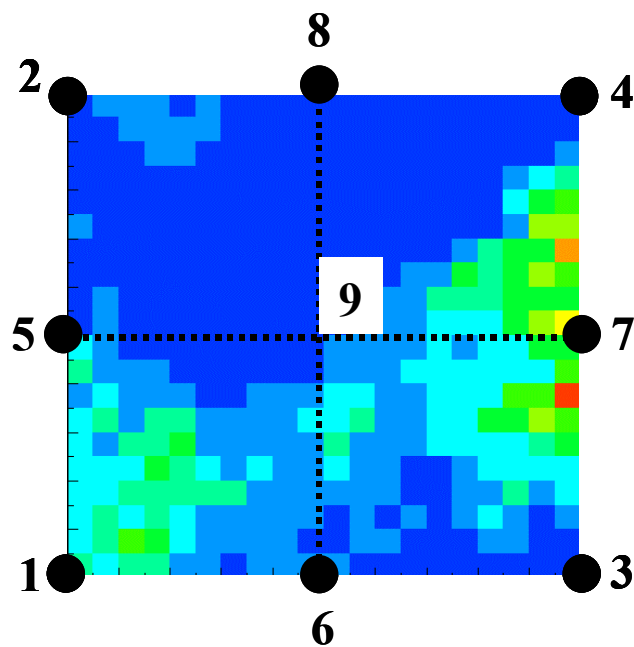


Figure 4.3 - Velocity Comparison for NRU Field Example. On the Top is from Streamline Simulator, On the Bottom is from Eclipse.



(a) before Infill



(b) after Infill

Figure 4.4 - Well Pattern and Reference Permeability Field for the Synthetic Example. Well # 9 is Injection Well.

found in the Pedibholta *et al.*¹² **Fig. 4.3** shows the velocity fields for both simulation techniques. It could be observed that both velocity fields are very similar in magnitude.

Changing velocity conditions arising from rate changes or infill drilling are accounted for in the usual manner, i.e., via pressure updating followed by regeneration of the streamlines and reinitialization of the saturations along the streamlines.

4.3 Assisted History Matching : A Synthetic Example with Infill Wells

This example consists of a mesh size of 21x21x1 with a total of 441 grid cells. Four infill wells introduced after initial 300 days of production. **Fig. 4.4** shows that reference permeability field and well locations. We used uniform initial permeability field for the assisted history matching purpose.

We carried out assisted history match for 600 days to reproduce the water cut response from the reference model. The assisted history match approach included the integration of water cut data obtained from ECLIPSE run. Water cut response match obtained from the initial model and final model are presented in **Fig. 4.5**. As one might expect, there is significant improvement in the match compared to the initial model. Initial and final permeability multipliers are presented in **Fig. 4.6**. It can be observed that there is maximum variation in permeability multipliers after first iteration. **Fig. 4.7** shows reference and the final permeability field which clearly indicates that use of information from finite difference simulator contributes to significant improvement in the final match of the water cut responses.

Fig. 4.8 shows the initial and final travel time match for the above case and **Fig. 4.9** shows the reduction in errors vs. iterations. It can be observed that the reduction in error vs. iteration for assisted history matching is very rapid with most of the reduction taking place in the first 6 iterations.

4.4 Assisted History Matching : Field Applications

4.4.1 Goldsmith Field Example

We applied our approach to water flooding in a CO₂ pilot project area in the Goldsmith San Andres Unit (GSAU), a dolomite formation located in west Texas. The pilot area consists of nine inverted 5-spot patterns covering around 320 acres with an average thickness of 100ft and has over 50 years of production history prior to CO₂ project initiation in Dec. 1996. **Fig. 4.10**

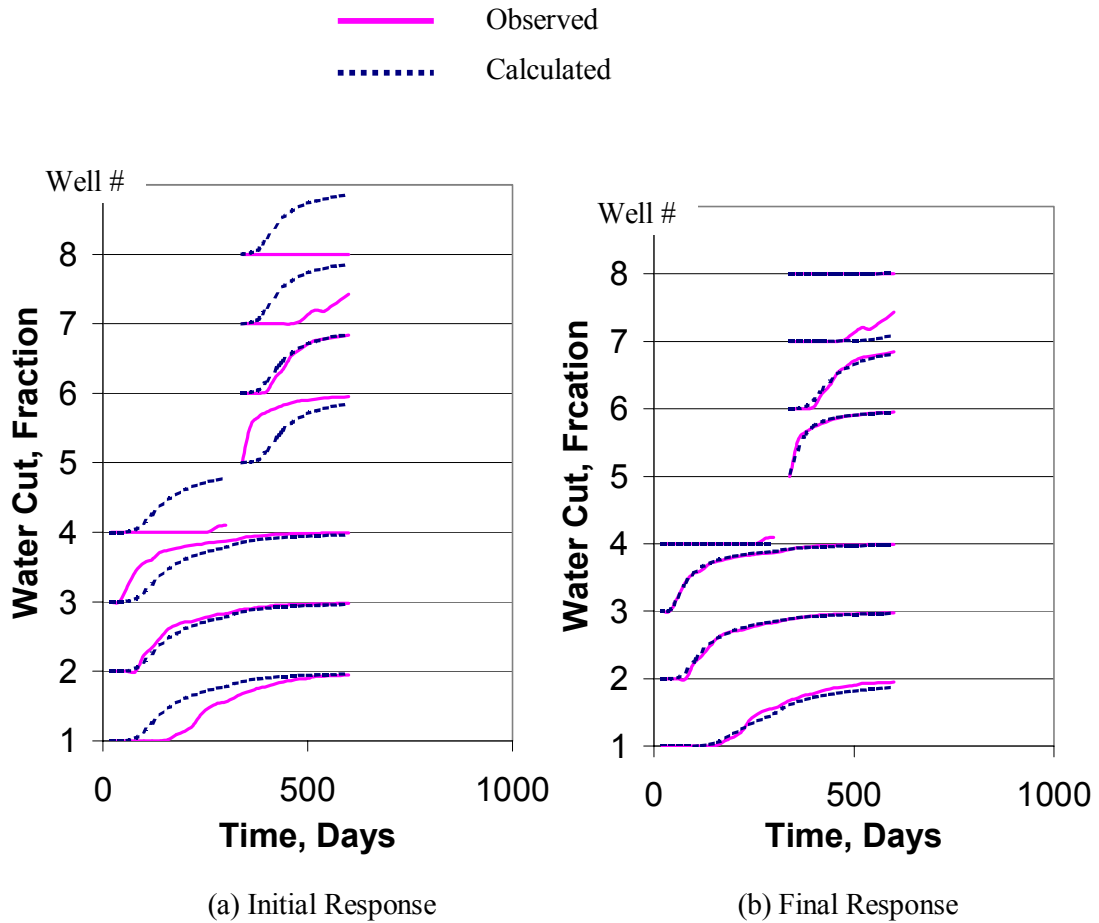


Figure 4.5 - Water Cut Response from Initial and Final Model for Synthetic Example.

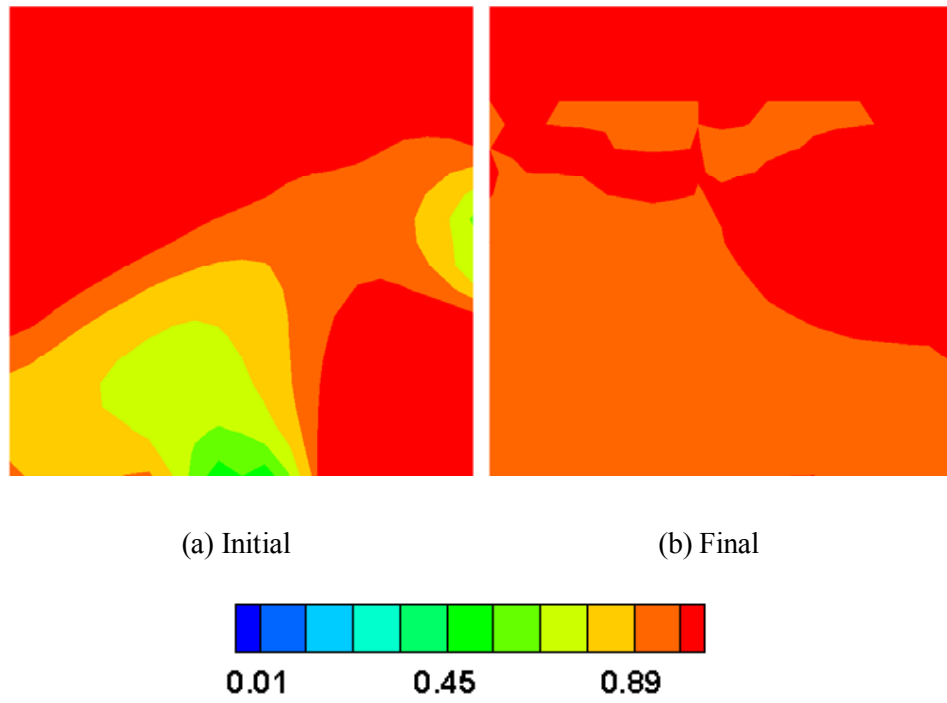


Figure 4.6 - Initial and Final Permeability Multipliers for the Synthetic Example.

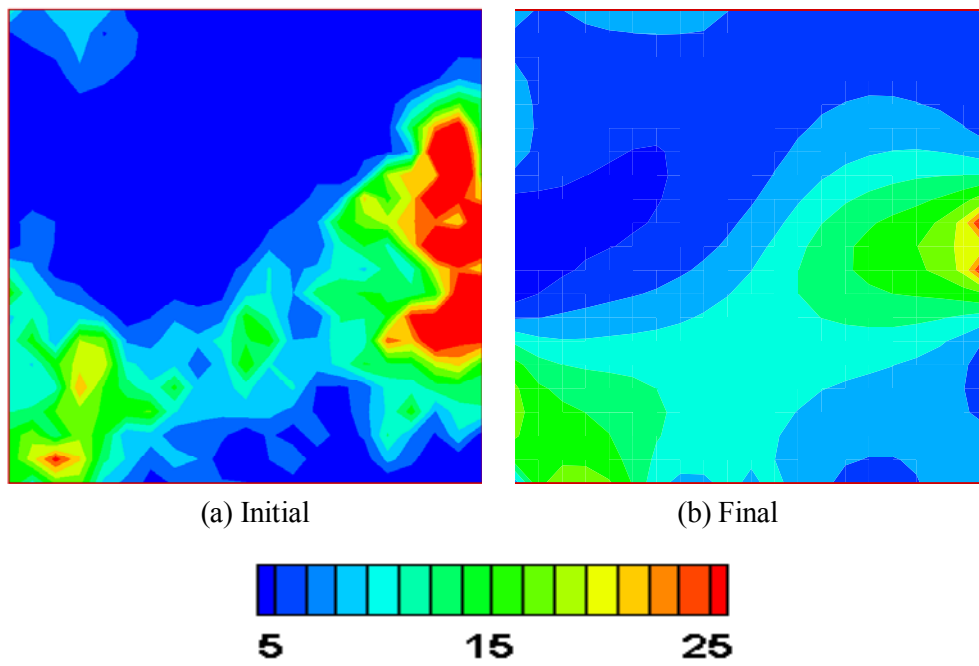


Figure 4.7 - Initial and Final Permeability Distribution for the Synthetic Example.

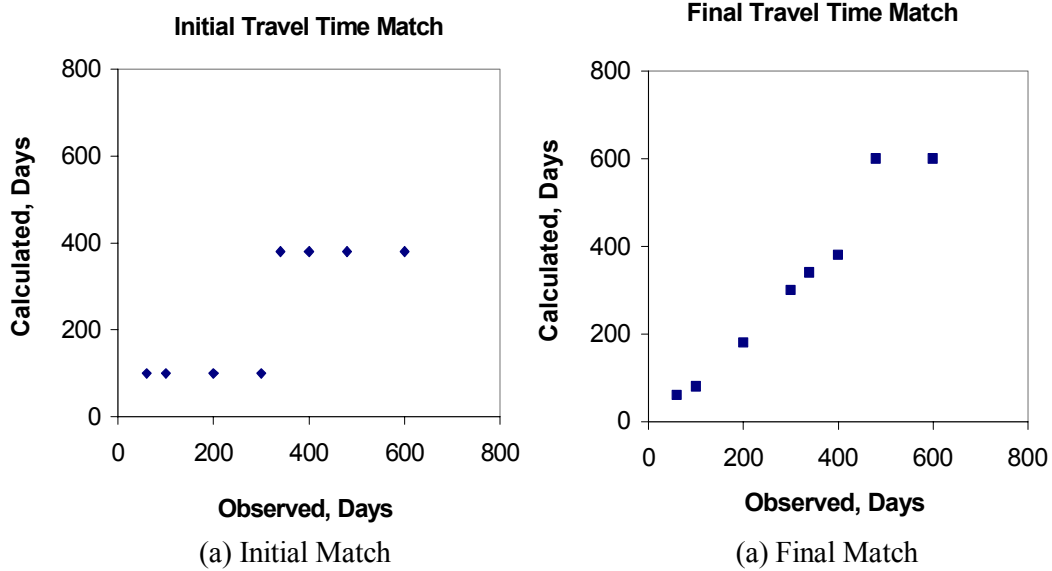


Figure 4.8 - Initial and Final Travel Time Match for the Synthetic Example.

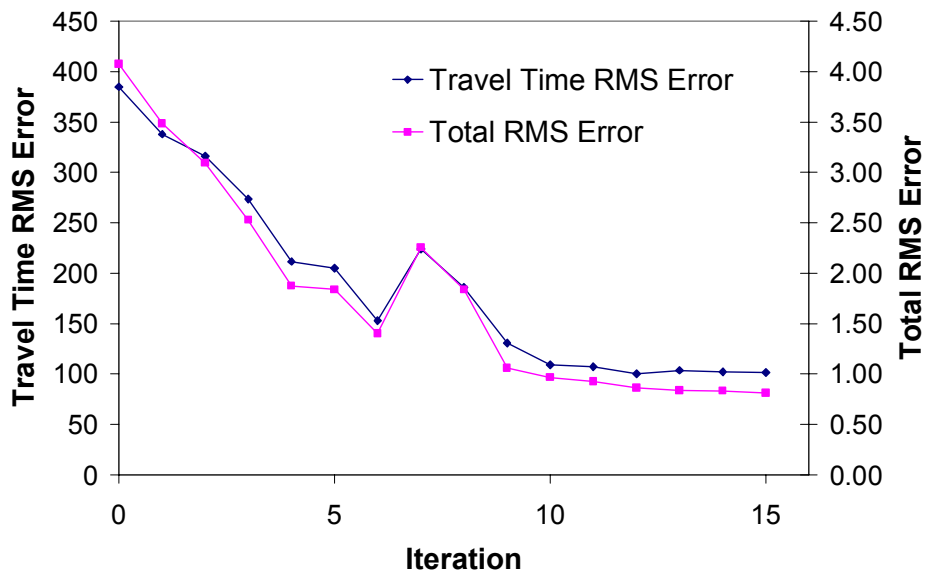


Figure 4.9 - Reduction in Travel Time RMS Error and Total RMS Error for Different Iterations for the Synthetic Example.

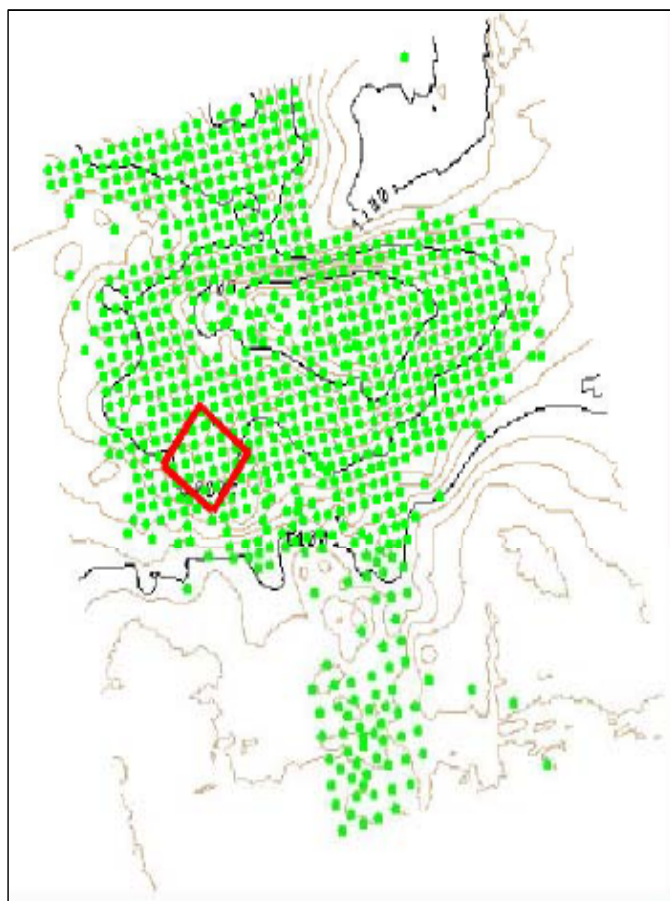


Figure 4.10 - Goldsmith Study Area.

shows the CO₂ pilot project site in the GSAU. Detailed well rates and well schedules have been presented by He *et al.*¹⁶. We performed a history matching for 20 years of waterflood prior to the initiation of CO₂ injection. Because of the practical difficulties in obtaining correct boundary conditions for the pilot area, extra wells located outside the pilot area were included in this study. The extended study area is included 11 water injectors and 31 producers. Among the producers within the study area, 9 wells showed significant water-cut response before the initiation of the CO₂ injection and are used for data integration. To account for the changing production rates and different starting times of the injection and production wells, 11 pressure updates were used in the simulation. The study area is discretized into 58x53x10 mesh or a total of 30,740 grid cells. The initial permeability field is generated via a cloud transform based on the porosity-permeability relationship (**Fig. 4.11(a)**). The porosity field, shown in **Fig. 4.14(b)**, is obtained by a Sequential Gaussian Simulation using the well log data and is not altered during the inversion.

We carried out assisted history match integrating 20 years of production response for the 9 producers for the period May 1968 to Dec. 1989. **Fig. 4.12** shows the water cut response obtained from initial and final model. Overall, we see a significant improvement in the production history match. **Fig. 4.13** shows initial and final perm multipliers. The final permeability field and the changes from the initial model are shown in **Fig. 4.14**. Notice that because of the ‘norm’ constraint in Eq.(2.18), the changes to the initial permeability model are kept to a minimum while matching the production history. This allows us to preserve the geologic realism during history matching. **Fig. 4.15** shows travel time misfit. **Fig. 4.16** shows the misfit versus the number of iterations during the inversion. For this field example with 31 producers, 11 injectors and 11 pressure updates, the computation time requirement was less than 2 hours in a PC.

4.4.2 Giant Middle Eastern Field Example

We successfully applied the assisted history matching technique to the large scale field case described in Chapter III. It should be noted that here we carried out two step inversion process where we first match the travel time and then match the production amplitude responses. Here we included gravity and compressibility along with influx from aquifer which is modeled by using pore volume multipliers along three sides of the reservoir. We considered the geological model shown in **Figs. 3.2 to 3.8** in Chapter III.

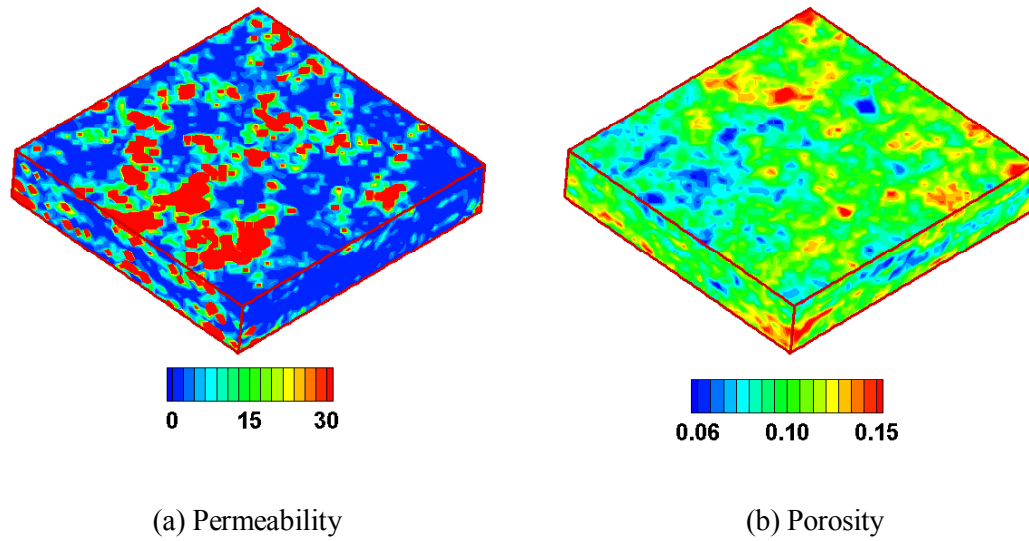


Figure 4.11 - Reference Permeability and Porosity Distribution for Goldsmith Field Example.

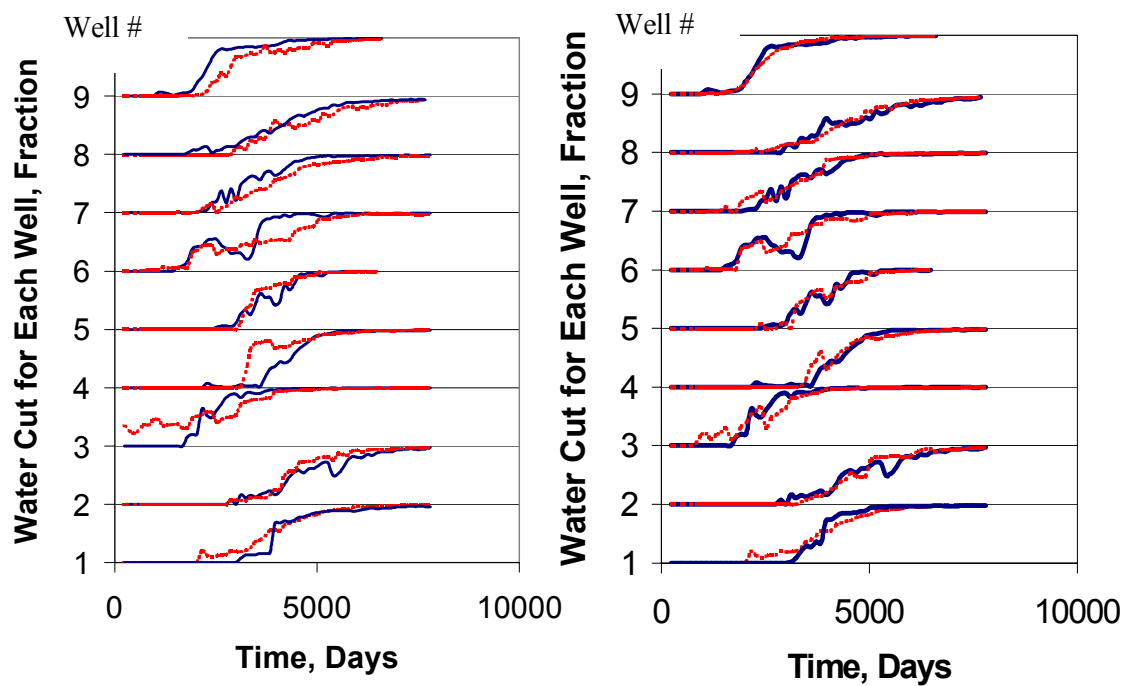


Figure 4.12 - Initial and Final Water Cut Matches for Goldsmith Field Example.

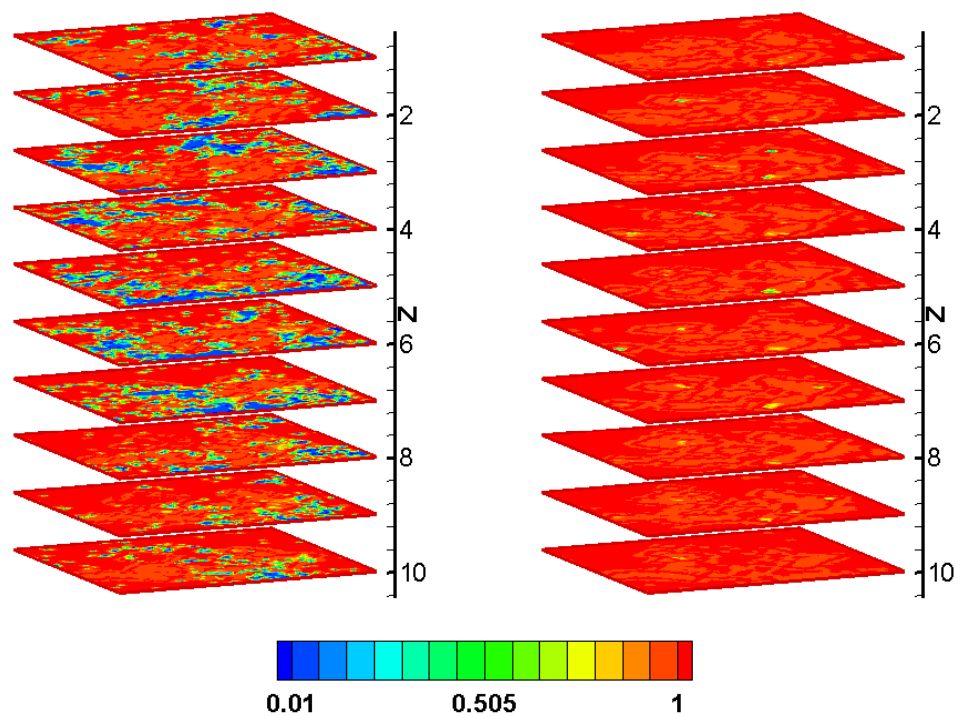


Figure 4.13 - Initial and Final Permeability Multipliers for Goldsmith Field Example.

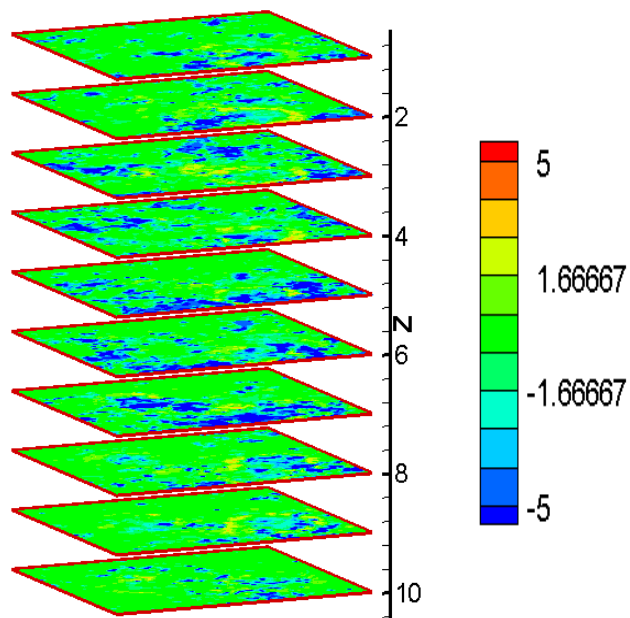
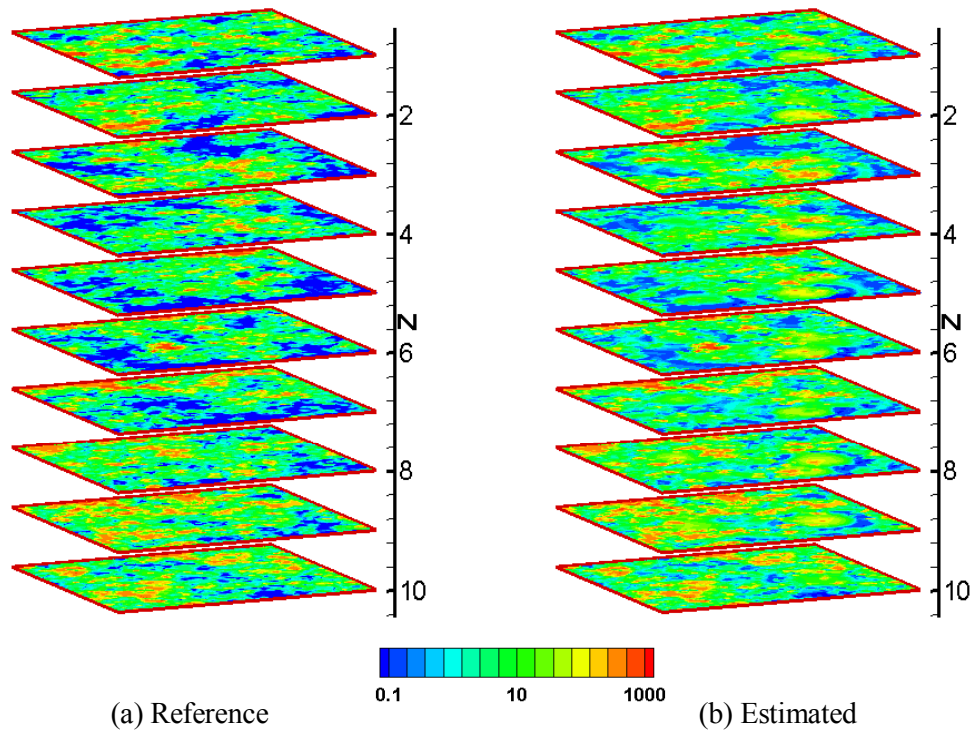


Figure 4.14 - Reference, Final and Change in Permeability for Goldsmith Field Example. All in Log Scale.

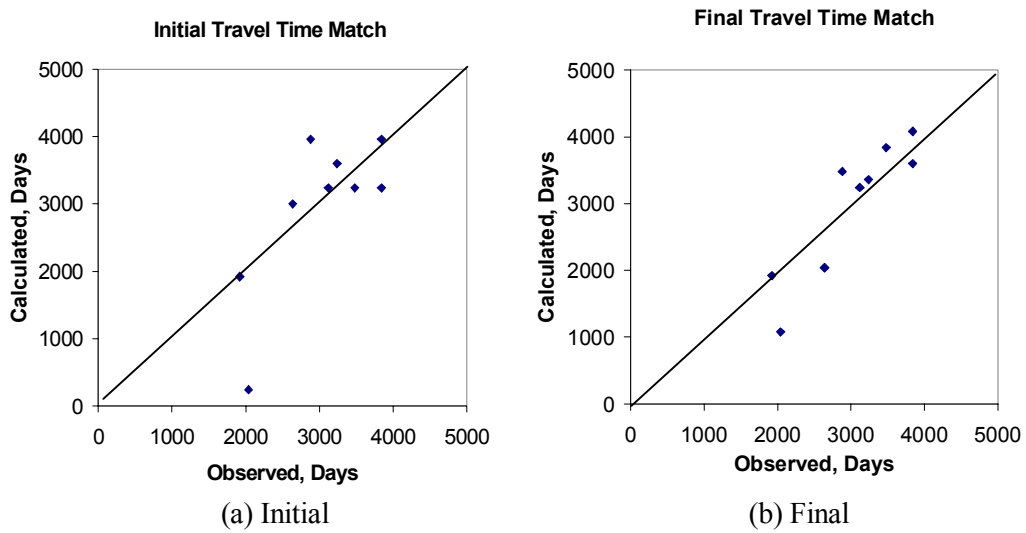


Figure 4.15 - Initial and Final Travel Time Match for Goldsmith Field Example.

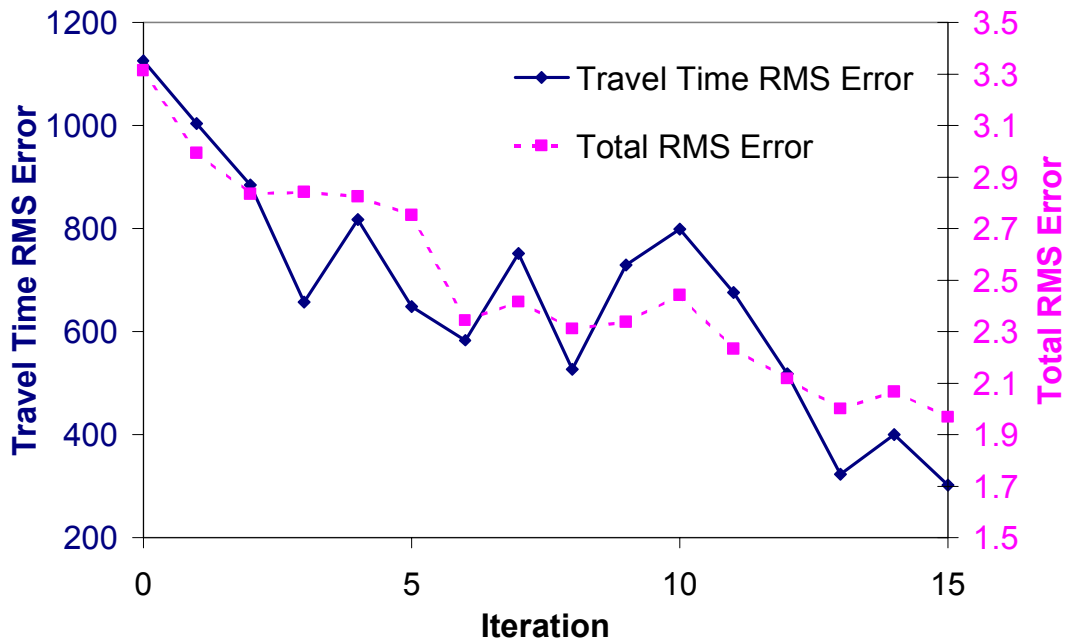
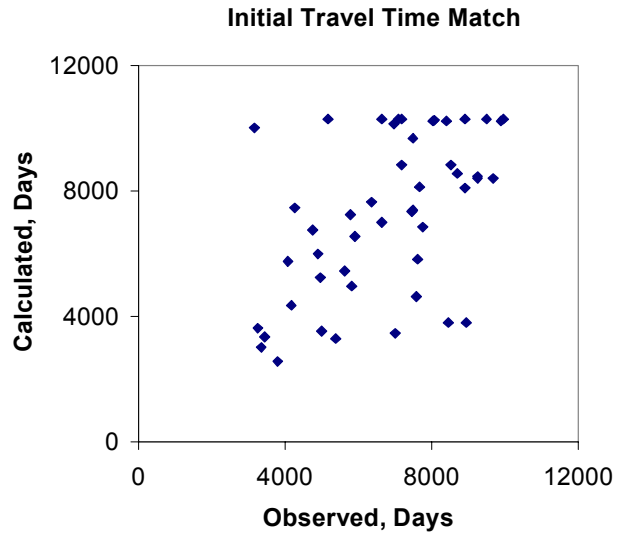
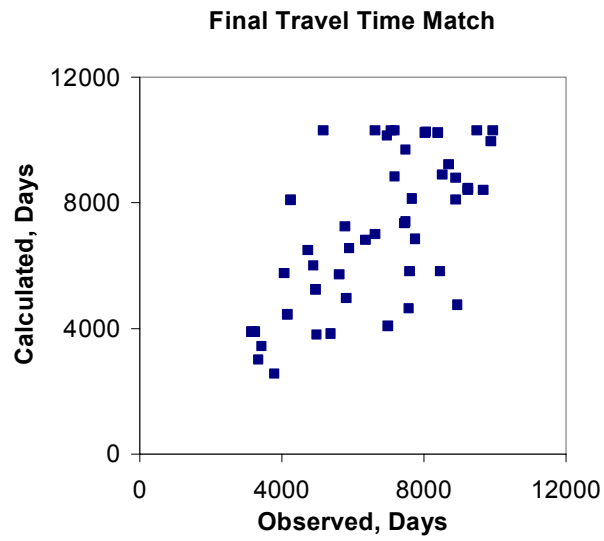


Figure 4.16 - Reduction in Error for Goldsmith Field Example.



(a) Initial Match



(b) Final Match

Figure 4.17 - Initial and Final Travel Time Matches for Giant Middle Eastern Field Example.

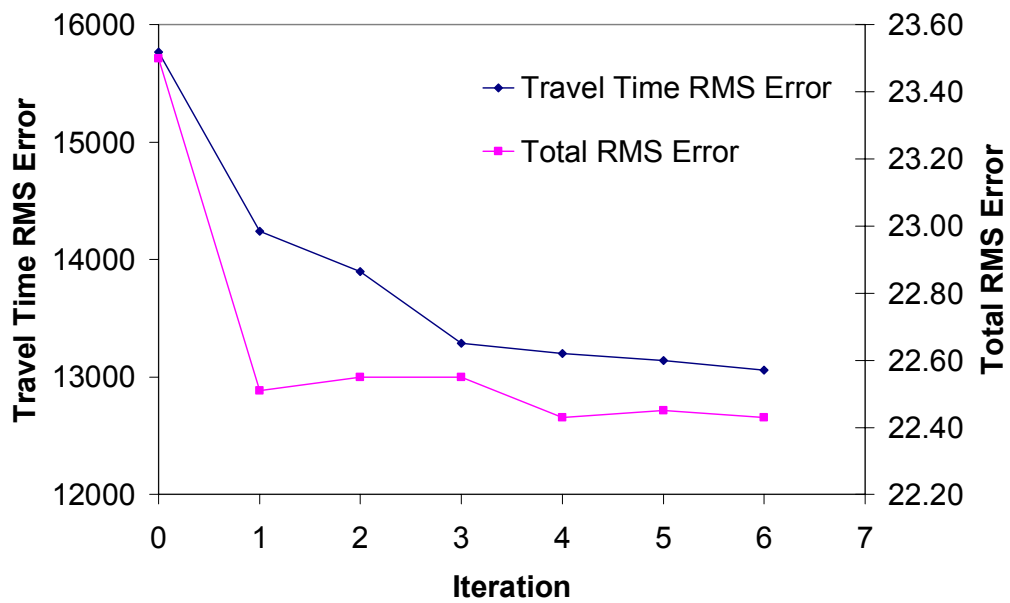
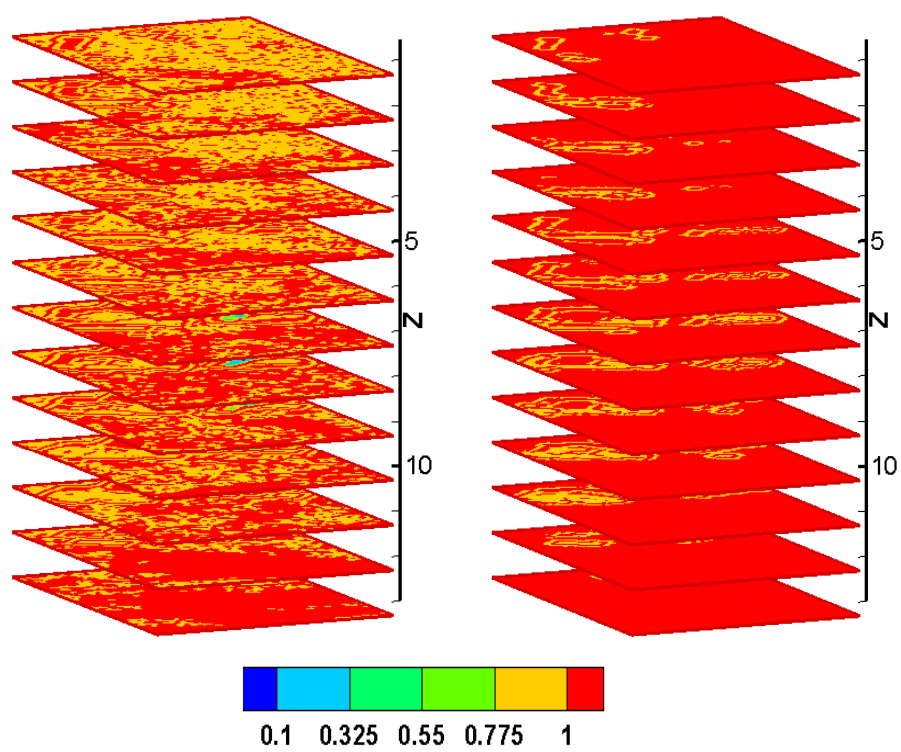


Figure 4.18 - Reduction in Travel Time RMS Error and Total RMS Error for the Giant Middle Eastern Field Example.



(a) Initial

(b) Final

Figure 4.19 - Initial and Final Permeability Multipliers for the Giant Middle Eastern Field Example.

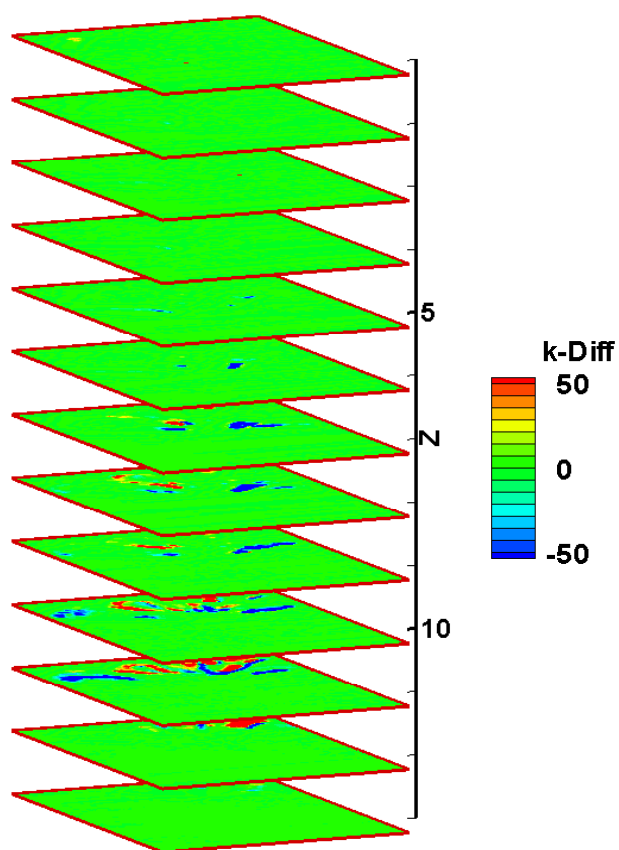


Figure 4.20 - Permeability Difference (md) for the Giant Middle Eastern Field Example.

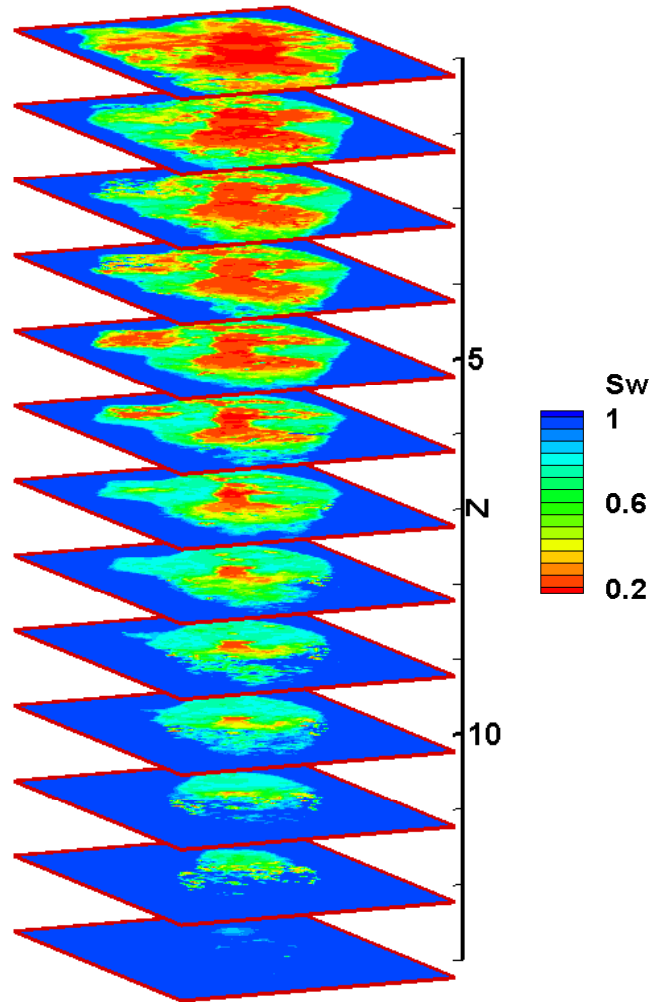


Figure 4.21 - Final Water Saturation Profile for the Giant Middle Eastern Field Example.

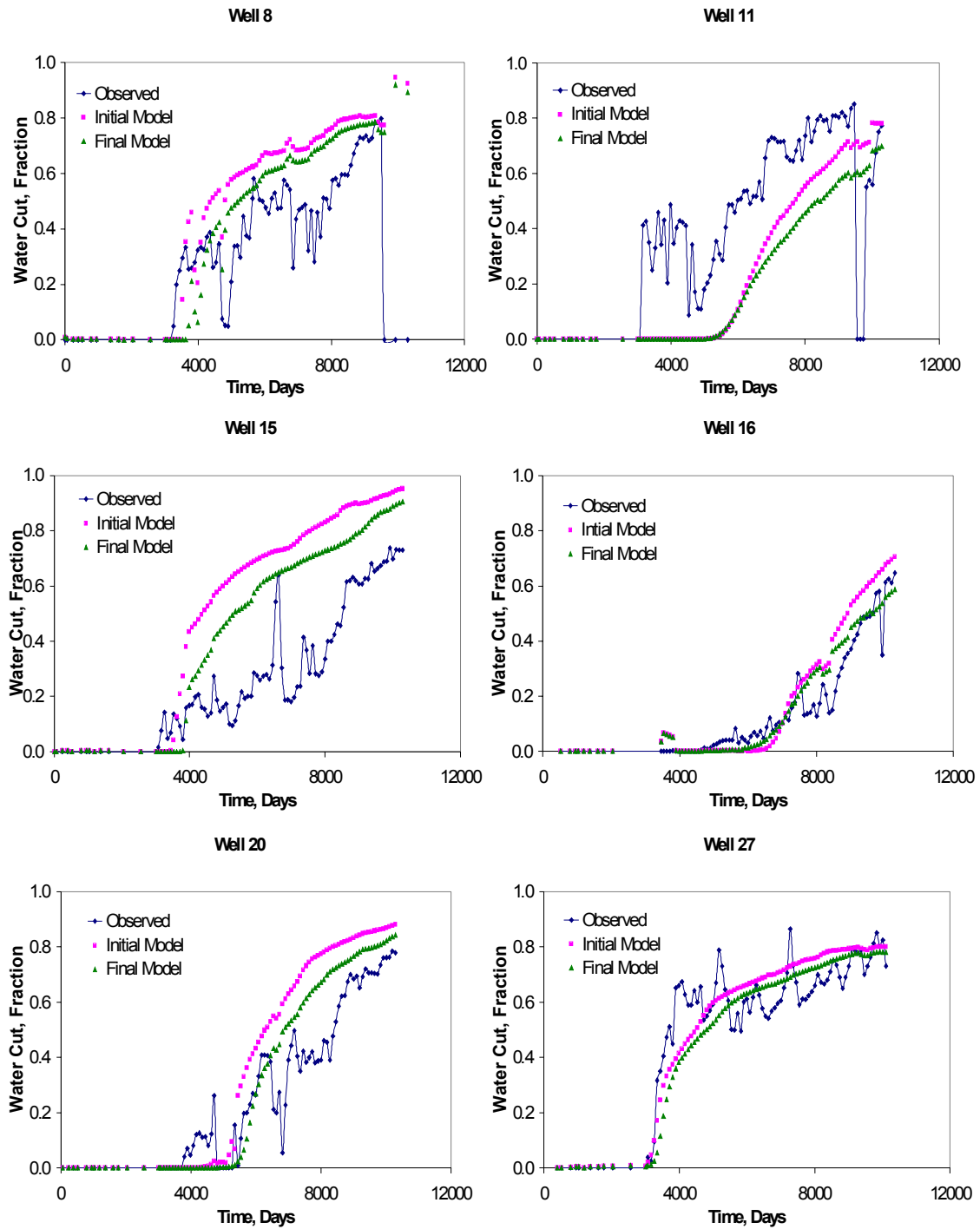


Figure 4.22 - Examples of Water Cut Match for the Giant Middle Eastern Field Example.

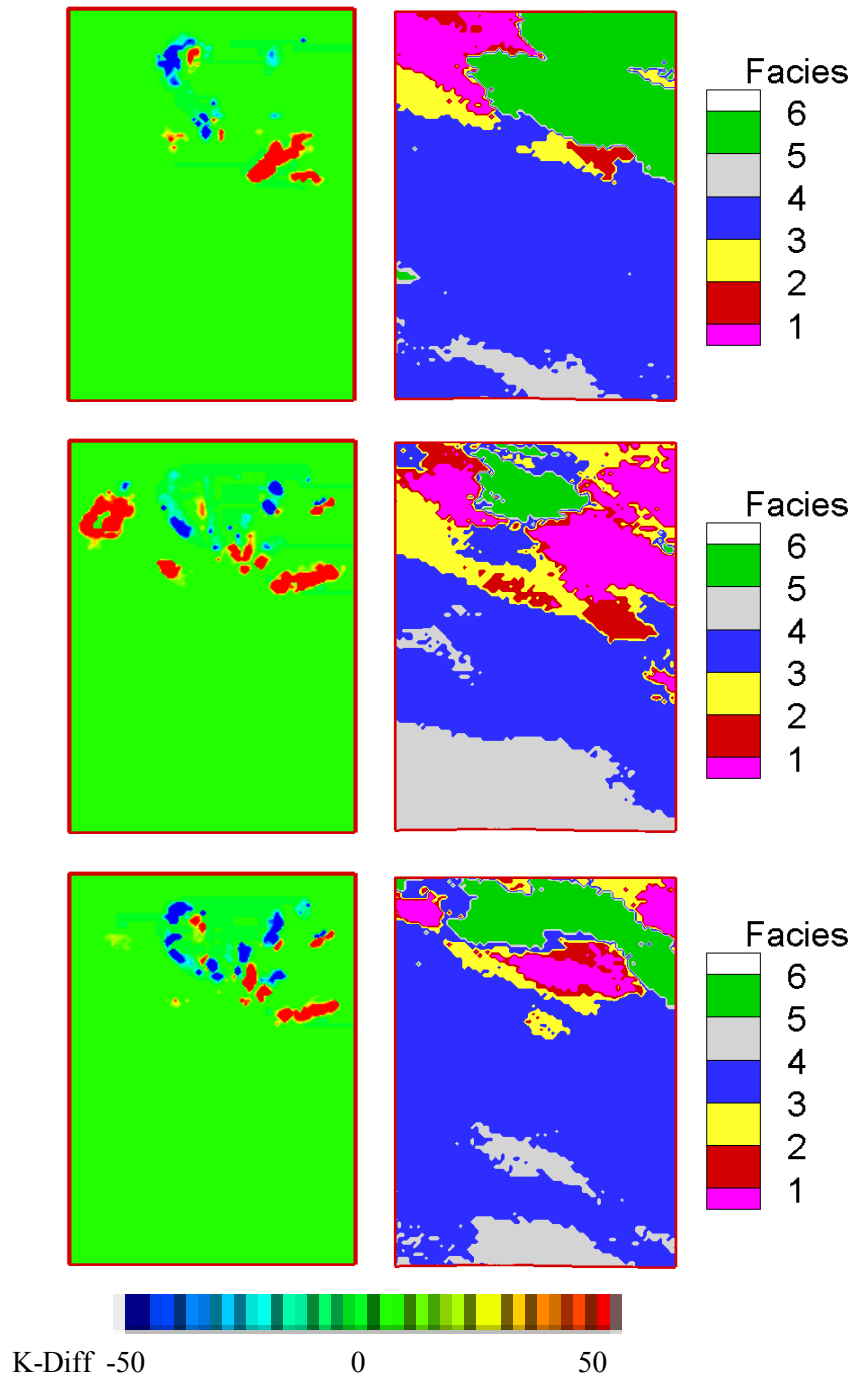


Figure 4.23 - Comparison of Facies Trends with Change in Permeability (md) for Layer 58, 64 and 67 Respectively from Top to Bottom. Left Hand Side Shows Change in Permeability. Right Hand Side Shows Facies Trend.

Fig. 4.17 shows the traveltime match for the initial and final model. **Fig.4.18** shows the reduction in misfit for various iterations. **Figs. 4.19** and **4.20** show the initial and final permeability multipliers and change in permeability respectively.

Fig. 4.21 shows water saturation profile at the end of simulation. Corresponding water cut response matches are shown in **Fig. 4.22** for a few representative wells. Unlike Goldsmith example, the matches here are less satisfactory. However, we can see some improvements in history match.

Fig. 4.23 compares the permeability change from the initial model with facies distribution at different layers in fine scale model, mainly located in between the upper and the middle region of the reservoir. As shown in **Fig. 4.23**, the trends of permeability changes are seen to follow the same trends as the facies distribution. An examination of the permeability changes appears to indicate that most of the dominant trends are along the ‘good’ facies. This is consistent with prior observations and has been found to be geologically realistic. This also reflects the trend obtained in **Fig. 3.31** in Chapter III.

This history matching was carried out in a Pentium IV machine in 4.0 hours of CPU time.

4.5 Sensitivity Studies for the History Match Process

In streamline simulation, saturation is mapped onto the streamline trajectory from the underlying grid. Then saturation equations are solved along the streamlines. During this saturation advance calculations, a streamline is divided into several nodes based on time of flight information. Speed of saturation calculation depends on number of nodes present in the streamline. Increasing the number of nodes increases the calculation time but results in improved accuracy. On the other hand, decreasing the number of nodes speeds up the calculations, but may result in less accurate estimates of saturation.

This section presents the results obtained by use of decreased number of nodes (nfactor = 1) in a streamline and results are compared with all the previously obtained results which use almost twice the number of nodes (nfactor = 2).

4.5.1 Goldsmith Field Example

Fig. 4.24 shows comparison of reduction in misfit for both cases. **Fig. 4.25** shows the travel time match. **Figs. 4.26** through **4.29** show the comparison for permeability multipliers, reference permeability and estimated permeability and permeability difference at the end of

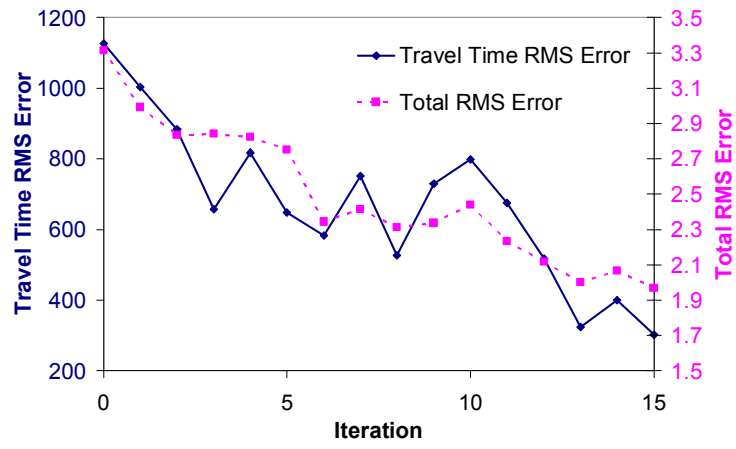
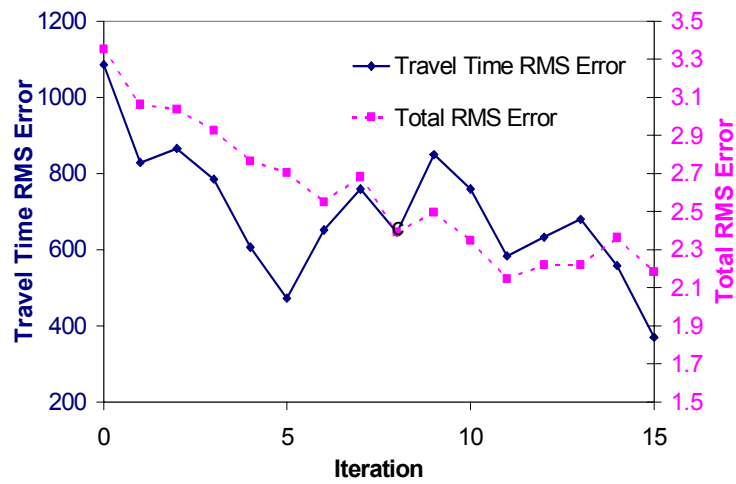
(a) $nfactor = 2$ (b) $nfactor = 1$

Figure 4.24 - Comparison of Misfit Reduction for Goldsmith Example. (a) $nfactor=2$, (b) $nfactor = 1$.

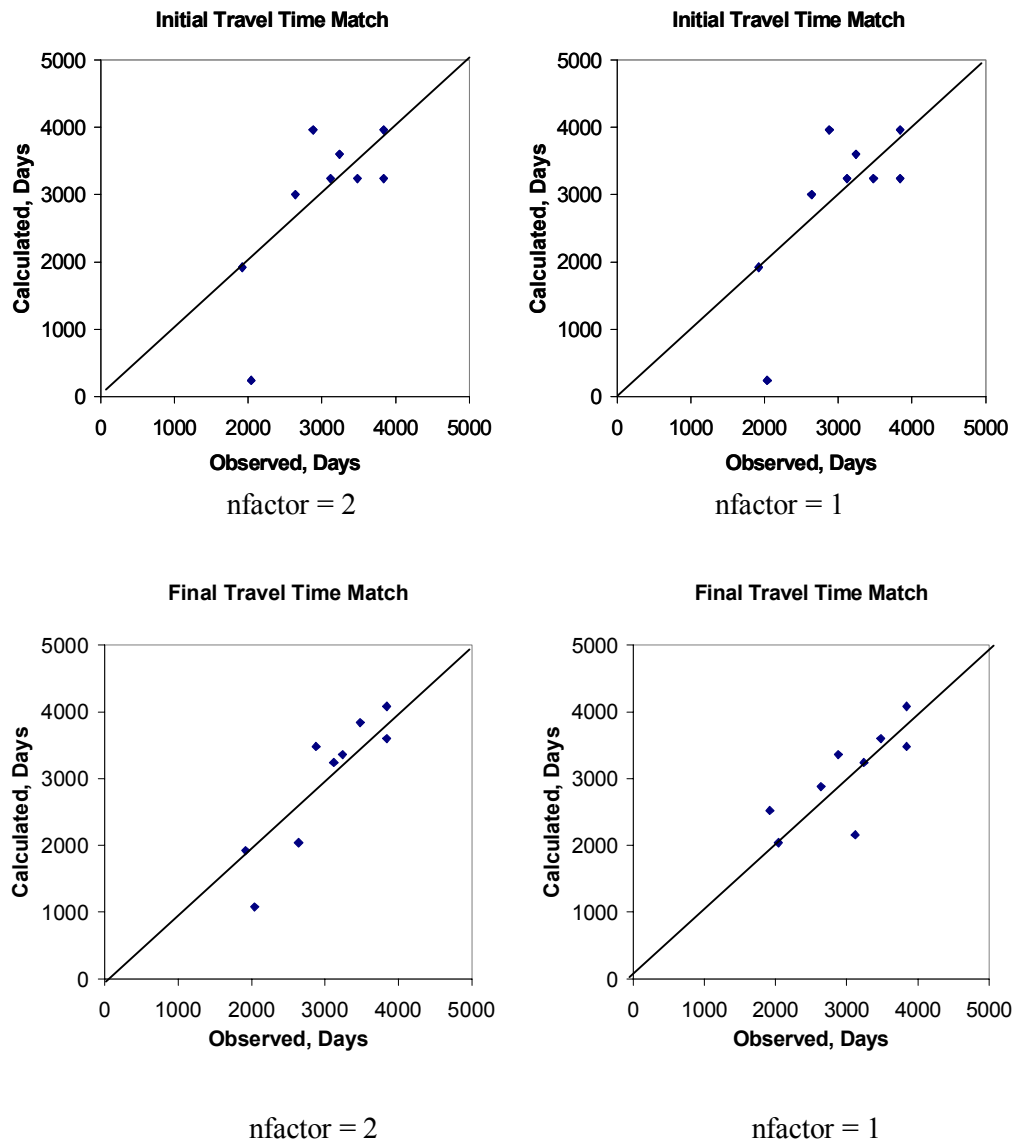


Figure 4.25 - Comparison of Initial and Final Travel Time Matches for the Goldsmith Field Example.

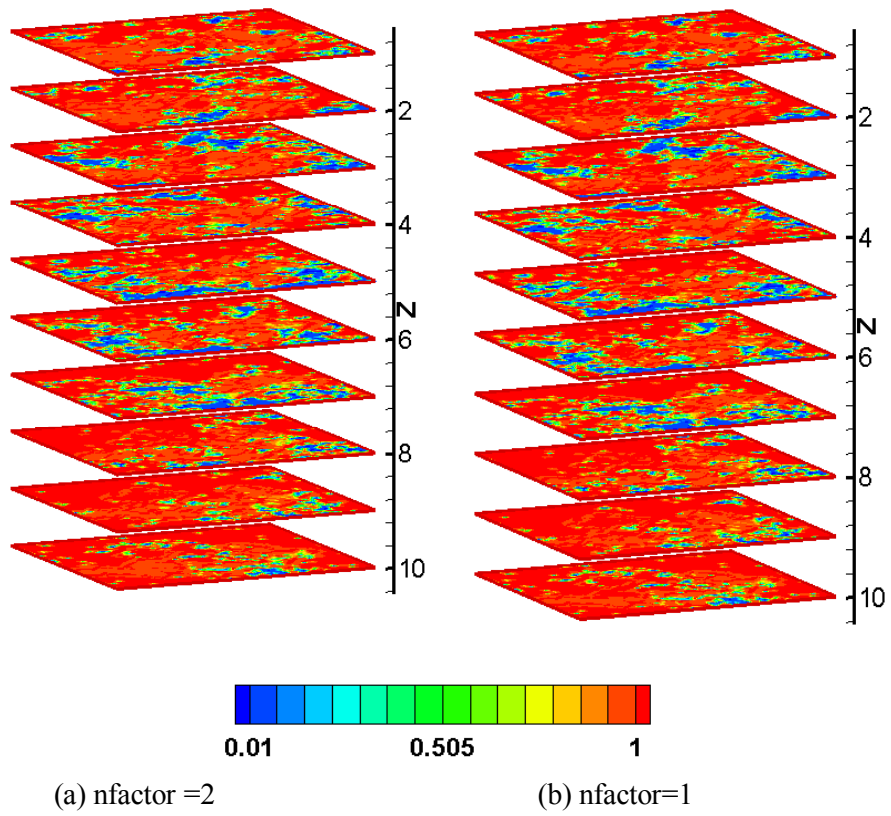


Figure 4.26 - Comparison of Initial Permeability Multipliers for the Goldsmith Field Example.
(a) nfactor=2, (b) nfactor = 1.

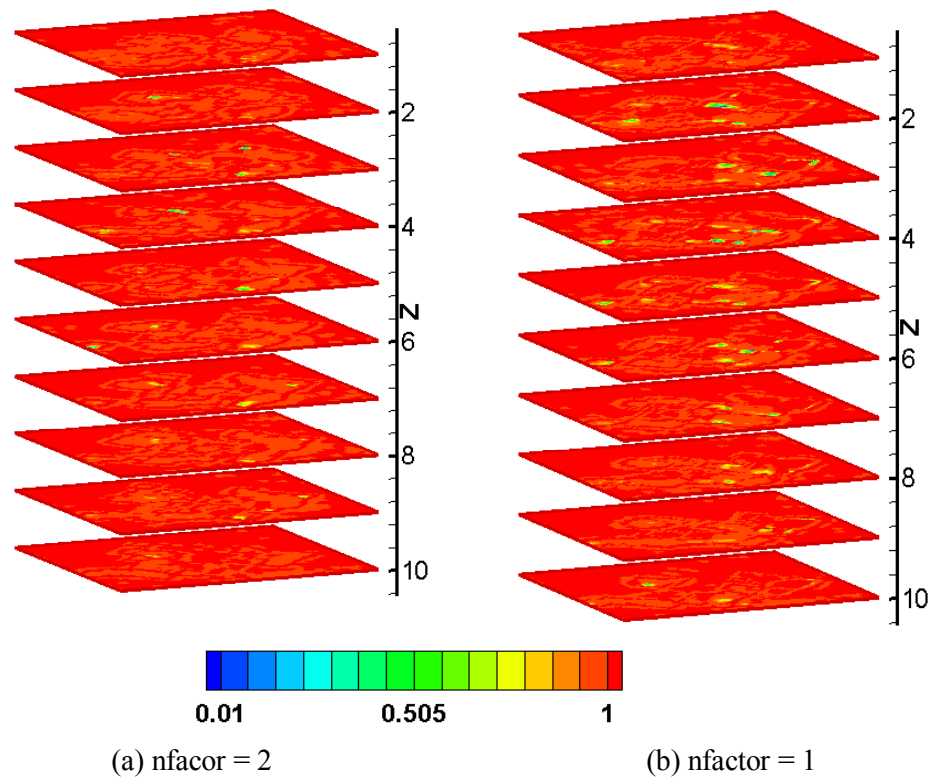


Figure 4.27 - Comparison of Final Permeability Multipliers for the Goldsmith Field Example.
(a) nfactor=2, (b) nfactor = 1.

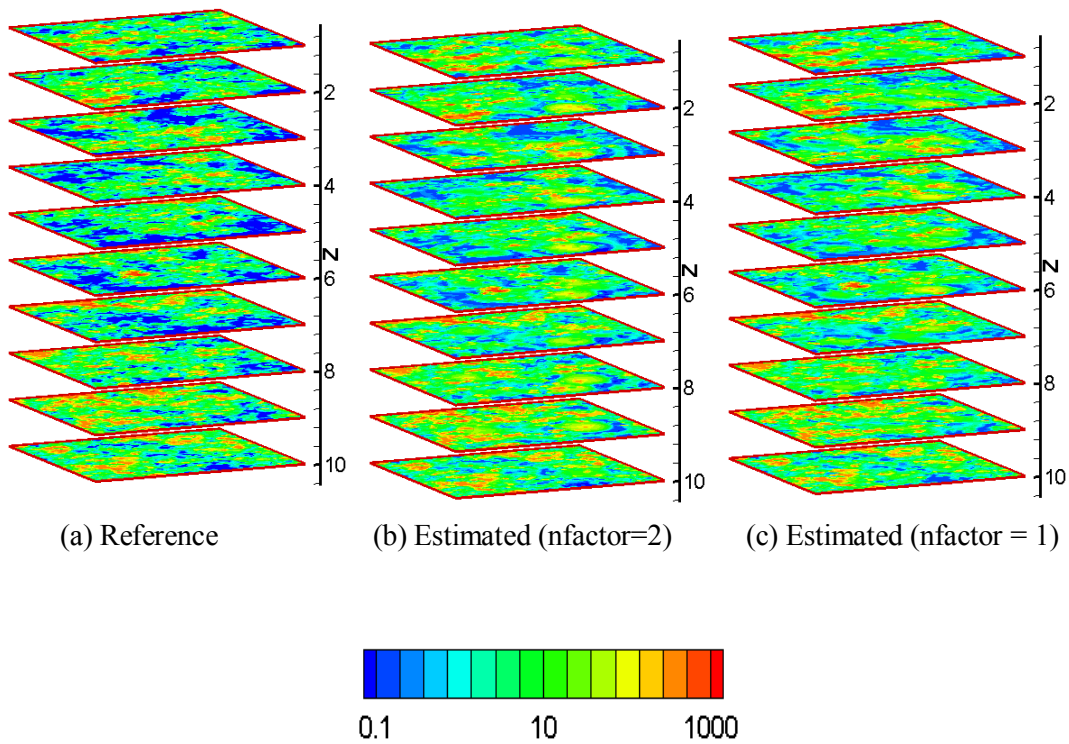


Figure 4.28 - Comparison of Estimated Permeability with Reference Model for the Goldsmith Field Example. (a) Reference, (b) Estimated with nfactor=2, (c) Estimated with nfactor = 1. All in Log Scale.

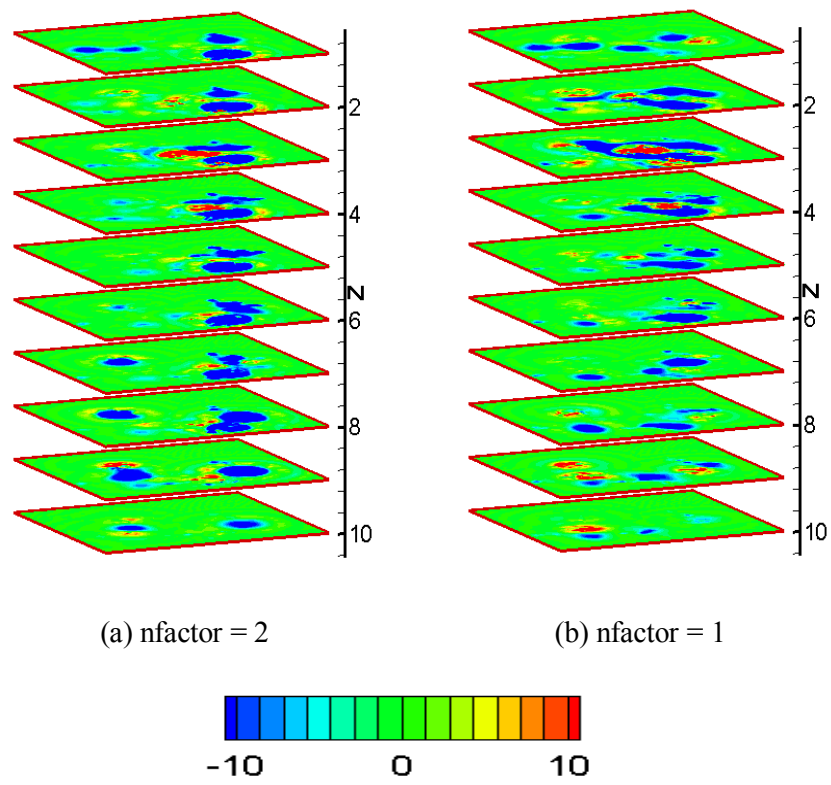


Figure 4.29 - Comparison of Permeability Change for the Goldsmith Field Example. (a) nfactor=2, (b) nfactor = 1. (Not in Log Scale)

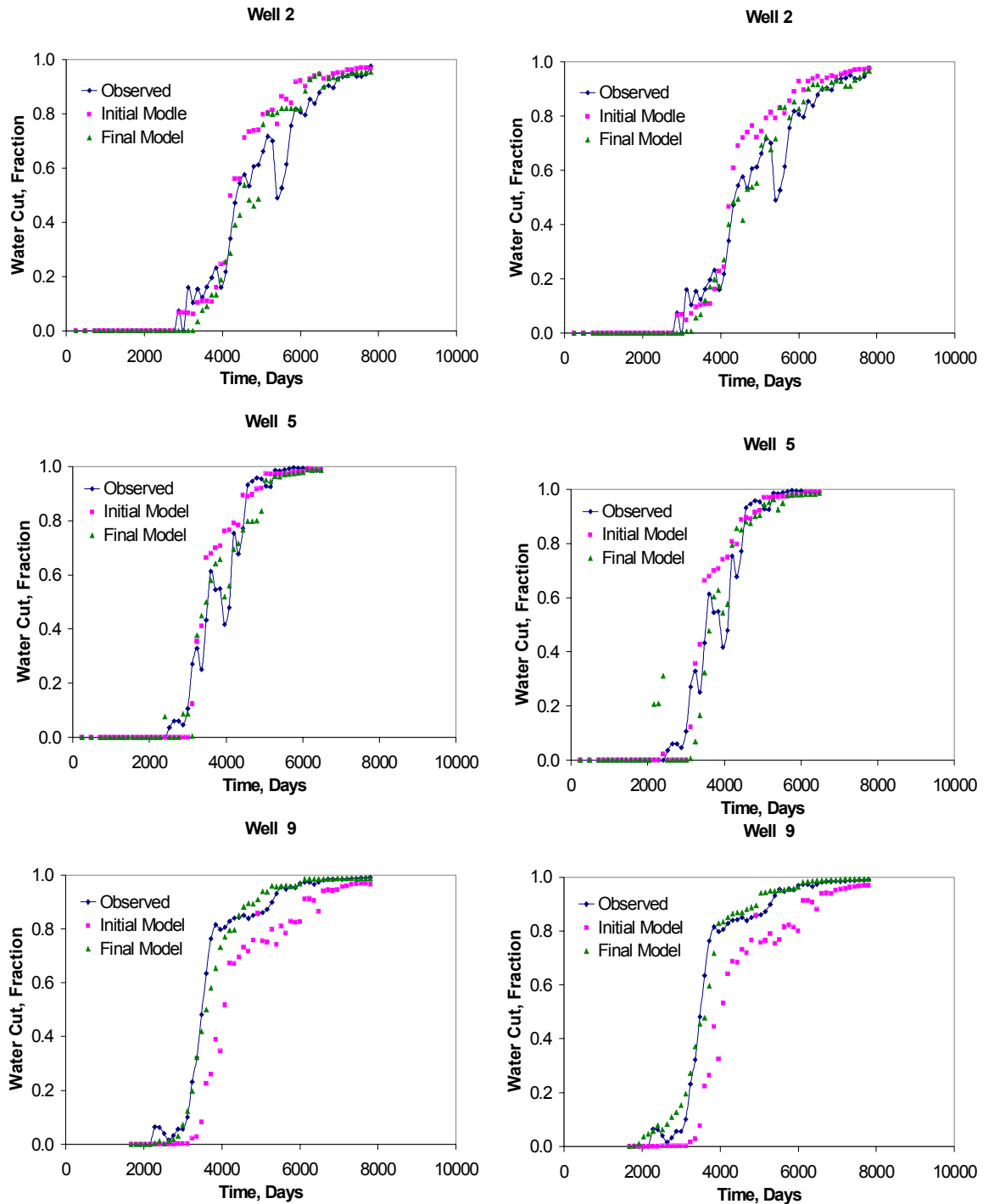


Figure 4.30 - Comparison of Initial and Final Water Cut Matches for the Goldsmith Field Example. Left Hand Side with $nfactor=2$, Right Hand Side with $nfactor=1$.

history match process. **Fig. 4.30** presents the comparison for water cut responses for both cases. It should be observed that results are almost identical in both cases, however, time required for the case $nfactor=1$ is 1.19 secs for 1 iteration while for $nfactor=2$ requires 2.58 secs for one iteration. Thus the computation time is reduced by more than 50%.

4.5.2 Giant Middle Eastern Field Example

Fig. 4.31 compares the reduction in misfit. **Fig. 4.32** shows the comparison of travel time match for both cases. **Figs. 4.33** through **4.35** show comparison for permeability multipliers and difference in permeability at the end of history match process. **Figs. 4.36** and **4.37** present the comparison for final water saturation profiles and water cut responses for both cases. Again, the results do not appear to change much by reducing the number of nodes for this case.

4.6 Time Comparison

Time comparison for different scenarios for Goldsmith and the giant middle eastern field examples has been shown in **Tables 4.1** and **4.2**. It should be observed that significant CPU time reduction could be obtained with $nfactor=1$ for both the cases without much sacrifice of the accuracy of the results.

4.7 Advantages of Assisted History Matching

This is a novel approach and is associated with several advantages:

- It speeds up the history match process considerably. This can potentially lead to a significant savings in time and man power.
- It allows us to use full physics finite difference simulators while retaining the benefits of streamline-based analytic sensitivity computations.
- Modeling of reservoirs with different shapes and sizes can be carried out easily (e.g. corner point geometry, fractured system) because we use a commercial finite difference simulator.

4.8 Chapter Summary

This chapter presents the details of the novel assisted history match approach developed based on streamline derived sensitivity computations with input from finite difference simulator. The synthetic and field examples show the efficiency of the methodology in terms of robustness,

computational time and improved accuracy. Major advantages of the method have been outlined.

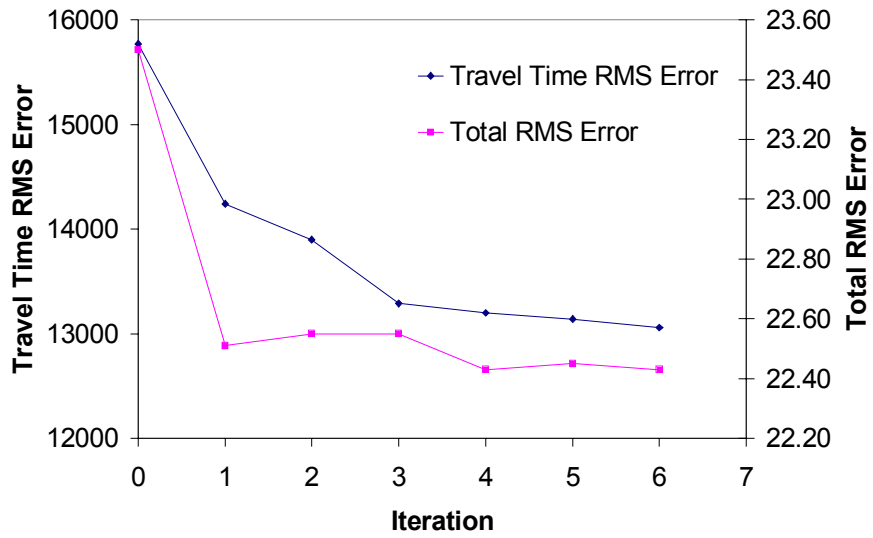
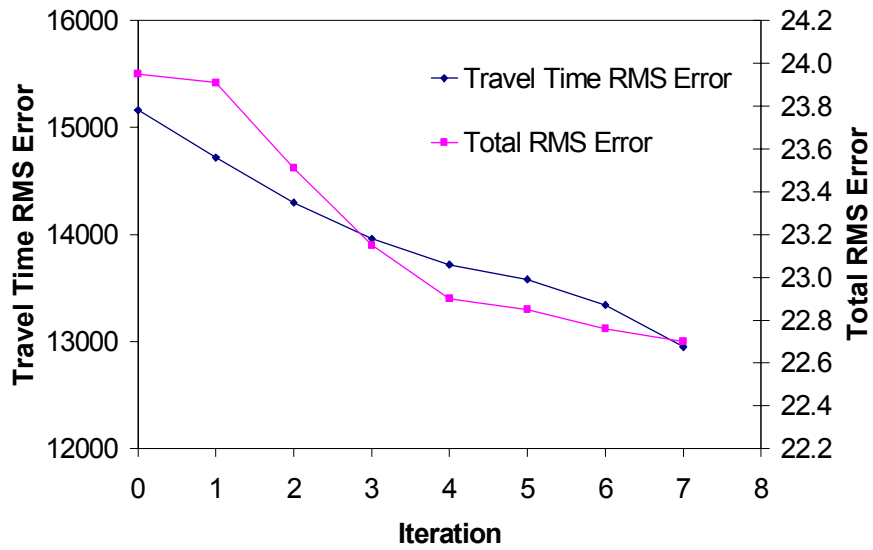
(a) $nfactor = 2$ (b) $nfactor = 1$

Figure 4.31 - Comparison of Reduction in Errors for Giant Middle Eastern Field Example. (a) $nfactor=2$, (b) $nfactor = 1$.

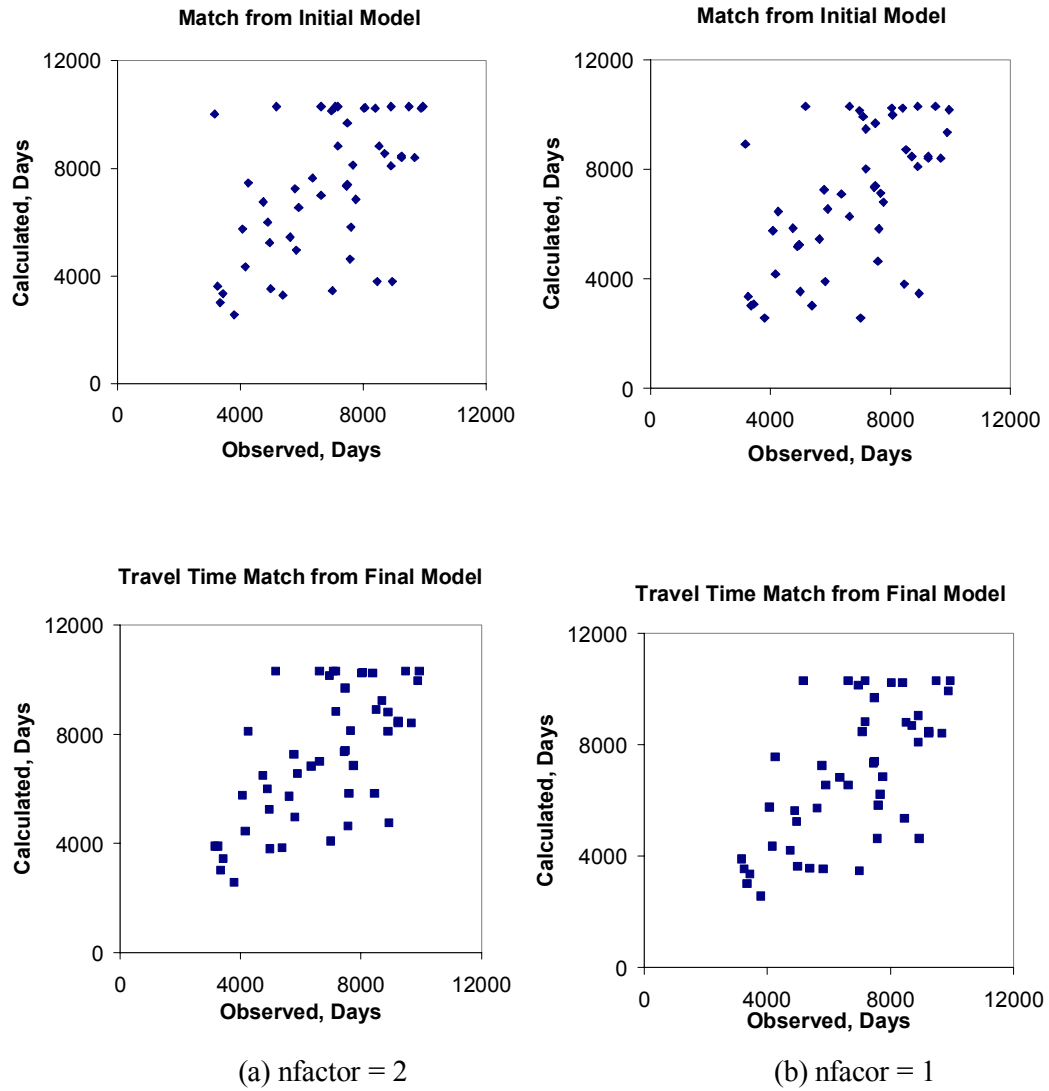


Figure 4.32 - Comparison of Initial and Final Travel Time Match for the Giant Middle Eastern Field Example. (a) nfactor=2, (b) nfactor = 1.

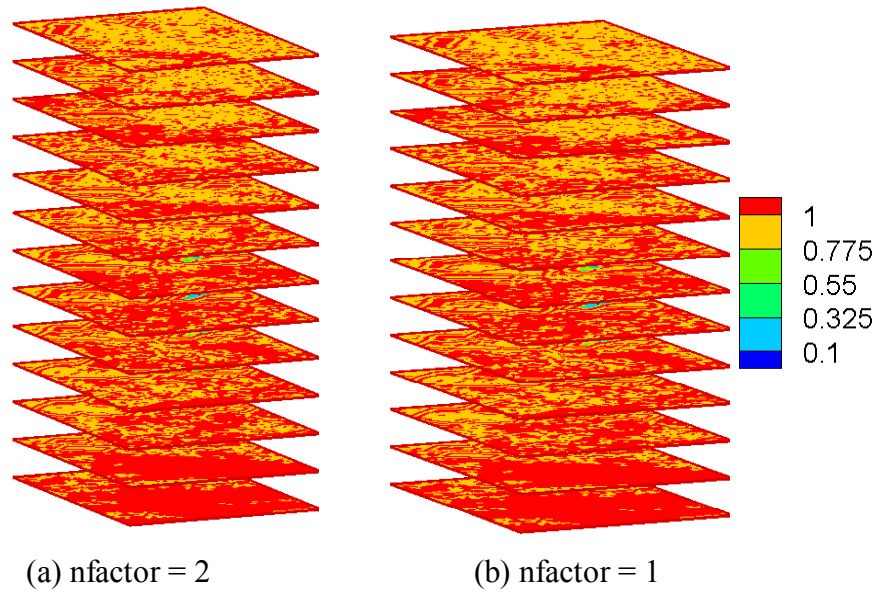


Figure 4.33 - Comparison of Initial Permeability Multipliers for the Giant Middle Eastern Field Example. (a) nfactor=2, (b) nfactor = 1.

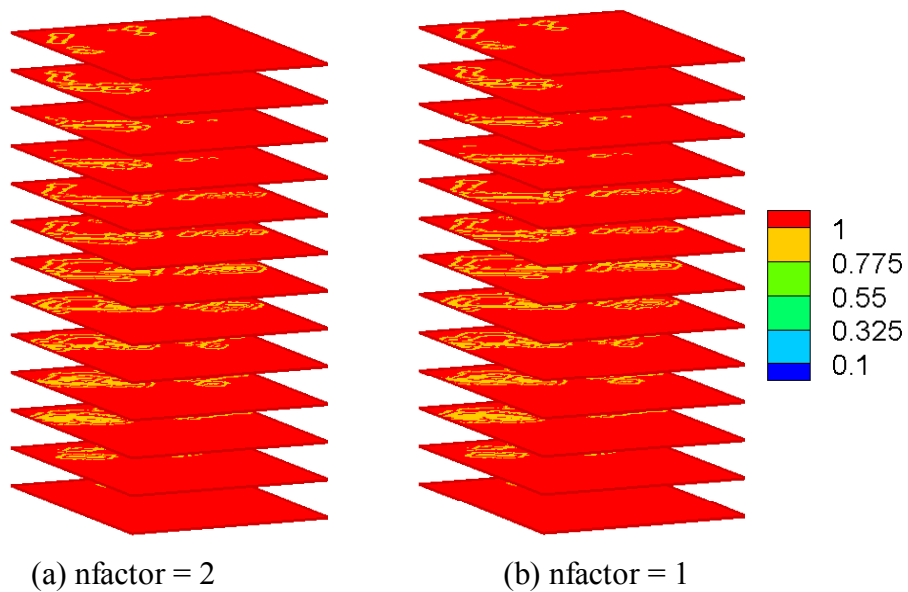


Figure 4.34 - Comparison of Final Permeability Multipliers for the Giant Middle Eastern Field Example. (a) nfactor=2, (b) nfactor = 1.

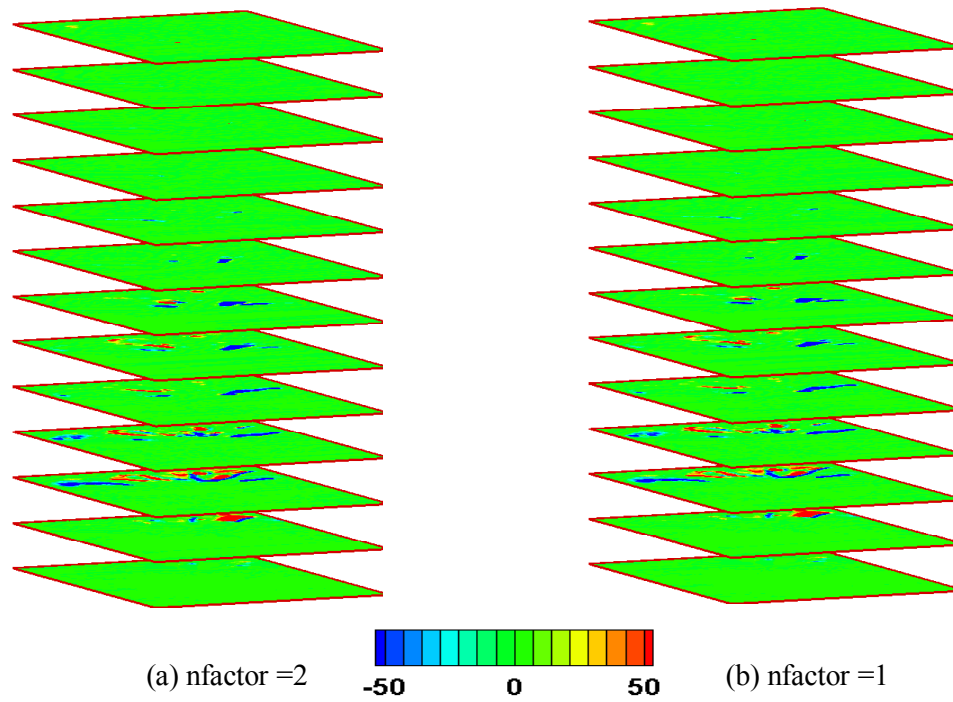


Figure 4.35 - Comparison of Permeability Difference for the Giant Middle Eastern Field Example. (a) nfactor=2, (b) nfactor = 1.

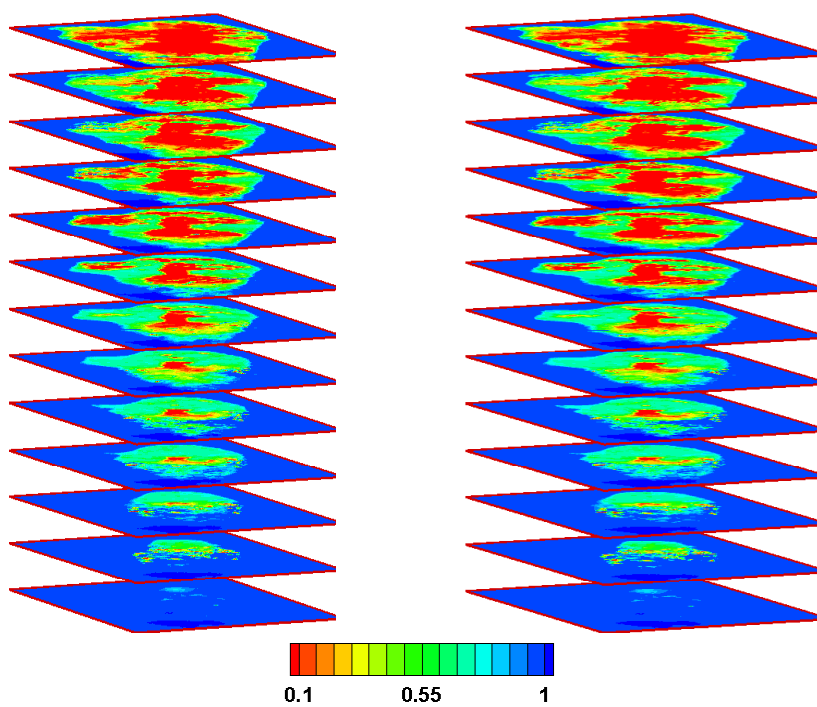
(a) $nfacotr = 2$ (b) $nfactor = 1$

Figure 4.36 - Comparison of Final Water Saturation Profiles for the Giant Middle Eastern Field Example. (a) $nfactor=2$, (b) $nfactor = 1$.

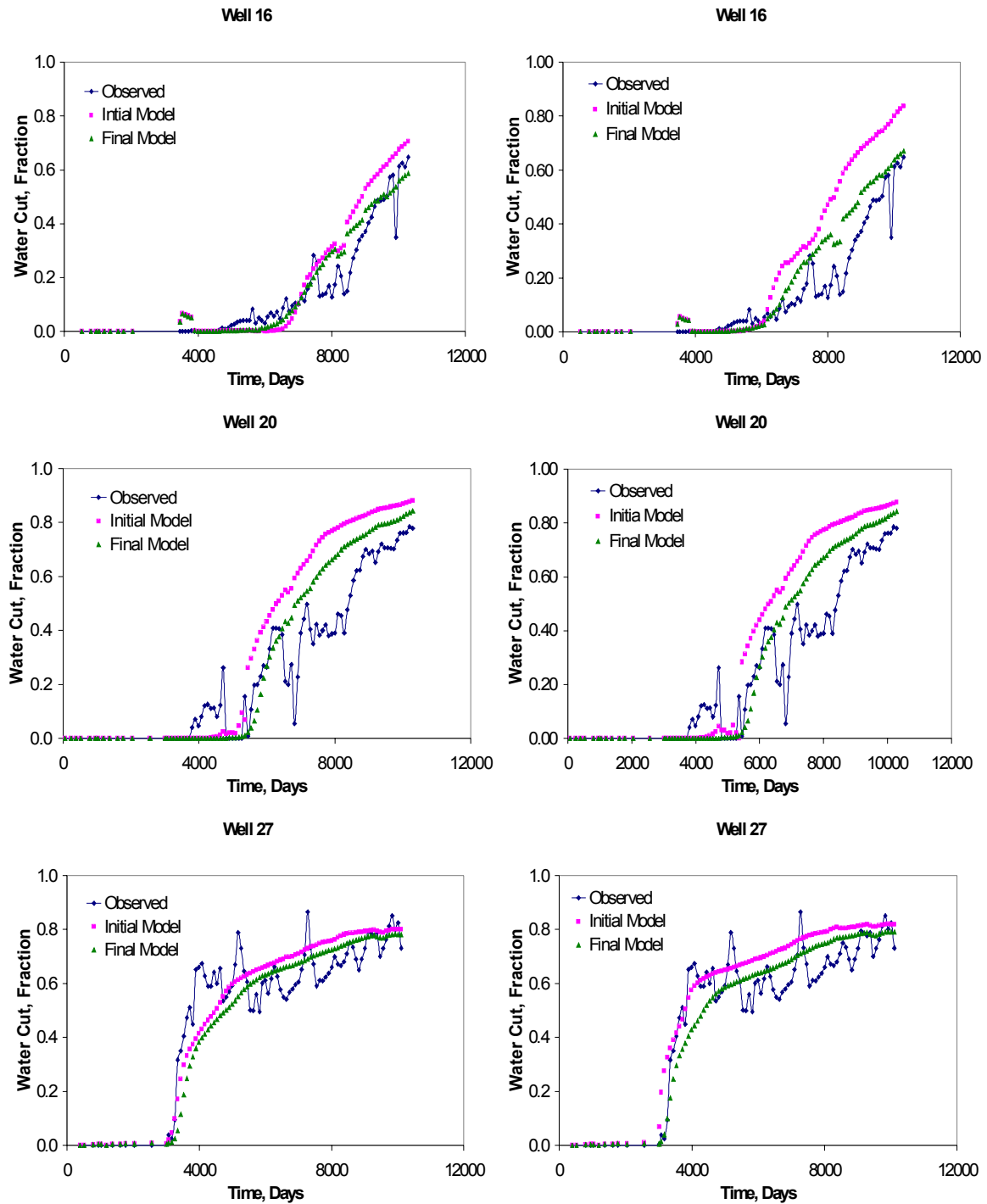


Figure 4.37 - Comparison of Water Cut Response from Initial and Final Models for the Giant Middle Eastern Field Example. Left side : nfactor=2, Right Side : nfactor = 1.

Table 4.1 : CPU Time Comparison for Goldsmith Field Case for Different Scenarios. (Pentium IV)

Scenario	CPU Time (mins)
Streamline + Eclipse : nFactor=2	38.70
Streamline + Eclipse : nFactor=1	17.85

Table 4.2 : CPU Time Comparison for Giant Middle Eastern Field Case (Upscaled Model) for Different Scenarios.(Pentium IV)

Scenario	CPU Time (Hrs)
Streamline + Eclipse : nFactor=2	4.03
Streamline + Eclipse : nFactor=1	2.25

CHAPTER V

CONCLUSIONS AND RECOMMENDATIONS

5.1 Conclusions

In this work, a streamline based inversion technique has been successfully demonstrated for a large scale field application. The streamline based flow simulator was used as a forward model. The inversion process involves analytical computations of the sensitivities along the streamlines which requires only a single forward run. A two-step approach that utilizes an upscaled model for production data integration and then propagates changes to the fine scale model through downscaling was developed. The two-step approach appears to be robust, computationally efficient (about 6 hrs in a PC) and result in significant improvement in the production history match. Almost all (about 90%) of the wells showed improvement in the breakthrough time matches. About 70% of the wells exhibited good to moderate matches in the overall production history.

A comparison of the saturation distribution derived from streamline simulation with the field surveillance data appear to indicate that the model reproduces the gross fluid movement in the reservoir quite well. The waterfront movement and aquifer encroachment are consistent with field observations. The model indicates water coning and bypassed oil as observed in the field. Also, the unswept areas in the model are consistent with field observations. Finally, an examination of the permeability changes resulting from production data integration appears to indicate that most of the dominant trends are along the 'good' facies. These changes are considered geologically plausible and are consistent with prior observations.

The integrated geological model derived after incorporating the water-cut history should significantly reduce the cycle time for full-physics history matching. This is confirmed by preliminary comparison of the streamline simulation results with those from a commercial numerical simulator (ECLIPSE). The results obtained have demonstrated the accuracy and robustness of the inversion methodology with the use of streamline simulator as a forward model.

A novel methodology for assisted history match has been developed and tested for both synthetic and field examples. This methodology involves use of a finite difference simulator in IMPES mode for obtaining pressure, velocity and water saturation profiles and subsequently

using them as input for streamline based dynamic data integration procedure. This results in a faster algorithm that incorporates the accuracy of finite difference simulator and estimation of sensitivities analytically along the streamlines which in turn reduces the in CPU time requirement to complete the history matching process.

The major conclusions of this work are summarized as follows.

1. Use of Streamline Simulator as Forward Model

Streamline simulation serves as an efficient forward model for inversion process. It can be order of magnitude faster compared to conventional finite difference simulator because of decoupling of flow from transport by use of streamline time of flight formulation. Streamline simulation technique can also be efficiently applied to changing field conditions with rate changes or infill drilling.

2. Analytic Sensitivity Computation Along Streamline

Streamline simulation technique provides a unique way to estimate the parameter sensitivities during inverse calculations. The parameter sensitivities can be calculated analytically with single streamline simulation run. This in turn results in significant savings in history matching cycle time. We have demonstrated the applicability of the analytic sensitivity computation with gravity and changing field conditions.

3. Two Step Inversion Procedure

Streamline based production data integration follows the simple analogy from seismic ray tracing where arrival time is matched first followed by amplitude match. In streamline based dynamic data integration process, this involves iterative linearization of the time of flight expression about a known initial model based on static data to match the arrival time first followed by amplitude matching. The travel time inversion is very robust and is particularly well suited for field applications.

4. Streamline Simulation and Large Scale Field Application

Our results showed that streamline simulation can be very efficiently applied for history matching process for large scale field application. The giant middle eastern field example presented in Chapter III consisted of 34 pressure updates with infill drilling schedules,

gravity and rate changes with 30 years of production and injection history. This study utilizes a two-step approach consisting of the following major steps:

- Upscaling to set up coarse scale model
- Inversion to generate coarse scale model conditioned to water cut response at wells,
- Downscaling to update the fine scale model based on permeability changes in the upscaled model, and
- Fine scale simulation with the updated model.

5. Enhancement to Streamline Simulator

In order to carry out the large scale field application, several enhancement have been made to the existing streamline simulator. These include:

- **Boundary Condition for Aquifer Flux**

In order account for the unknown aquifer size, we use pore volume multiplier in aquifer regions to obtain reasonable overall field pressure and fluid flow rates. In this study, we used a PV multiplier of 20 at the edge grid blocks along three sides: North, East, and West. A sensitivity study was carried out to investigate the effect of pore volume multipliers on the matching of individual wells before selecting the optimal multiplier.

- **Gravity Effect and Compressibility of Fluids**

Commonly, streamline models assume incompressible multiphase flow in the reservoir. However, in this study, we accounted for rock and fluid compressibility and also aquifer expansion during solution of the pressure equation and also via pressure updating and streamline regeneration. The present formulation accounts for slight compressibilities. We used an oil compressibility of $16.1 \times 10^{-6}/\text{psi}$ and an water compressibility of $3.3 \times 10^{-6}/\text{psi}$ at reservoir condition. We also accounted for gravity effects during the simulation via operator splitting. The gravity force caused by the density difference of oil and water ($\rho_w = 61.582 \text{ lb/ft}^3$, and $\rho_o = 45.979 \text{ lb/ft}^3$) can impact the final saturation distribution and water-cut responses. In this study we, for the first time, extend the streamline-based history matching technique to include gravity and compressibility of fluids.

6. Assisted History Matching Using Streamline Derived Sensitivity Calculation

This study presents a novel approach for assisted history matching approach which uses the streamline simulator for assisted history matching using finite difference simulation models. In this approach, pressure and velocity distributions are obtained from finite difference simulator and supplied as input for the streamline simulator. Based on these information, streamline trajectories are calculated and also sensitivities along the streamline are calculated and finally mapped back to the underlying grids for inverse modeling purposes. The method has been demonstrated using synthetic and field examples.

7. Reduction in CPU Time for Data Integration

The Assisted History Matching approach presented in this study has been tested for both synthetic and field examples and results in significant savings in history matching cycle time. The results presented show that the new approach reduces the computational CPU time to almost half without losing the accuracy of the calculations.

5.2 Recommendations

Following recommendations could be suggested for the present streamline simulator:

1. The present streamline code could be modified to take into account the generation of streamlines from aquifer, thus taking into account the flow from aquifer. This will require small change in algorithm during Buckley-Leverett calculations.
2. The present could be extended to trace back streamlines from the missing blocks. This will require small modifications in the streamline tracing routines, but would result in significant improvement in the mapping the water saturation back to the grid blocks at the end of simulation.
3. The present streamline code is capable of handling multiple pressure updates, however it appears that during each pressure update, there occurs a slight change in the production responses even without any infill wells. The sensitivity or the effect of pressure updates on production responses should be studied in more detail.

The methodology developed for assisted history match procedure is a very promising tool for wide variety of applications in reservoir engineering application. In this study, although we investigated the applicability of the methodology for synthetic and field examples, however, this could easily be extended to some major applications mentioned below:

1. Since the method utilizes the input from a finite difference simulator for streamline generation, it will be easier to implement different reservoir systems with minimum changes to the streamline simulator. This may include modeling complex systems like fractured system and system with corner point geometry.
2. The methodology could be used to extend streamline technology to easily incorporate three phase system. At present, streamline simulation could handle two phase system very efficiently, however, if total velocity field for all the phases are obtained from finite difference module, it would be easier to handle three phase saturation calculations.

NOMENCLATURE

A	= large sparse unsymmetric matrix
B	= bidiagonal matrix
C	= covariance matrix
<i>C</i>	= tracer concentration or covariance
<i>c</i>	= velocity of propagating wave
d	= data vector
D	= dispersion coefficient
<i>f_w</i>	= water fractional flow
g	= forward model or computed model response
G	= sensitivity matrix
I	= identity matrix
<i>J</i>	= objective function
<i>k</i>	= permeability
K	= permeability tensor
L	= spatial difference operator
<i>M</i>	= number of parameters
m	= parameter vector
<i>N</i>	= number of dynamic data observations
<i>P</i>	= pressure
<i>q</i>	= source/sink or number of fine grids within a coarse grid
<i>s</i>	= slowness
<i>S_w</i>	= water saturation
<i>S_{wi}</i>	= initial water saturation
<i>t</i>	= time
v	= velocity vector
ε	= residual vector
<i>ρ</i>	= phase density
<i>φ</i>	= porosity

- λ_t = total relative mobility
 τ = streamline time of flight or phase function
 ψ, χ = bi-streamline functions
 γ = weighting factor

REFERENCES

1. Muskat, M.: *Flow of Homogeneous Fluid*, International Human Resources Development Corporation, Boston, Massachusetts (1973).
2. Fay, C. H. and Pratts, M.: "The Application of Numerical Methods to Cycling and Flooding Problems," *Proc. 1951 Third World Pet. Cong.*, The Hague, Netherlands, 29 May - 6 June.
3. Higgins, R. V. and Leighton, A. J.: "A Computer Method to Calculate Two Phase Flow in Any Irregularly Bounded Porous Medium," *JPT* (June 1962) 679.
4. Pitts, G. N. and Crawford, P. B.: "Low Areal Sweep Efficiencies in Flooding Heterogeneous Rocks," paper SPE 2866 presented at the 1970 9th Biennial Symposium, Production Techniques, Wichita Falls, Texas, 14-15 May.
5. Martin, J. C. and Wagner, R. E.: "Numerical Solution of Multiphase Two Dimensional Incompressible Flow Using Streamtube Relationships," *SPEJ* (October 1979) 313.
6. Datta-Gupta, A. and King, M. J.: "A Semianalytical Approach to Tracer Flow Modeling in Heterogeneous Permeable Media," *Advances in Water Resources* (1995) **18**, No. 1,9.
7. Batycky, R. P., Blunt, M. J. and Thiele, M. R.: "A Streamline Based 3-D Field Scale Simulator with Gravity and Changing Well Conditions," paper SPE 36726 presented at the 1996 Annual Technical Conference and Exhibition, Denver, Colorado, 6-9 October.
8. King, M. J. and Datta-Gupta, A.: "Streamline Simulation : A Current Perspective," *In Situ* (1998) **22**, No. 1,91.
9. Datta-Gupta, A.: "Detailed Characterization of a Fractured Limestone Formation by Use of Stochastic Inverse Approach," *SPEFE* (September 1995) 133.
10. Vasco, D. W. and Datta-Gupta, A.: "Integrating Field Production History in Stochastic Reservoir Characterization," *SPEFE* (September 1997) 149.
11. Xue, G. and Datta-Gupta, A.: "Structure Preserving Inversion : An Efficient Approach to Conditioning Stochastic Reservoir Models to Dynamic Data," paper SPE 38727 presented at the 1997 Annual Technical Conference and Exhibition, San Antonio, Texas, 5-8 October.
12. Peddibholta, S. Helber, C., Datta-Gupta, A. and Wu, C. H.: "Rapid Simulation of Multiphase Flow Through Fine Scale Geostatistical Realizations Using a New, 3-D Streamline Model : A Field Example," paper SPE 36008 presented at the 1996 Petroleum Conference, Dallas, Texas, 2-5 June.

13. Vasco, D. W., Yoon, S. and Datta-Gupta, A.: "Integrating Dynamic Data into High Resolution Reservoir Models Using Streamline Based Analytic Sensitivity Coefficients," paper SPE 49002 presented at the 1998 Annual Technical Conference and Exhibition, New Orleans, Louisiana, 27-30 September.
14. Yoon, S., Barman, I., Datta-Gupta, A. and Pope, G. A.: "In-Situ Characterization of Residual NAPL Distribution Using Streamline Based Inversion of Partitioning Tracer Tests," paper SPE 52729 presented at the 1999 SPE/EPA Exploration and Production Environmental Conference, Austin, Texas, 1-3 March.
15. Yoon, S., Malallah, A., Datta-Gupta, A., Vasco, D. W. and Behrens, R. A.: "A Multiscale Approach to Production Data Integration Using Streamline Models," paper SPE 56653 presented at the 1999 Annual Technical Conference and Exhibition, Houston, Texas, 3-6 October.
16. He, Z., Datta-Gupta, A. and Yoon, S.: "Streamline Based Production Data Integration Under Changing Field Conditions," paper SPE 71333 presented at the 2001 Annual Technical Conference and Exhibition, New Orleans, Louisiana, 30 September-3 October.
17. He, Z., Parikh, H., Datta-Gupta, A. and Perez, J. and Pham, T.: "Identifying Reservoir Compartmentalization and Flow Barriers Using Primary Production : A Streamline Approach," paper SPE 77589 presented at the 2002 Annual Technical Conference and Exhibition, San Antonio, Texas, 29 September-2 October.
18. Yoon, S.: "Dynamic Data Integration into High Resolution Reservoir Models Using Streamline Based Inversion," PhD Dissertation, Texas A&M University, Texas (2000).
19. McLaughlin, D. and Townley, L. R.: "A Reassessment of the Groundwater Inverse Problem," *Water Resources Research* (1996) **32**, No. 5, 1131.
20. Tikhonov, A. N. and Arsenin, V. Y.: *Solution of Ill Posed Problems*, Halsted Press, New York (1977).
21. Paige, C. C. and Saunders, M. A.: "LSQR : An Algorithm for Sparse Linear Equations and Sparse Least Squares," *ACM Transactions on Mathematical Software* (1982) **8**, No. 1, 43.
22. Golub, G. H. and C. F. Van Loan: *Matrix Computations*, John Hopkins University Press, Baltimore (1996).
23. Scales, J. A.: "Tomographic Inversion via the Conjugate Gradient Method," *Geophysics* (1987) **52**, No. 2, 179.
24. Nolet, G. and Snieder, R.: "Solving Large Linear Inverse Problems by Projection," *Geophysics. J. Int.* (1990) **103**, 565.

25. VanDecar, J. C. and Snieder, R.: "Obtaining Smooth Solutions to Large, Linear, Inverse Problems," *Geophysics* (1994) **59**, No. 5, 818.
26. Idrobo, E. A., Choudhary, M. K. and Datta-Gupta, A.: "Swept Volume Calculations and Ranking of Geostatistical Reservoir Models Using Streamline Simulation," paper SPE 62557 presented at the 2000 SPE/AAPG Western Regional Meeting, Long Beach, California, 19-23 June.
27. Osako, I., Datta-Gupta, A. and King, M. J.: "Timestep Selection During Streamline Simulation via Transverse Flux Correction," paper SPE 79688 presented at the 2003 SPE Reservoir Simulation Symposium, Houston, Texas, 3-5 February.
28. Thiele, M. R.: "Modeling Multiphase Flow in Heterogeneous Media Using Streamtubes," PhD Dissertation, Stanford University, California (1994).
29. Kulkarni, K. N. and Datta-Gupta, A.: "Estimating Relative Permeability from Production Data : A Streamline Approach," *SPEJ* (December 2000) 402.
30. Peaceman, D. W.: "Representation of Horizontal Well in Numerical Reservoir Simulation," paper SPE 21217 presented at the 1993 Reservoir Simulation Symposium, Anaheim, California, 17-20 February.
31. Hisham, M. A., Basem, A. R., Mohammed, A., Bassam, A. and Sarkar, A.: "Conditioning Integrated Geologic Models to Dynamic Flow Data of Giant Saudi Arabian Reservoir," paper SPE 71319 presented at the 2001 Annual Technical Conference and Exhibition, New Orleans, Louisiana, 30 September-3 October.

APPENDIX A

DYNAMIC MEMORY ALLOCATION

Modifications to the existing Streamline Simulation code was carried out to take into account the dynamic memory allocations thus making it capable of handling large scale simulation cases. The existing code was compiled under F77 environment, however to introduce dynamic memory allocation for the arrays, F90 is used for the modified version.

Followings are the major changes made to the existing code:

1. All the arrays of the parameter file 'flocom' were defined separately in a module (called module Dynamic in the file Module.f90) as dynamic arrays using F90 syntax as below.

```
integer, dimension(:),allocatable,save::iwp
real*8, dimension(:, :, :),allocatable,save::tx
```

2. The dynamically defined arrays are then allocated memory at run time using the F90 syntax as below:

```
! comment - allocate the arrays
if(.not. allocated(tx) .or. .not. allocated(ty) .or.&
    .not. allocated(tz)) then

    allocate (tx(ndxp,ndyp,ndzp), STAT=ierr1)
    allocate (ty(ndxp,ndyp,ndzp), STAT=ierr2)
    allocate (tz(ndxp,ndyp,ndzp), STAT=ierr3)

    if(ierr1.ne.0 .or. ierr2.ne.0 .or. ierr3.ne.0) then
write(*,*) 'Memory problem for trans arrays ...'
stop
endif
endif
```

It should be noted that the array dimensions for the above arrays are passed only during run time and once their role in the simulation run is over (for some arrays this happens before the end of complete simulation run), the arrays are destroyed as below:

```

if(allocated(tx))      deallocate(tx)
if(allocated(ty))      deallocate(ty)
if(allocated(tz))      deallocate(tz)

```

Two notable differences of using F90 compared to F77 compiler can be observed in the above procedure

- The comment line in F90 starts with an '!' sign rather than 'c' or 'C' as in F77
- The continuation of a code line is maintained by the use of an '&' sign at the end of the first line rather than using an integer value at the 6th column of the second line as in F77.

Followings are the major points to be noted :

1. A new subroutine called 'DynamicSubrouitnes.f90' has been added to the code where allocation and deallocation of the arrays are taken care of.
2. Local arrays used in a particular subroutine are defined and destroyed in the particular subroutine in the same manner as above.
3. The changes are documented at the end of the main routine where S3D development history can be found.

Comparison of the Non-Dynamic Version with the Dynamic Version

Since no theoretical changes have been made to the code, the results obtained from both non Dynamic and Dynamic version should be essentially similar. This has been demonstrated in the following section with examples.

Example 1 : Example with Infill Drilling

A 49 x 49 X 10 homogeneous system was considered for this purpose. Infill drilling was started after 2000 days of initial production. **Figs. A.1** through **A.7** are presented to show the similarities in results obtained from both non dynamic and dynamic version of the Streamline code. The plots presented show identical results for both versions of the code.

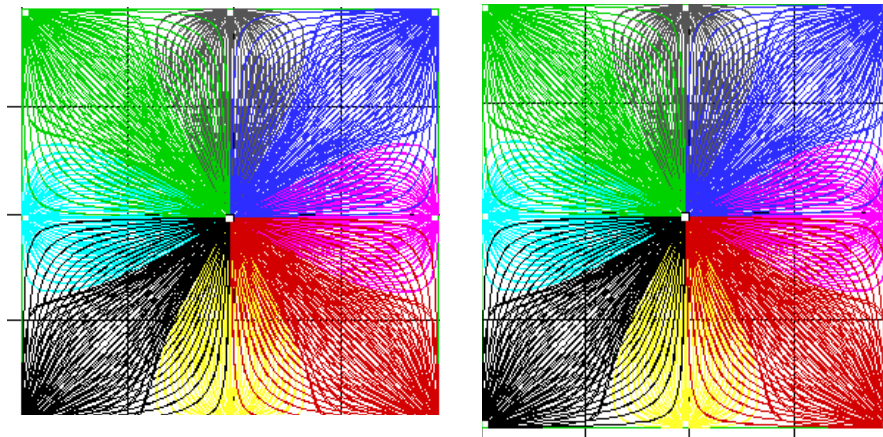


Figure A.1a : non-Dynamic
(after infl)

Figure A.1b : Dynamic
(after infl)

Figure A.1 - Comparison of Streamlines.

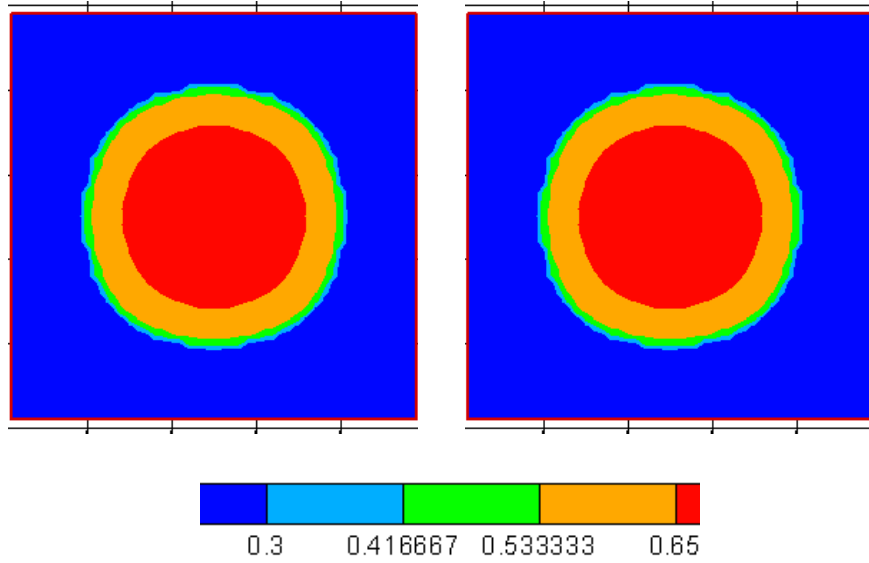


Figure A.2a
Non- Dynamic

Figure A.2b
Dynamic

Figure A.2 - Comparison of Water Saturation Profiles.

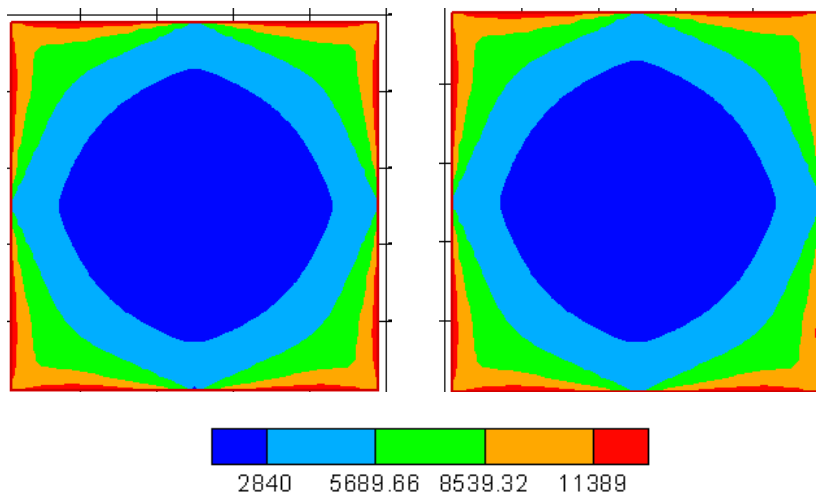


Figure A.3a
Non-Dynamic

Figure A.3b
Dynamic

Figure A.3 - Comparison of Time of Flight.

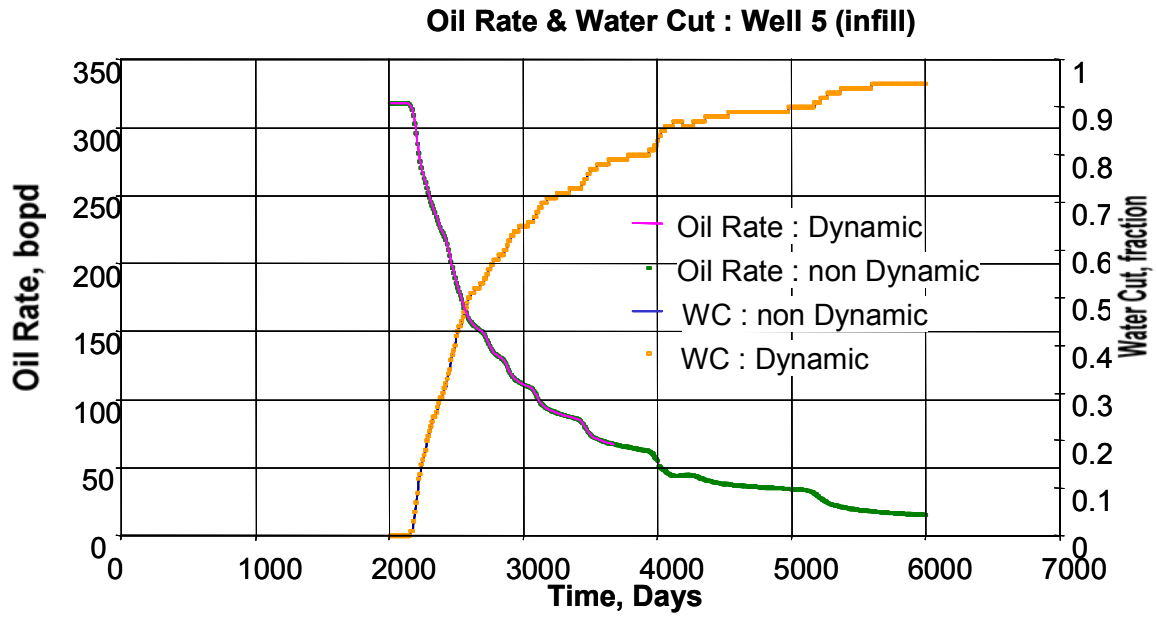


Figure A.4 - Oil Rate and Water Cut Comparison for Well 5.

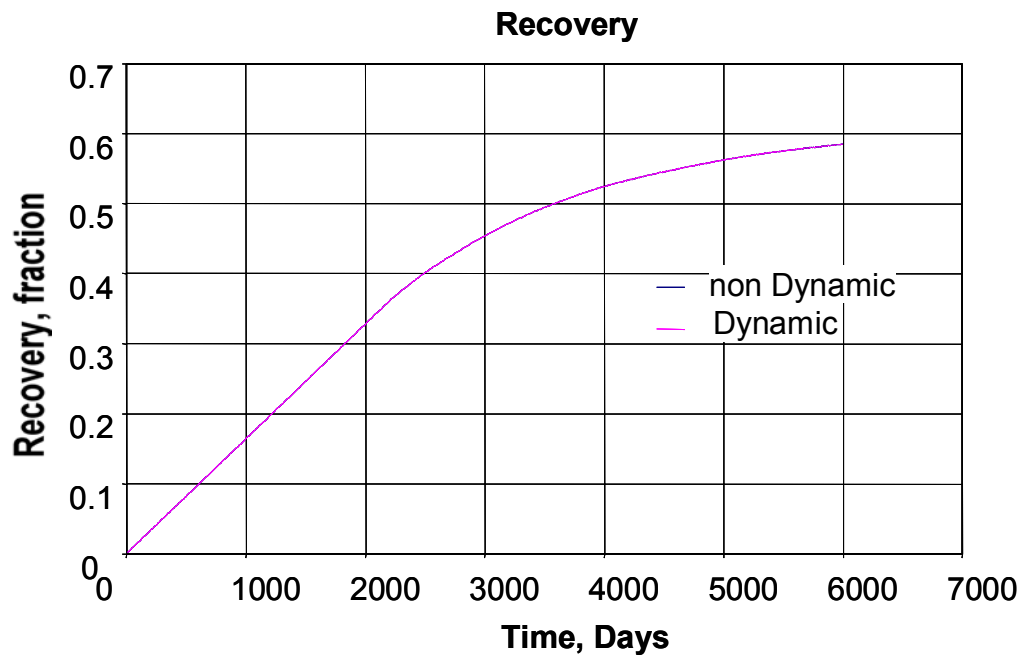


Figure A.5 - Recovery Comparison for nonDynamic and Dynamic Routines..

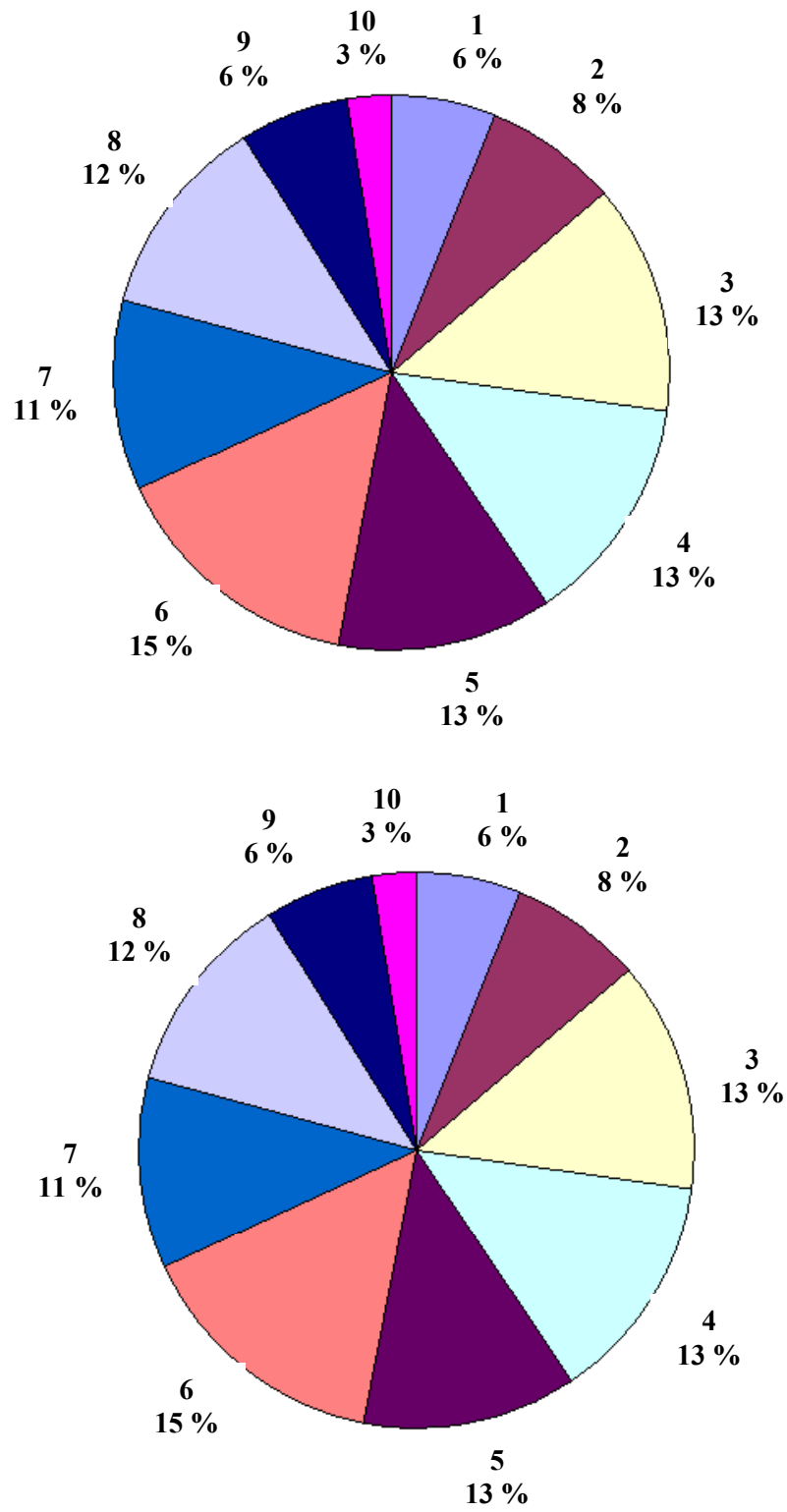


Figure A.6 - Sweep Volume Comparison.

Example 2 : North Robertson Unit

This example consists of 50 x 25 x 12 heterogeneous system with 27 producers and 15 injectors. Results of the simulations runs obtained from dynamic as well non dynamic versions are presented in **Figs. A.7** through **A.11**. The plots presented show identical results for both versions of the code.

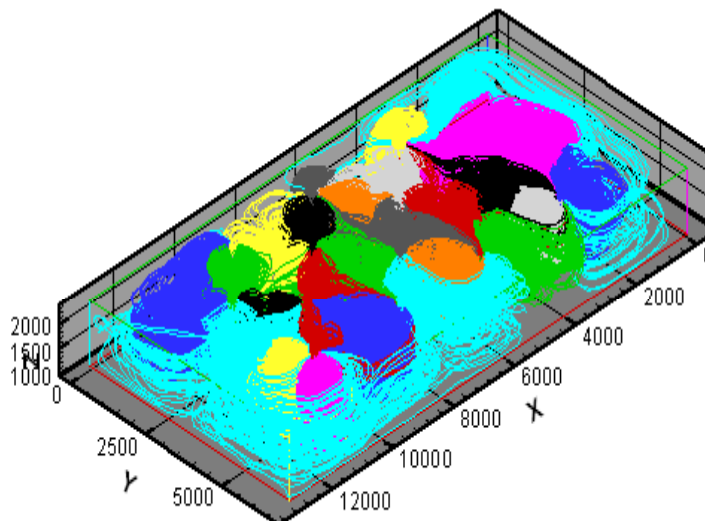
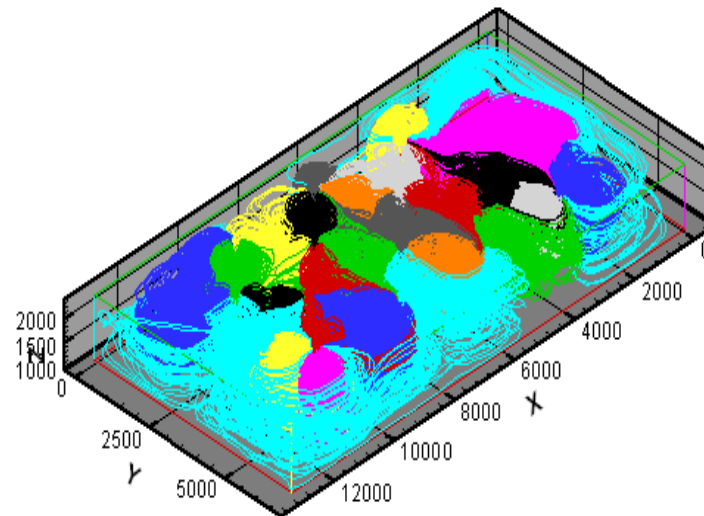


Figure A.7 - Streamlines from non-Dynamic Routine (On the Top) Compared to Streamlines from Dynamic Routine (On the Bottom).

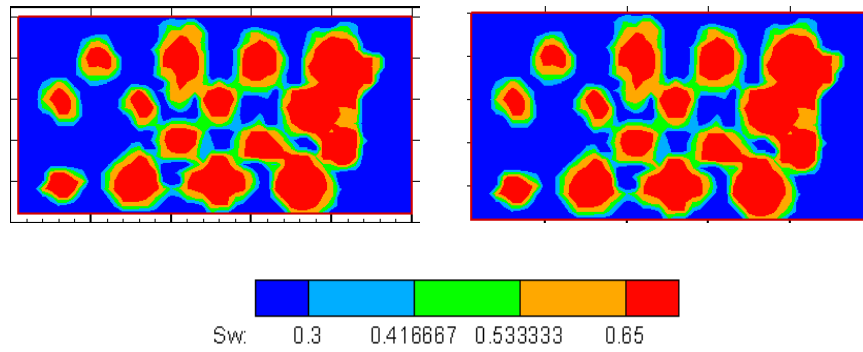


Figure A.8 - Saturation Profile from non-Dynamic Routine (On the Left) Compared to Saturation Profile from Dynamic Routine (On the Right).

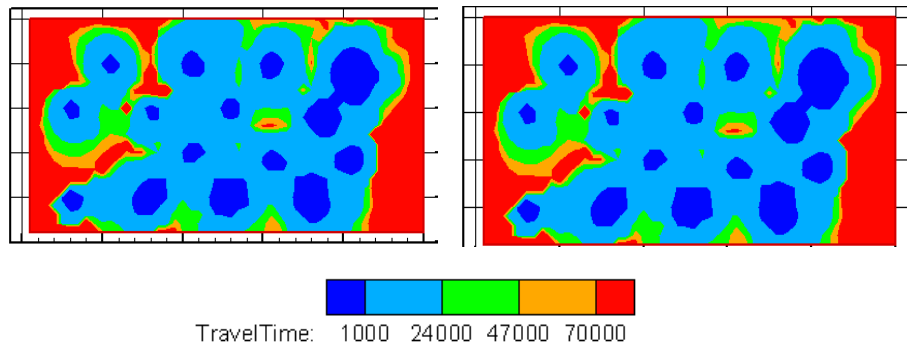


Figure A.9 - Time of Flight from non-Dynamic Routine (On the Left) Compared to Time of Flight from Dynamic Routine (On the Right).

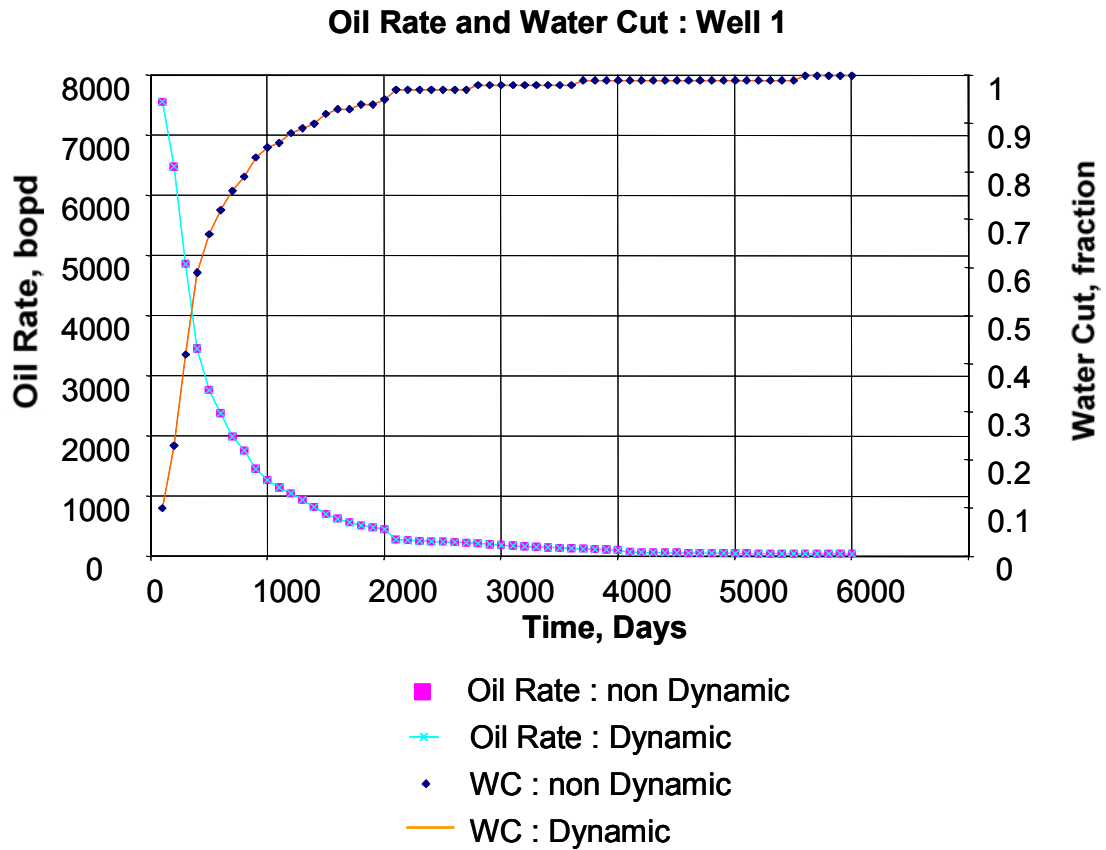


Figure A.10 - Oil Rate and Water Cut Comparison for Well 1.

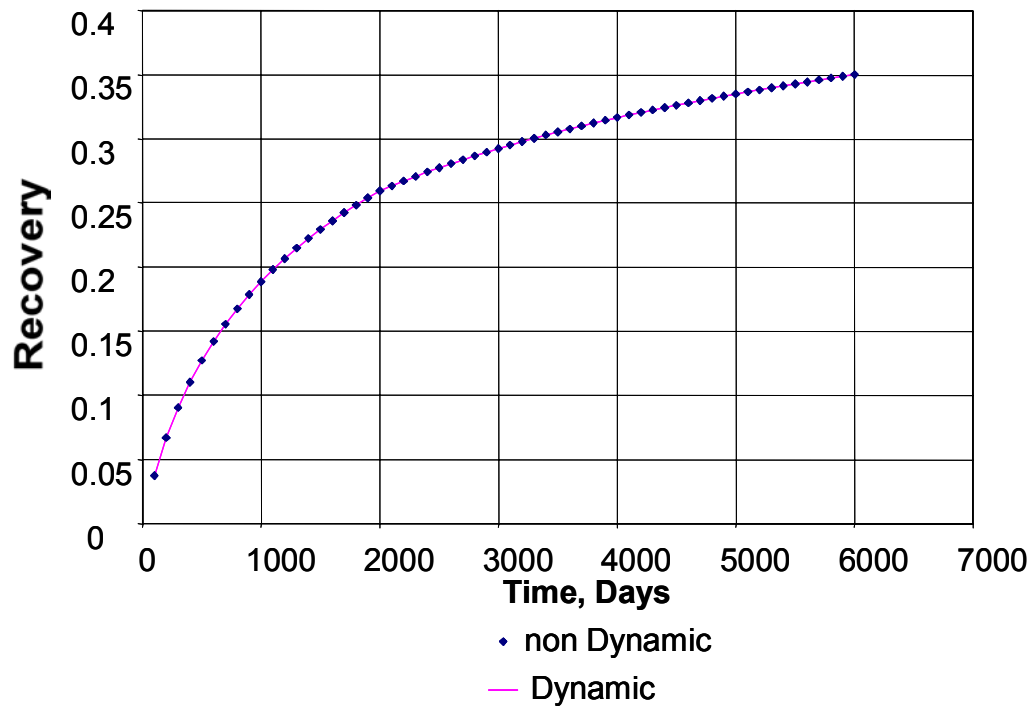


Figure A.11 - Recovery Comparison.

APPENDIX B

HORIZONTAL WELL

The existing Streamline has been modified to incorporate the dynamic memory allocation capability. This version is also capable of handling relative permeability tables and different rock types. A new subroutine called 'Horizontal.f90' has been added to this version of the code to make it capable of handling horizontal wells in both x and y directions. A horizontal well is treated as a rectangular pipe with interconnected blocks in either in x or y direction depending on the direction of the well. Also, special care has been taken to ensure that interconnected faces of the horizontal well are not active for launching streamlines. Productivity index for the horizontal well is calculated using the equivalent well block radius proposed by Peaceman,³⁰ (as given below).

In x - direction:

$$r_o = 0.28 \frac{\left(\left[\frac{K_y}{K_z} \right]^{0.5} \Delta z^2 + \left[\frac{K_z}{K_y} \right]^{0.5} \Delta y^2 \right)^{0.5}}{\left[\frac{K_y}{K_z} \right]^{0.25} + \left[\frac{K_z}{K_y} \right]^{0.25}} \quad (\text{B.1})$$

In y - direction:

$$r_o = 0.28 \frac{\left(\left[\frac{K_x}{K_z} \right]^{0.5} \Delta z^2 + \left[\frac{K_z}{K_x} \right]^{0.5} \Delta x^2 \right)^{0.5}}{\left[\frac{K_x}{K_z} \right]^{0.25} + \left[\frac{K_z}{K_x} \right]^{0.25}} \quad (\text{B.2})$$

In order to accommodate the horizontal well data, datafiles 'data01' and 'data05' have been modified. At this point, only horizontal producers are considered. The code will require modification if horizontal injectors are modeled.

Figs. B.1 & B.2 show the Streamlines for a horizontal well system and comparison of the performance of the horizontal well from the streamline module and ECLIPSE commercial reservoir simulator.

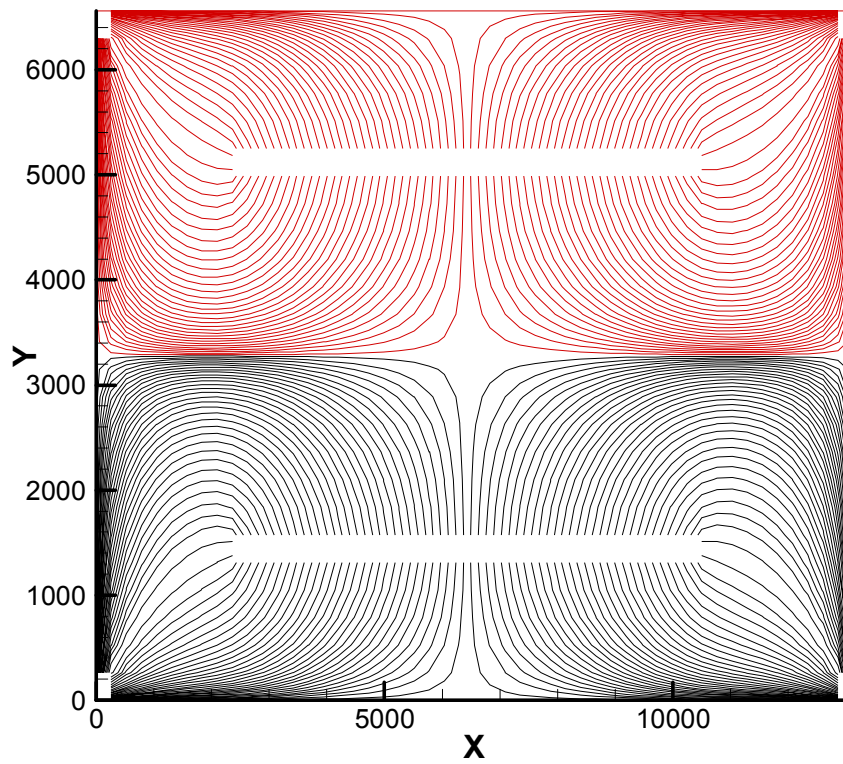


Figure B.1 - Streamline Generated in a 2D System with Two Horizontal Wells.

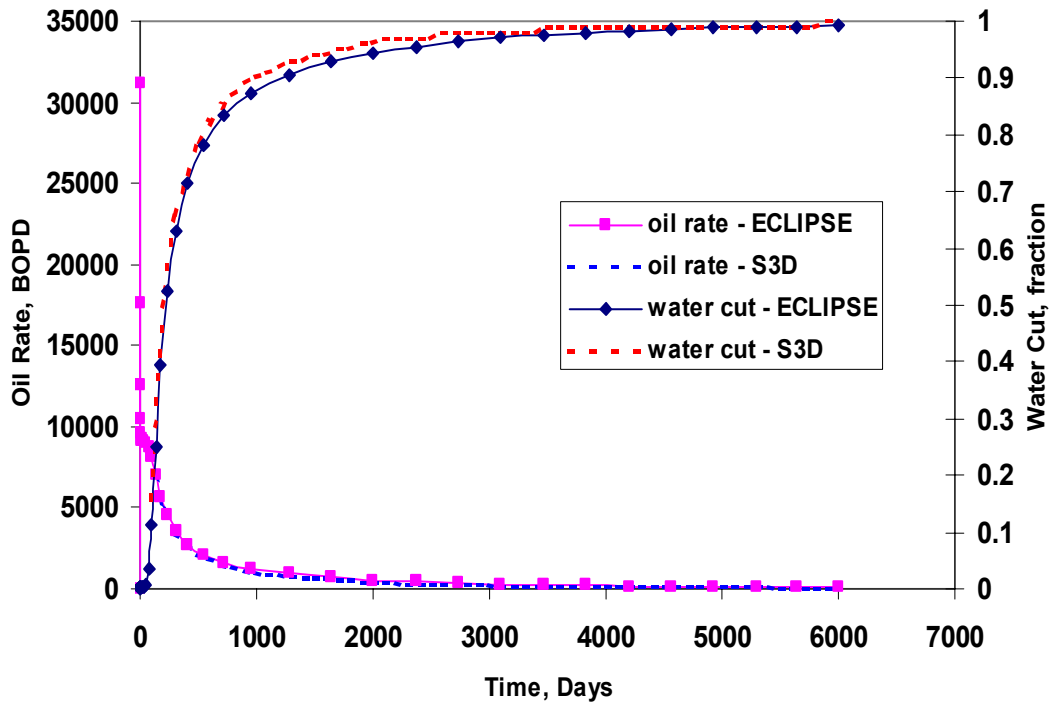


Figure B.2 - Performance Comparison of Horizontal Wells with ECLIPSE.

APPENDIX C

USER INTERFACES

In order to facilitate the ease of using streamline simulator in a more user-friendly manner, a graphical user interface has been developed. Similar interfaces are also designed for the inverse module and electrofacies modules. Following sections briefly describe the user manuals for these three interfaces. These interfaces have been developed using Borland C++ Builder version 5. Some of the 3D visualization plots (e.g. permeability distribution, streamlines) use OpenGL based components. Fortran executables are linked from the interface for execution purposes. The interfaces could be easily installed (and uninstalled) in PC with windows operating system.

C.1 Screenshots from Interface Version of S3D



Figure C.1 – Screenshot of the Launch Panel from S3D.

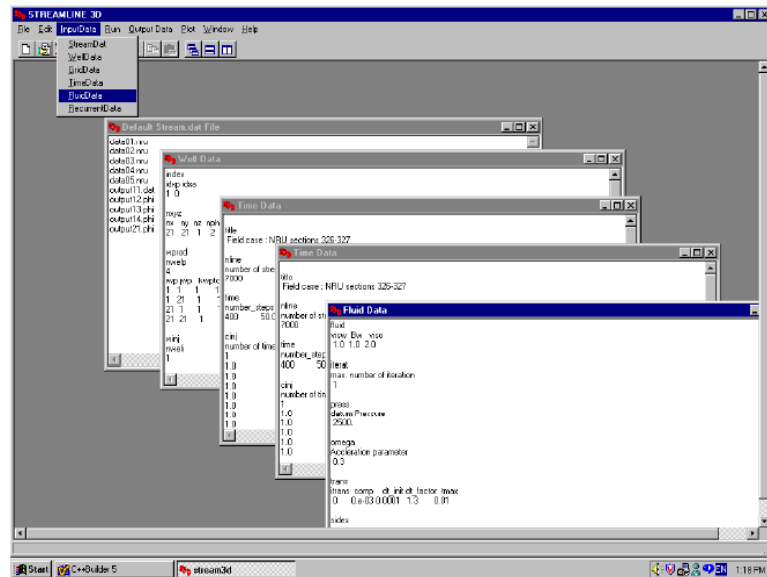


Figure C.2 – Screenshot of the Input Data Panel from S3D.

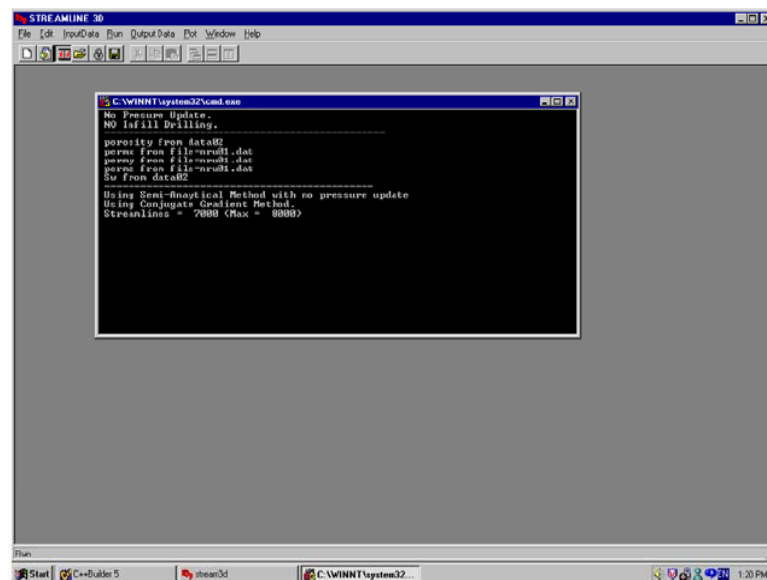


Figure C.3 – Screenshot of the Execution Panel from S3D.

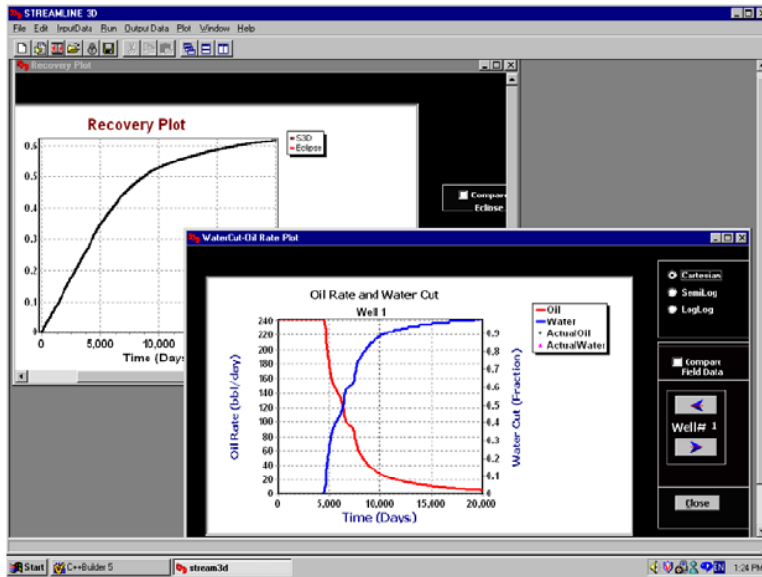


Figure C.4 – Screenshot of the Plot (Oil-Water Rates, Recovery) Panel from S3D.

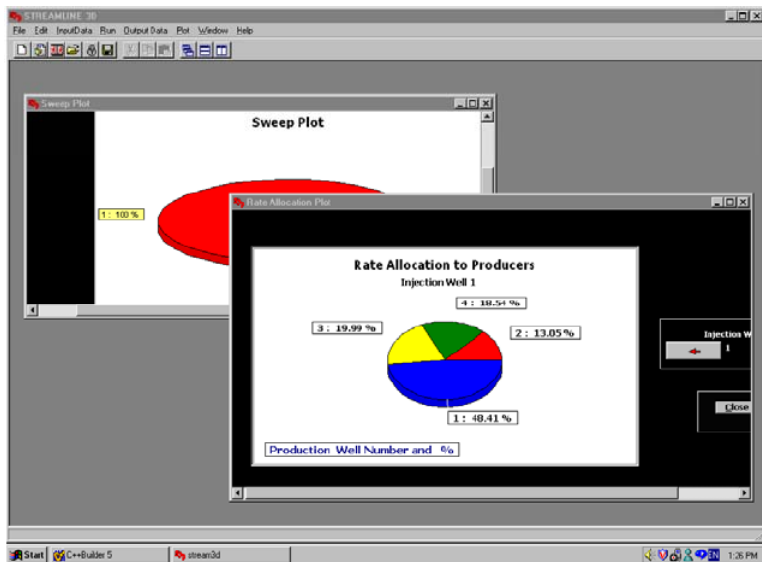


Figure C.5 – Screenshot of the Plot (Sweep, Rate Allocation) Panel from S3D.

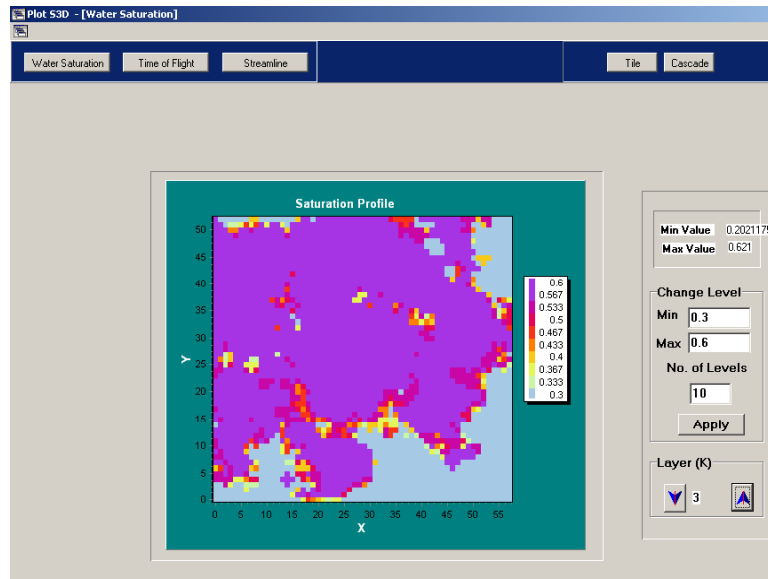


Figure C.6 – Screenshot of the Final Water Saturation Profile from S3D.

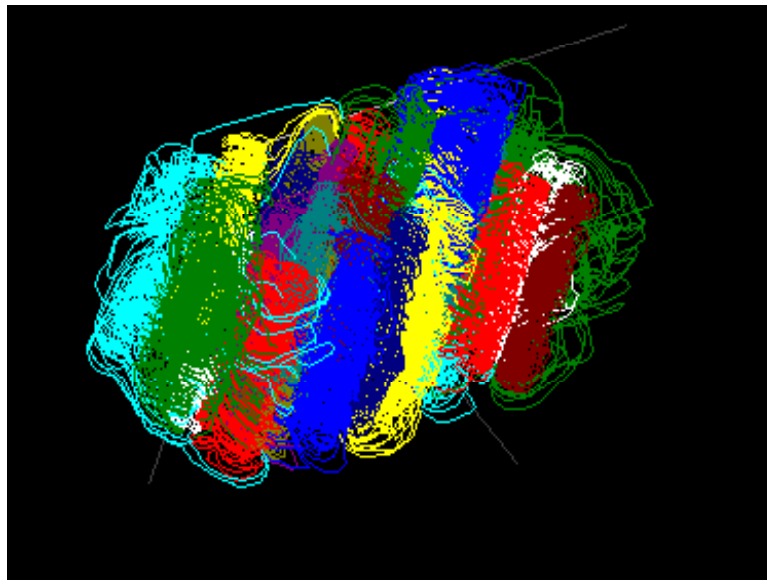


Figure C.7 – Screenshot of the Streamline from S3D.

C.2 Screenshots from Interface Version of PHIS3D

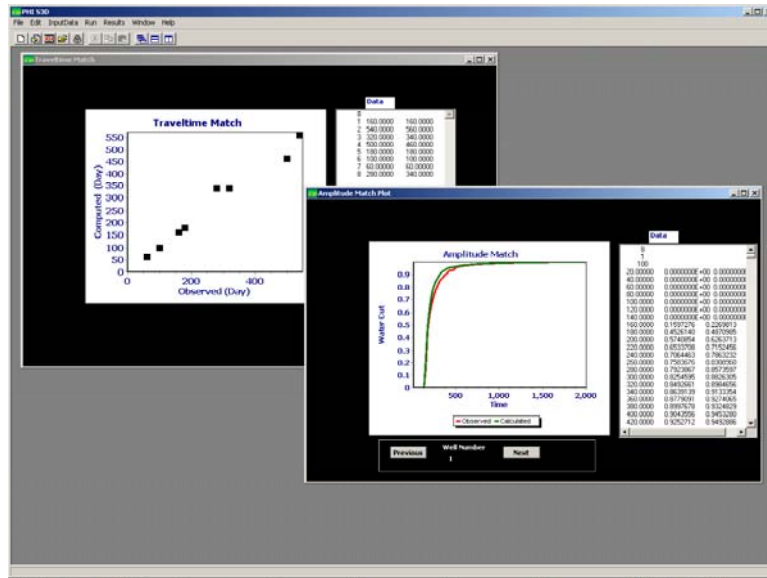


Figure C.8 – Screenshot of the Plot (Travel Time and Amplitude Match) Panel from PHIS3D.

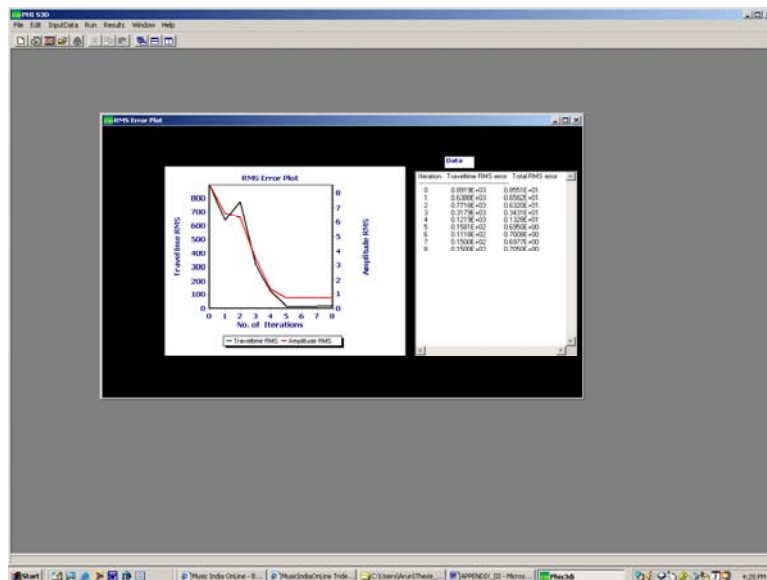


Figure C.9 – Screenshot of the Plot (Error vs. Iterations) Panel from PHIS3D

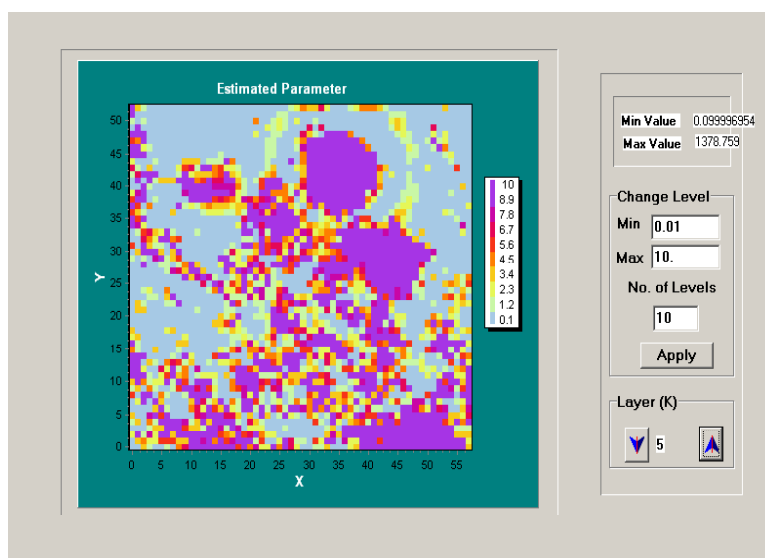


Figure C.10 – Screenshot of the Estimated Parameter from PHIS3D.

C.3 Screenshots from Interface Version of EFACIES

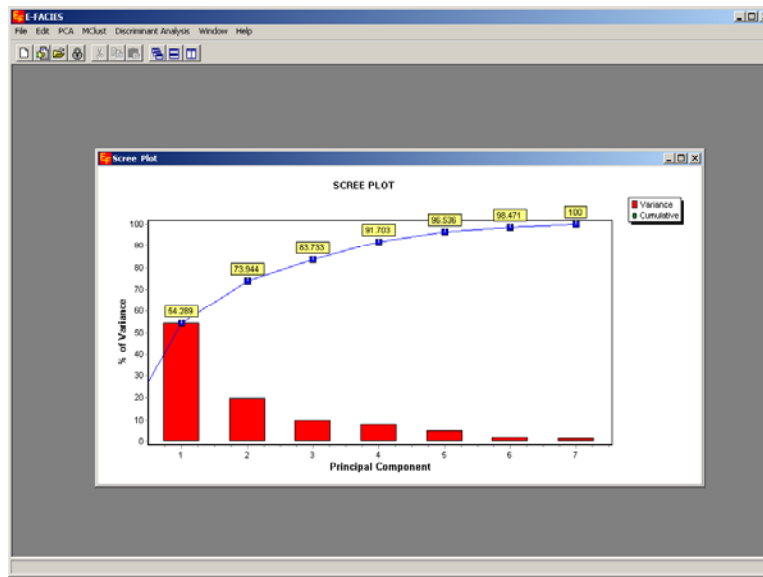


Figure C.11 – Screenshot of the Scree Plot from Efacies.

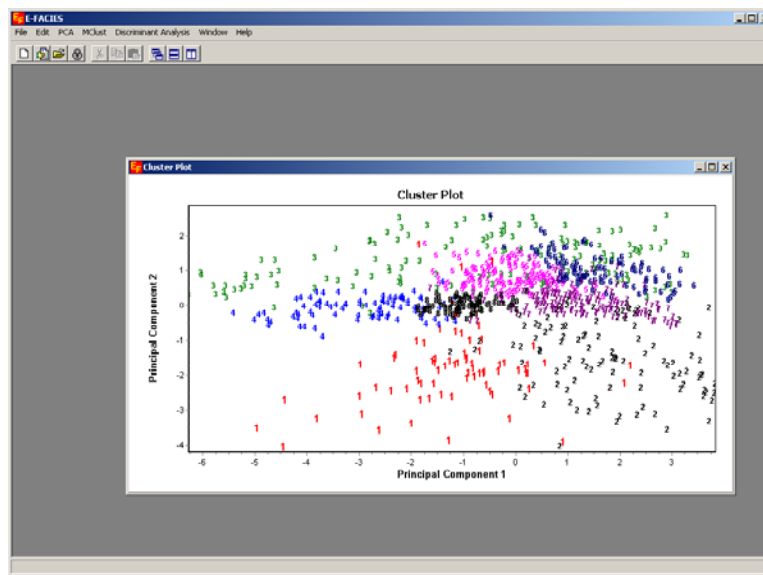


Figure C.12 – Screenshot of the Cluster Plot from Efacies.

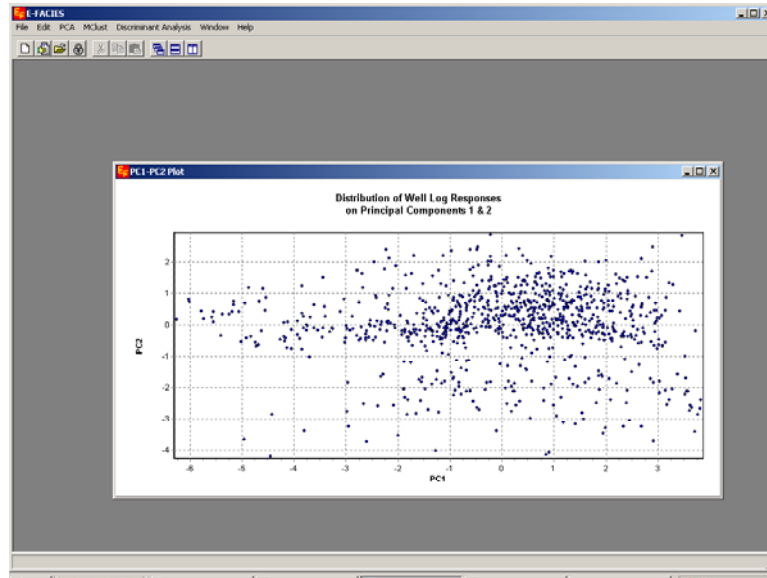


Figure C.13 – Screenshot of Principle Components Plot from E-facies.

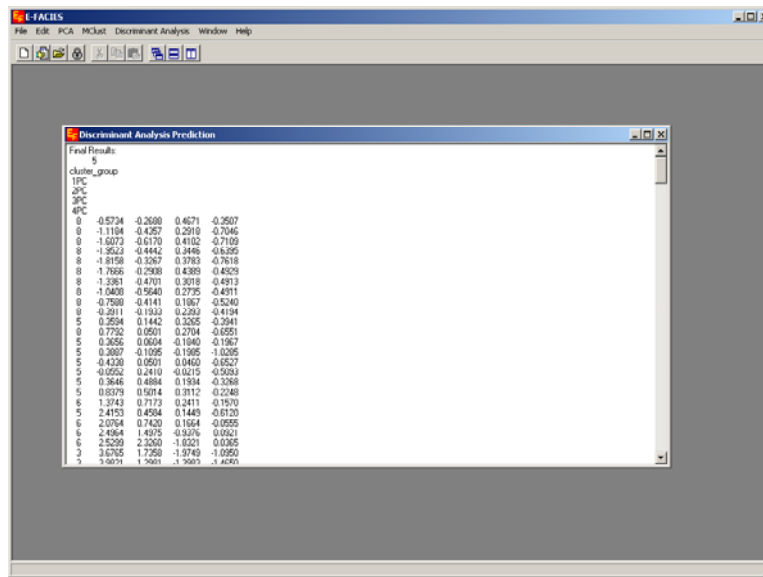


Figure C.14 – Screenshot of Prediction of Discriminant Analysis from E-facies.

VITA

Arun Kharghoria was born in Dhemaji, India, on March 1, 1973. He received his Bachelor of Technology in petroleum engineering from Indian School of Mines, Dhanbad, India in June 1994. He started his first on-the-job assignment with Assam Barytes and Chemical (Pvt.) Limited as a trainee drilling engineer in Assam. Later, he worked for Oil India Limited as a reservoir engineer in Duliajan, India. He obtained his Master of Science degree in petroleum engineering from the University of Tulsa in 1999 and Doctor of Philosophy in petroleum engineering from Texas A&M University, College Station in 2003. His other experience includes two summer internships with Schlumberger in Houston, TX. His permanent address is Milon Nagar, Dhemaji, Assam, India, 787057.

This dissertation was typed by the author.